THE EFFECT OF FIELD-OF-VIEW ON THE MANUAL CONTROL OF VISUALLY SIMULATED AIRCRAFT ROLL

by

EDWARD WILLIAM KNELLER

SB Aeronautics and Astronautics, MIT (1984)

Submitted in partial fulfillment of the
requirements for the degree of

MASTER OF SCIENCE
IN
AERONAUTICS AND ASTRONAUTICS

at the

MASSACHUSETTS INSTITUTE OF TECHNOLOGY

June 1986

Signature of Author _____
Department of Aeronautics and Astronautics
May 22, 1986

Certified by _____
Professor Robert V. Kenyon
Thesis Supervisor

Accepted by _____
Professor Harold Y. Wachman
Chairman Departmental Graduate Committee

THE EFFECT OF FIELD-OF-VIEW ON THE MANUAL CONTROL OF VISUALLY SIMULATED AIRCRAFT ROLL

by

EDWARD WILLIAM KNELLER

Submitted to the Department of Aeronautics and Astronautics
on May 22, 1986 in partial fulfillment of the requirements for the
Degree of Master of Science in Aeronautics and Astronautics

ABSTRACT

Subjects were tested in a manual control task of visually simulated aircraft roll motion to study how field-of-view size affects control response. Two experiments were performed to study different elements of the control response: the Critical Control Experiment and the Tracking Experiment. An apparatus was built for these experiments which displayed a computer generated image with a maximum field-of-view of 120°.

Five subjects were tested in the Critical Control Experiment in which they stabilized the roll motion of a time varying system. During a test the instability of the control element increased until the subject lost control. This experiment measured the time delay and control accuracy of the subjects for field-of-view sizes of 10°, 20°, 40°, 80° and 120° under two conditions: 1) the visual field rolled according to the system dynamics and 2) the visual field was stationary and the subject controlled a small center display. For the moving field condition the RMS errors and time delays were lowest at mid-range field-of-view sizes. For the stationary field condition RMS errors and time delays were lowest at the extreme field-of-view sizes. These results indicate an optimum field-of-view where the visual field has the most influence on the subject's perception of roll motion.

The Tracking Experiment was a similar roll control task but the system was time invariant so that the data analysis produced a quasi-linear model of the subject's control response. Field-of-view sizes of 10°, 40° and 120° were tested at three levels of instability. The resulting quasi-linear model was divided into two elements: 1) the subject's non-linear remnant and 2) a linear transfer function from which gain, phase, and crossover frequencies were extracted. The effect of field-of-view on control response was different for the three instability levels. The crossover frequencies showed that the subject's control response was best at 40° when the instability was moderate but when the instability was high, control response was best at 120°. The average roll velocity, which increased with the instability level, was a likely cause of this phenomenon. Perception is less accurate for higher velocities than lower velocities, and because the velocities of points are proportional to their radial distance from the field center, the periphery will be the first place for inaccuracies in perception to occur. An interaction between the periphery and the average velocity of points in the visual field forms the basis for a hypothesis which explains the varying effect of field-of-view on control response.

Thesis Supervisor: Professor Robert V. Kenyon
Title: Associate Professor of Aeronautics and Astronautics.

ACKNOWLEDGEMENTS

I thank Professor Kenyon for acting as my thesis supervisor for the past two years. His willingness to spend much time with students and freely discuss ideas is greatly appreciated.

Thanks go to Dr. Mohammed Massoumnia, Dr. Alan Natapoff, Steve Adkins and David Bower. All four gave help in great quantities and at critical times during this project.

I thank my parents, A. William and Mary Kneller, who gave me moral support and personal independence.

Finally, I thank the students of the Man-Vehicle Lab who made the tedious days fun and the most frustrating situations laughable.

This research was performed under a U.S Air Force contract, no. F33615-83-D-0603, technical monitor Dr. Kent Gillingham.

TABLE OF CONTENTS

TABLE OF FIGURES

CHAPTER 1: INTRODUCTION

1.1 Motivation for Research

When a helicopter pilot puts on a standard set of helmet-mounted, night-vision goggles, his field-of-view is often limited to less than sixty degrees. Because these goggles provide the pilot with his only image of the outside world, any effect of restricted field-of-view on the aircraft's controllability is critical. Visual displays with a limited field-of-view such as the night-vision goggles are becoming more common as pilots are required to fly missions using processed images, simulated scenes, or video pictures sent from remote cameras.

Two recent examples of aircraft with limited fields-of-view are the FAA's Controlled Impact Demonstration and the LHX helicopter. In the Controlled Impact Demonstration a ground based pilot, using remote controls, flew a Boeing 720 through a critical landing test. The only visual reference of the outside world was a nineteen inch video monitor located approximately four feet in front of the pilot. A forward looking camera on the nose of the aircraft provided the image [Aviation Week, December 10, 1984].

Plans for the LHX advanced helicopter call for the pilot to use a computer generated, virtual image of the outside world, to guide the helicopter in attack missions. Prototype displays for the LHX have been tested using 40°, 90° and 120° field-of-view sizes [Aviation Week, January 14, 1985].

1.2 Research Objective and Approach

The purpose of the current research was to describe how a pilot's control response is affected by limiting his field-of-view. Two experiments were designed to measure various aspects of a subject's control response for field-of-view sizes ranging from 10° to 120°. The field-of-view used was circular with its center aligned with the roll axis. Subjects in both experiments used a force-stick to control the roll motion of a simulated visual scene; their task was to keep the roll angle as close to zero degrees as possible. The control plants in both experiments were unstable, first order systems.

The first experiment, called the Critical Control Experiment, showed how field-of-view influenced the subjects' time delay and control accuracy. The basic characteristic of this experiment was that the plant dynamics became more unstable during the course of an individual test until the subject lost control. Ten experimental cases were tested: five field-of-view sizes for both moving field and stationary field conditions. The five field-of-view sizes were 10°, 20°, 40°, 80° and 120°. In the moving field condition the simulated visual scene rolled according to the control-loop dynamics. In the stationary field condition the simulated visual scene remained fixed with zero degrees roll while the subject controlled only a small center horizon indicator.

The second experiment, the Tracking Experiment, resulted in a quasi-linear model of the human operator. This model consisted of the subject's linear transfer function and a non-linear residual. The plant dynamics in the Tracking Experiment were time-invariant over the length of an individual test; the duration of a test was set at 147 seconds.

Nine experimental cases, resulting from the combination of three field-of-view sizes and three control plant instability levels, were tested in the Tracking Experiment. The three field-of-view sizes tested were 10°, 40° and 120°. The three instability levels changed the subject's difficulty in controlling the roll motion.

A fixed base simulator, used in both experiments, decreased the realism of the simulation, however, the purpose of the current research was to study only the importance of visual information, so the lack of bodily motion was not critical. The lack of bodily motion relates the current research directly to flight simulators and teleoperation stations that use fixed base systems.

Limiting the control task to roll motion simplified the data analysis and allowed a single input control response to be studied with greater accuracy than a multi-degree-of-freedom control task. Roll motion about the visual axis was chosen over pitch and yaw because, even with a very limited field-of-view, the roll angle can be seen easily, while this is not the case with pitch or yaw. For roll motion the radial velocity of objects in the periphery is much higher than that of objects in the center of the field. Decreasing the field-of-view removes these high velocity visual cues in the periphery which may have an effect on the subject's control response.

The Critical Control Experiment provided the subject's time delay and control accuracy which was measured by the root mean square (RMS) roll error. The Tracking Experiment resulted in a quasi-linear model which describes how the subject processed his input signal to produce his output signal. This quasi-linear model was divided into a linear transfer function and a non-linear, random, signal called remnant.

These results described how limiting a subject's field-of-view affects his control response for visually simulated roll motion.

1.3 Background Research

The relation between central vision and peripheral vision must be understood in order to study the importance of field-of-view in manual control. Past research covering peripheral and central vision in perception and manual control is presented in chapters 1.3.1 to 1.3.3. Chapter 1.3.1 covers the basic physiology of the human visual system and visual perception. Chapter 1.3.2 discusses a research paper on vection, the perception of self motion produced by purely visual cues. Chapter 1.3.3 discusses two recent papers, both on the role of the visual periphery in manual control tasks.

1.3.1 Vision

A basic understanding of visual physiology explains important aspects of motion perception. When the eye focuses on a scene, an image is produced on the retina, the inner surface of the eyeball which contains light sensitive cells. There are two types of light sensitive cells in the retina: rods, which measure the intensity of light, and cones, which are sensitive to the wavelength of light stimulating them, enabling a person to distinguish colors.

The fovea is the center of the retina which subtends approximately 2° of visual arc. The fovea has a higher density of light sensitive cells than any other part of the retina. Since visual resolution is

roughly proportional to the density of light-sensitive cells, the center of the visual field has the highest resolution. Another characteristic of the fovea is that it only contains the color sensitive cones. The density of the rods increases from zero at the fovea to a maximum at a position on the retina corresponding to a visual angle of 20° from the center of the visual field; the cone density drops off rapidly when moving from the fovea to the periphery. The periphery of the retina is populated primarily with rods and, although it has lower resolution and color sensitivity than the fovea, the periphery has a lower intensity threshold and therefore is more effective than the fovea when light levels are very low [Pirenne, 1967], [Cornsweet, 1970].

Since the center of the visual field has the highest resolution, it is used for perceiving patterns and tracking object motion. When a person uses visual information to orientate themselves spatially, she relies primarily on peripheral vision. Peripheral vision also contributes greatly to a person's sense of motion.

The combination of central vision which perceives the motion of an object relative to the observer, and peripheral vision which perceives self-motion, allows the observer to track an object while undergoing active locomotion [Held, Leibowitz, Teuber, 1978].

1.3.2 Vection and Field-of-View

Vection is a phenomena where a person perceives the motion of a visual field as self-motion. The study of vection shows the importance of the central and peripheral vision, and the vestibular system in spatial orientation. The vestibular system, or inner ear, provides the

brain with a second source of information for spatial orientation. The vestibular system measures bodily accelerations, both linear and rotational. In a normal environment, the motion of the visual field and the bodily motion a person experiences coincide and the information sent to the brain by the visual system and the vestibular system agree. However, some situations provide conflicting information for the visual and vestibular systems. A fixed base flight simulator with a full field display system provides an example of such a situation.

Motion of the visual scene tells the pilot that he is moving while the vestibular system receives no such signal. Due to process by which the brain combines the two signals, the pilot feels as if he is actually moving in many situations. A more common example is a passenger sitting in a stationary train. A nearby train perceived in the passenger's peripheral visual field, may start to move, causing the passenger to feel he is moving in the opposite direction.

Brandt, Dichgans and Koenig (1972), presented a series of experiments showing some of the relationships between vection and field-of-view. Their experiments support the assumption that central vision is used for detecting object motion and peripheral vision is used to detect self-motion. The basic experiment consisted of exposing an upright subject to a visual field rotating about the subject on a vertical axis. The visual field was the inside of a large, brightly lit cylinder covered by a high contrast pattern. The subject, who was always stationary, would either perceive a moving visual field have the illusion of self-motion (vection).

If the subject was presented with motion over the full visual field then the subject usually experienced vection which was indistinguishable

from actual rotation. When a peripheral mask was placed around the subject such that she saw only the moving pattern in a limited central area, the subject usually experienced little if any vection, even if the central field subtended an angle as great as 60°. If a central mask was placed in front of the subject such that she was exposed to field motion only in periphery, vection usually did not fall from its maximum level, even if the central mask subtended an angle of 120°.

Brandt, et al (1972), discussed other findings that should be considered when designing an experiment involving motion perception. They indicated that patterns perceived in the background of a scene produced stronger vection than patterns perceived in the foreground. Increasing the spatial frequency, or detail of visual detail, of the visual field increases the strength of vection; a greater amount of detail in the scene provides more indicators of motion. The strength of vection was greater if the subject lets her eyes move freely across the field than if the subject keeps his eyes fixed on a non-moving point in the field's center. This may be due to cells in the retina being exposed to the motion of the field.

Finally, the magnitude of circular vection reaches a limit when the field rotates about the subject at greater than 90°/second. Above this speed the subject would rarely perceive full self-motion with the visual field being stationary. Instead, the subject would sense self-motion and motion of the visual field relative to an inertially fixed coordinate system.

1.3.3 Central and Peripheral Vision in Manual Control.

The work of Hosman and van der Vaart (1981), is closely related to the subject of this report in that it examines the pilot performance in controlling simulated aircraft roll, when using peripheral or central displays. In the van der Vaart experiment the pilot's task was to keep the aircraft roll as close to wings-level (0° with respect to the horizon) as possible. The aircraft dynamics were modelled as a neutrally stable second order system. A quasi-random disturbance signal was used to produce a roll error which the pilot attempted to correct. For one experimental case the subject was shown a central display alone and in another case the subject was presented with the central display and left and right peripheral displays. The peripheral displays were 50cm wide TV monitors displaying a black and white checkerboard pattern at the subject's eye level. The right monitor was located 50 cm from the subject, and the left monitor was at a distance of 140 cm. The central display was a 10 cm wide monitor which displayed a simple horizon indicator. The motion of both visual systems corresponded to the simulated roll motion of the aircraft.

The subject's performance was measured by both the RMS error of the aircraft's roll and by analysis of the pilot's transfer function using the crossover model. Measurements of the RMS roll error showed a significant improvement when the pilot used peripheral displays in addition to the central display. Analysis of the transfer function showed that the pilot's crossover frequency increased when the peripheral displays were added to the central display, indicating a greater stability margin.

Further effects of field-of-view on pilot performance are found in Zacharias (1983). This study developed an optimal control model to measure the ability of a pilot to fly a simulation of a low-level, terrain-following mission. In this model the pilot estimated the direction of the aircraft by the flow-field of visible landmarks about an expansion point. During a time period, dt, the aircraft flew toward a point on the terrain which remained fixed in the field-of-view. All other points in the visual field moved along paths radiating directly away from this expansion point. The model predicted that a pilot would estimate the aircraft's flight path based on this flow-field. A least squares fit of the paths of the points in the flow-field indicated the center of the flow-field and therefore direction in which the aircraft was flying. The model also predicted that the error of the estimation was caused by inaccuracies or noise in the visual perception process.

A major prediction of this model is that there is an optimal field-of-view for estimating the aircraft's flight path. A narrow-field-of-view does not give enough information for the pilot to make an accurate estimation while a very wide field-of-view introduces a large amount of noise into the system. There was so much information in the periphery that the pilot's visual perception system was saturated and he tracked the landmarks with less accuracy.

1.4 Thesis Organization

This thesis is divided into two major parts, each describing a separate experiment. Part one covers the Critical Control Experiment and Part Two covers the tracking experiment. Part One contains chapters

2 through 6. Chapter 2 discusses the development of the Critical Control Experiment which includes the theory of a past experiment on which the Critical Control Experiment is based and how the theory was implemented for the current research. Chapter 3 covers the equipment that was used for the experiment, much of which was developed for the current research. Chapter 4 describes the experimental procedure including the design of the Critical Control Experiment, the subjects who participated, and the experimental process. Chapter 5 describes the data analysis which produced the results that are presented in Chapter 6.

Part Two of this report begins with Chapter 7 and ends with Chapter 9. Chapter 7 covers the experimental procedure for the Tracking Experiment which includes the implementation of a tracking task, the equipment used, and the experimental process. Chapter 8 describes the data analysis and Chapter 9 presents the results.

This report concludes with Chapter 10 which is a discussion of the results from both the Critical Control Experiment and the Tracking Experiment.

PART ONE: THE CRITICAL CONTROL EXPERIMENT

CHAPTER 2: DEVELOPMENT OF THE CRITICAL CONTROL EXPERIMENT

The Critical Control Experiment measured two parameters of the subject's control response: time delay and control accuracy. Results of the Critical Control Experiment showed how changes in the field-of-view affected these parameters. The Critical Control Experiment used in the current research was based on the Critical Tracking Task described by Jex, McDonnel and Phatak (1966), which was designed to measure a subject's effective time delay. The control element dynamics and the method of measuring the time delay in the Critical Control Experiment were the same as those developed for the Critical Tracking Task. Chapter 2.1 gives a brief overview of the experimental theory described by Jex, et al (1966), and chapter 2.1 describes how the concepts of the Critical Tracking Task were implemented in the Critical Control Experiment of the current research.

2.1 Theory of the Critical Tracking Task, circa 1966

The Critical Tracking Task was a closed-loop control system with an unstable, first-order control plant. The subject used a force-stick to control the vertical motion of a horizontal line displayed on a CRT screen; the neutral position of the line was at the center of the CRT. During a single run of this experiment, the instability level of the control plant slowly increased. At first the operator had little trouble controlling the vertical motion of the line, but the task became increasingly difficult and reached a critical instability level where the operator lost control of the line's motion. This critical instabil-

ity level was a measure of the operator's effective time delay. To show how the Critical Tracking Task measured the subject's effective time delay, equations for the human-operator and the control-element were developed and combined to produce a model of the closed-loop system.

2.1.1 The Human-Operator Model

A first order human-operator model, given in equation 2.1, is the first step in showing how the Critical Tracking Task measures the subject's effective time delay. This model was chosen because its is simple but still able to show the theory behind the Critical Control Task.

$$Y_H(s) = K_p\, e^{-\tau_e s} \qquad 2.1$$

Y_H is the human operator transfer function

K_p is the subject's gain

τ_e is the subject's effective time delay

The subject's time delay for this control task was the length of time it takes for the operator to respond to the signal input. This includes the time that the central nervous system takes to process the visual information, the time for central nervous system to send neural signals to the muscles, and the time for the muscles to respond. This equation can be approximated by the first order Pade polynomial:

$$Y_H(s) = K_p \frac{-(\tfrac{1}{2}\tau_e)s + 1}{(\tfrac{1}{2}\tau_e)s + 1} \qquad 2.2$$

2.1.2 The Control Element

The first-order divergent control element has the transfer function:

$$Y_C = \frac{-K_c}{(-Ts + 1)} \qquad 2.3\ (a)$$

$$Y_C = \frac{-K_c/T}{(-s + 1/T)} \qquad 2.3\ (b)$$

The time constant of the controlled element, T, was the parameter that controlled the stability of the system. If T was relatively high, the system reacted slowly and was easy for the operator to control. As the value of T decreased, the system reacted faster and became more difficult to control. This can be seen in equation 2.3 (b) where $-K_c/T$ is the loop sensitivity gain. When T is small, the loop sensitivity gain is high and the system reacts quickly forcing the operator to also act quickly in order to maintain control.

2.1.3 The Closed-Loop Characteristics

The equations for the human-operator and the control element are combined into a closed-loop system, that describes how the Critical Tracking Task measures the human-operator's effective time delay. The block diagram of the closed-loop system is shown in figure 2.1.

Before the actual closed-loop equations are examined, a root-locus diagram will graphically depict how the Critical Tracking Task measures the subject's effective time delay. The movement of the closed-loop

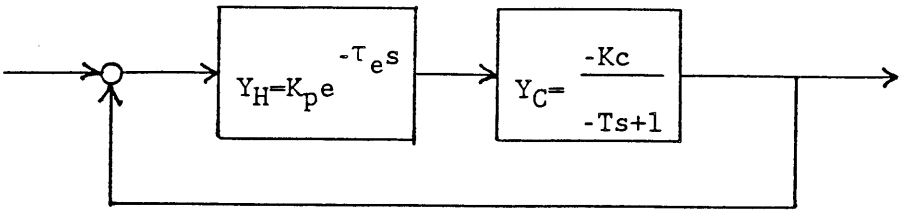

Figure 2.1: Block diagram of closed-loop system

poles are shown in figure 2.2 as the subject increases her gain from zero to infinity. If the closed-loop poles are in the left-half plane of the coordinate system, the system is stable. If the poles are in the right-half plane, the system is unstable.

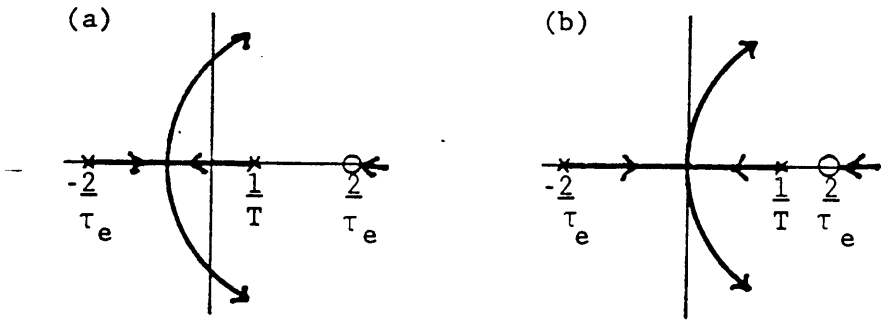

Figure 2.2: (a) Root locus at a low instability level.
(b) Root locus at the critical instability level.

Figure 2.2 (a) represents a system where the control element has a relatively low value for 1/T. In this case the closed-loop system is stable when the subject adopts a gain such that both poles are in the left-half plane. This corresponds to an subject's gain high enough such that the 1/T closed-loop pole moves into the left hand plane, yet low enough such that both the 1/T and the $-2/\tau$ closed-loop poles do not move back into the right-half plane.

Figure 2.2 (b) shows the same system except that 1/T has increased to a level $1/T_c$, where T_c is the critical time constant. The operator's gain is constrained to a very limited range in order for the system to be stable; the value of the gain must be such that the two poles move to the origin. Both the phase margin and the gain margin vanish so the subject is not able to adopt lead or lag equalization, the operator must adopt a pure gain response. Lead and lag equalization are methods of making a system easier to control, which the subject adapts by trading off her gain and phase in such a way as to optimize the control response.

A mathematical explanation of the Critical Control Task provides an analytical alternative to the root-locus diagram. If the open-loop operator/control element transfer function is estimated as:

$$G = Y_H Y_C = \frac{-K e^{-\tau_e s}}{(-Ts + 1)} = \frac{-K(-\frac{1}{2}\tau_e s + 1)}{(-Ts + 1)(\frac{1}{2}\tau_e s - 1)} \qquad 2.4$$

then the closed-loop function is:

$$H = \frac{G}{1 + G} = \frac{-\frac{K}{T}(s - \frac{2}{\tau_e})}{s^2 + (\frac{2}{\tau_e} - \frac{1}{T} - \frac{K}{T})s + 2\frac{K - 1}{\tau_e T}} \qquad 2.5$$

The denominator of H has the form:

$$s^2 + 2\zeta\omega_n + \omega_n^2 \qquad 2.6$$

$$\text{where } \omega_n^2 = \frac{2(K - 1)}{\tau_e T} \qquad 2.7$$

$$2\zeta\omega_n = \frac{2}{\tau_e} - \frac{1}{T} - \frac{K}{T} \qquad 2.8$$

When $T = T_c$ then $\omega_n = 0$ since the closed-loop poles are at the origin and ω_n is equal to the distance between the closed-loop pole and the origin. Therefore

$$\omega_n^2 - \frac{2(K - 1)}{\tau_e T_c} = 0 \qquad 2.9$$

$$2\zeta\omega_n - \frac{2}{\tau_e} - \frac{1}{T_c} - \frac{K}{T_c} = 0 \qquad 2.10$$

Solving equation 2.9 for K and 2.10 for τ_e results in:

$$\tau_e = T_c \qquad 2.11$$

By this simplified model the subject's effective time delay is equal to the critical time constant of the control element. In practice, the operator is not able to maintain a precise pure gain response and he is likely to reach a critical point where control is lost, when T_c is less than τ_e.

2.1.4 Adjusting the Instability Level

In order to measure T_c with reasonable accuracy, the adjustment itself of T, during a run, must not greatly influence the outcome of the experiment. Since T is often used in the form of 1/T, the variable will be defined as $\lambda = 1/T$. For the critical time constant T_c, $\lambda_c = 1/T_c$. λ is called the inverse time constant or the instability level, λ_c is the critical instability; as λ increases, the instability of the system increases.

The preferred adjustment scheme described in Jex, et al (1966), had λ starting at a low level where the system was easy to control. During

a single run of the experiment, λ increased at a relatively rapid rate $\dot{\lambda}_1$, until a point was reached where the subject's performance deteriorated past a predetermined level, indicating that λ was close to its critical value, λ_c. λ then increased at about 1/4 its previous rate until λ_c was reached and the operator lost control. The fast rate allowed the operator to move from a relatively stable level to the near critical level over a period of 20 to 40 seconds, therefore avoiding fatigue. The second rate $\dot{\lambda}_2$, lasts up to 20 seconds, did not fatigue the operator, but was slow enough to approximate a time invariant system. If the second rate was too high, the λ_c values may have been optimistic due to λ increasing a significant amount during the moment after the operator had lost control but before the display had reached its characteristic limit.

2.1.5 Results of the Critical Tracking Task

Preliminary experiments conducted in Jex, et al (1966), resulted in three key points which were taken into account for the experiments of this report. First, the subject's learning time was quite short, after a few tests, the subject's critical instability reached a level $\lambda_c = 5$, then increased over 170 tests and a month's time, to an average value, $\lambda_c = 6.5 \pm 0.7$. Jex found that three to five tests gave a stable value of λ_c, having little variation as successive test scores were added.

Second, experiments showed that the operator was able to compensate for a wide range of force-stick gains. Even stick gains differing by two orders of magnitude had little effect on the critical instability levels. The third and final key point was that the Critical Tracking

Task experiments were run both with and without a random disturbance function input. The experiments without a disturbance input used the subject's remnant to drive the system away from its neutral position. The critical instability values for these experiments were generally higher and had a lower standard variation than the tests run with a disturbance function. This was due to the forcing function sometimes driving the display to its limit before the operator actually lost control.

2.2 Implementation of the Critical Control Experiment

For the current research the concepts of the Critical Tracking Task were applied to a visual, roll control experiment in which field-of-view was the primary experimental variable. The experiment of this report used the same theory and control equations as the task described by Jex, et al, (1966), but the display that the subject controls was changed from a linear tracking task to a roll control task. The result is referred to, in this report, as the 'Critical Control Experiment'.

2.2.1 Calculation of the Discretized Control Equations

The roll dynamics of the simulated scene were calculated by a control loop which was programmed into a digital computer. The first order divergent system implemented in the computer was

$$Y_C = \frac{\Theta}{X} = \frac{-K_c}{-Ts + 1}$$

and are the Laplace transforms of the roll angle of the scene and the operator's stick input respectively. The corresponding differential equation is

$$\frac{d\theta}{dt} = \frac{1}{T}\theta + \frac{1}{T}K_c x = \lambda\theta + \lambda K_c x \qquad (2.11)$$

To implement this differential equation digitally, it was converted to a difference equation. This difference equation was used to calculate a value for the new roll position based on the current roll position and the subject's current control input. The roll velocity was not calculated explicitly. Equation (2.11) has the form

$$\dot{\theta}(t) = F\,\theta(t) + Gx(t) \qquad (2.12)$$

If x_n and θ are assumed to be constant over the interval $\Delta t = h$, then the corresponding exact difference equation is

$$\theta_{n+1} = A\theta_n + Bx_n \qquad (2.13)$$

$$A = e^{F\Delta t} = e^{\lambda h}$$

$$B = \int_0^{\Delta t} e^{F(\Delta t - \tau)}G\,d\tau = e^{\lambda h} - 1$$

2.2.2 Adjustment of the Instability Level

The instability level, λ, was incremented by a value $\Delta\lambda$, each time the computer program executes the control loop. The current value of λ was used to calculate the coefficients A and B which were then used in equation 2.13 to calculate the new value for the roll angle of the display. The value of $\Delta\lambda$ can be one of two values, a high value for the

initial, rapidly increasing, instability level and a low value for the second, slower rate of increase.

The criteria for switching from the high to the low $\Delta\lambda$ value was based on a measure of the operator's performance degradation. When the average absolute error of the display, over 2/3 second, was greater than 13°, $\Delta\lambda$ was switched from its first value to its second value.

The rate at which the computer runs through the program loop was 15 Hz, therefore, h = 0.0667 seconds. The initial instability level was $\lambda_0 = 1.5$. Its initial rate of increase was $\dot{\lambda}_1 = 0.112$ rad/sec corresponding to $\Delta\lambda_1 = 0.0075$. Its second rate of increase was $\dot{\lambda}_2 = 0.03$ rad/sec, corresponding to $\Delta\lambda_2 = 0.002$. The limit of the displayed roll angle was ±100°. When the roll angle reached this limit, by definition, the operator had lost control and the test was over. Roll angle limits as high as 200° were tested and found not to increase the critical instability level, obtained with the 100° display limit.

2.2.3 Using Operator Remnant as a Forcing Function

The Critical Control Experiment of this report does not use a forcing function. The operator's remnant, which by definition is not

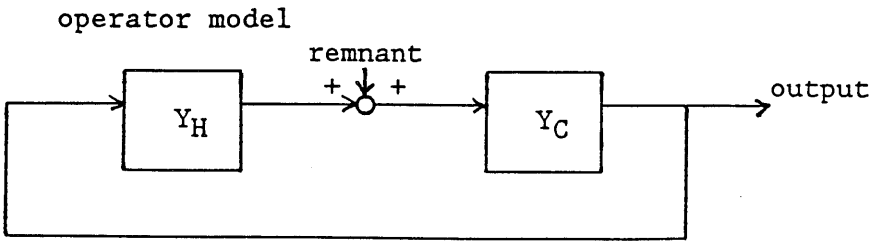

Figure 2.3: Operator model including remnant

correlated with the linear part of the operator's transfer function, acted as a disturbance function which drove the display away from its neutral position (see figure 2.3). The remnant is generally modeled as white noise with a Gaussian distribution and a time varying component [Sheridan, 1974].

2.3.4 Data Provided by the Critical Control Experiment

In addition to measuring the critical time constant of the control element, the roll angle of the display was sampled at 15 Hz throughout the test allowing the RMS roll error to be measured. RMS roll error indicates how accurate the subject's control input was for a particular field-of-view.

CHAPTER 3: EQUIPMENT FOR CRITICAL CONTROL EXPERIMENT

3.1 Equipment Overview

The Experimental apparatus that was needed to perform the Critical Control Experiment consisted of three major components. First, a method for simulating visual roll motion according to the dynamics equations; second, a method for presenting the simulation to the subject with as wide a field-of-view as possible; and finally, equipment to provide the subject with a control input to the control element.

The first requirement was satisfied by the IRIS 2400, a dedicated graphics computer manufactured by Silicon Graphics, Inc. The IRIS was capable of producing real-time, graphic simulations, with solid-modelling and red, green and blue (RGB) color mapping; the graphic simulations were displayed on a high-resolution color monitor. The control equations for these simulations were also programmed into the IRIS. The second requirement was satisfied by the Expanded Field Display, an optical system developed under the current research, which displayed the IRIS's computer generated image with a maximum field-of-view of 120°. The third requirement, for the subject's control input, was satisfied by a force-stick hand-control and an analog-to-digital (A/D) card. The subject applied lateral pressure on the stick, producing a voltage signal. The voltage level was converted to a digital signal by the A/D card and then was read by the IRIS graphics computer.

The overall system of generating a computer image and then displaying the image through the Expanded Field Display was originally developed under a US Airforce contract for a flight-simulator display. The

design requirements for the flight simulator were low cost, wide-field-of-view and small size. The IRIS 2400 was chosen to generate the image, based on its high quality graphics and low cost. The Expanded Field Display was developed under this contract, by the MIT Man-Vehicle Lab. It was designed to be compact, inexpensive and display a computer generated image with a 120° field-of-view. A more detailed description of the individual components of this system is given in appendix 3.1.

3.2 The Expanded Field Display

The Expanded Field Display is an optical system that displays a computer generated image with a maximum field-of-view of 120°. The subjects of the Critical Control Experiment looked through the Expanded Field Display, when viewing the visually simulated roll motion. The main components of the Expanded Field Display are two projection lenses, a ground glass projection screen and a binocular viewer which houses two wide-field-of-view lenses. The basic principle of the Expanded Field Display was to project a two-dimensional, external image onto a sheet of ground glass, using the two projection lenses. This produced two separate, side-by-side images. The subject then viewed these ground glass images through the wide-field-of-view lenses (see figure 3.1).

3.2.1 The Binocular Viewer

The binocular viewer was manufactured by Pop Optix of Waltham, MA. It was originally designed along with a stereoscopic camera as part of the Large Expanse Extra Perspective (LEEP) Stereoscopic Imaging System

[Howlett, 1983]. When used in the Expanded Field Display, the LEEP viewer distorts images spatially and produces chromatic abberations, where the primary colors of the original become slightly separated. The LEEP viewer was also originally designed to view film images; each image had an approximate size on film of 7 cm by 6 cm (see figure 3.2).

The spatial distortions of the viewer are described by the equation:

$$r = M (\theta - k\theta^3) \qquad 3.1$$

θ is the angle from the optical axis of the camera.

r is the corresponding radial distance from the center of the image.

For r in centimeters and θ in radians, k = 0.22 rad^{-2}, M = 3.7 cm. Figure 3.3 shows the theoretical, spatial distortion of an image as seen through the LEEP viewer.

3.2.2 The Projection Screen

In the Expanded Field Display the film images are replaced by a sheet of ground glass onto which the computer generated image is projected. The ground glass is placed approximately 1 cm in front of the viewer, in the position normally occupied by the film. The images projected onto the ground glass were the same size as the original film images therefore, a 7 cm x 6 cm area of the ground glass was seen under

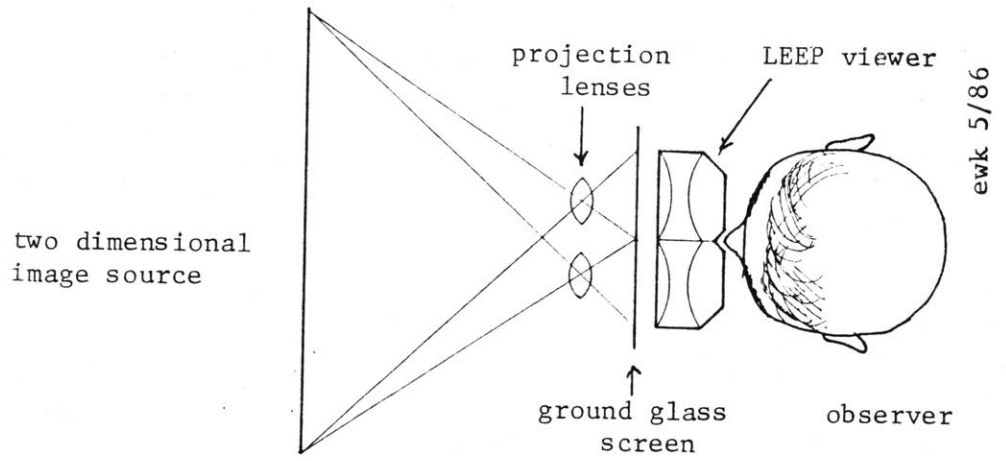

Figure 3.1: Schematic top view of the Expanded Field Display.

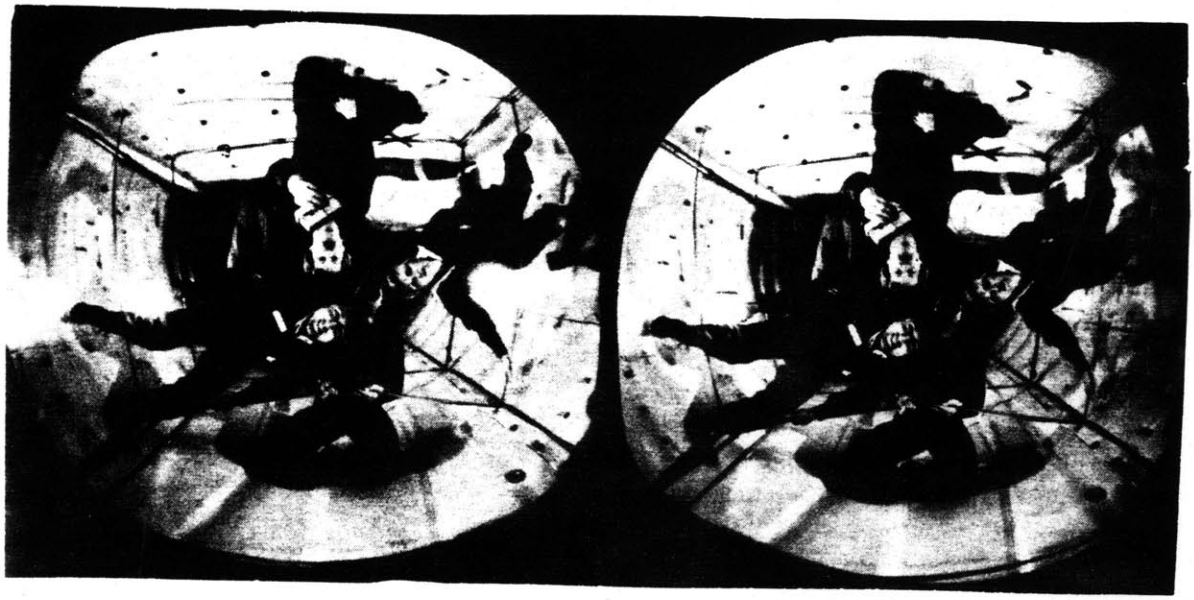

Figure 3.2: Film images normally seen through the LEEP viewer.

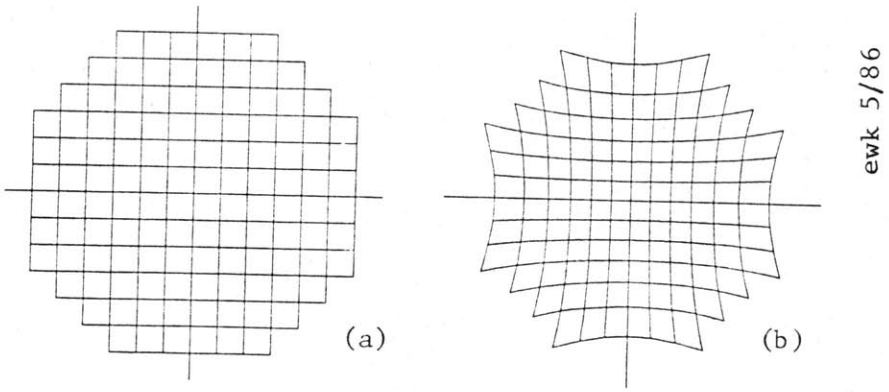

Figure 3.3: Undistorted grid pattern (a) and subsequent distortions as seen through the LEEP viewer

high magnification. Therefore, a very fine grain ground glass was used in order to have a high image resolution.

If the ground glass image was viewed directly through the LEEP viewer, the intensity of the image was seen to fall off rapidly in the periphery. This intensity fall-off was corrected by placing two fresnel lenses against the far side of the ground glass so that light from the periphery was directed towards the eye. One fresnel lens was used for each projected image. The focal length of the fresnel lenses was 10 cm.

3.2.3 The Projection Optics

The computer generated image is projected onto the ground glass with two 80mm projection lenses, producing two duplicate images. A partition between the two lenses, that extends to the ground glass screen, stops the two images from overlapping. As with any focused image produced by a positive lens, the image on the ground glass was reversed from top to bottom and from left to right. Therefore, the computer generated image was displayed with a 180° rotation, so that the image seen through the LEEP viewer appeared with the proper orientation.

3.2.4 Integration of the Expanded Field Display Components

An aluminum frame was built to house the lenses, the projection screen and the viewer. The frame held the optics in a position that did not move unless purposely adjusted. The Expanded Field Display frame was mounted on an optical bench which was then positioned in front of the graphics computer monitor. Sections of black matte paper were cut

and placed on the frame of the Expanded Field Display in order to shield the subject form any stray light. The only light which reached the subject was projected from the monitor, through the lenses of the Expanded Field Display.

3.2.5 Setting the Field-of-View Size

Masks were cut from black matte paper, and placed directly in front of the LEEP viewer in order to limit the subject's field-of-view. The masks were 2½" x 4" sections of paper in which circular holes were cut. The size of the circular hole for a particular field-of-view was calculated using equation 3.1. Two masks were needed for each field-of-view size, one for each lens of the LEEP viewer. Two paper-clips were taped to each mask and these were used to slide the mask onto the frame of the LEEP viewer; the masks could be attached quickly and with little effort. When in place the masks rested on the outer rim of the LEEP viewer lenses which are highly concave.

3.2.6 Use of the Expanded Field Display

In order to obtain the widest possible field-of-view and the clearest image, the subject's head was held in a fixed position, with the brow and the bridge of the nose touching the LEEP viewer lenses. For these experiments a contoured, adjustable, chin rest stabilized the head in the desired position. The chin rest is mounted on the same optical bench as the Expanded Field Display.

When using the Expanded Field Display the subjects had to make several adjustments in order to suit their individual eyesight. The vergence angle that the eyes must assume when looking through the viewer can be adjusted by the horizontal spacing of the projection lenses. This spacing affects the distance between the two separate images; an average distance of 5.5 cm between the optical axes of the two lenses is comfortable for most people. The subject also needed to adjust the distance between the LEEP viewer and the ground glass in order to match the normal focusing distance of their eyes.

Adjustments of the components when first setting up or altering the system included focusing the projected image onto the ground glass; setting the size of the projected image and setting the tilt of the viewer about its optical axis, so that the subject does not have to tilt his head in order to see the image clearly. Figure 3.4 shows the important adjustments associated with the Expanded Field Display.

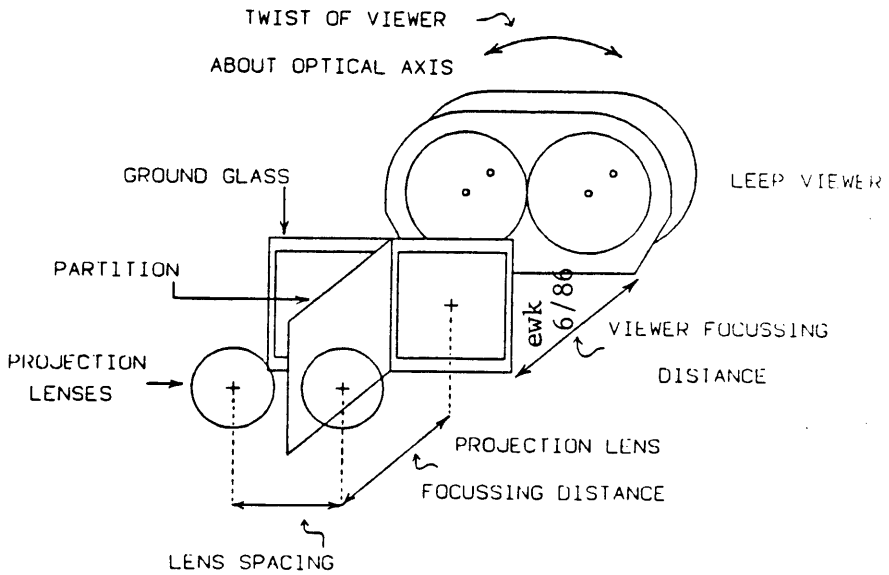

Figure 3.4: Adjustments for the Expanded Field Display

3.3 Control Input Hardware

A simple one degree-of-freedom, force-stick was used by the subject to control the roll motion of the scene. The force stick was a four inch long, aluminum shaft, which was supported by a fixed base assembly. A small rubber knob was placed on the tip of the shaft in order to ease the pressure on the subjects fingers. The subject was told to hold the knob between the pad of the thumb and the right forefinger. The base assembly of the force-stick was mounted securely to the right hand armrest of a steel frame chair in which the operator sat. During the experiments the subject's forearm rested securely in a contoured armrest attached to the chair.

The lateral force that the subject applied to the stick is converted to an analog voltage which varies linearly with the force level. The maximum voltage output of the force-stick was ±10V, the voltage/force ratio is 22mV/N. When the voltage input was converted to a variable in the control equation, the resulting ratio was 0.09 radians/N. A signal generator supplied the force-stick with power and an input signal.

In order to insure the stick output was suitable for digital analysis, the stick signal was sent through a low pass filter. The filter had a break frequency of 3.8 Hz, which attenuated high frequency signals which were not important to the results but could impair the data analysis. The filter is a simple RC circuit. The analog output signal from the force-stick is converted to a digital signal by an A/D card installed in the IRIS 2400.

McDonnell and Jex [1967], in a follow-up study to their original Critical Tracking Task, stated several reasons for using a force stick instead of other input devices such as a self centering displacement stick or a rotating knob. The primary reason is that any displacement device increases the subject delay time due to limb positioning and muscle dynamics. A force stick with very little motion, avoids increasing the subject's effective time delay.

3.4 The Graphics Computer

The Iris 2400, a dedicated graphics computer, was programmed to run each test of the Critical Control Experiment once the experimenter had entered the starting command and a name for the current test. Once an experiment started, the IRIS displayed the simulated roll motion, read the subject's control input, and stored the input and output data. The graphics output of the Iris 2400 was an analog RGB signal which was sent to a high-resolution, 30 Hz interlaced, color monitor. The monitor had a 19" diagonal measurement with a resolution of 768 x 1024 RGB pixels.

3.4.1 Graphics for the Roll Motion Simulation

In order to display computer generated images, the IRIS 2400 was programmed using a library of graphics commands which included drawing commands, color definitions, coordinate transforms, and display commands. Simple drawing commands create lines, polygons and circles based on a previously defined coordinate system. Color commands specify a color with which to draw the current graphics. The graphics software

allowed the user to define colors by specifying red, green and blue intensity levels. Each color has 256 possible levels of intensity which combine to produce 256^3 possible colors. In normal operations between 64 and 256 colors could be defined at one time. Once a series of graphical commands was compiled the defined image could be displayed on the graphics monitor.

The scene that displayed the roll motion showed a stylized landscape as viewed from an aircraft with approximately 500 feet altitude. The scene was highly stylized because its basic elements were solid-shaded polygons. The scene had three characteristics that were considered important in the simulation of visual aircraft roll: a well defined horizon, distant landscape features, and high spatial frequency. Because the subject's task in the Critical Control Experiment was to keep the roll angle of the scene at 0°, a well defined horizon line gave the subject a strong indication of the roll angle. A fixed crosshairs symbol, in the center of the display, gave the subject a reference for 0° roll angle.

Landscape features such as hills, clouds and trees were included in the stylized scene to give an impression of distance. In addition to making the scene more realistic, moving objects that are perceived to be far away have a greater effect on a person's perception of motion than objects that are near [Brandt, et al, 1972]. The scene was also designed with high-spatial frequency, by including many small polygons, since high spatial frequency also adds to the perception of motion [Brandt, et al, 1972]. Figure 3.5 shows a photograph of the scene for the roll motion simulation.

10°
20°
40°
80°
120°
ewk 5/86

In the stationary field cases the scene remained at 0° roll, and a small center display rolled according to the system dynamics. This roll indicator had a visual angle of 10° and consisted of two semicircles which formed an 'artificial' horizon line. The scene for the stationary field cases is shown in figure 3.6.

Figure 3.7 shows a set of circles overlaid on the display. These circles represent the field-of-view limits for the masks that were placed in the Expanded Field Display. For the case where the field-of-view was 10° and the artificial horizon was displayed, no part of the out-the-window visual field could be seen, since the artificial horizon itself had a visual angle of 10°.

3.4.2 Control Program Description

The computer program for the Critical Control Experiment modeled the closed-loop control system, displayed the graphical simulation of the roll motion dynamics, and performed the sequence of steps which measured the subject's time delays and RMS roll error. A flow chart of the Critical Control Experiment program is shown in figure 3.8. The actual code for the program is given in appendix 3.2.

When the program is initialized for a test it displayed the scene but did not start the control loop until the experimenter typed in a keyboard command. Once the command was given a countdown sequence was initiated which prepared the subject for the start of the closed-loop control process. Two vertical red lines appeared, within the central 10° field-of-view, on either side of the display's center, and moved towards each other. The lines met in five seconds and disappeared, at

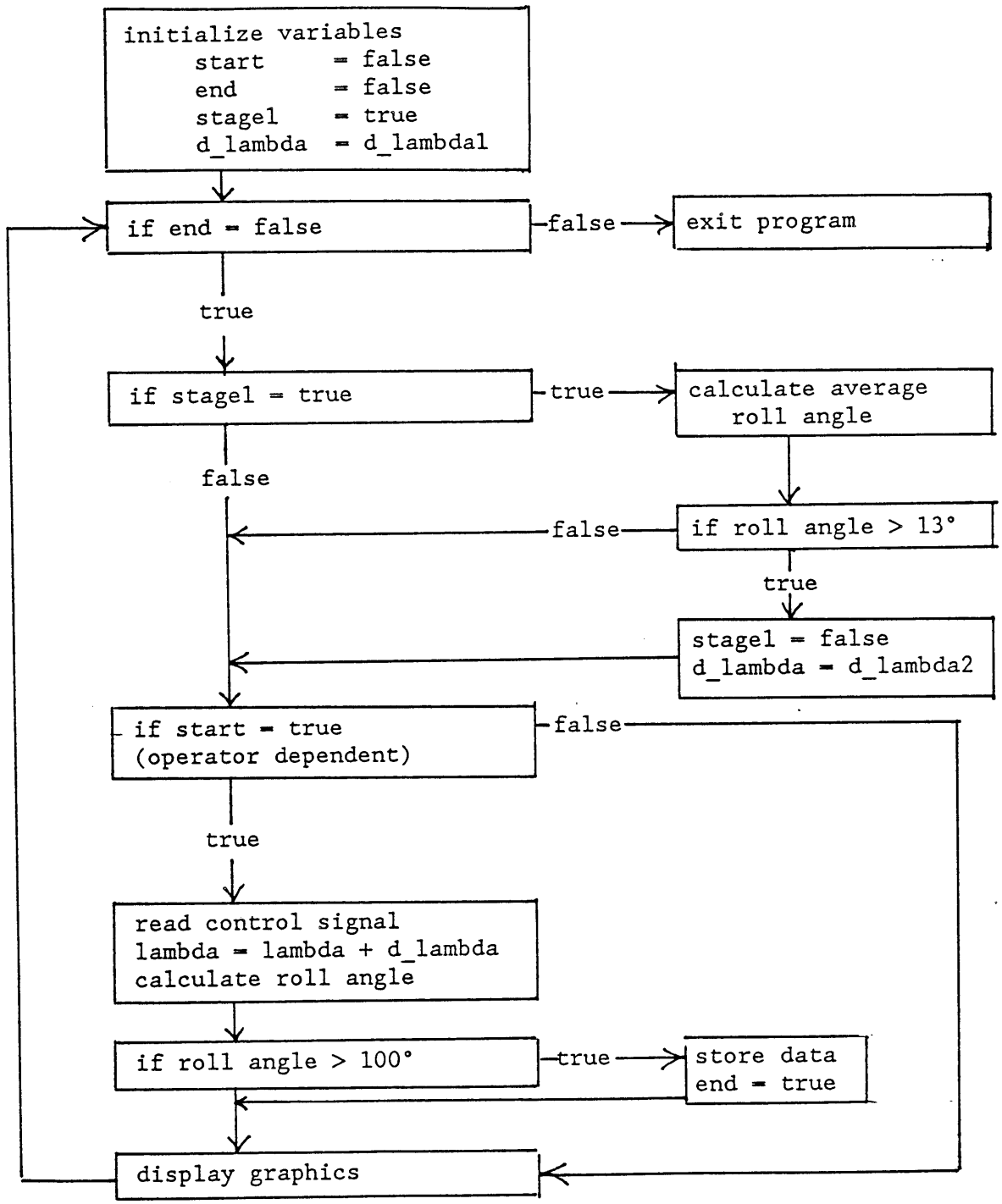

Figure 3.8: Flow chart of Critical Control Experiment program.

which instant the control process was activated and the display began to move. The display would not rest at zero degrees roll since the output of the stick contained a slight amount of noise, and any stick offset would cause the display to diverge from its neutral position.

Each time the program passed through the main control loop the subject's input signal was read from the A/D card and was used along with the previous roll angle to calculate the current roll angle. The scene was displayed with the current roll angle and the roll angle was then tested to see if it had exceeded its limit for loss of control; if so, the control process stopped and the data from the experiment was stored in a file. The program also incremented the instability level by the current $\Delta\lambda$ value, each time through the program loop, and the program performed a test of the roll angle to determine whether the first or second $\Delta\lambda$ value should be used.

One of the main concerns with this program was that it had to run at a constant update rate. The digital control equations were calculated for a specific time increment so if the update rate changed the control dynamics would change. A signal generator set at a frequency of 15 Hz, acted as a control clock for the program's update rate. The programm was tested every day before any experiments were run and during the actual testing. No timing results ever showed an update rate that deviated from 15Hz by more than one percent.

3.5 Experiment Preparation

The experiments for this report were conducted in an 8' x 12' room which was well shielded from external sources of light and noise. The

graphics computer monitor and the Expanded Field Display were fixed in position, throughout the experiments, so that projected image was in sharp focus and centered in the viewer. The subject needed only to adjust the distance between the LEEP viewer and the ground glass, to set the focus for their individual eyesight.

The subject prepared for an experiment by adjusting the chair so that he could look comfortably through the Expanded Field Display. The subject also positioned the chin rest so that his head was stable, and then focussed the LEEP viewer. When the final adjustments were made, the subject was leaning slightly back in the chair, the right forearm comfortably held in the armrest, and the hand control held between the thumb and forefinger. The subject's head was upright with the brow resting against the LEEP viewer (see figure 3.9). During the tests the experimenter sat off to the side of the subject with the computer keyboard. In this position the experimenter had a clear view of the subject and the monitor screen, and could enter all program parameters through the computer's keyboard. Figure 3.10 shows a schematic of the equipment layout.

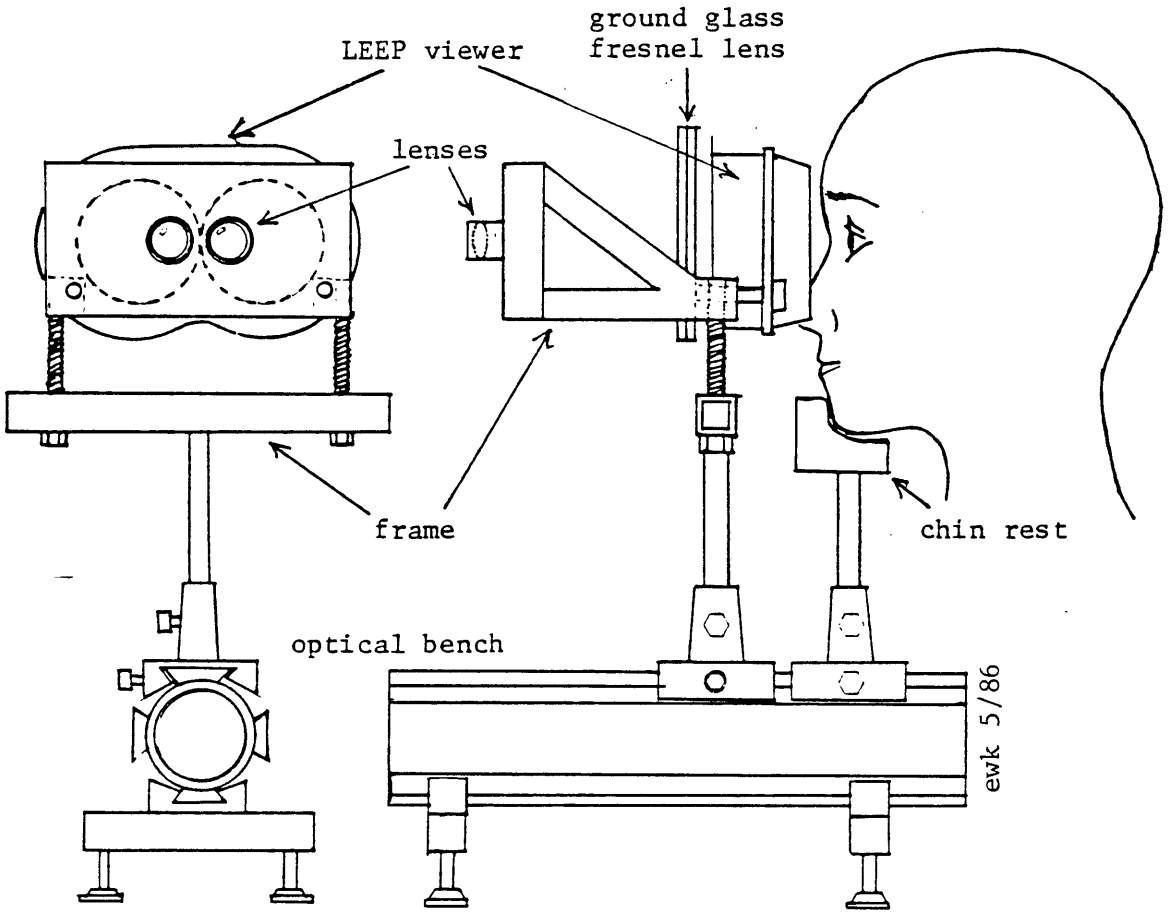

Figure 3.9: Front and side views of the Expanded Field Display.

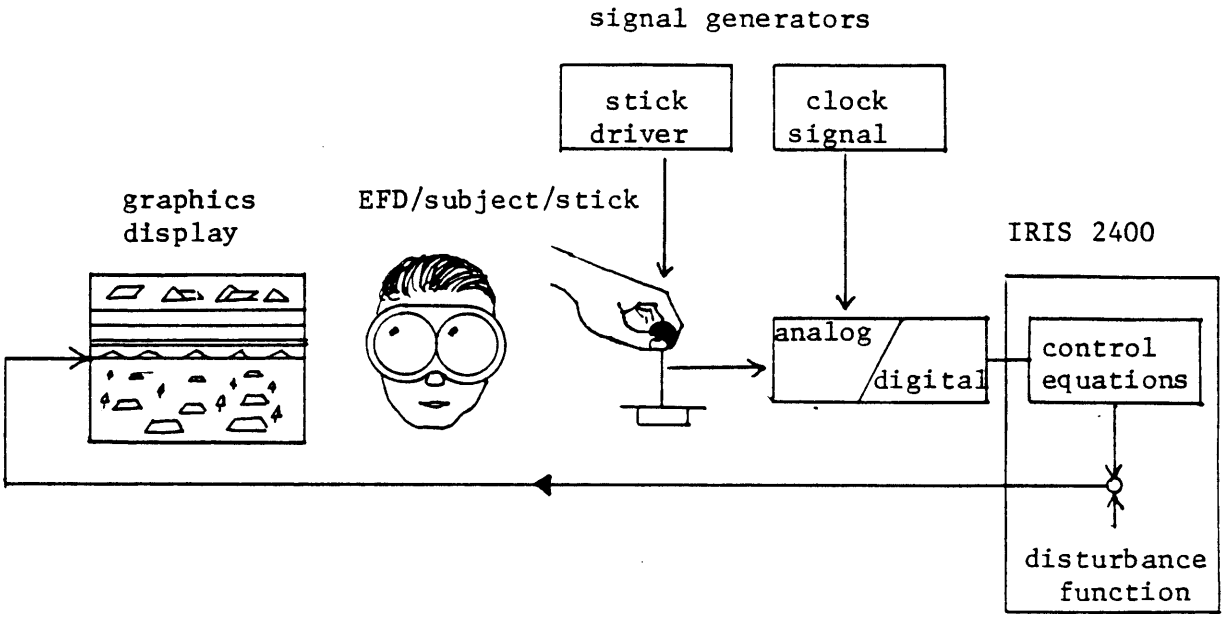

Figure 3.10: Schematic diagram of equipment layout.

CHAPTER 4: EXPERIMENTAL PROCEDURE FOR THE CRITICAL CONTROL EXPERIMENT

4.1 Design of the Critical Control Experiment

The Critical Control Experiment was conducted to show how field-of-view size affects a subject's reaction time and accuracy in controlling visual roll motion. This experiment was designed so that any change in these parameters would be clearly caused by changes in the field-of-view of the moving visual scene. Chapter 4.1.1 presents the test-matrix which determined the individual cases of this experiment and chapter 4.1.2 shows how these cases were ordered.

4.1.1 Test Matrix

Five field-of-view sizes were tested for the Critical Control Experiment: 10°, 20°, 40°, 80° and 120°. The subject could not see any light outside the boundary set by the field-of-view. These five sizes were tested under both moving field and stationary field conditions. The stationary field condition was designed as a control experiment against which the affect of field-of-view could be compared. One hypothesis of this experiment is that the size of the subject's field-of-view affects the subject's performance, due to the added roll motion information in the periphery. Therefore, it must be shown that it is not the mere presence of the visual field that affects performance. The stationary field tests were designed to show any effect due changes in size of a stationary visual field. In these tests the roll motion was shown with a small, center display, similar to the roll indicator in an

aircraft. This display had a field-of-view size of 10°. The out-the-window visual scene that surrounded the roll indicator display remained fixed at 0° roll angle.

Each field-of-view was tested with both the moving visual field and the stationary visual field making a total of ten separate cases for this task. A test trial was a set of each of the ten cases. Every subject ran six trials which produced six sets of data for each case. The subjects ran three trials per day over two consecutive days. A trial lasted approximately twenty to twenty-five minutes and on each day there was a five minute break between the first and second trials and between the second and third trials. This method of testing should have avoided any long term changes in a subject's effective time delay [Jex, et al, 1966].

4.1.2 Ordering of Cases

Care was be taken when gathering data to avoid artificial trends which could be caused by the order of tests within a trial. The effect of one case on the case that immediately follows, and the affect of a particular position within a trial, such as the first position, were the main areas of concern.

After reviewing the variety of tests, a set of rules was created for the ordering of cases within a trial: 1) Each separate field-of-view size had to be presented as the first case in at least one of the six trials. 2) The stationary field condition for the 10° field-of-view was visually unique since it was the only case that showed no out-the-window scene. This extreme case may have had an influence on the

subject which would carry over to the case that followed it. Therefore, each field-of-view size immediately followed this baseline case in at least one of the six trials. 3) For each field-of-view size there were two cases which were considered counterparts, the moving field case and the stationary field case. In a trial, each of the five sets of counterparts had to be separated by at least two but no more than six other cases. By separating the field-of-view counterparts the subject did not become accustomed to a particular field-of-view size. 4) Within the conditions set by the first three rules, the order of cases within a trial was chosen at random.

4.2 Description of Subjects

The basic experiment addressed by this report modeled roll control of an aircraft. However, the dynamics have been modified and the visual field motion is limited to one degree of freedom. Because of these changes, and the simplicity of the task, it was felt that trained pilots were not needed as subjects, in order to obtain relevant data concerning the effect of field-of-view size on manual control. Five subjects, referred to in this report as subjects A through E, were selected for the critical control experiments. This number of subjects should give an indication of how a larger population would react to this experiment; more subjects were not tested primarily due to time constraints and the fact that the experiment was previously untested and may undergo a considerable amount of development before the effort is expended to test a larger population sample.

All subjects were males, in good health, with vision corrected to at least 20/40 at a far distances. Each subject was able to adjust the position of the viewer so that the image was in sharp focus. No subjects were aware of having any motor coordination anomalies. Subject C used his left hand for writing but his right hand for throwing and other manual tasks and therefore felt comfortable using the right-handed control stick. Other than subject E who had fifty hours of VFR flight time in light aircraft and subject B who had 10 hours in advanced flight simulators, no other subjects had flight training. Further subject information is given in appendix 4.1.

In order for the results of these experiments to be consistent and relevant to manual control tasks, the subject's had to be well trained before collecting the final data. A well trained subject's data would not show any significant learning effects. Also, a trained and highly motivated subject performs close to an optimal level, devoting their attention and skill to performing the task as best as possible, within their inherent limits.

Before attempting the control task for the first time, each subject was given a set of written instructions (appendix 4.2) and an oral briefing. The written instructions stated the nature of the basic task: to keep the displayed roll angle as close to 0° as possible, while the instability increased; the control stick motion corresponds to controlling aircraft roll velocity, if the scene rotates clockwise the corrective stick force is to the right; the task measures the subject's effective time delay so the subject should react quickly and accurately. During the control task the subject was instructed to look only at the center of the display, so the direction of the subject's gaze would not

be a factor in the data analysis. The instructions also stated that the subject should hold the knob of the control stick with the right hand, between the pad of the thumb and the side of the forefinger. Finally, the subjects were told that during the tests they should not be under the influence of the influence of caffeine, alcohol, stimulants, depressants, narcotics or hallucinogens. A brief, confidential questionnaire was included at the end of the instructions, where the subjects noted their age, height, weight, profession, visual or coordination impairments, medication that may have affected the test results and previous flying experience. On the basis of this questionnaire, all subjects were felt to be qualified for the experiments.

The subjects were given an oral briefing where the instructions were discussed and the subject was able to ask any questions; all questions were answered without intentionally holding back any information. Familiarization runs were conducted where the subject viewed the computer graphics monitor directly, without using the Expanded Field Display. During these runs the experimenter confirmed that the subject was holding the control stick correctly and that the subject was looking at the center of the display. Several subjects adopted an initial control strategy of using step responses to control the roll motion. The subjects were asked to adopt a more continuous control response, which they soon agreed was a more accurate strategy.

After approximately ten trial tests when viewing the monitor directly, the subjects felt comfortable enough with the task that they could start practicing with the Expanded Field Display. The initial training requirements were that a subject would run one practice trial a day, which contained all ten cases, for three days. The data from the

last two trials is checked for learning effects and if none are found, the subject is cleared for the true experimental tests. Subjects C and D received the minimum amount of required training, while subjects A, B and E had on the order of ten practice trials each, since they were involved in the development of the experiment.

4.3 Conducting the Critical Control Experiment

A subject was scheduled to start a set of experimental trials at the same time each day. The experimenter prepared for the subject by giving a command that starts the task program and displays the out-the window scene in a fixed position. The subject sat down and adjusted the chair, the focus of the LEEP viewer, the position of the chin rest and then told the experimenter that they were ready to start testing. The experimenter placed the desired masks in the Expanded Field Display to set the field-of-view size; the subject made fine position adjustments of the masks by checking that the boundary of the right and left mask matched the same locations on the out-the-window display. The subject then gave a final signal that he was ready to start the test. The experimenter started the count-down sequence and the test started.

During a test the experimenter usually made no comment to the subject. The one occasional exception was if the test had to be stopped and then restarted before the critical condition was reached. The main reasons for a test being stopped were a hard-disk access by the computer which causes a noticeable slowing of the programs update rate, a premature loss of control by the subject due to an itchy nose or a loss of concentration, or a mistake of the experimenter setting up the wrong

case. The last two situations occurred less than five times throughout the whole set of experiments.

When a test was completed the experimenter exited from the program which automatically stored the collected data in a specified file. The starting command was given again, a new set of field-of-view masks was placed in the Expanded Field Display, the subject made the necessary adjustments, and the new case was started. Each case lasted between twenty-five and sixty seconds and the set of three trials per day lasted approximately one hour and fifteen minutes.

CHAPTER 5: DATA ANALYSIS OF THE CRITICAL CONTROL EXPERIMENT

Data analysis of the Critical Control Experiment was based on four sets of measurements: two root mean square (RMS) roll error measurements and two time constant measurements. These values were recorded for each individual test and then were analyzed to determine how they were affected by changes in the field-of-view size.

5.1 Time Constant Analysis

In the Critical Control Experiment the time constant of the control element decreased continually, making the subject's task increasingly difficult. The value of the time constant at a given subject performance level provided information on how the subject was affected by the display's field-of-view. The time constant of the control element was measured at two specific levels of subject performance. The first time constant measurement is called the 'transition time constant' since its value was measured when the instability level, lambda, had its rate of increase changed from a high value to a low value. The second time constant is called the 'critical time constant' since its value was measured at the point when the subject lost control of the displayed roll motion.

The transition time constant is defined as the value of the control elements time constant when the lambda rate of increase was switched to its lower value. The lambda increase rate was changed when the subject's average roll error, over 0.667 seconds, first exceeds 13°. However, the lambda increase rate cannot be changed until lambda reaches

a minimum value of 3.2. Therefore, the transition time constant had a maximum value of 1/3.2 or 0.3125 seconds.

As stated in Section 2.1 the critical time constant was the value of the control element's time constant when the subject lost control of the displayed roll motion. This time constant was shown to be closely related to the subject's effective time delay.

5.2 RMS Analysis

Two root mean square (RMS) roll error values were measured for each test. These two independent measurements came from two separate stages of a Critical Control Experiment test. Both RMS roll error values were based on roll error measurements which were recorded at 15 Hz throughout the test.

Stage-one RMS roll error was obtained from roll error measurements from the beginning of the test, when lambda = 1.5, to the point where lambda reached a value of 3.2. This was a period of 15.1 seconds consisting of 226 roll error measurements. Since the control element was time varying due to the increasing value of lambda, the RMS value obtained was not valid for a time-invariant control system. However, every single test of this experiment followed the same time course for this period of 15.1 seconds; the lambda rate of increase could not switch to its lower rate until lambda reached 3.2 so the instability increased at the same rate for all tests. Therefore, stage-one RMS values can be compared to other stage-one RMS values in order to find any RMS variation caused by changes in field-of-view.

Roll error measurements from the time when lambda = 3.2 to till the end of the test were used to calculate stage-two RMS error values. During this period of time the system dynamics were time dependent and, additionally, the time courses followed by the tests were variable. This was due to the variation of the final lambda value, the variation of the total time of stage-two and the variation of the time at which the lambda rate of increase was switched to its low value.

Several techniques were used to partially normalize the stage-two RMS error. The first technique gave a higher weighting to the roll error measurements taken during the period when lambda increased rapidly. The weighting was equal to the ratio of $\Delta\lambda_1/\Delta\lambda_2$. The rational for this method was based on the assumption that if lambda increased at a slow rate during all of stage-two, the period during which lambda actually increased rapidly would produce more roll error measures which would be approximately the same the roll error values that were actually collected.

The second technique for normalizing the RMS value was used when calculating the mean and standard deviation of the six individual RMS values of each experimental case. Each individual RMS value was weighted by the actual number of roll error measurements from which the RMS value was calculated. Therefore, RMS values from tests that lasted a longer period of time, would affect the mean and standard deviation more than RMS values from tests which lasted a shorter period of time.

No steps were taken to normalize the RMS values for the variation in the final lambda values. The relation between RMS roll error and lambda was not developed in the current research, and a simple linear approximation of the relation does not appear to be a good choice based

on the initial data analysis. Therefore, the RMS values for stage-two do not account for the different critical lambda values of each test.

5.3 Least-Squares Data Analysis

The least-squares method was used to estimate a second order equation that best related the stage-one RMS values to their corresponding field-of-view sizes. Field-of-view size was the independent variable and RMS roll error was the dependent variable. The form of the equation was chosen to match a hypothesized relationship between RMS roll error and field-of-view size. The resulting equations, each described by three coefficients, were evaluated as to how well they matched the hypothesis based on the accuracy of their prediction.

The analysis of how well the predicted equation matched the data was evaluated using the chi-square test. The chi-square test produced a chi-square value based on the RMS roll error predicted by the equation, and the mean and standard deviation of the actual RMS roll error. The chi-square value gave a confidence percentile as to how accurately the predicted equation matched the experimentally determined values.

In addition to predicting the coefficients of the equation, the least-squares analysis produced the standard deviations of the coefficients based on their ability to fit the actual data. These standard deviations were needed since the predicted equation was only an estimate of a 'true' underlying function; the standard deviations give the likely range of the coefficients for the true function.

CHAPTER 6: RESULTS OF THE CRITICAL CONTROL EXPERIMENT

The subject's task in the Critical Control Experiment was to keep the roll angle of a display as close to zero degrees as possible. The results of the experiment show how the subject's field-of-view affected his reaction time and his tracking accuracy. The transition and critical time constants indicate how quickly the subject was able to react to the displayed motion. The stage-one ($1.5 < \lambda < 3.2$) and stage-two ($\lambda > 3.2$) RMS roll errors measured the subject's control accuracy. Results are presented for both the moving field cases, in which the whole visual field rolled according to the control equations, and the stationary field cases, where the visual field remained fixed and the subject controlled only the motion of a small center display.

Section 6.1 presents the transition time constant, Section 6.2 presents the critical time constant, Section 6.3 presents the stage-one RMS roll errors, and Section 6.4 presents the stage-two RMS roll errors. Within each section the results from the moving field cases are presented first followed by the results from the stationary field cases.

Results for each of the five subjects, A to E, are presented separately in a series of figures, (a) to (e). Each figure contains a plot showing the values of the parameters as a function of field-of-view; a square marks the mean of the six individual tests and plus signs (+) mark the sample standard deviations of the mean. Directly below each plot is a table of student-t test values. These values indicate the level of significance between parameters due to changes in field-of-view size. Student-t values marked with a single asterisk (*) indicate a 95% confidence level that a mean for one field-of-view was higher than

a mean for another field-of-view. Student-t values marked with a double asterisk (**) indicate an 99% confidence level or greater.

The data analysis for the stage-one RMS roll error was taken one step further by predicting a function relating RMS roll error to the field-of-view size. This analysis was performed using the least squares method for fitting a curve to data. The results are presented in section 6.5.

6.1 Transition Time Constants

The transition time constant was not a measure of any specific subject parameter but it does indicate how quickly the subject reacts to the display error: the transition time constant was low if the subject reacted quickly. It also indicates the subject's ability to keep roll motion deviations relatively small. When the Critical Control Experiment was designed, the transition time constant was not planned to be part of the data analysis. Therefore, the transition time constant's maximum limit of 0.3125 seconds had already affected the data adversely. This limit affected the data in the more difficult tests such as narrow field-of-view and stationary field cases.

As figures 6.1 (a) to 6.1 (e) show for the motion field cases, all subjects had transition time constants that decreased as the field-of-view increased from 10° to 80°. Approximately half of the field-of-view intervals had a significant effect on the transition time constant. Four out of the five subjects show a trend for the transition time constant to increase when the field-of-view was increased from 80° to 120°. Subject B shows a highly significant increase in the transition

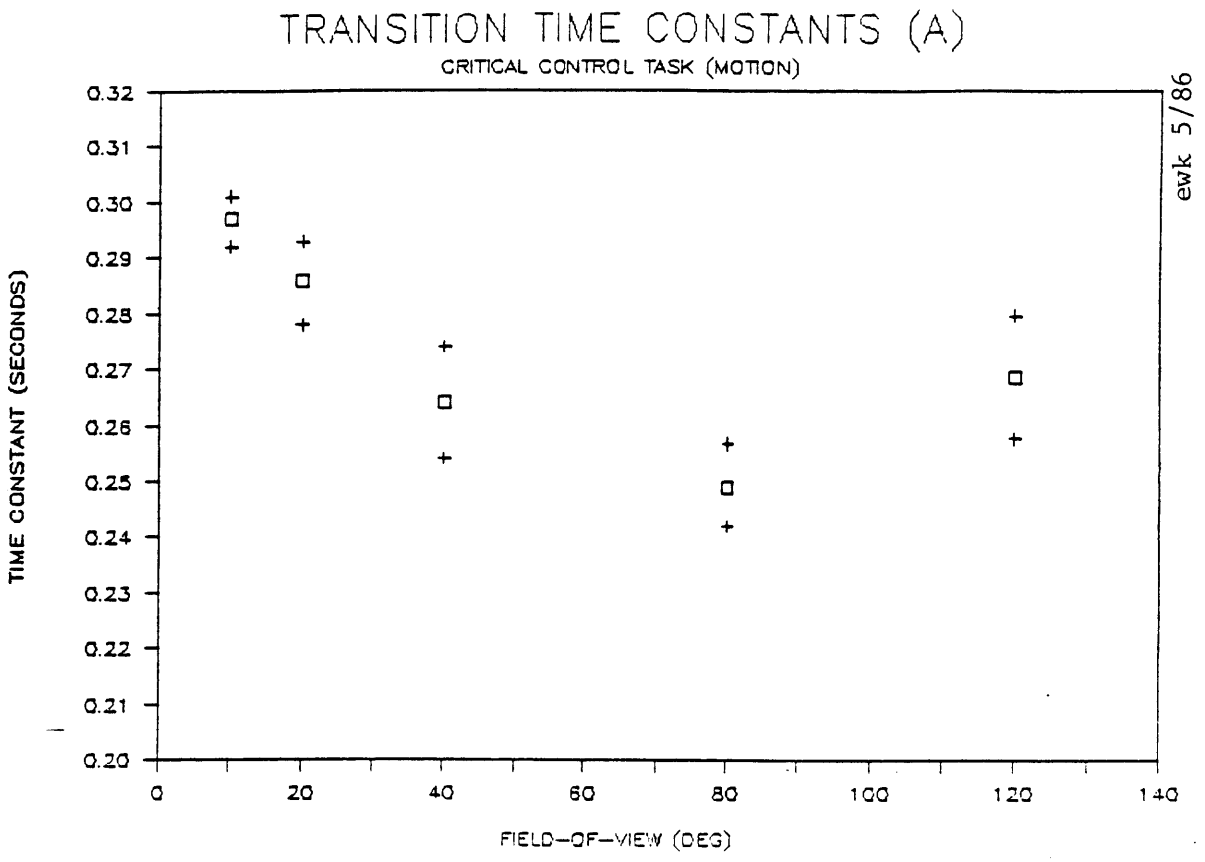

	10°	20°	40°	80°
20°	1.2273			
40°	3.0618 **	1.7605		
80°	5.5736 **	3.4628 **	1.2247	
120°	2.3525 *	1.2613	-0.3390	-1.5097

Figure 6.1 (a)

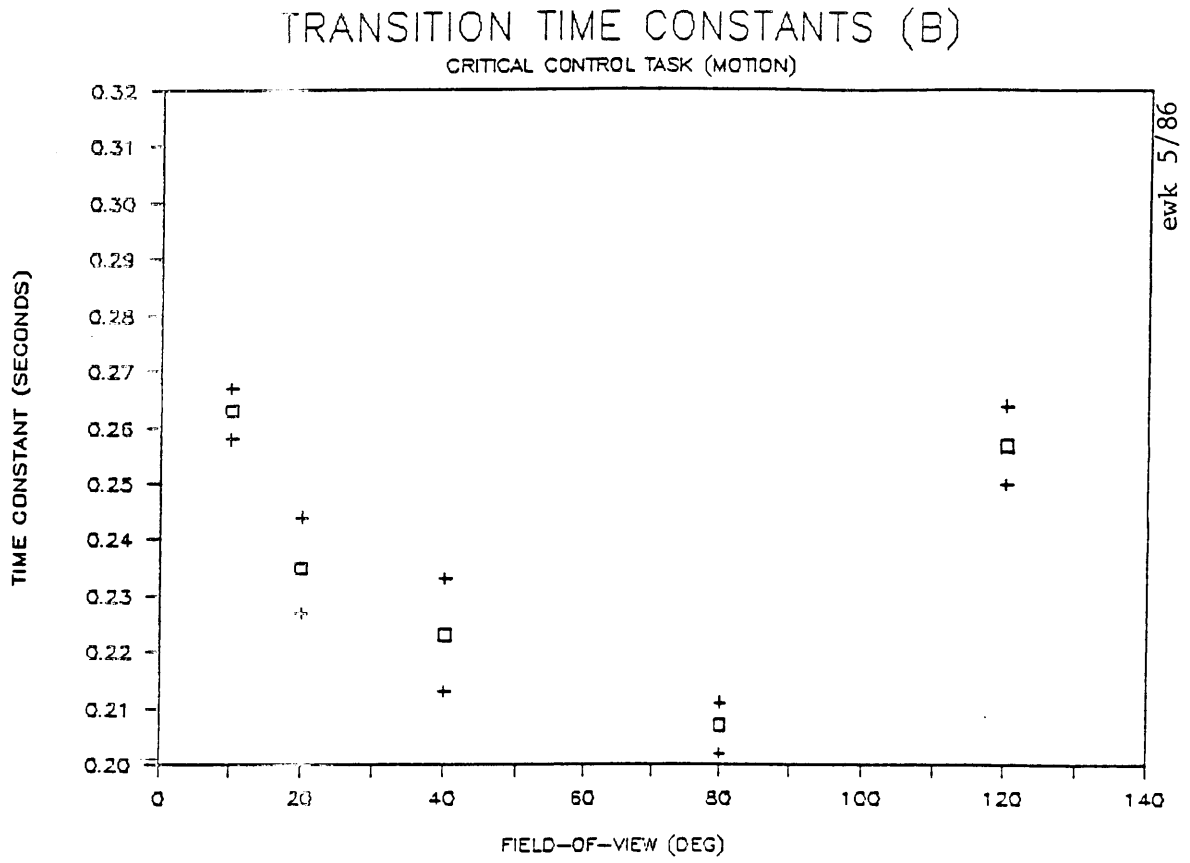

	10°	20°	40°	80°
20°	3.0048 **			
40°	3.5873 **	0.9181		
80°	8.8177 **	3.0048 **	1.4349	
120°	0.7258	-2.0530 *	-2.7547 *	-6.0486 **

Figure 6.1 (b)

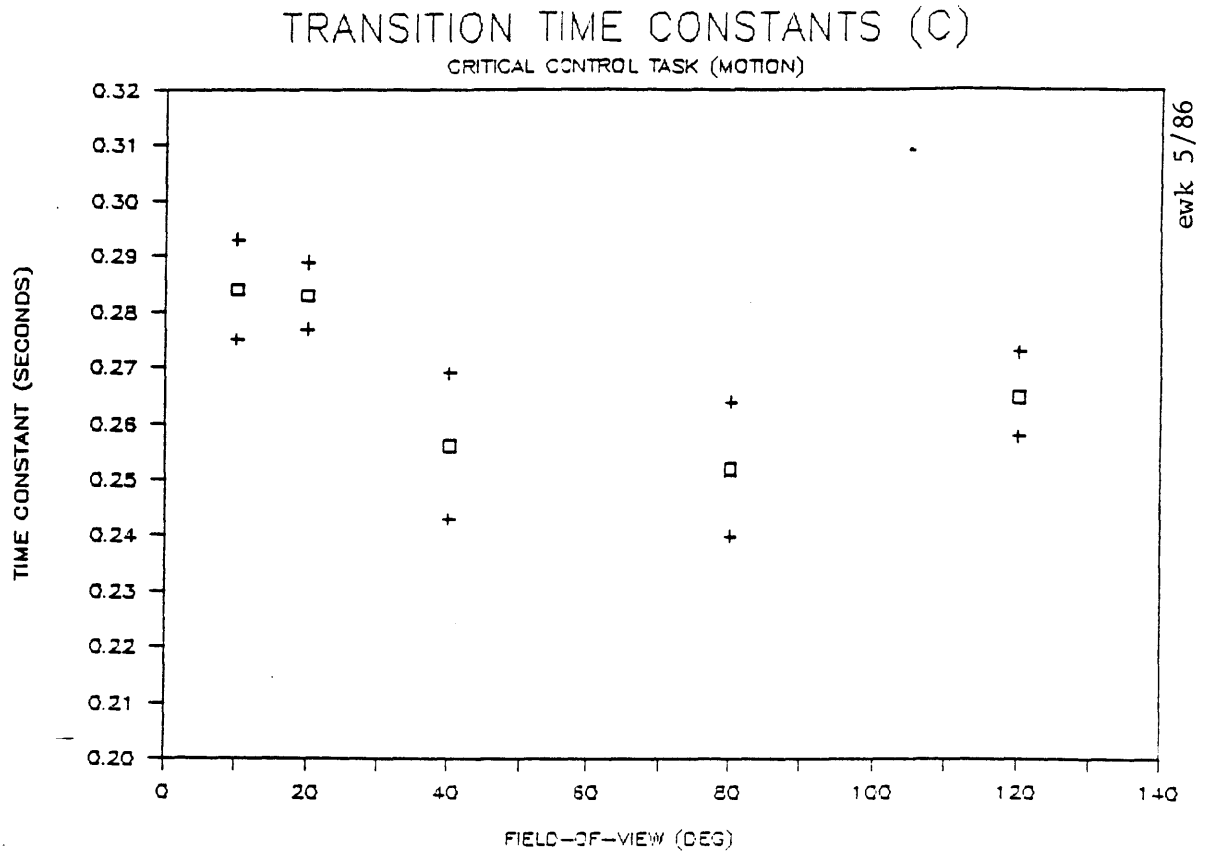

	10°	20°	40°	80°
20°	0.0892			
40°	1.7404	1.8714 *		
80°	2.1177 *	2.3257 *	0.2268	
120°	1.5935	1.8818 *	-0.6004	-0.9329

Figure 6.1 (c)

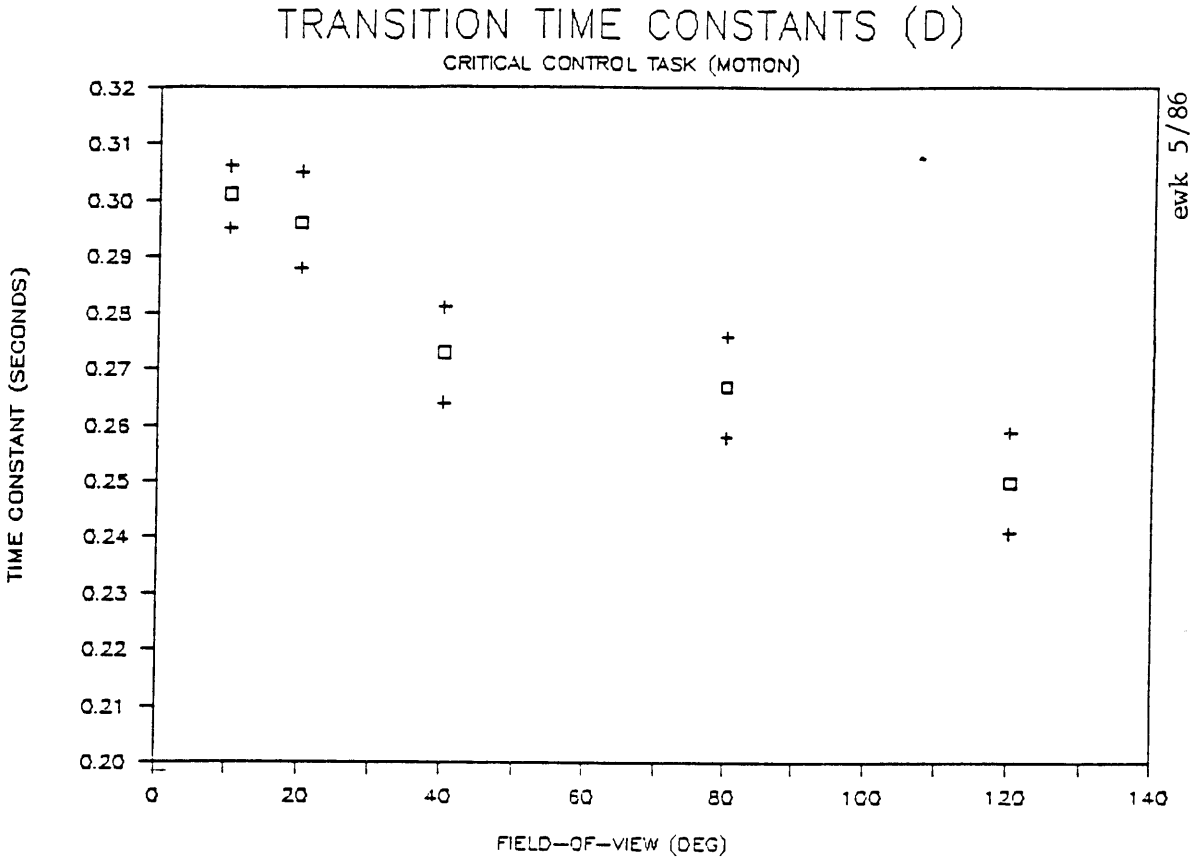

	10°	20°	40°	80°
20°	0.5016			
40°	2.7175 *	1.9427 *		
80°	3.1937 **	2.3892 *	0.4832	
120°	4.7906 **	3.7897 **	1.8524 *	1.3384

Figure 6.1 (d)

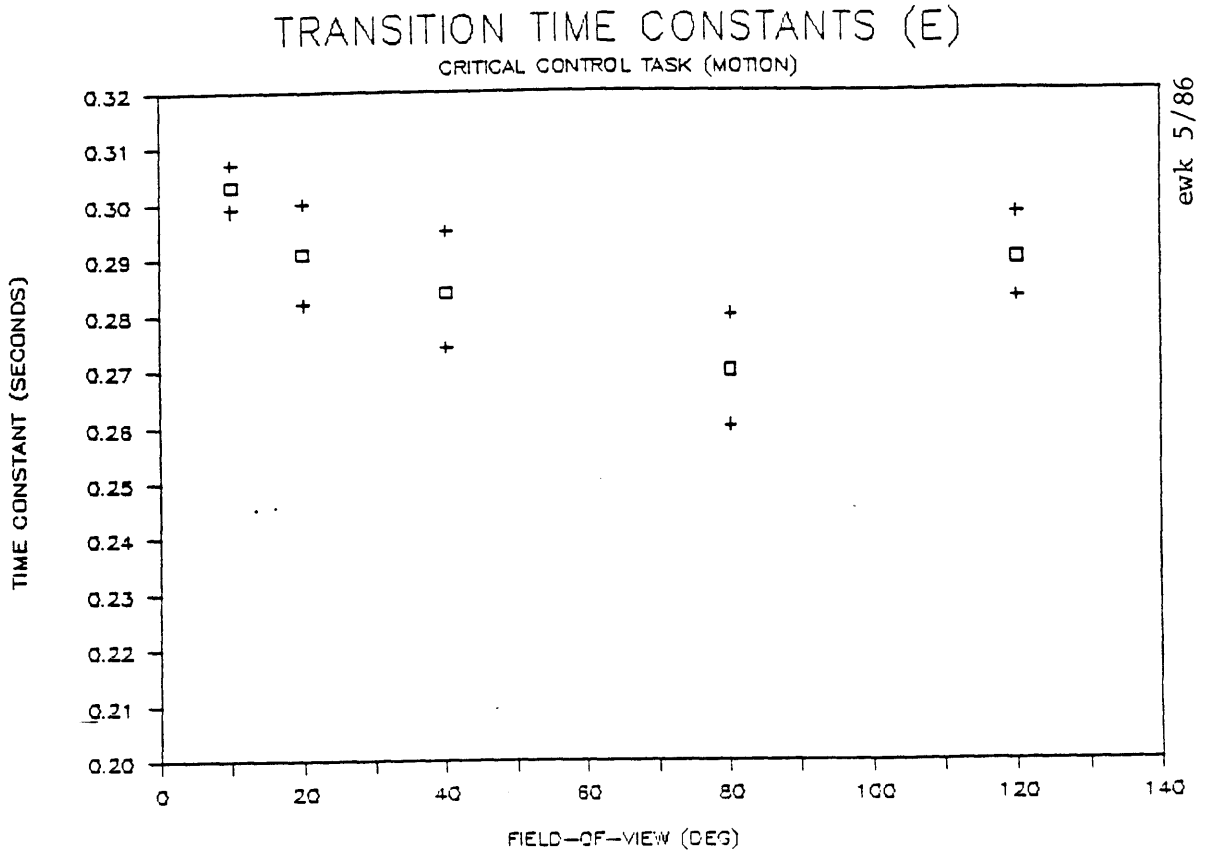

	10°	20°	40°	80°
20°	1.2865			
40°	1.7516	0.5251		
80°	3.1536 **	1.6130	0.9895	
120°	1.5823	0.8856	-0.4770	-1.633

Figure 6.1 (e)

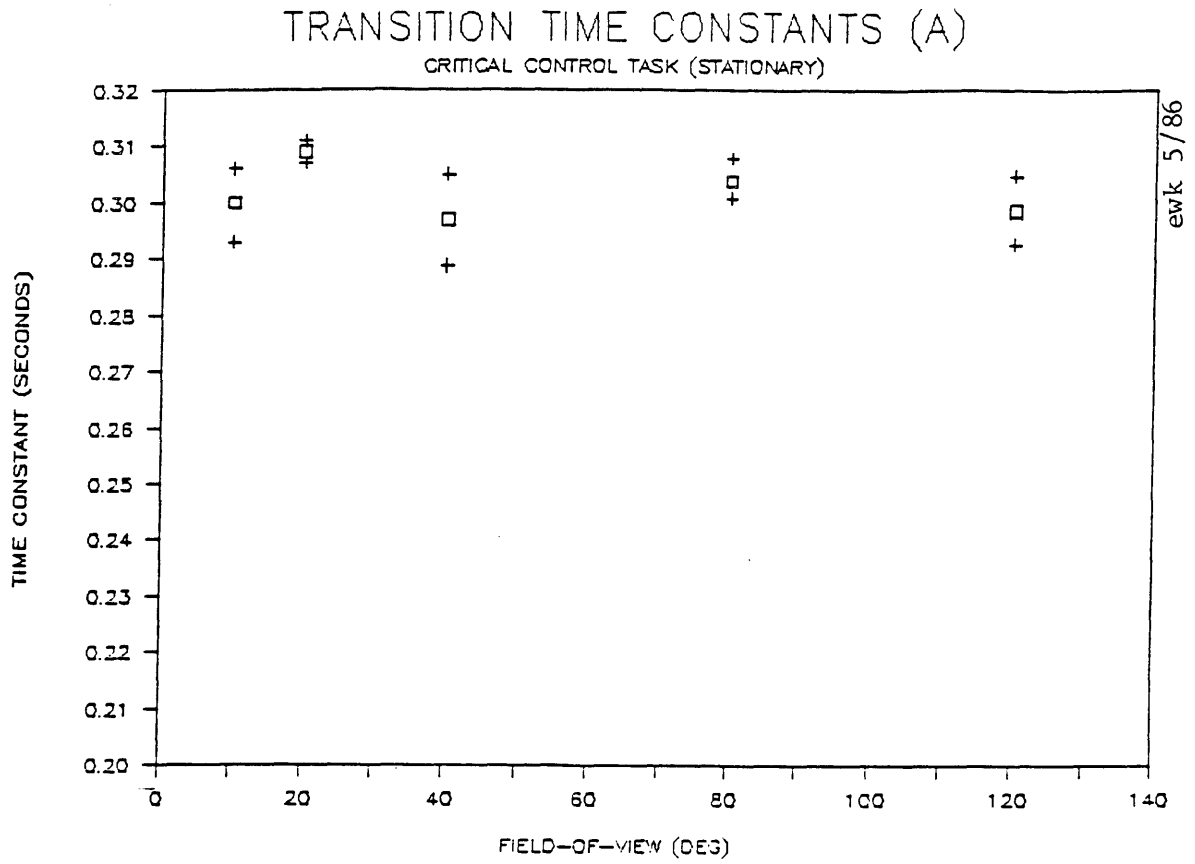

	10°	20°	40°	80°
20°	-1.3151			
40°	0.2869	1.4258		
80°	-0.5477	1.2982	-0.7960	
120°	0.1152	1.6477	-0.2006	0.7595

Figure 6.2 (a)

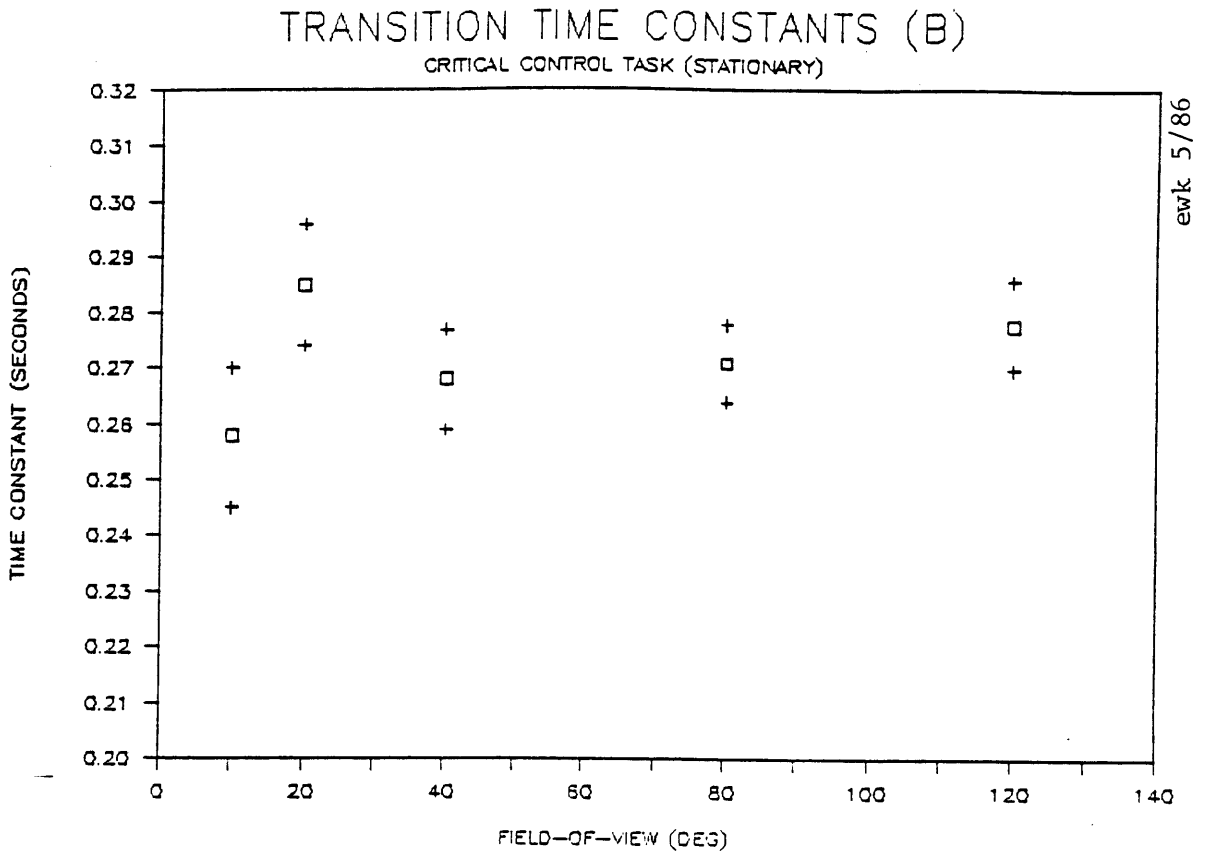

	10°	20°	40°	80°
20°	-1.6386			
40°	-0.6689	1.2174		
80°	-0.9365	1.0927	-0.2783	
120°	-1.3587	0.5103	-0.8446	-0.6694

Figure 6.2 (b)

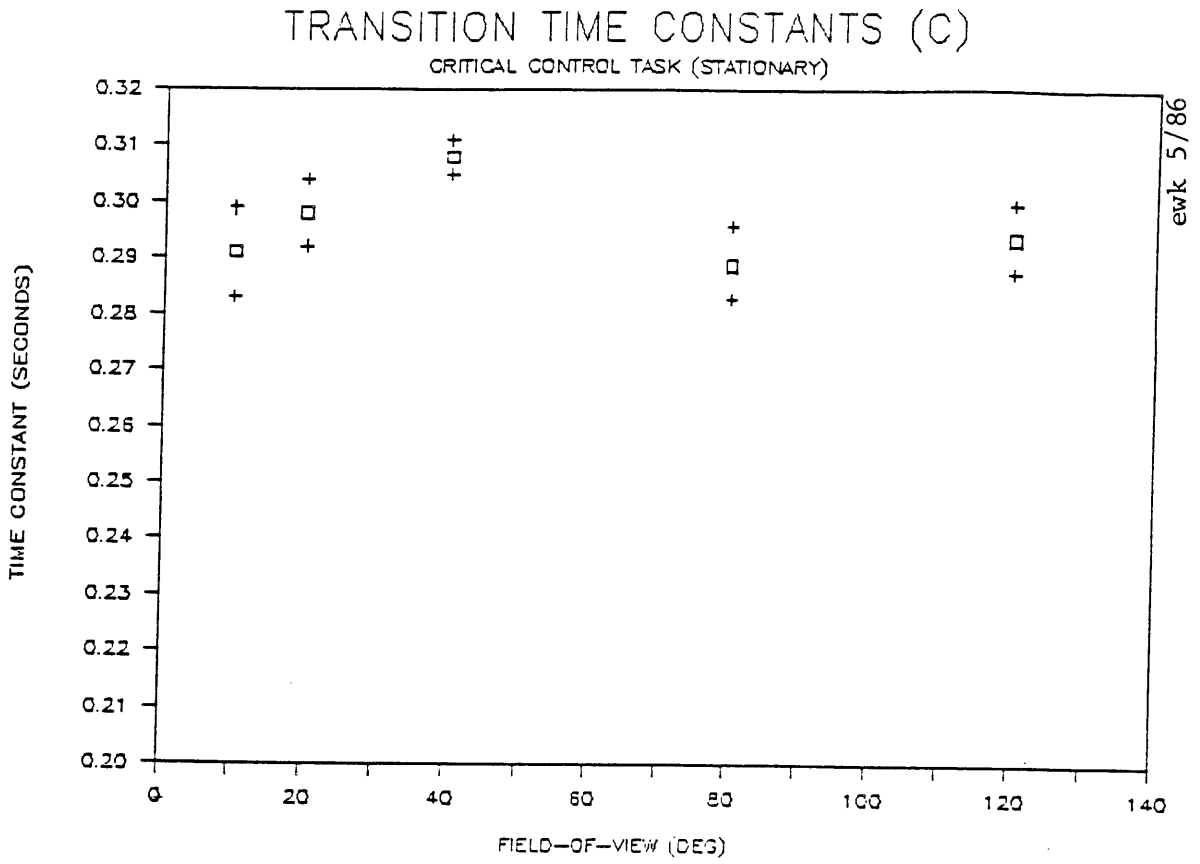

	10°	20°	40°	80°
20°	-0.7083			
40°	-2.0565 *	-1.4798		
80°	0.1921	0.9723	2.5315 *	
120°	-0.3113	0.4775	2.1909 *	-0.5561

Figure 6.2 (c)

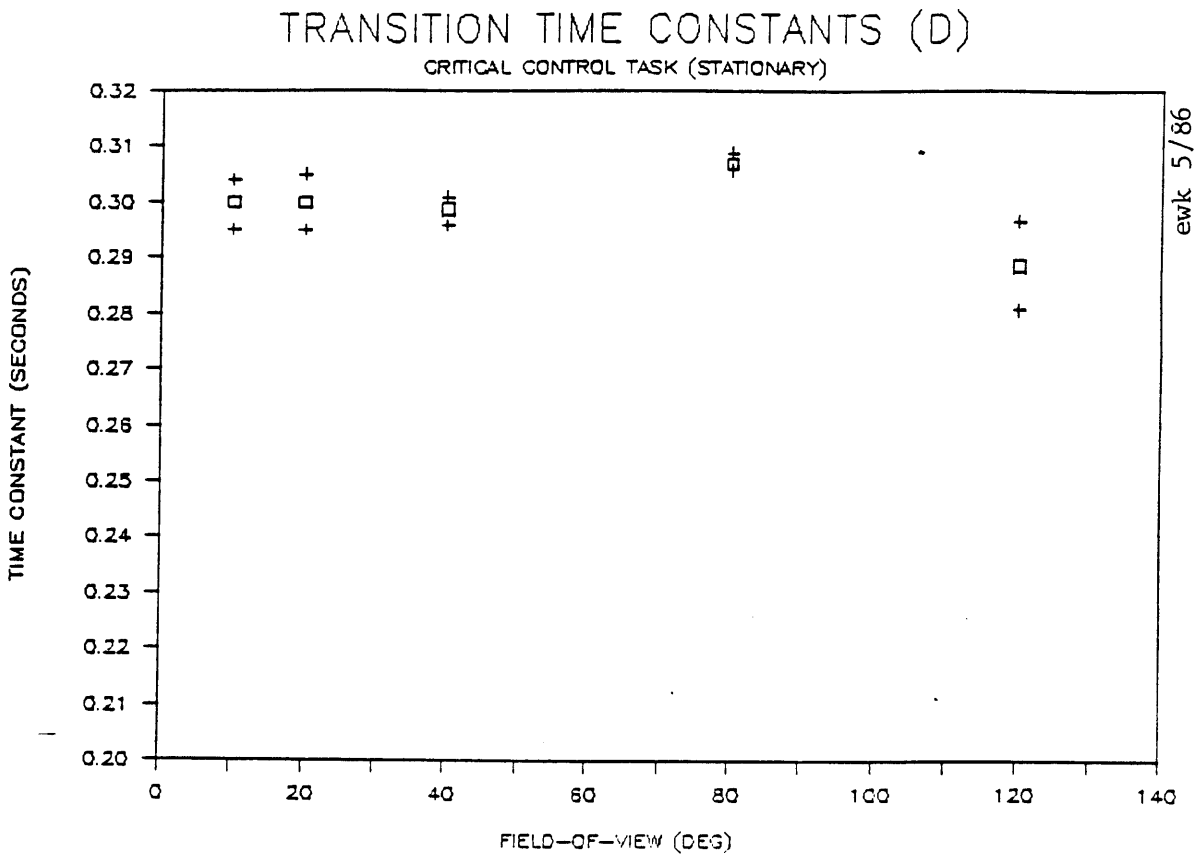

	10°	20°	40°	80°
20°	0.0000			
40°	0.1954	0.1710		
80°	-1.4649	-1.2606	-2.7175 *	
120°	1.1805	1.1296	1.1731	2.1617 *

Figure 6.2 (d)

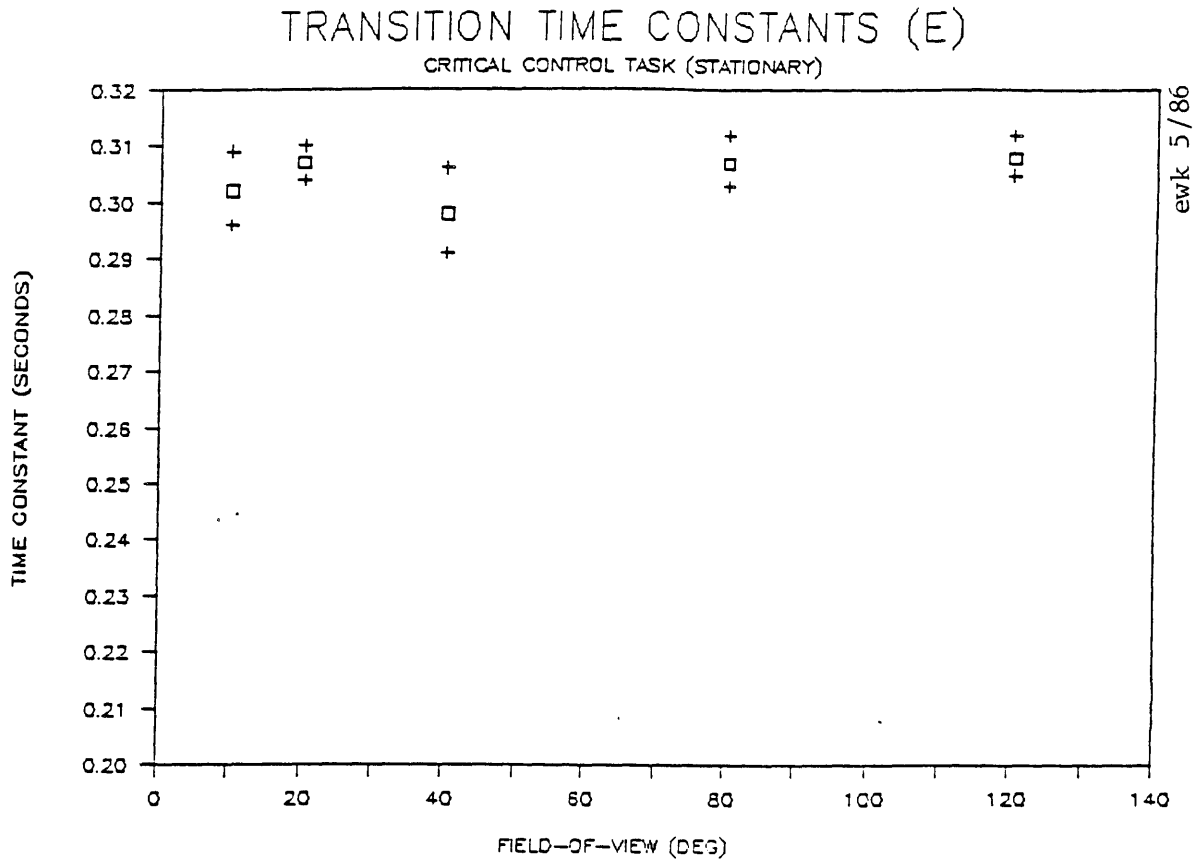

	10°	20°	40°	80°
20°	-0.6846			
40°	0.4197	1.1734		
80°	-0.6307	0.0000	-1.0887	
120°	-0.8215	-0.2165	-1.3037	-0.1800

Figure 6.2 (e)

time constant for this field-of-view interval. These figures suggest that there was an optimum field-of-view where the transition time was a minimum and, therefore, the subject's reaction speed was at a maximum. Error bars for subjects D and E indicate that the limit on the maximum transition time constant may have affected the data for the 10° and 20° field-of-view cases. This effect does not change the general trends of the transition time constant.

The transition time constants for the stationary field cases are presented in figures 6.2 (a) to 6.2 (e). Due to the effect of the maximum transition time constant, the data for the stationary field cases should be considered very inaccurate for subjects A, D and E. Subject B shows no significant effects due to field-of-view while subject C reacted slower when the field-of-view size was 40° as compared to 10°, 80° and 120°.

6.2 Critical Time Constants

The critical time constant was a close approximation of the subject's effective time delay; a low critical time constant means that the subject had a short reaction time. The results of moving field cases, shown in figures 6.3 (a) to 6.3 (b), are mixed and show no clear trends for the population of five subjects. Subjects A, B and E had significantly higher critical time constants for the 10° field-of-view case compared to the wider field-of-view sizes, in addition, subject A had a significantly higher critical time constant for a 20° field-of-view compared to the wider field-of-view sizes. Subject B may have had an optimum field-of-view for the critical time constant since the

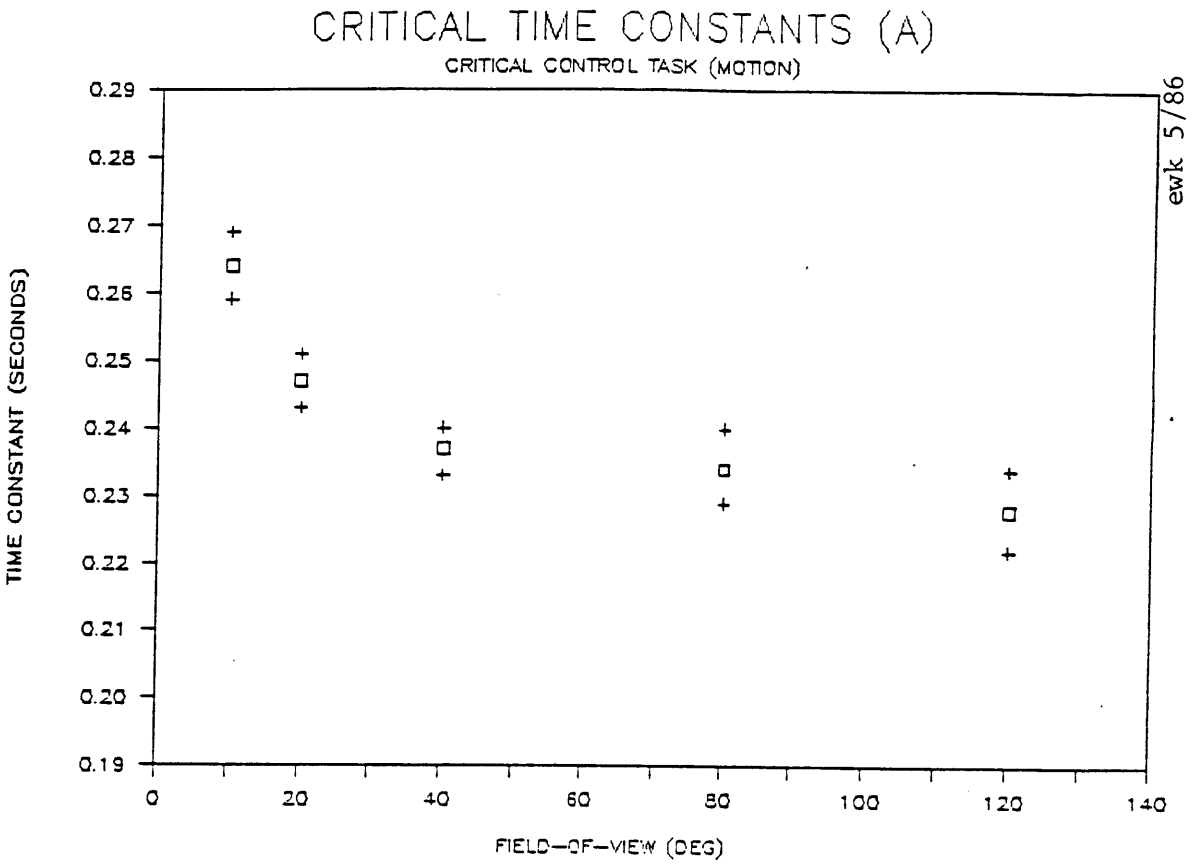

	10°	20°	40°	80°
20°	2.5389 *			
40°	4.1828 **	1.8207 *		
80°	3.9970 **	1.9415 *	0.4647	
120°	4.4425 **	2.5816 *	1.2603	0.7404

Figure 6.3 (a)

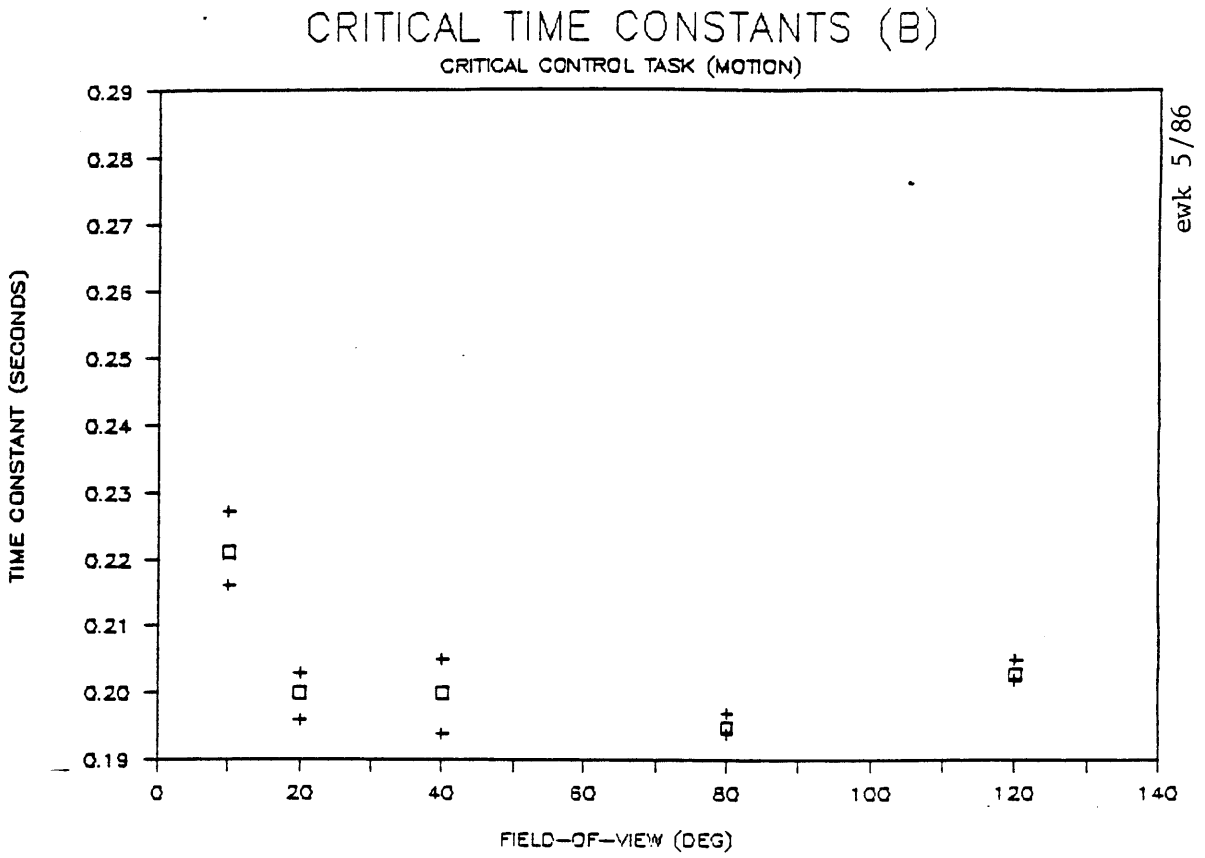

	10°	20°	40°	80°
20°	3.2533 **			
40°	2.6925 *	0.0000		
80°	4.5724 **	1.1896	0.8238	
120°	3.2416 **	-0.7461	-0.5046	-3.0604 **

Figure 6.3 (b)

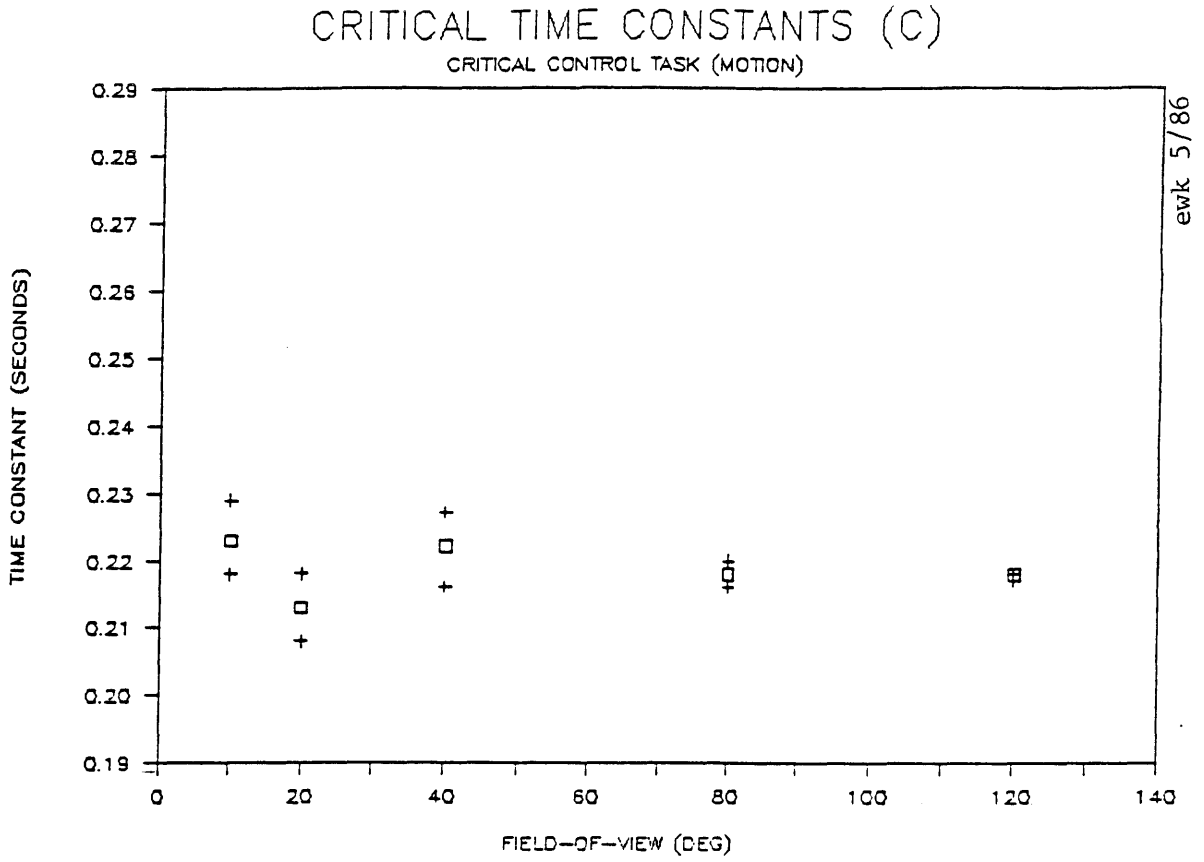

	10°	20°	40°	80°
20°	1.3845			
40°	0.1332	-1.2461		
80°	0.8793	-0.9421	0.7034	
120°	0.9311	-1.0067	0.7449	0.0000

Figure 6.3 (c)

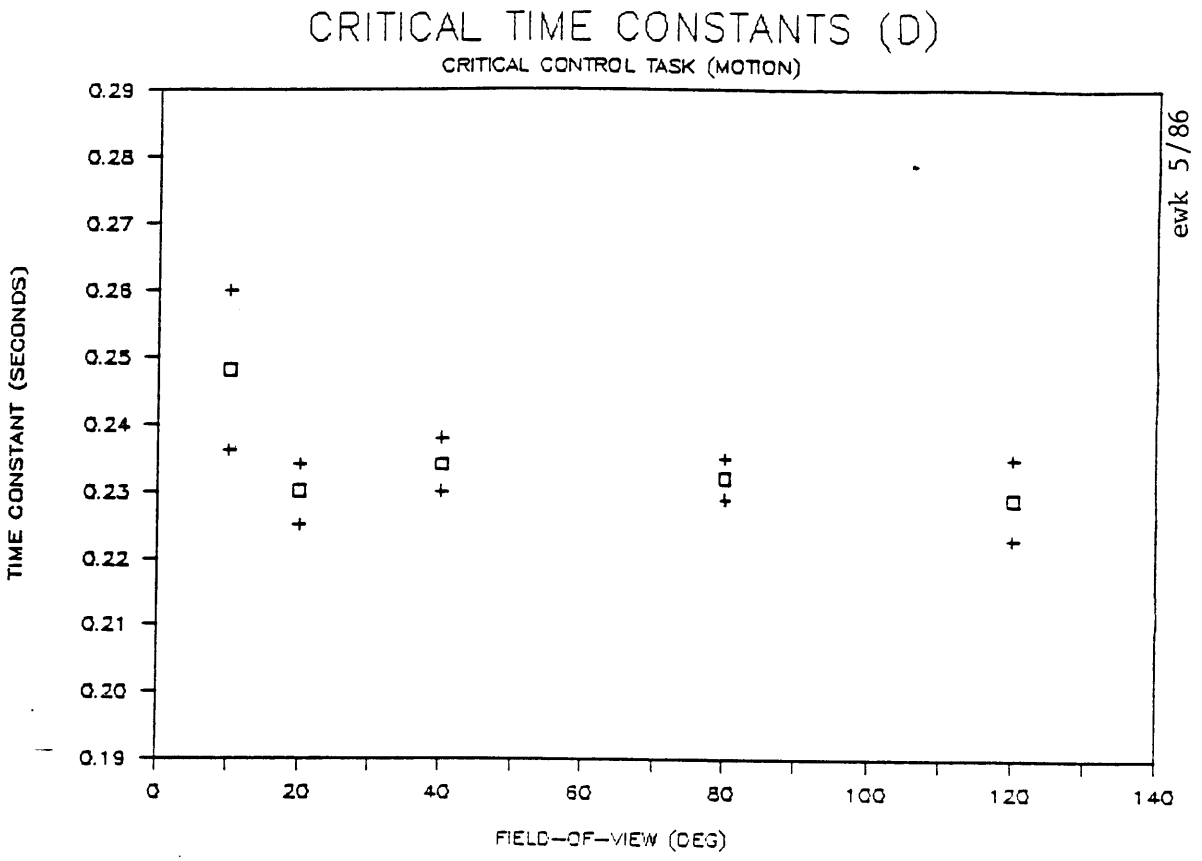

	10°	20°	40°	80°
20°	1.4049			
40°	1.1294	-0.6532		
80°	1.3137	-0.3526	0.4296	
120°	1.4254	0.1275	0.7001	0.4439

Figure 6.3 (d)

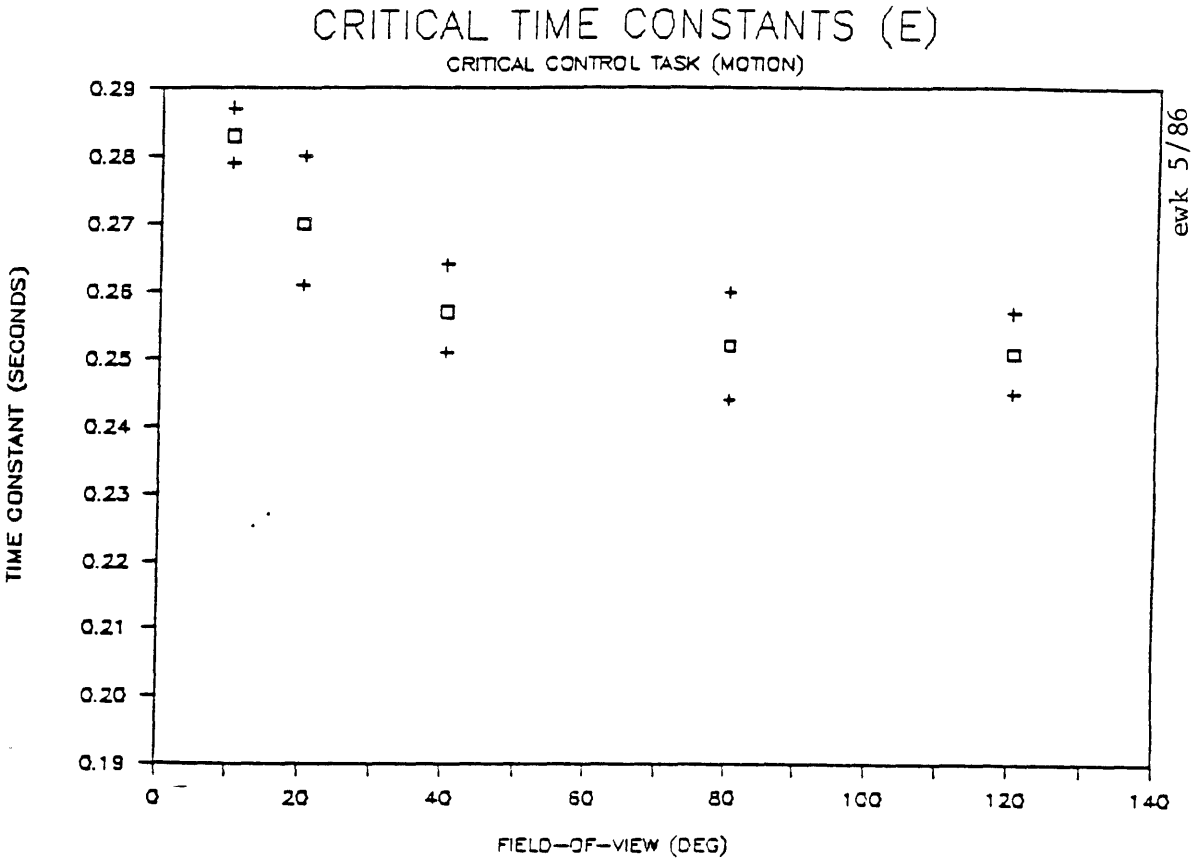

	10°	20°	40°	80°
20°	1.2893			
40°	3.3109 **	1.1134		
80°	3.6118 **	1.4779	0.4803	
120°	4.7096 **	1.7285	0.6673	0.1037

Figure 6.3 (e)

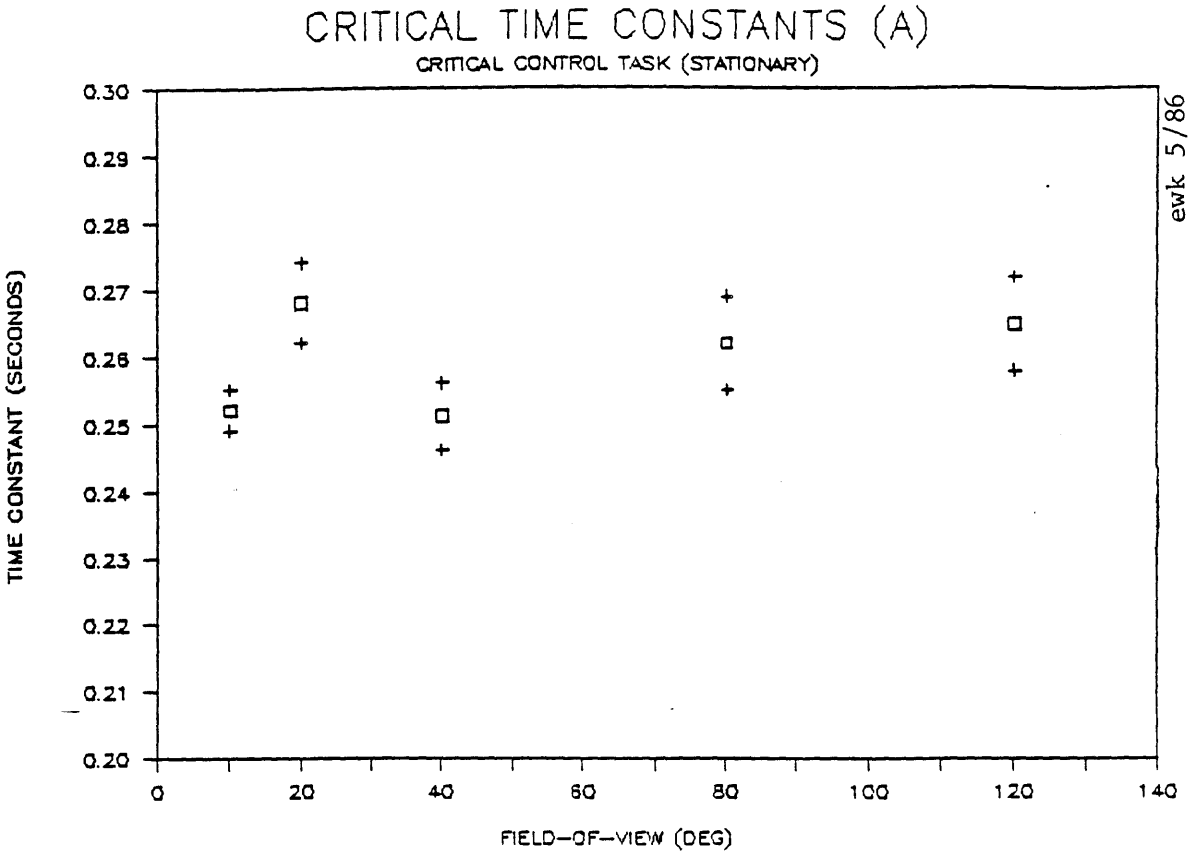

	10°	20°	40°	80°
20°	-2.3054 *			
40°	0.1604	2.0979 *		
80°	-1.3693	0.6701	-1.3070	
120°	-1.6949	0.3241	-1.6024	-0.3147

Figure 6.4 (a)

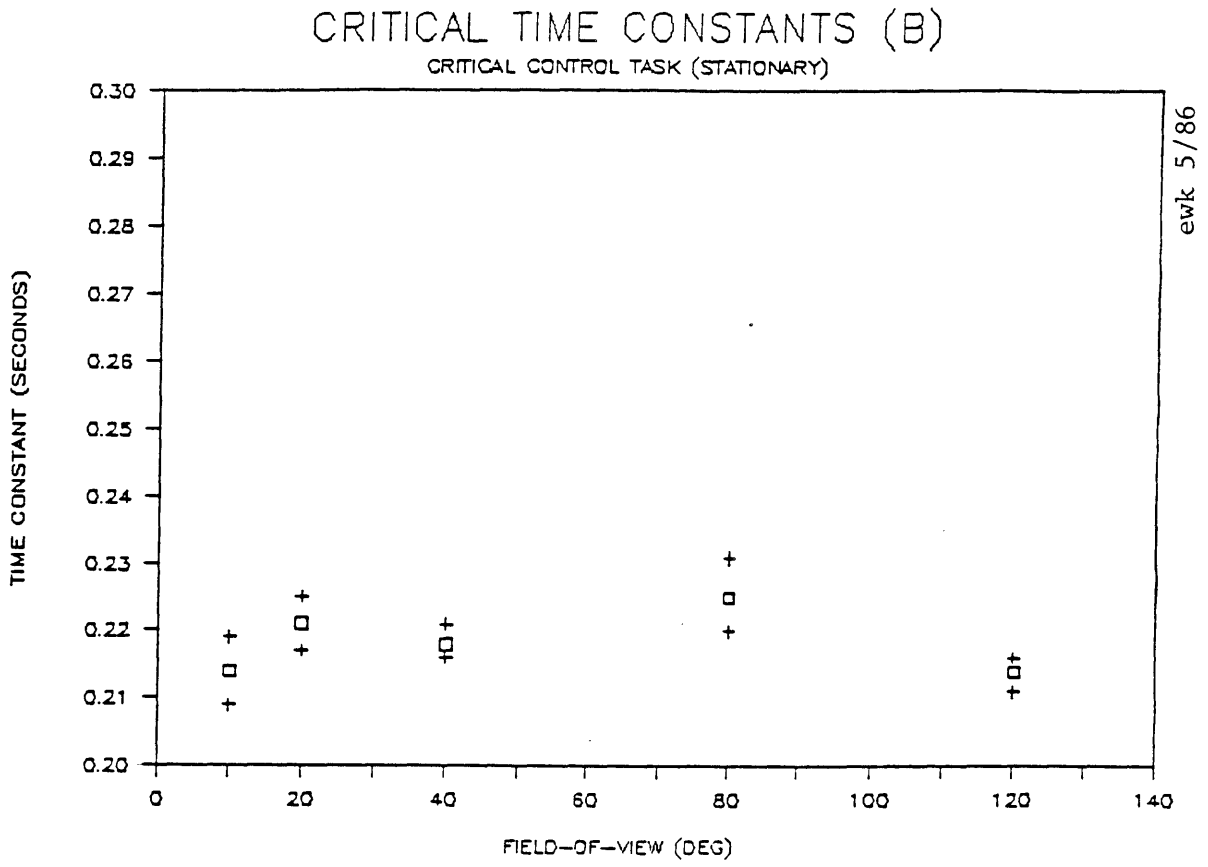

	10°	20°	40°	80°
20°	-1.0454			
40°	-0.6636	0.6020		
80°	-1.4656	-0.5973	-1.1613	
120°	0.0000	1.4703	1.0627	1.8819 *

Figure 6.4 (b)

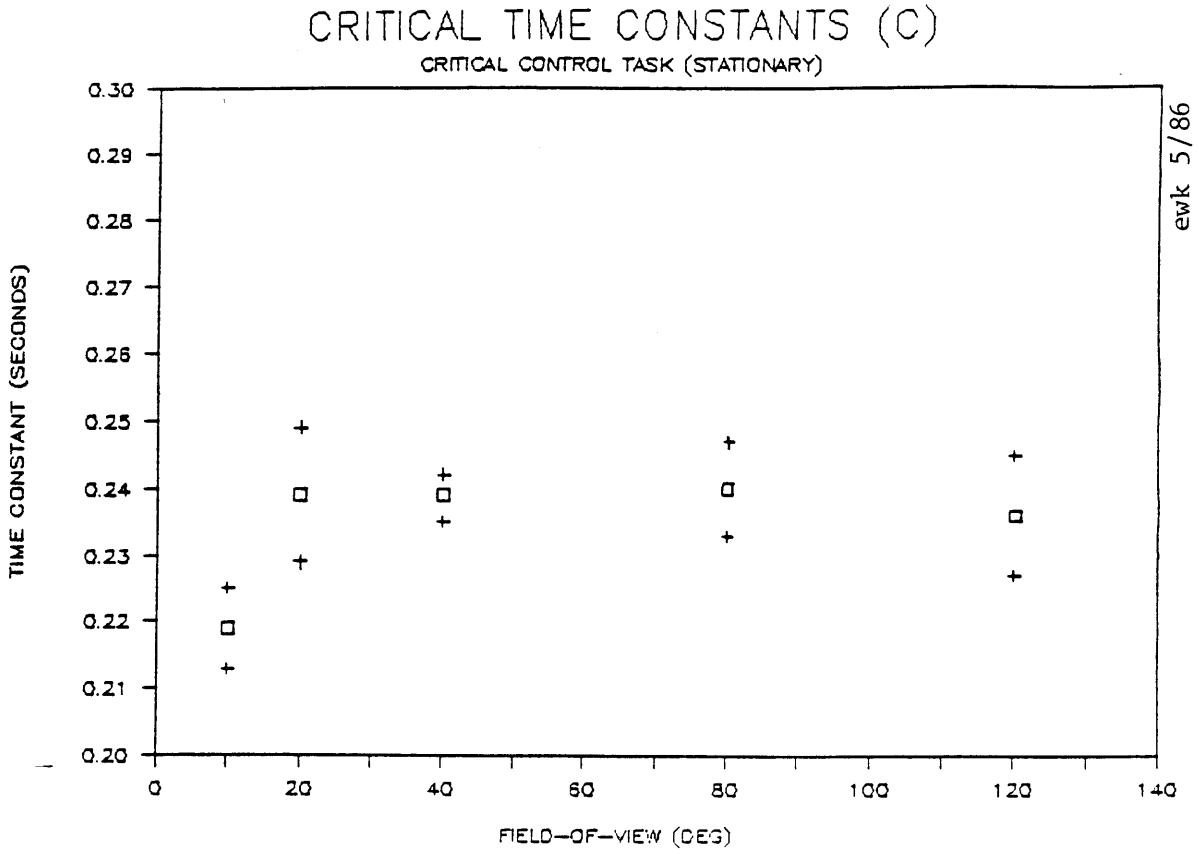

	10°	20°	40°	80°
20°	-1.7098			
40°	-2.9435 **	0.0000		
80°	-2.2558 *	-0.0795	-0.1217	
120°	-1.6499	0.2250	0.3216	0.3542

Figure 6.4 (c)

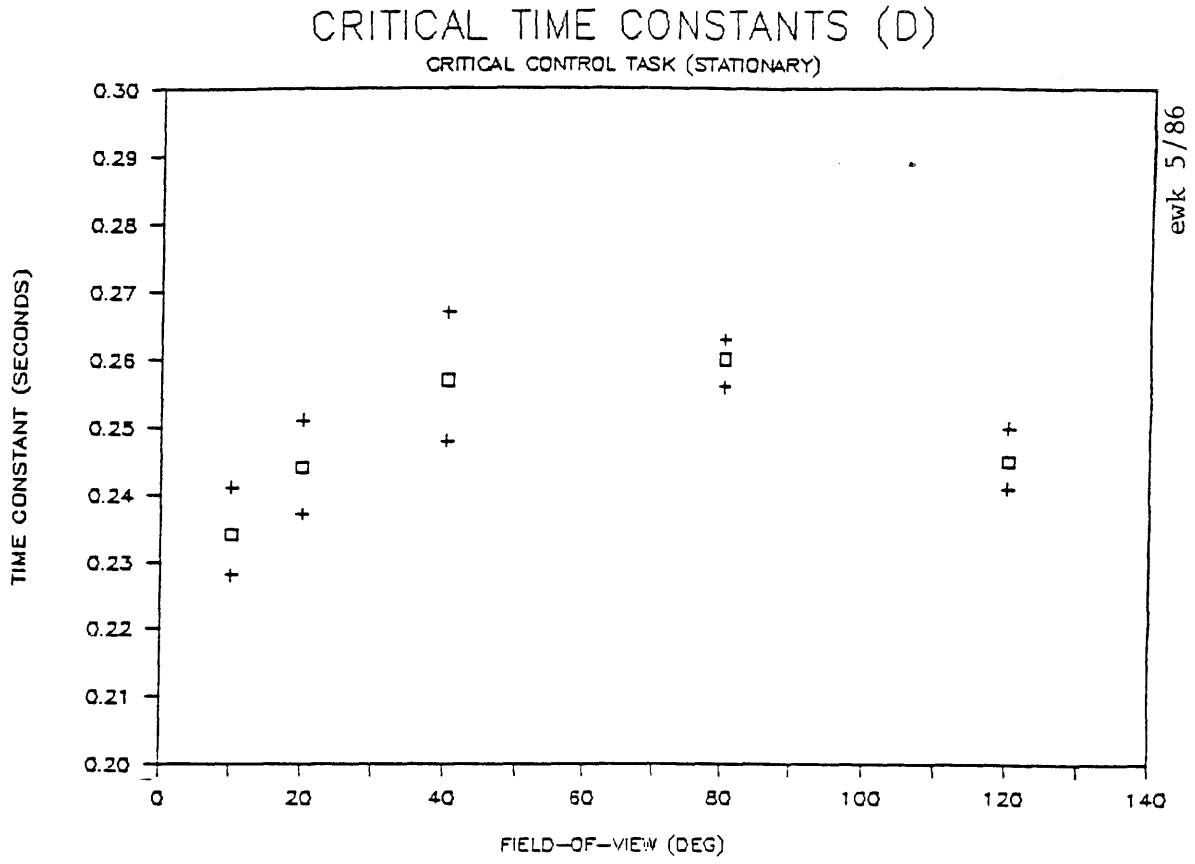

	10°	20°	40°	80°
20°	-1.0492			
40°	-2.0108 *	-1.1134		
80°	-3.4692 **	-2.0375 *	-0.2975	
120°	-1.3877	-0.1209	1.1529	2.5852 *

Figure 6.4 (d)

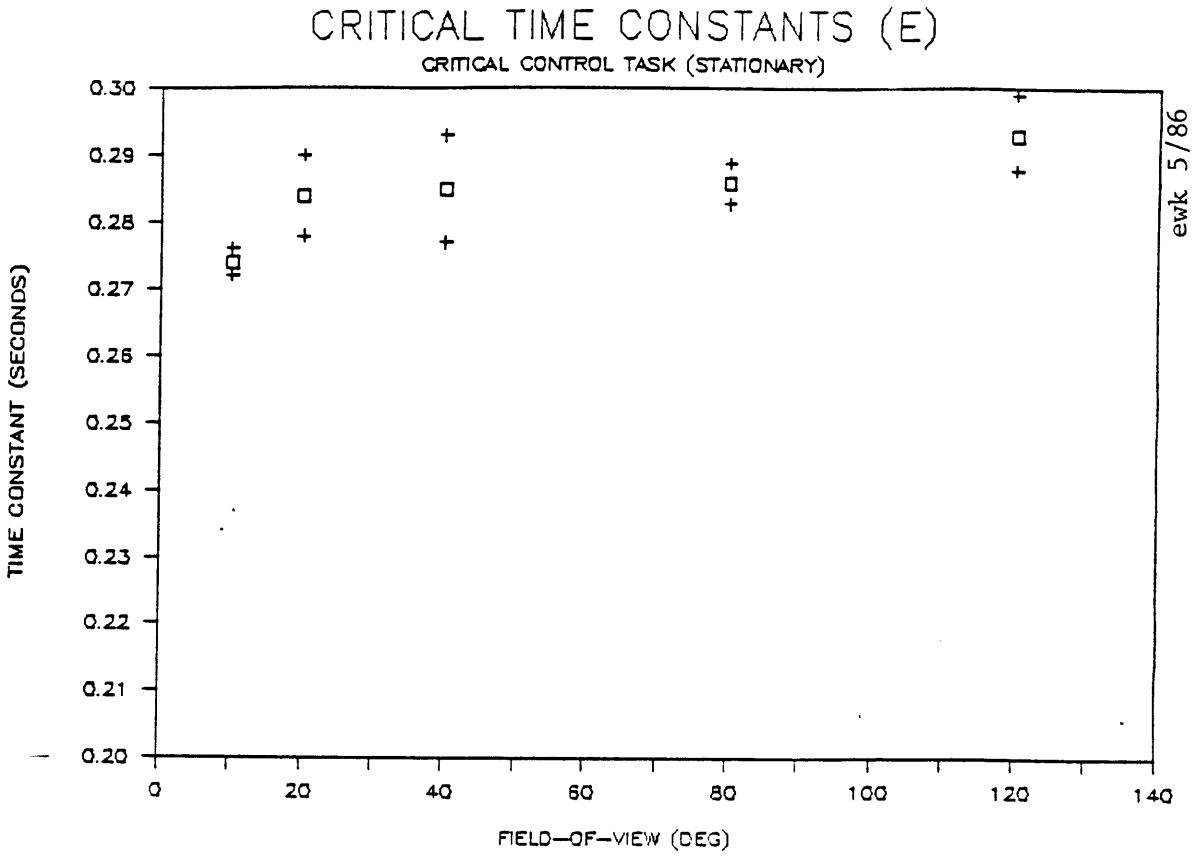

	10°	20°	40°	80°
20°	-1.5492			
40°	-1.3070	-0.0979		
80°	-3.1157 **	-0.2881	-0.1137	
120°	-3.3414 **	-1.1106	-0.8215	-1.1233

Figure 6.4 (e)

critical time constant at 120° was significantly higher than the 80° field-of-view case. Subjects C and D show no significant differences for the effects of field-of-view on their critical time constants.

Critical time constants for the stationary field cases are presented in figures 6.4 (a) to 6.4 (e). One general statement that can be made about the results is that four of the five subjects had significantly lower critical time constants for the 10° field-of-view as compared to wider field-of-view sizes; the fifth subject (B) shows the 10° field-of-view critical time constant was lower than the wider field-of-view sizes but not by a significant amount. Subjects B and D show the critical time constant at 120° was significantly less than the 80° field-of-view case. Therefore, four of the five subjects had a shorter time delay with the 10° field-of-view, and two subjects tend to have had shorter time delays at the extreme field-of-view sizes.

6.3 Stage-One RMS Roll Error

Stage-one RMS roll error measured how accurately the subject controlled the roll motion when the instability level, lambda, was less than 3.2. A low RMS roll error indicates accurate control by the subject. Since the instability level was relatively low during stage-one as compared to the rest of the test, the subject's task was relatively easy. Figures 6.5 (a) to 6.5 (e) show the RMS roll errors for the moving field cases. All subjects had significantly higher RMS roll errors for the 10° field-of-view case compared to wider field-of-view sizes. Subjects A, B and C had RMS roll errors that were significantly higher for 120° than for 80°. This indicates an optimum

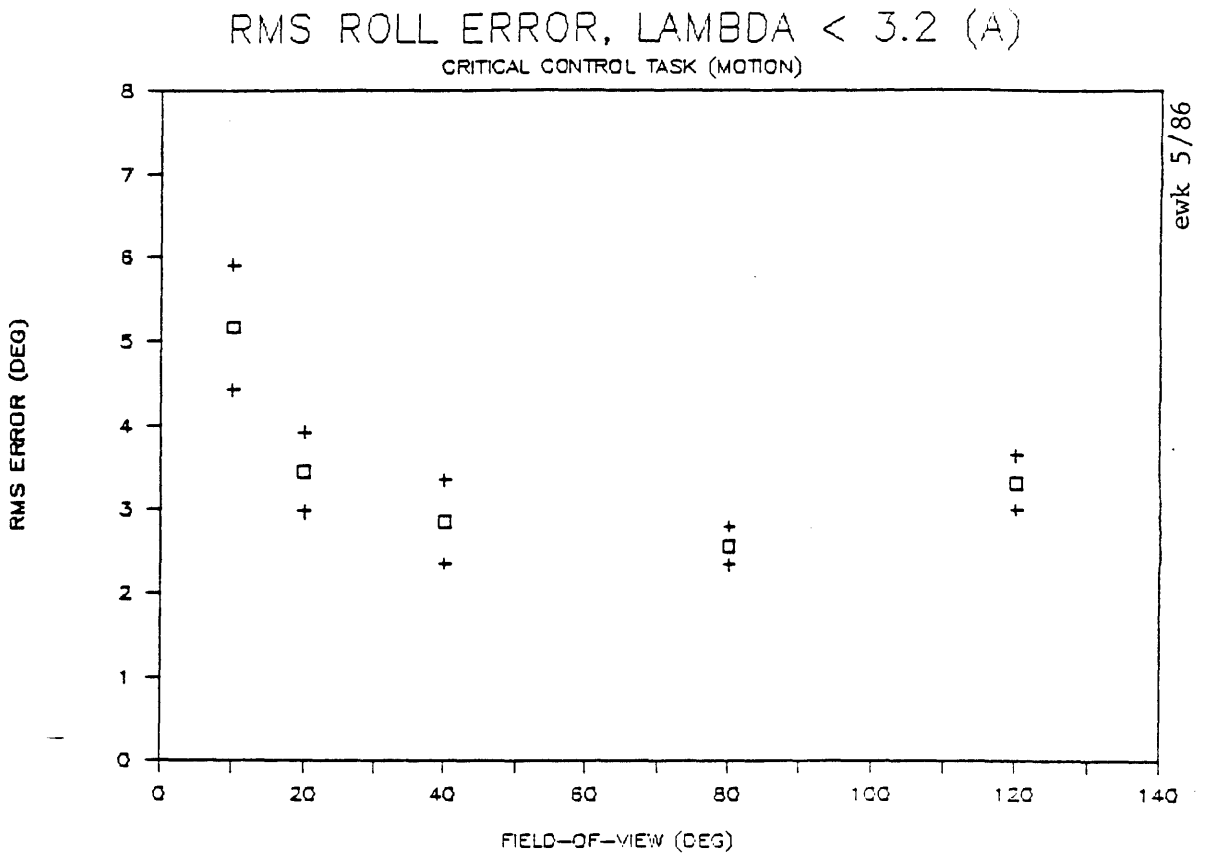

	10°	20°	40°	80°
20°	1.9493 *			
40°	2.5773 *	0.87281		
80°	3.3278 **	1.6852E	0.50749	
120°	2.2567 *	0.20982E	-0.80132	-1.9064 *

Figure 6.5 (a)

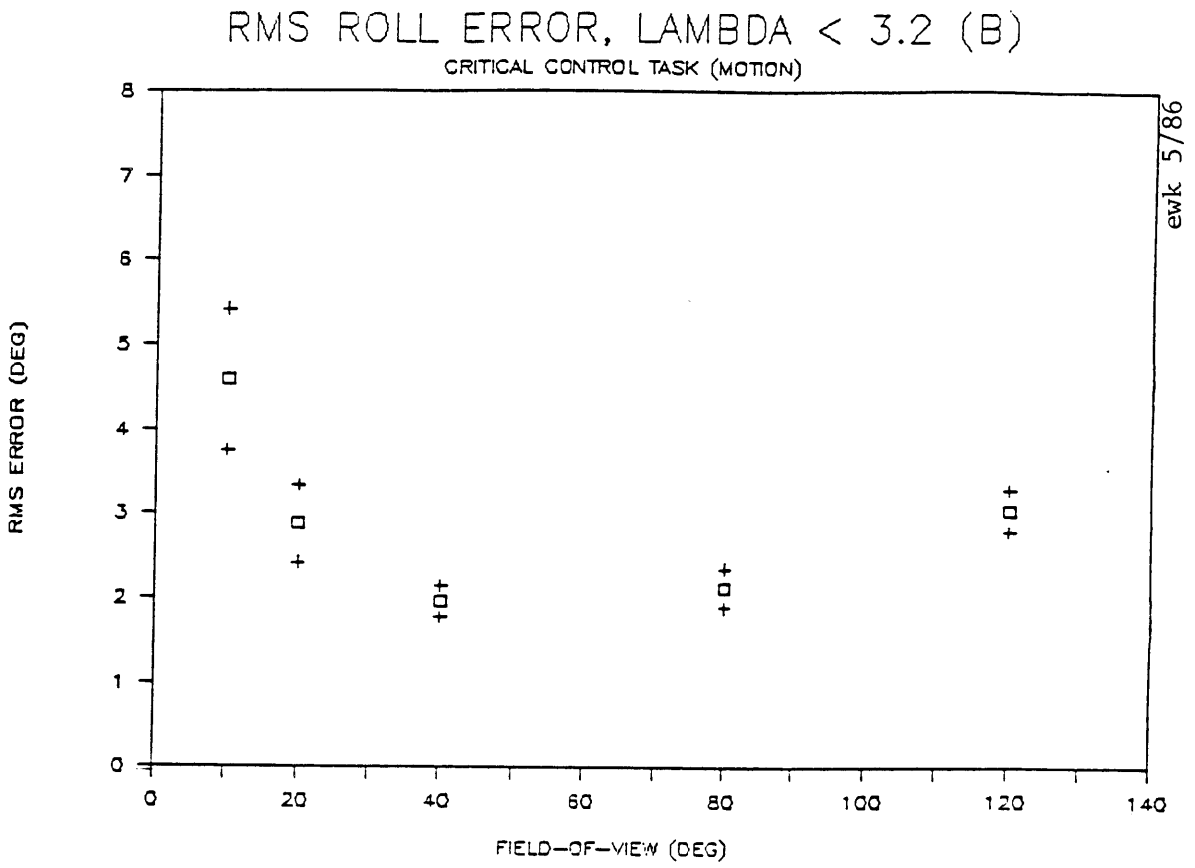

	10°	20°	40°	80°
20°	1.7894			
40°	3.0663 **	1.8471 *		
80°	2.8399 **	1.4657	-0.5294	
120°	1.7637	-0.3242	-3.4947 **	-2.7064 *

Figure 6.5 (b)

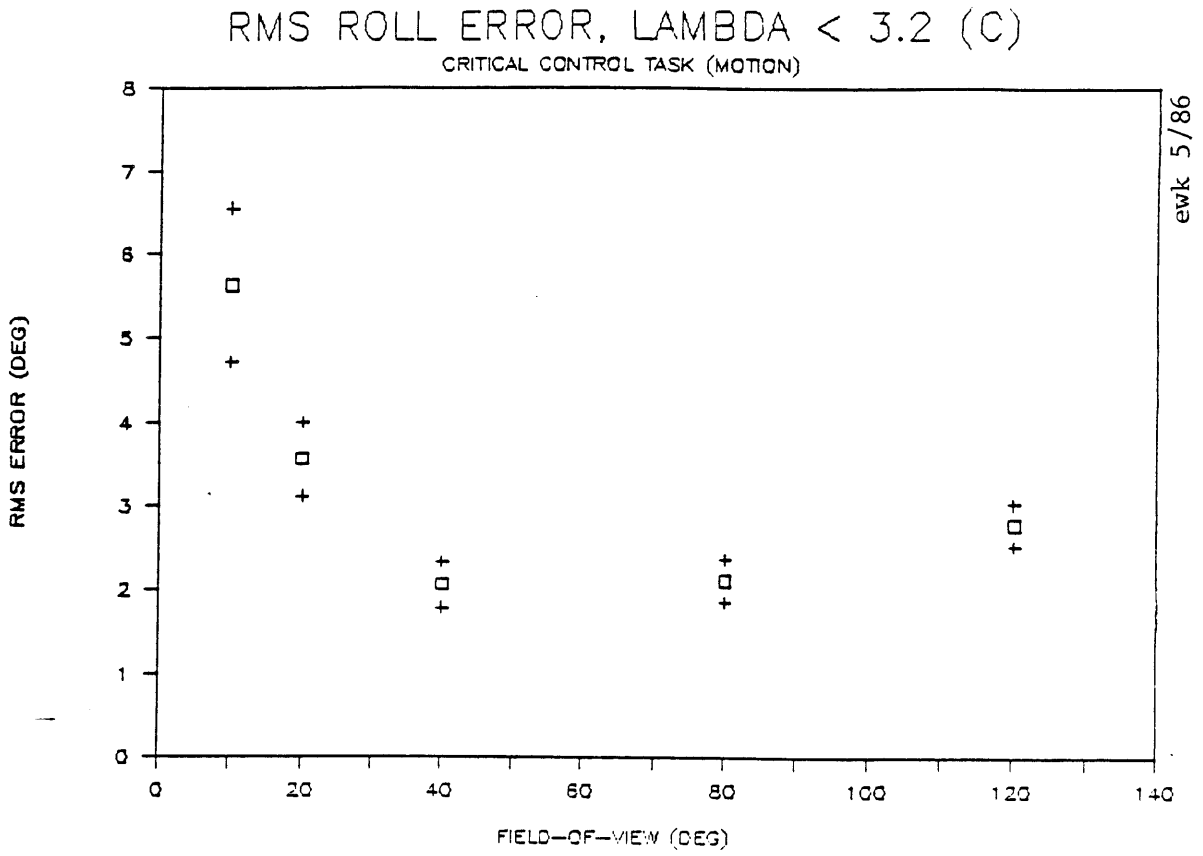

	10°	20°	40°	80°
20°	2.0278 *			
40°	3.7052 **	2.8981 **		
80°	3.6792 **	2.8721 **	-0.1330	
120°	2.9684 **	1.5252	-1.9432 *	-1.8997 *

Figure 6.5 (c)

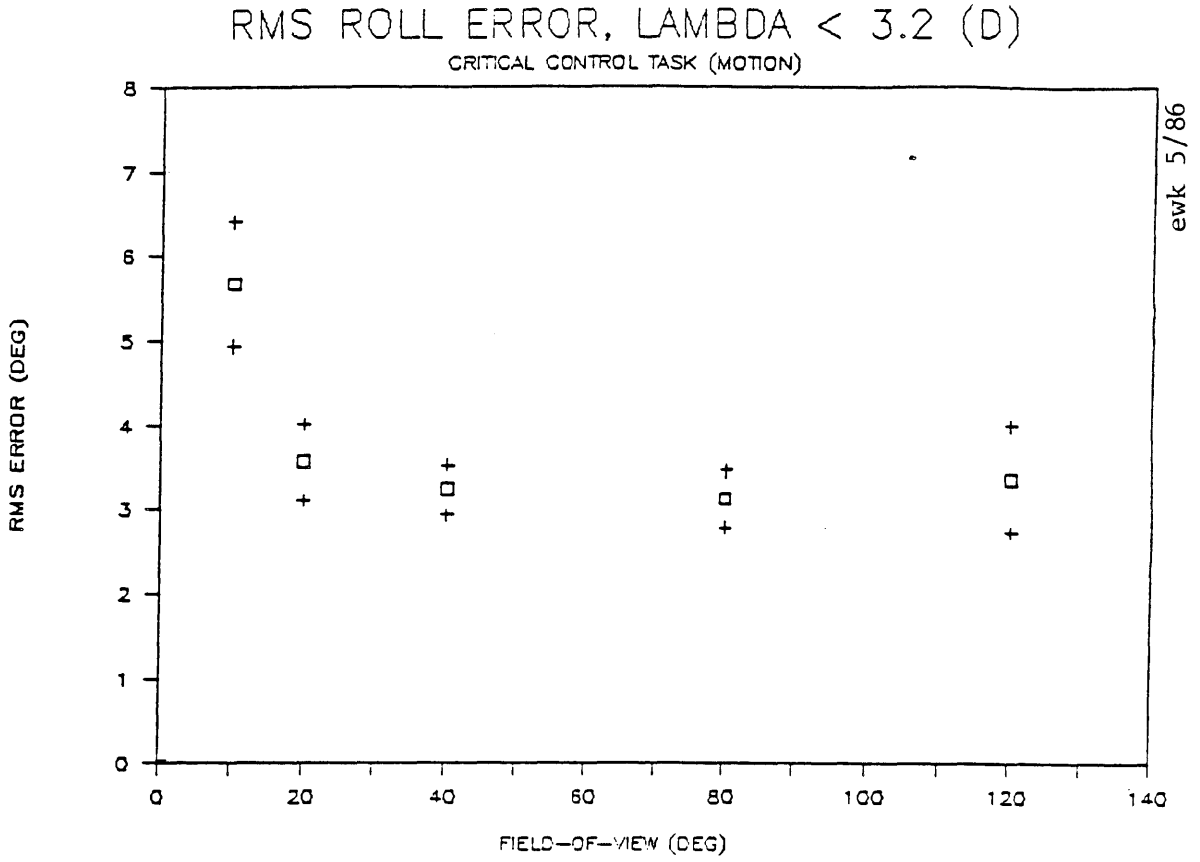

	10°	20°	40°	80°
20°	2.4539 *			
40°	3.0978 **	0.6109		
80°	3.1590 **	0.7742	0.2435	
120°	2.3897 *	0.2569	-0.1863	-0.3334

Figure 6.5 (d)

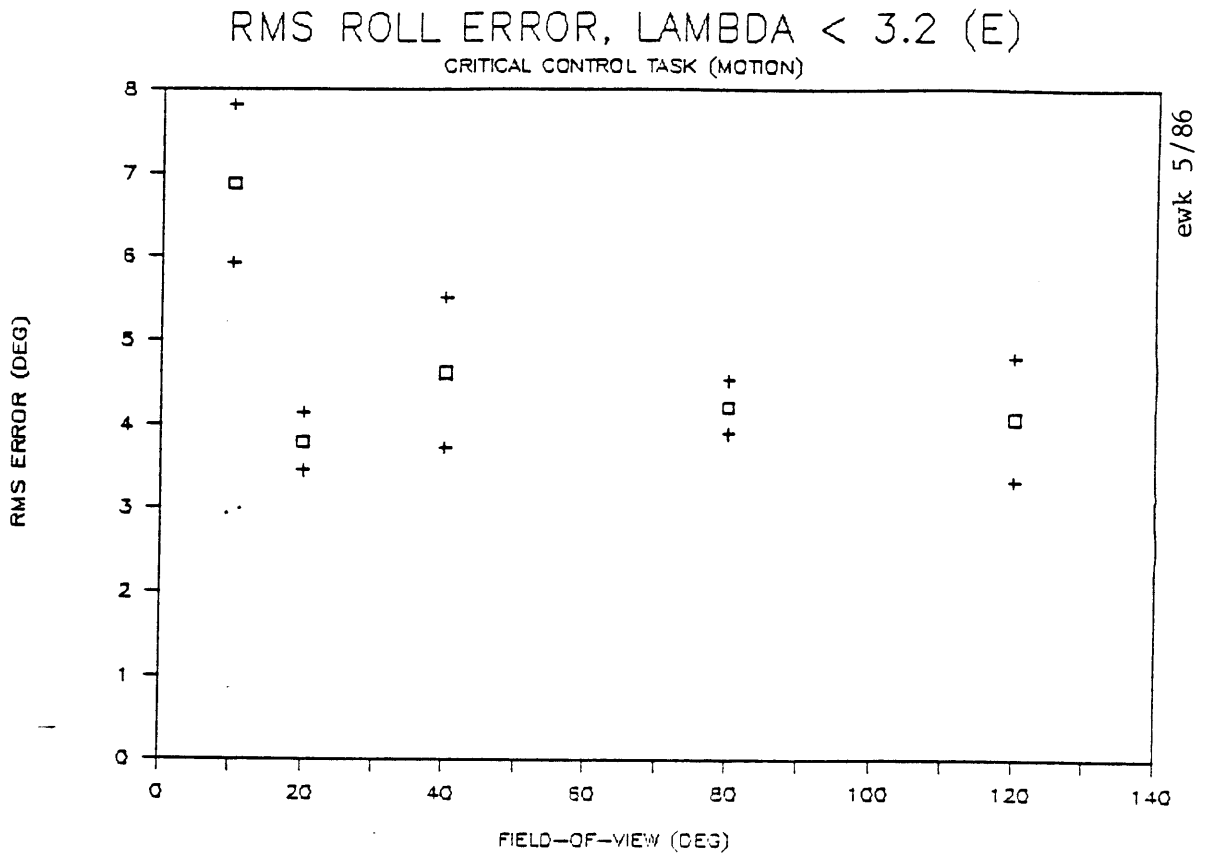

	10°	20°	40°	80°
20°	2.8423 **			
40°	1.7141	-0.8697		
80°	2.6727 *	-0.9156	0.4560	
120°	2.3350 *	-0.3317	0.47131	0.1739

Figure 6.5 (e)

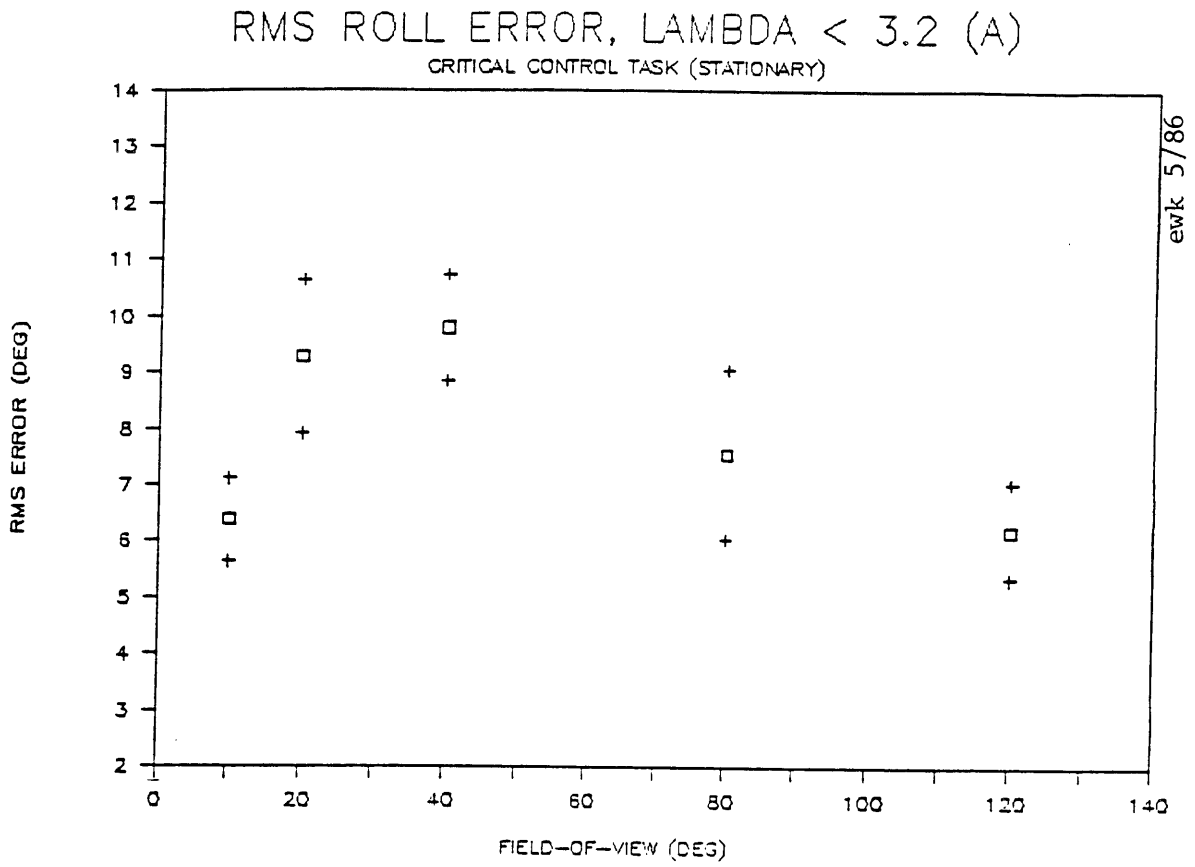

	10°	20°	40°	80°
20°	-1.9638 *			
40°	-2.8479 **	-0.3172		
80°	-0.7009	0.8299	1.2538	
120°	0.1502	1.9834 *	2.8217 **	0.7781

Figure 6.6 (a)

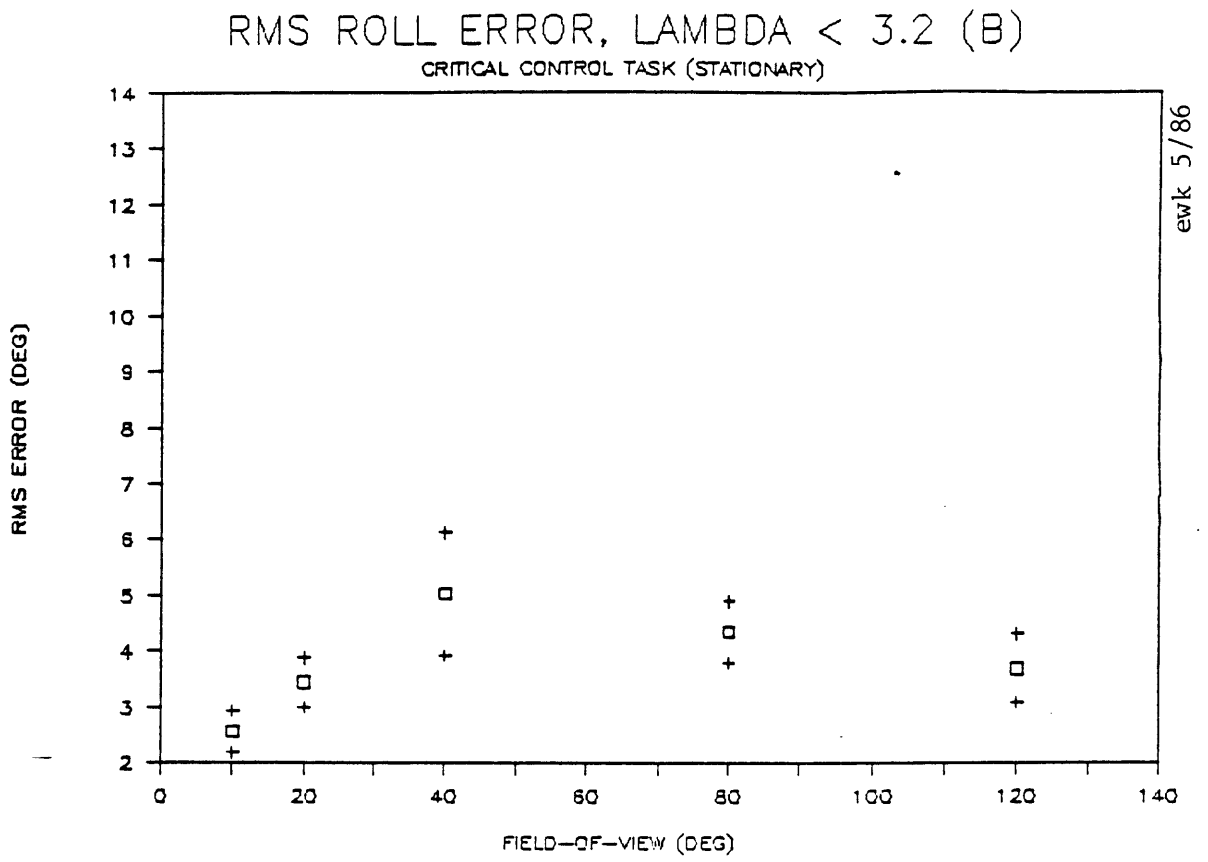

	10°	20°	40°	80°
20°	-1.4581			
40°	-1.9510 *	-1.3359		
80°	-2.5598 *	-1.2800	0.5517	
120°	-1.5811	-0.3498	0.9938	0.7899

Figure 6.6 (b)

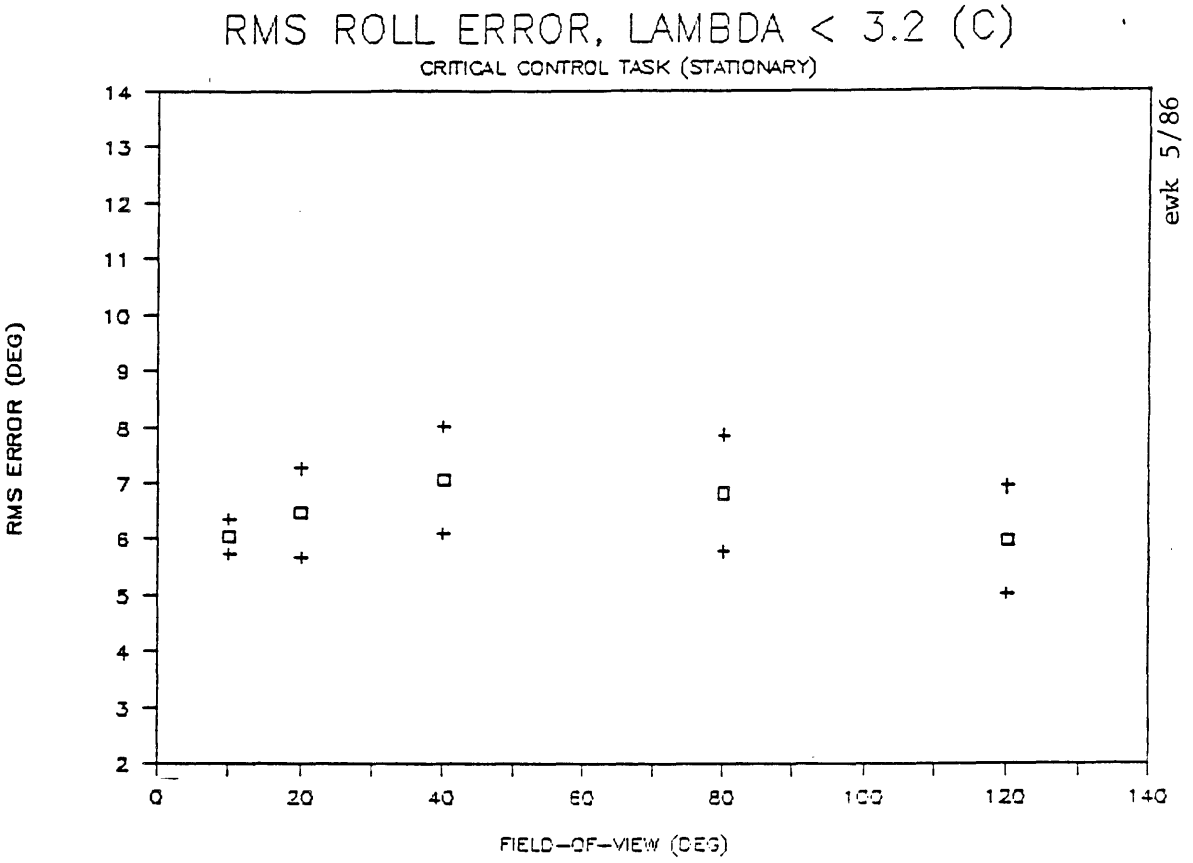

	10°	20°	40°	80°
20°	-0.5055			
40°	-1.0116	-0.4742		
80°	-0.7890	-0.2801	0.1622	
120°	0.0640	0.3965	0.7865	0.5982

Figure 6.6 (c)

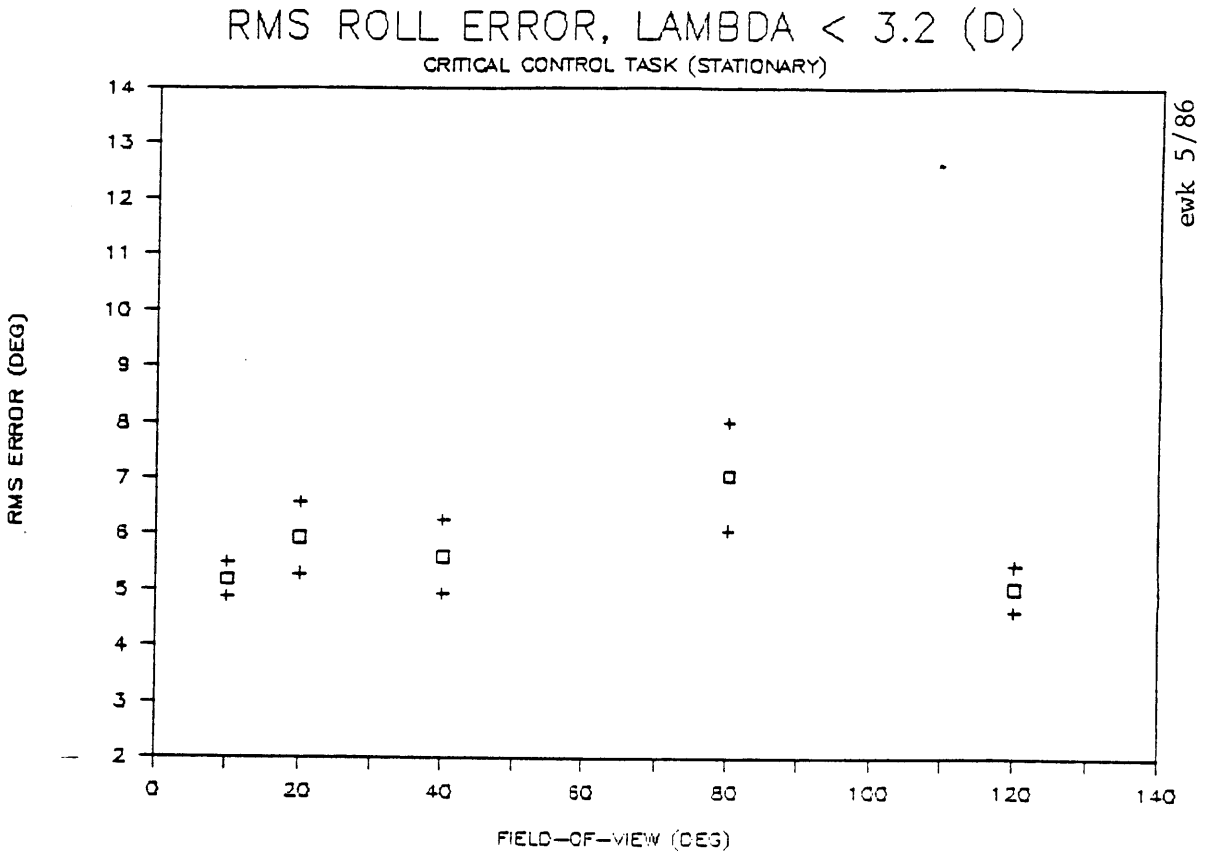

	10°	20°	40°	80°
20°	-1.1149			
40°	-0.5625	0.3639		
80°	-1.8427 *	-0.9199	-1.2457	
120°	0.2920	1.2183	0.7185	1.9206 *

Figure 6.6 (d)

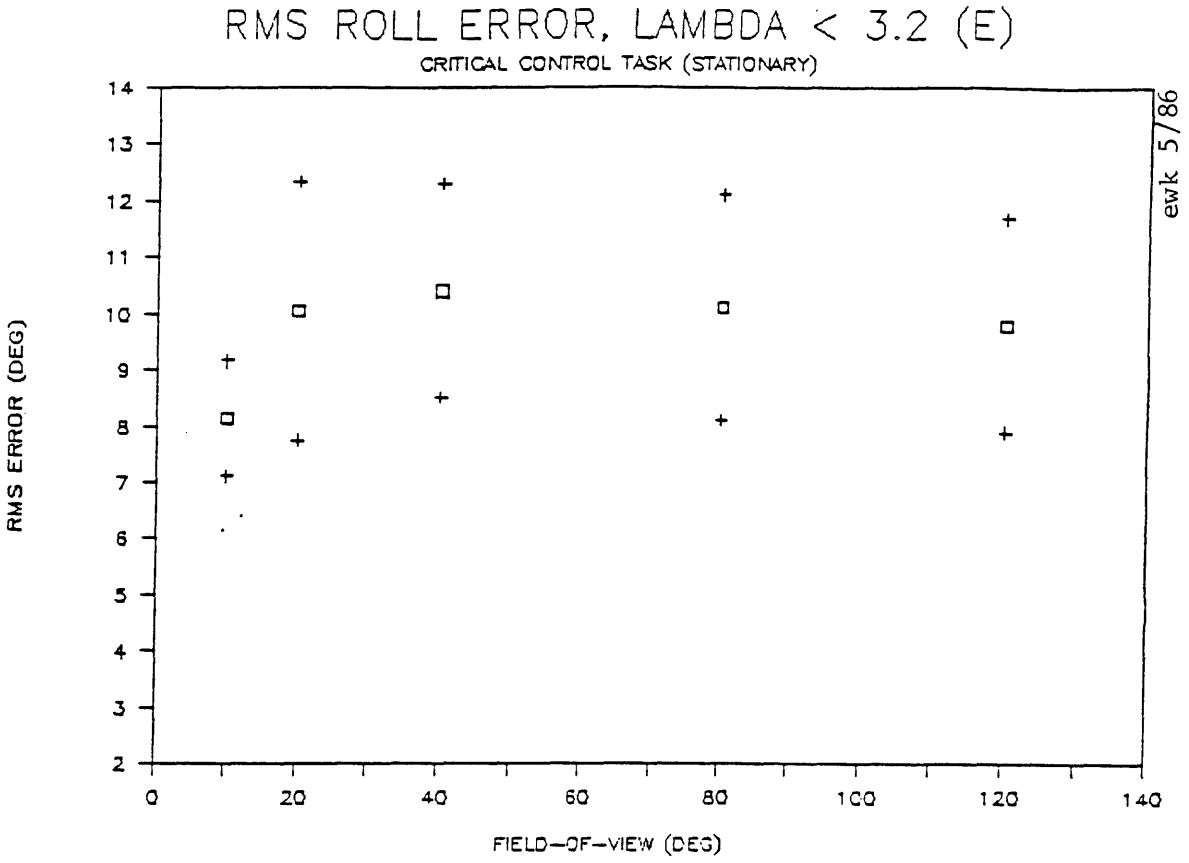

	10°	20°	40°	80°
20°	-0.7545			
40°	-1.0467	-0.1207		
80°	-0.8713	-0.0196	0.1087	
120°	-0.7675	0.0804	0.2232	0.1086

Figure 6.6 (e)

field-of-view size which would minimize a subjects RMS roll error for these three subjects. The curves for four of the five subjects look very similar so in order to further evaluate the effect of field-of-view on stage-one RMS roll error this data was evaluated using a least squares fit analysis of the measurements. The least squares analysis showed trends in the measurements with greater accuracy and confidence than a one-to-one comparison of values. This analysis method is presented in section 6.5.

Stage-one RMS roll errors for the stationary case are shown in figures 6.6 (a) to 6.6 (e). Subject A shows significantly lower RMS roll errors for the extreme field-of-view sizes, 10° and 120°, compared to the mid field-of-view sizes, 20° and 40°. Subjects B, C and D show weaker trends, similar to the results of subject A, with only a few intervals between the extreme field-of-view and the mid field-of-view sizes having any significance. This trend for more accurate control at the extreme field-of-view sizes is the opposite of the effect seen in the stage-one RMS roll error for the moving field case; the moving field case showed a trend for an optimum field-of-view size between the extremes.

6.4 Stage-Two RMS Roll Error

Stage-two RMS roll error measured the subject's tracking accuracy during the more difficult stage of the Critical Control Experiment. The roll error was measured from lambda = 3.2 till the end of the test. Figures 6.7 (a) to 6.7 (e) show the stage-two RMS roll error for the moving field cases. All subjects had significantly higher stage-two RMS

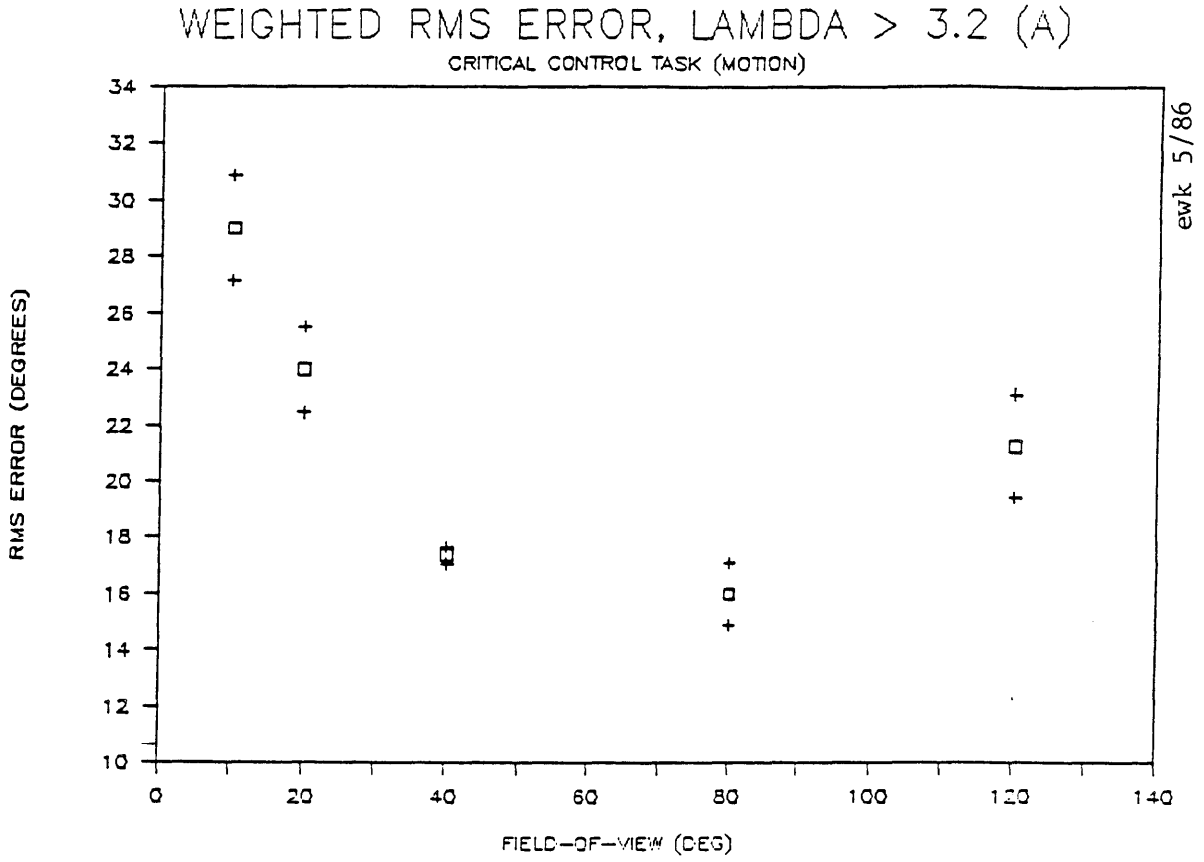

	10°	20°	40°	80°
20°	2.3056 *			
40°	6.8280 **	4.6363 **		
80°	6.6482 **	4.6405 **	1.3198	
120°	3.2534 **	1.2295	-2.3104 *	-2.7130 *

Figure 6.7 (a)

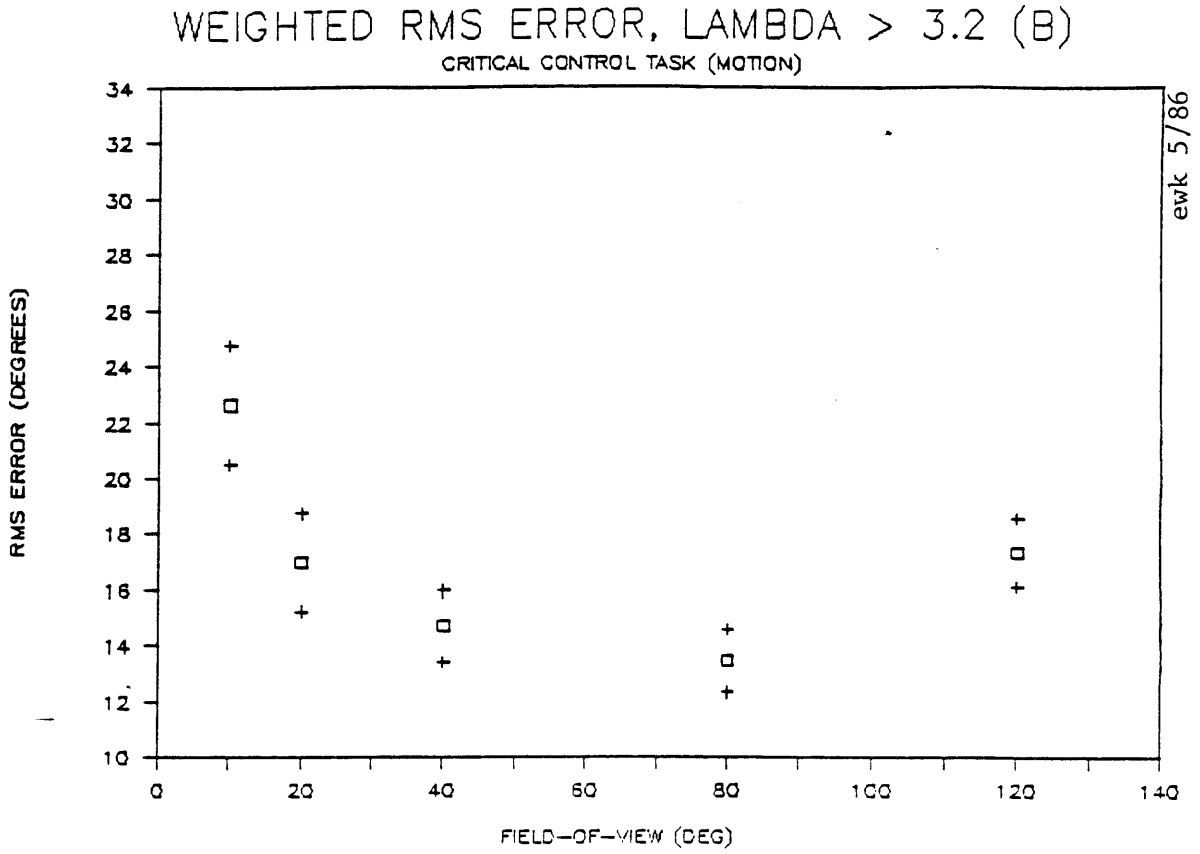

	10°	20°	40°	80°
20°	2.2374 *			
40°	3.5077 **	1.1493		
80°	4.1659 **	1.8350 *	0.7950	
120°	2.3461 *	-0.1931	-1.6483	-2.5495 *

Figure 6.7 (b)

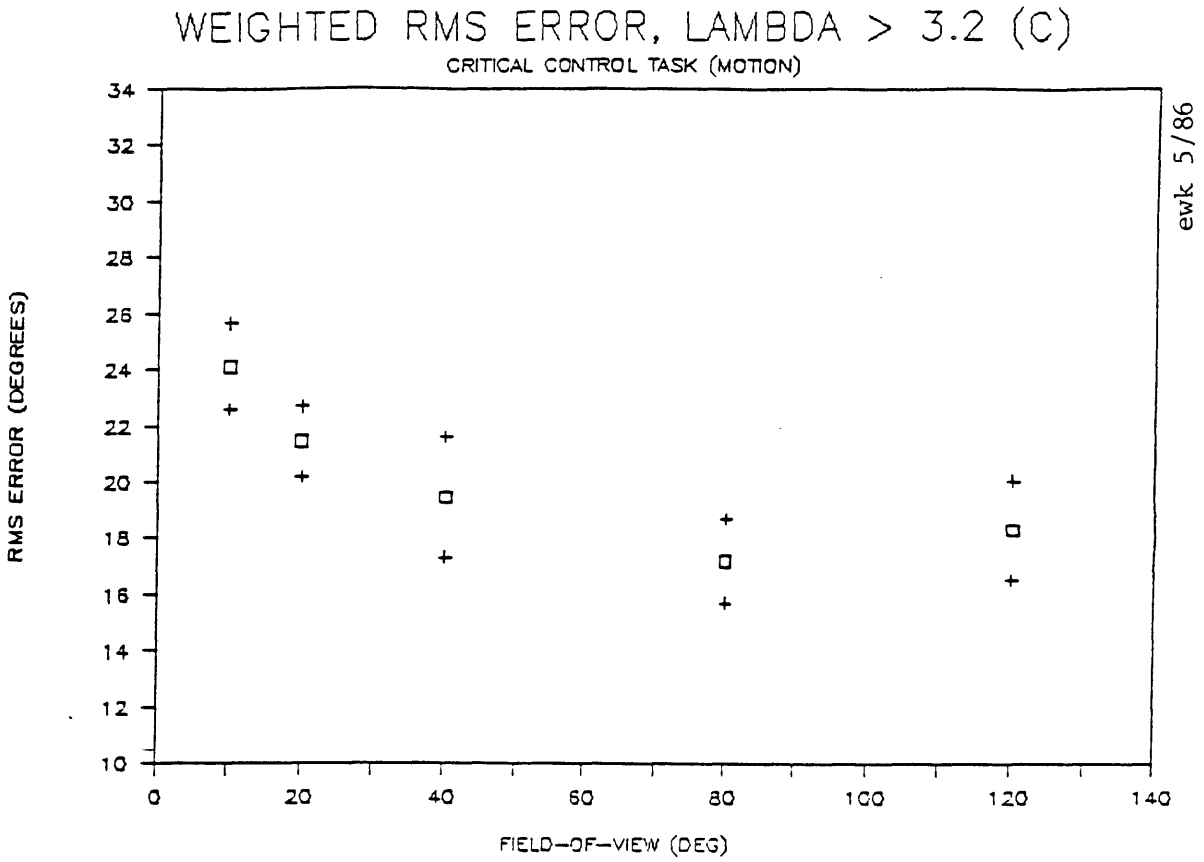

	10°	20°	40°	80°
20°	1.4844			
40°	1.9318 *	0.8722		
80°	3.5305 **	2.3725 *	0.9393	
120°	2.7218 *	1.5830	0.4491	-0.5250

Figure 6.7 (c)

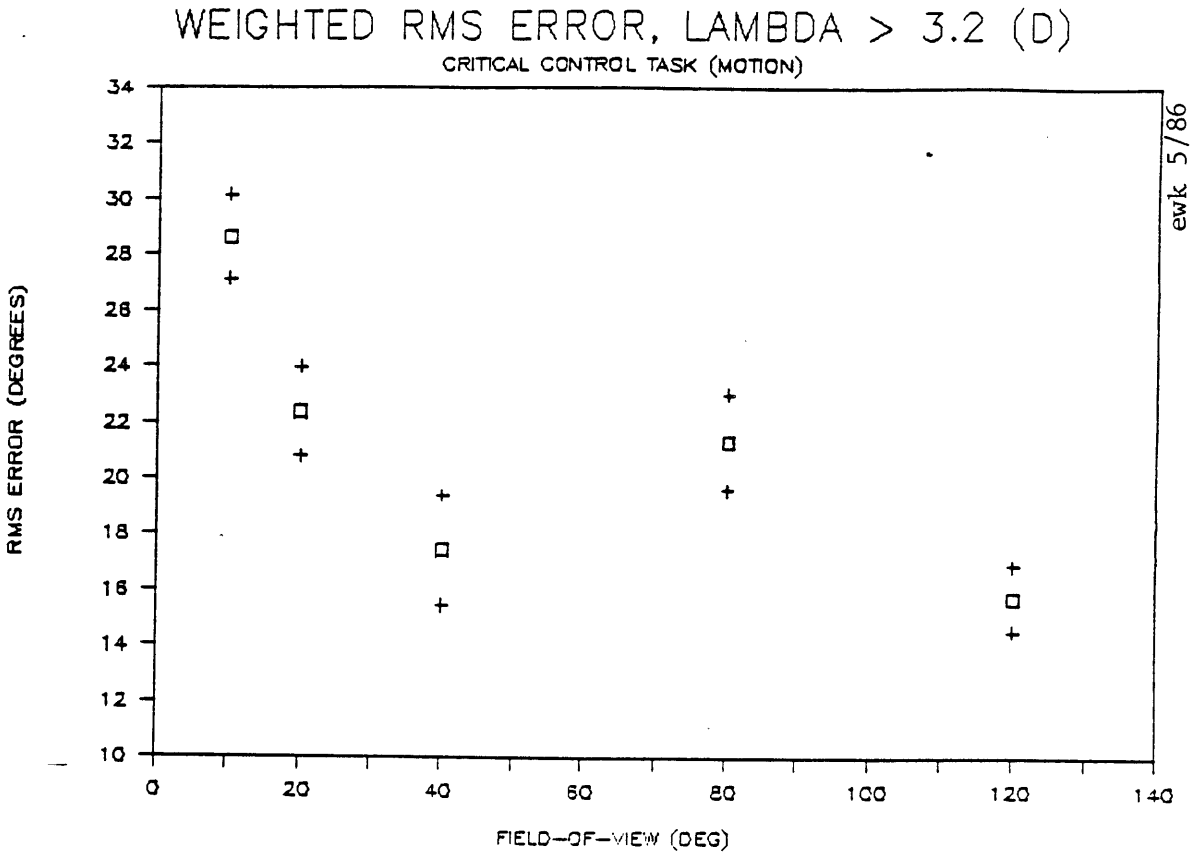

	10°	20°	40°	80°
20°	3.1087 **			
40°	4.9570 **	2.1511 *		
80°	3.4855 **	0.4951	-1.6361	
120°	7.3676 **	3.6863 **	0.8252	2.9437 **

Figure 6.7 (d)

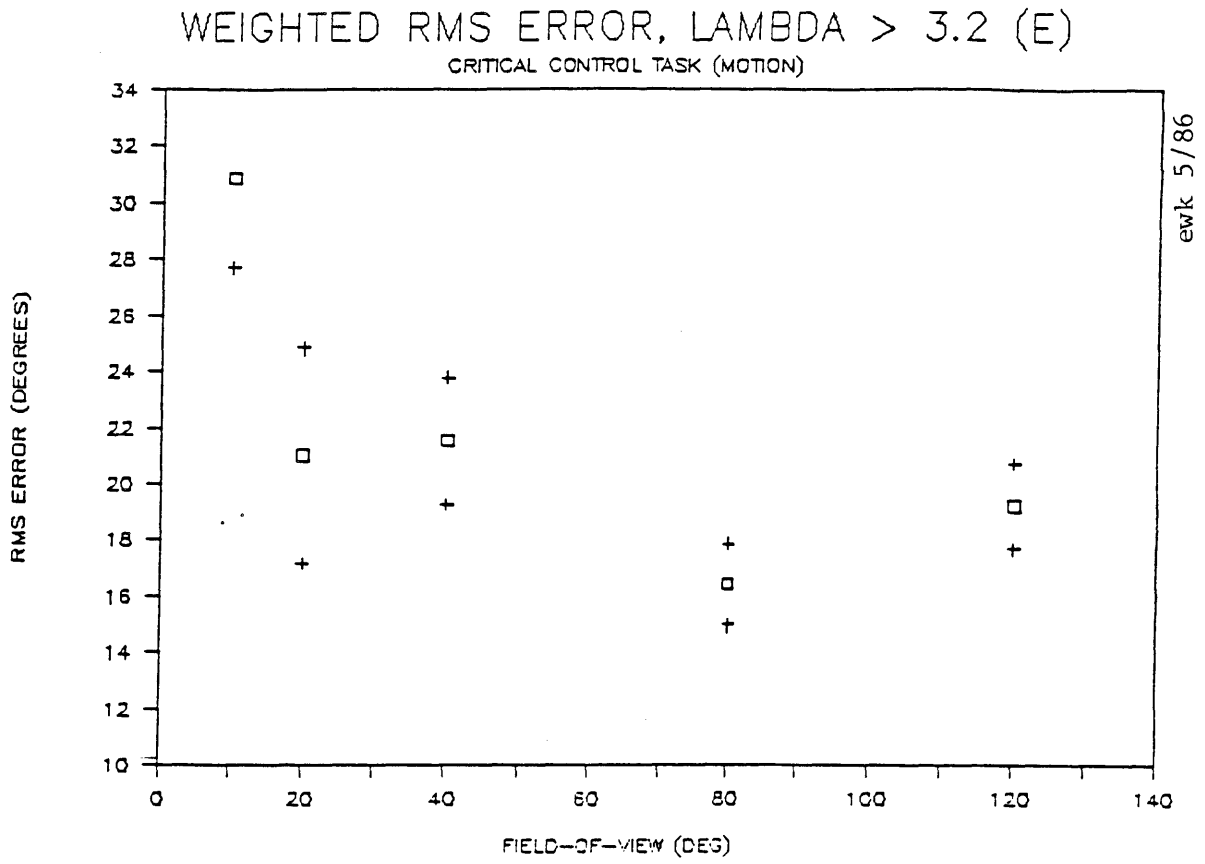

	10°	20°	40°	80°
20°	2.1645 *			
40°	2.6269 *	-0.1301		
80°	4.5469 **	1.2209	2.0947 *	
120°	3.6302 **	0.4736	0.9347	-1.4616

Figure 6.7 (e)

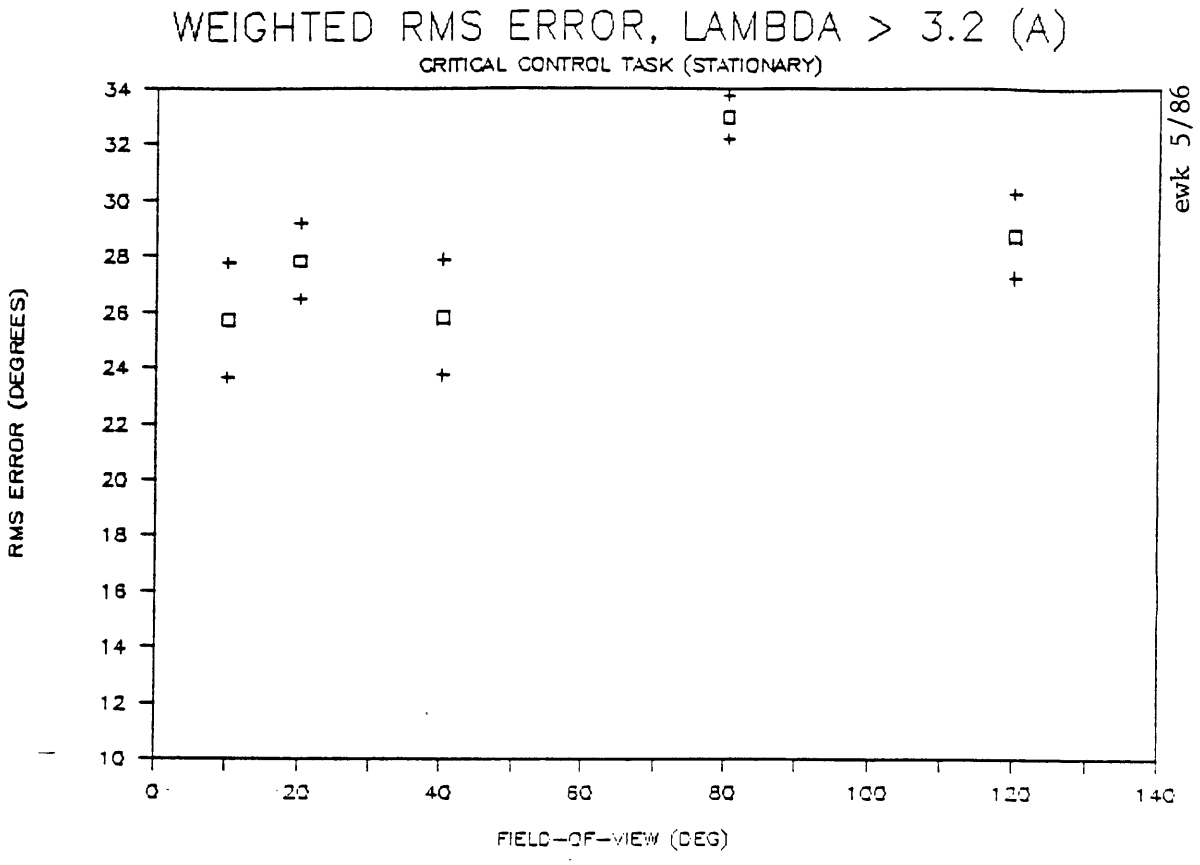

	10°	20°	40°	80°
20°	-0.9379			
40°	-0.0446	0.8808		
80°	-3.5961 **	-3.6245 **	-3.5167 **	
120°	-1.3239	-0.5276	-1.2671	2.7221 *

Figure 6.8 (a)

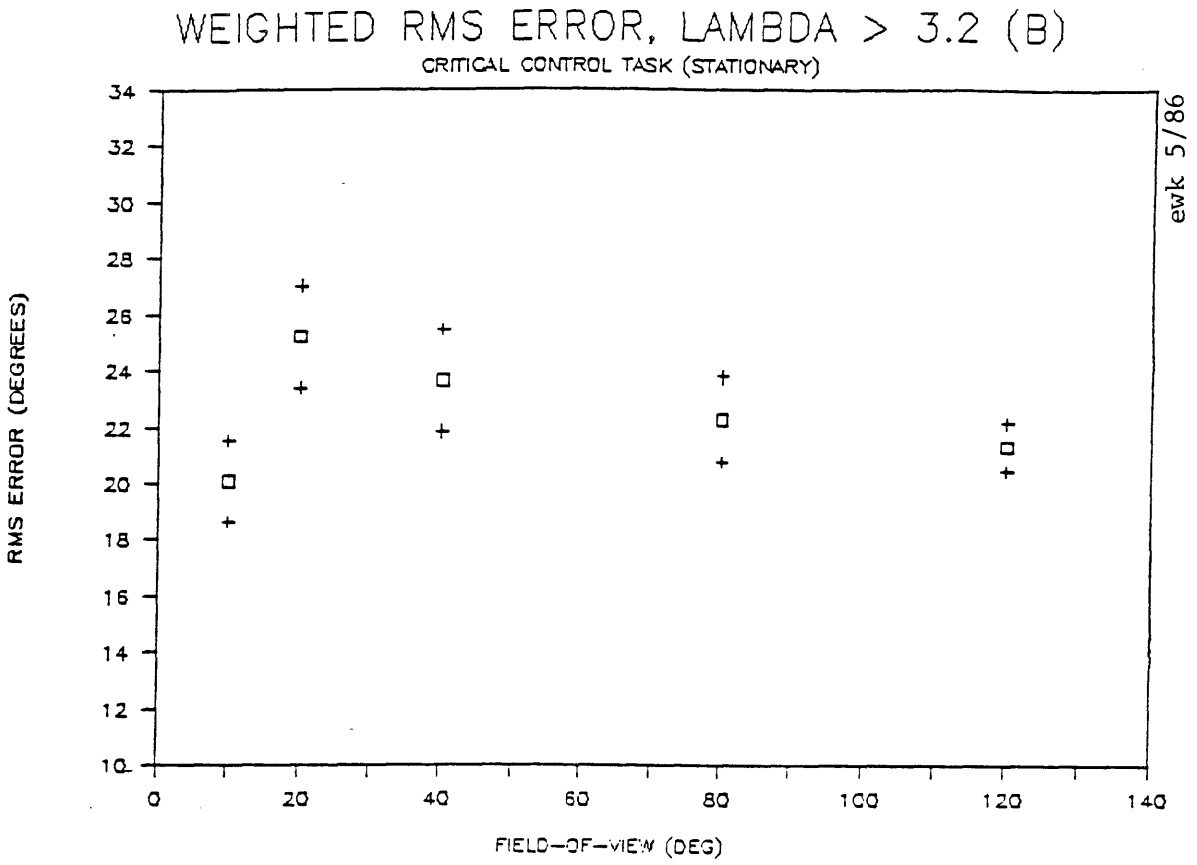

	10°	20°	40°	80°
20°	-2.4202 *			
40°	-1.6959	0.6671		
80°	-1.1559	1.3376	0.6241	
120°	-0.8173	2.1254 *	1.2834	0.6123

Figure 6.8 (b)

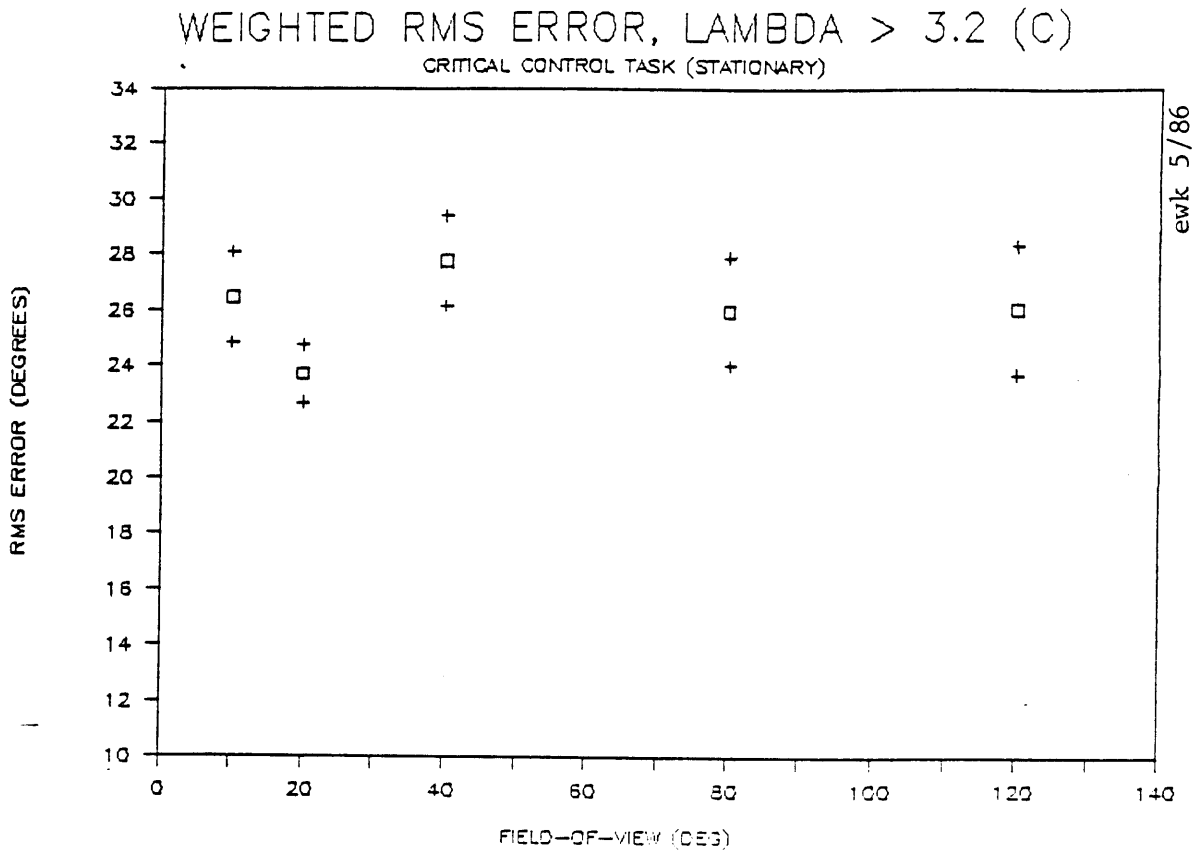

	10°	20°	40°	80°
20°	1.5522			
40°	-0.6406	-2.3416 *		
80°	0.1803	-1.1578	0.7650	
120°	0.1272	-1.0459	0.6511	-0.0325

Figure 6.8 (c)

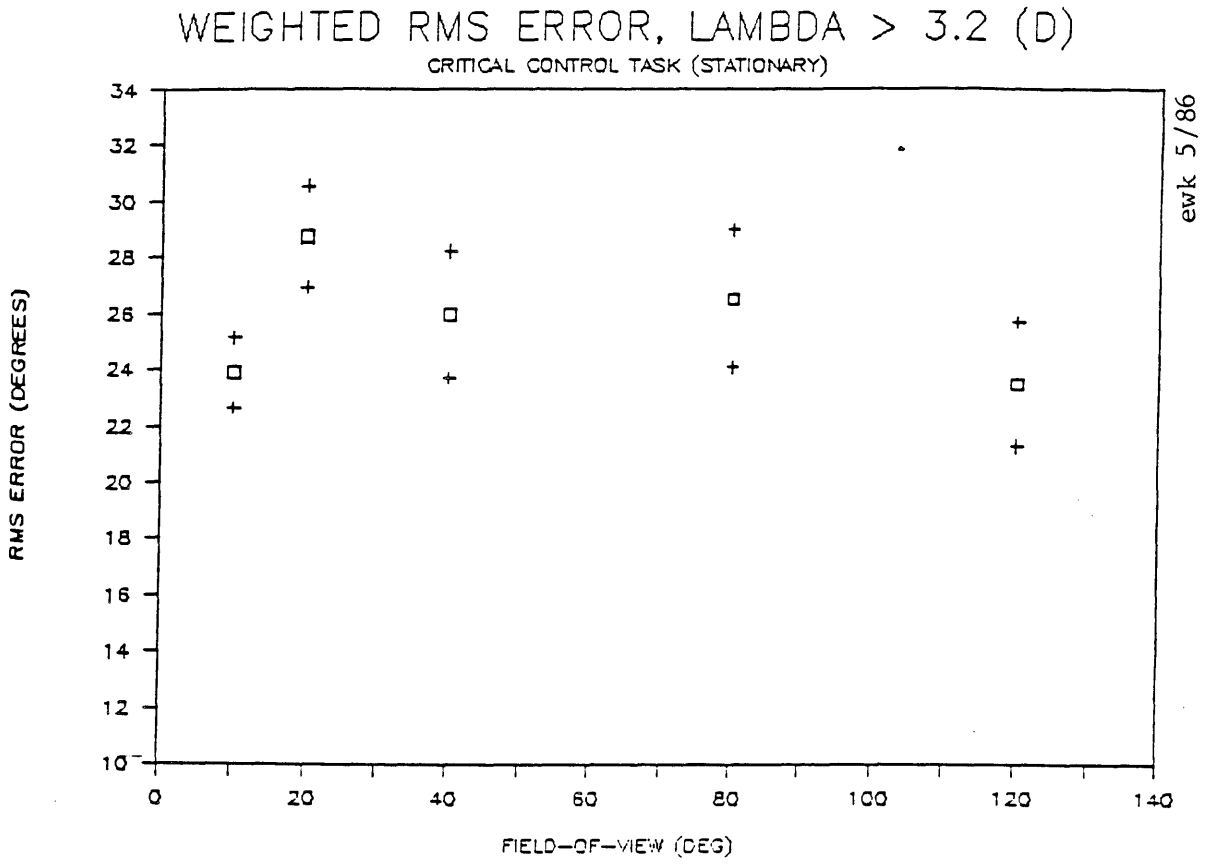

	10°	20°	40°	80°
20°	-2.4482 *			
40°	-0.8966	1.0469		
80°	-1.0754	0.7935	-0.1875	
120°	0.1388	2.0137 *	0.8476	1.0060

Figure 6.8 (d)

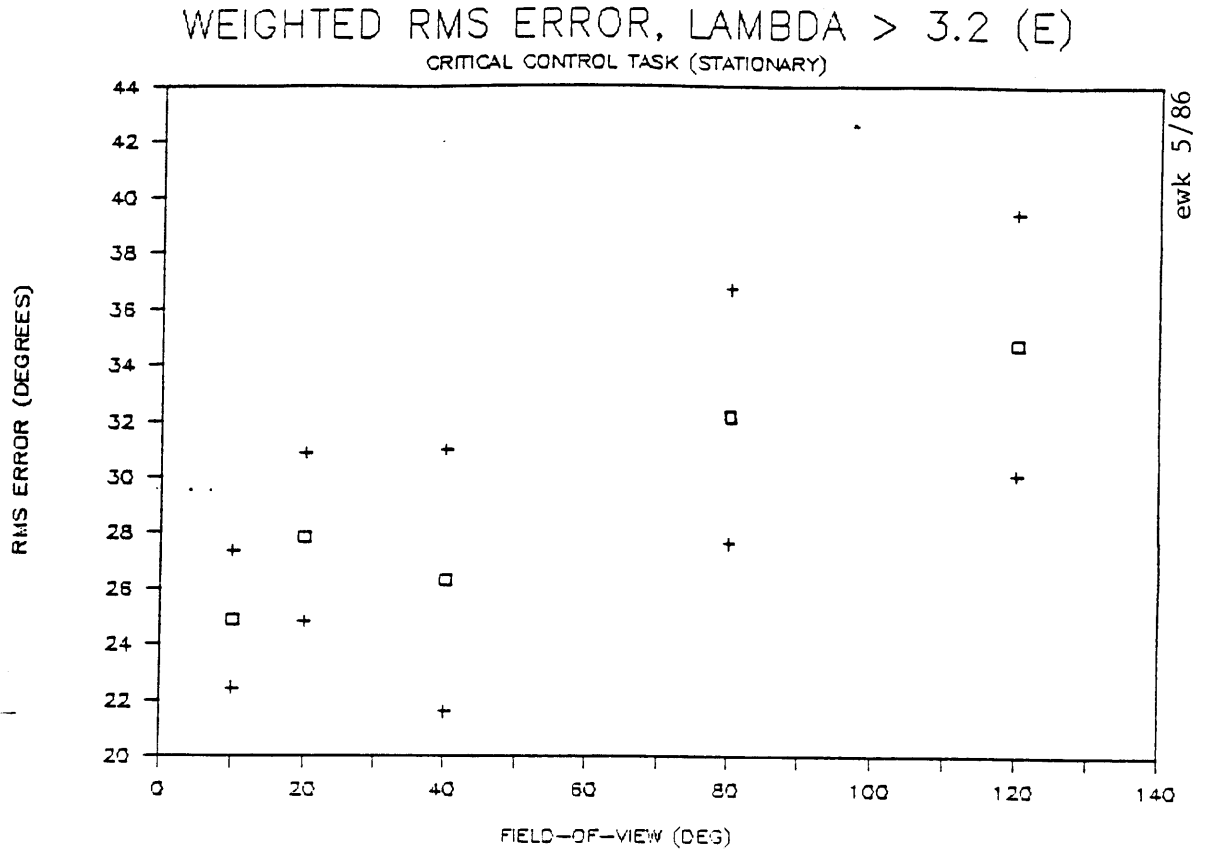

	10°	20°	40°	80°
20°	-0.8324			
40°	-0.2918	0.3041		
80°	-1.5476	-0.8709	-0.9882	
120°	-2.0614 *	-1.3712	-1.4095	-0.4396

Figure 6.8 (e)

roll errors for the 10° field-of-view case compared to the wider field-of-view sizes. Four of the five subjects show approximately half of the intervals between 20° and wider field-of-view sizes to be significant. Subjects A and B show an optimum field-of-view size since their stage-two RMS roll errors were significantly higher for 120° compared to 80°. Subjects C and E show similar trends though the differences between values were not significant.

Stage-two RMS roll errors for the stationary field case are shown in figures 6.8 (a) to 6.8 (b). There are only a few scattered significant differences between field-of-view sizes with no major trends within subject scores or between subject scores. Four of the five subjects had an RMS roll error value for the 10° field-of-view that was significantly lower than a single wider field-of-view size.

6.5 Least Squares Analysis of Stage-One RMS Roll Error

After studying the values shown in the stage-one RMS roll error plots for the moving field cases (figures 6.5 (a) to 6.5 (e)), a decision was made to analyze the data using a least squares fit of the data [J. Orear, 1958]. The least squares analysis begins by choosing an appropriate class of function which will relate the dependent variable (stage-one RMS roll error) to the independent variable (field-of-view size). Once the class of the function was chosen the analysis was performed using the experimental data, resulting in the determination of the function's coefficients. The function, which is now fully determined, shows the predicted values for a continuous range of input values.

The type of function chosen for the stage-one RMS roll error analysis was a second order function, with three undetermined coefficients, having the form:

$$y = A x^{-1} + B + Cx \qquad 6.1$$

x = field-of-view (degrees)

y = RMS roll error (degrees)

There were three reasons for choosing a function of this form: first, there was a rapid drop in RMS roll error between 10° and 20° field-of-view, and in the theoretical case where the field-of-view is 0° an infinite RMS roll error would be expected. This corresponds to a term of Ax^{-1}. Secondly, there was a gradual increase in RMS roll error as the field-of-view size increases above 80°. This increase was estimated by the linear term Cx. Finally, the coefficient B gives a baseline offset to the RMS roll error values.

The coefficients A, B, and C were determined in the actual analysis procedure. In addition to the values A, B, and C the least squares analysis also resulted in the expected standard deviations of A, B and C; these standard deviations were based on the errors between the values predicted by the function and the actual experimental data.

Once the function had been determined, its ability to fit the data was shown with the chi-square test. The chi-square value produces a percentage confidence level between the actual data and the predicted curve. The percentage level is the likelihood of the predicted curve being different from the experimental data. A low percentage would mean

that the predicted curve and the experimental data were essentially equal indicating a good theoretical model.

Figures 6.9 (a) to 6.9 (e) show the experimental data points for each subject along with the predicted second order function. The values for the coefficients and their standard deviations are given below each plot along with the chi-square value and its corresponding percentage. The means and standard deviations of the five sets of coefficients are:

$$A = 45.9 \pm 4.0 \qquad B = 0.764 \pm 0.396 \qquad C = 0.0192 \pm 0.0022$$

The x^{-1} coefficient, A, and the x coefficient, C, are both fairly consistant for the population while the constant offset, B, is quite variable and close to zero. The mean and standard deviation for C shows with reasonable certainty that wide-field-of-view has a negative effect on opperator control accuracy.

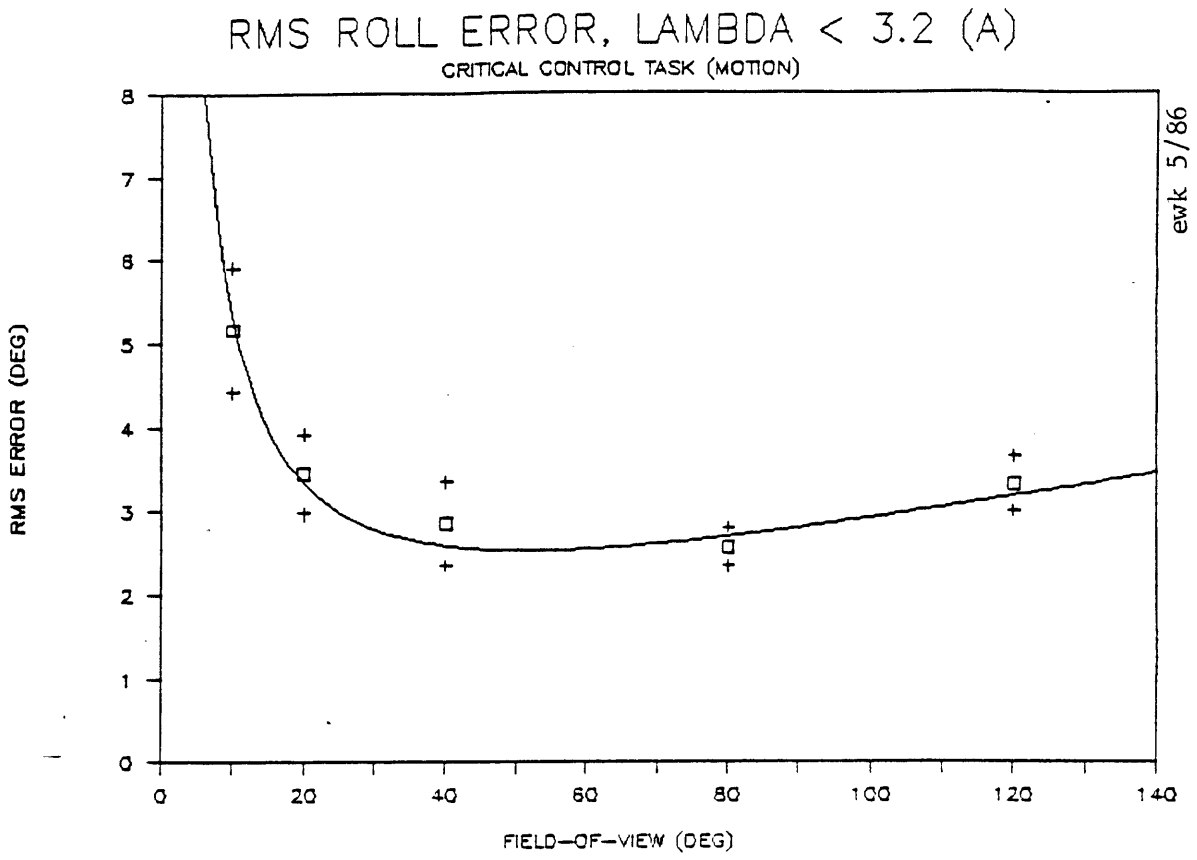

A =	43.542	ΔA =	12.706
B =	0.824	ΔB =	0.849
C =	0.017	ΔC =	0.008

$X^2 = 0.929$ (37%)

Figure 6.9 (a)

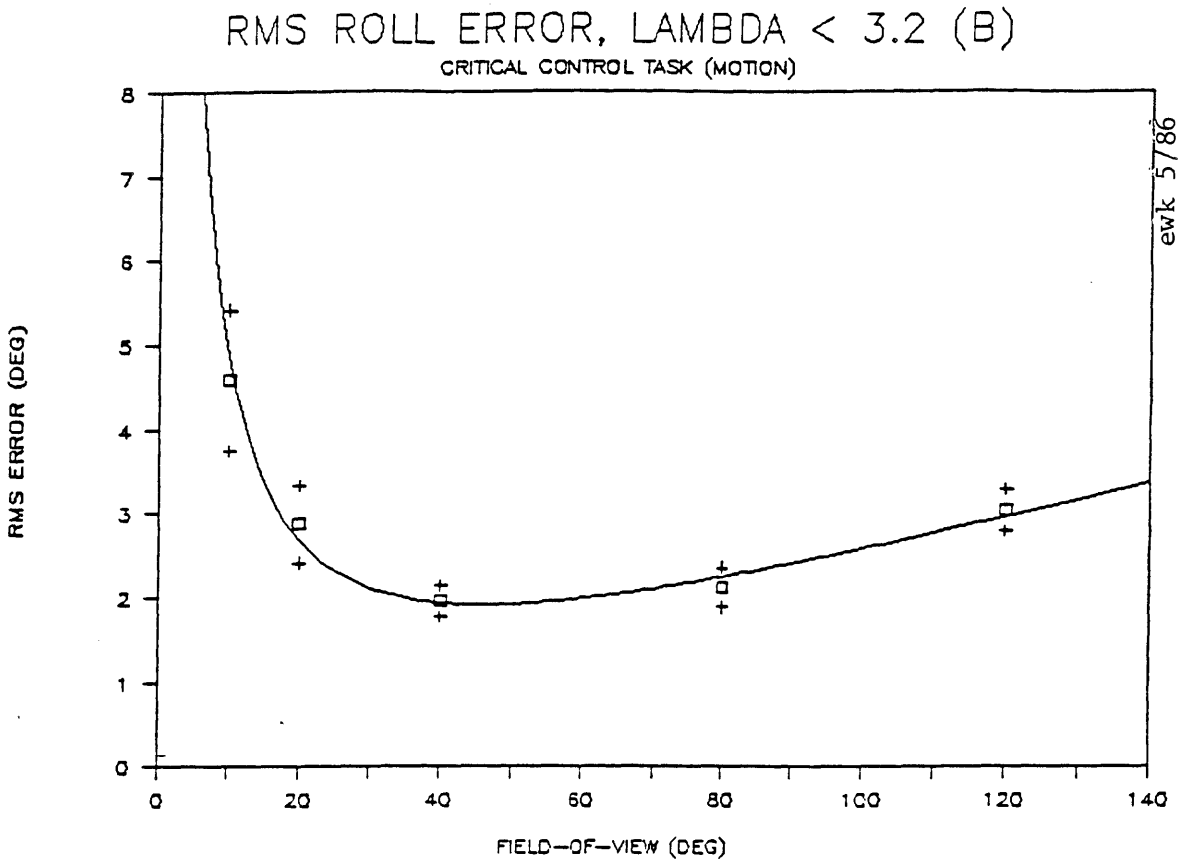

A =	48.463	Δ A =	11.634
B =	-0.195	Δ B =	0.576
C =	0.023	Δ C =	0.005

$X^2 = 0.721$ (30%)

Figure 6.9 (b)

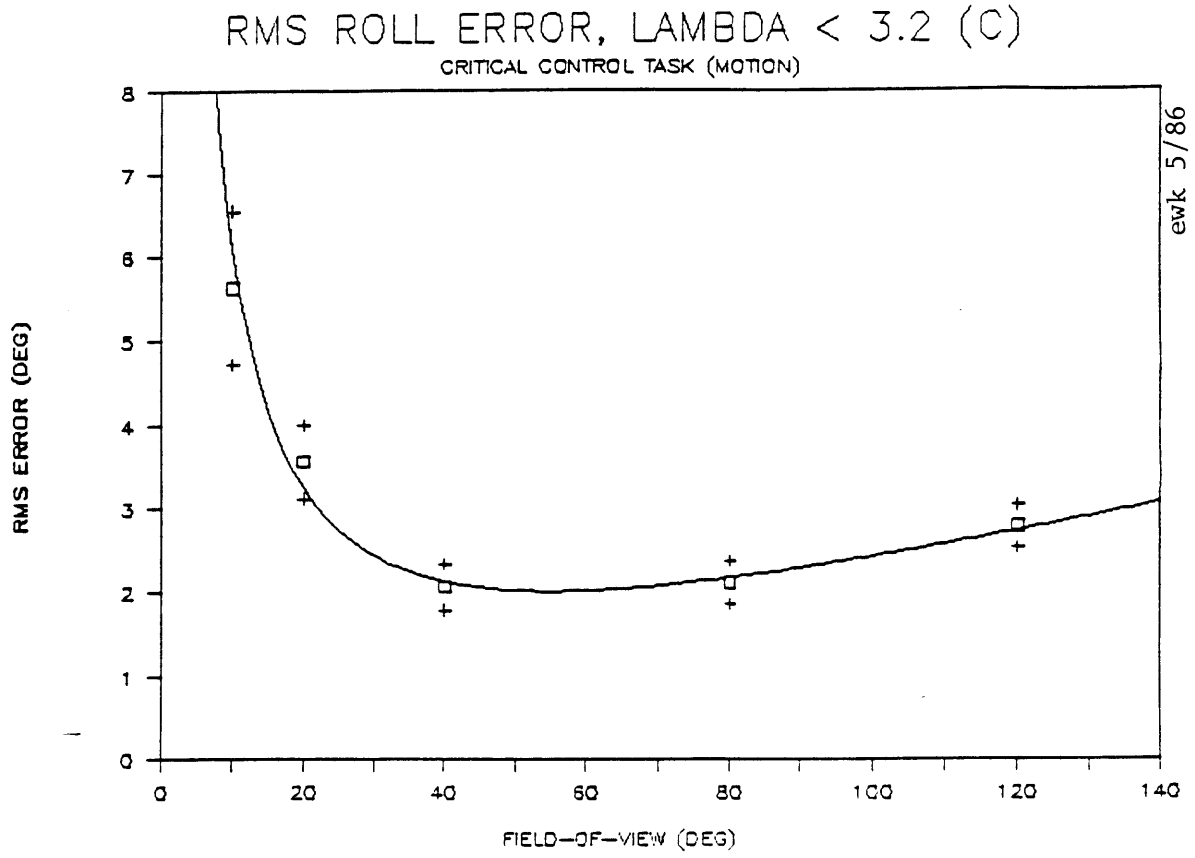

A =	61.443	Δ A =	13.053
B =	-0.240	Δ B =	0.704
C =	0.021	Δ C =	0.006

$X^2 = 0.942$ (38%)

Figure 6.9 (c)

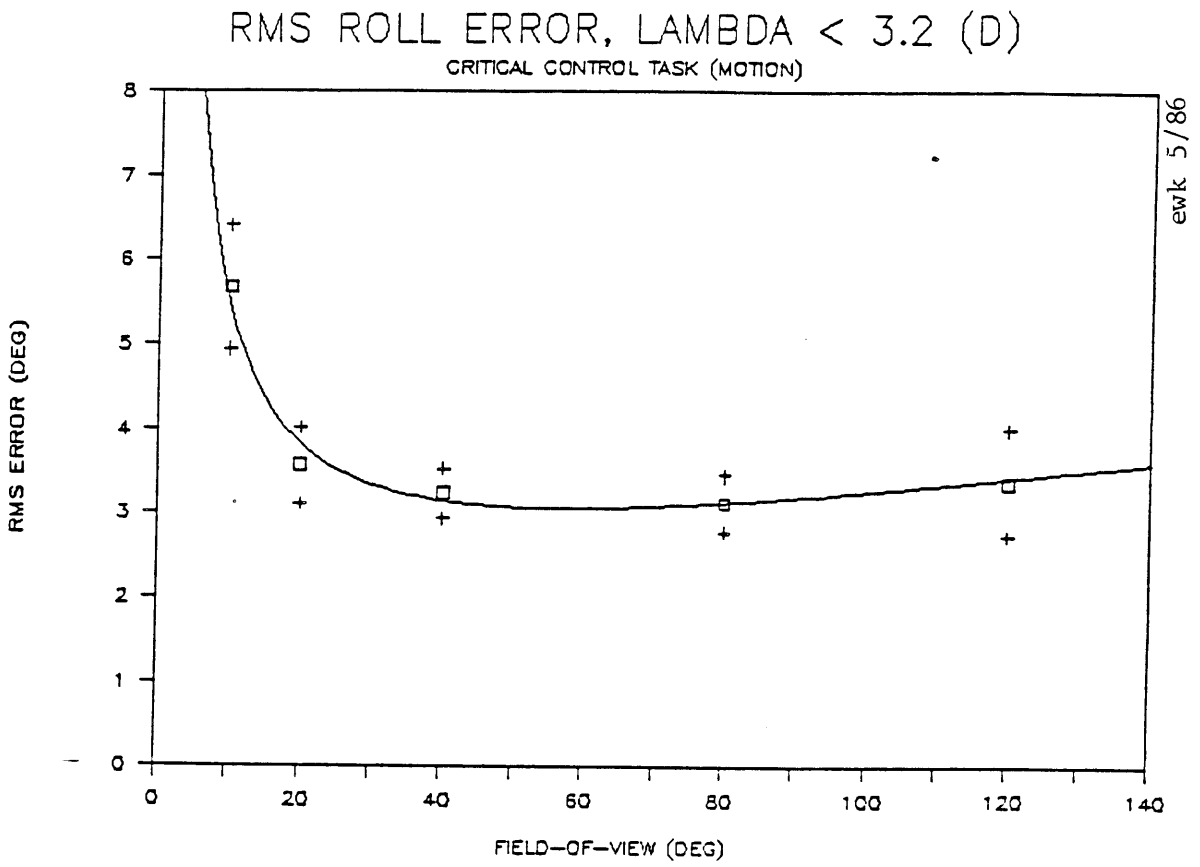

A =	35.482	ΔA =	12.548
B =	1.829	ΔB =	0.822
C =	0.011	ΔC =	0.009

$X^2 = 0.478$ (21%)

Figure 6.9 (d)

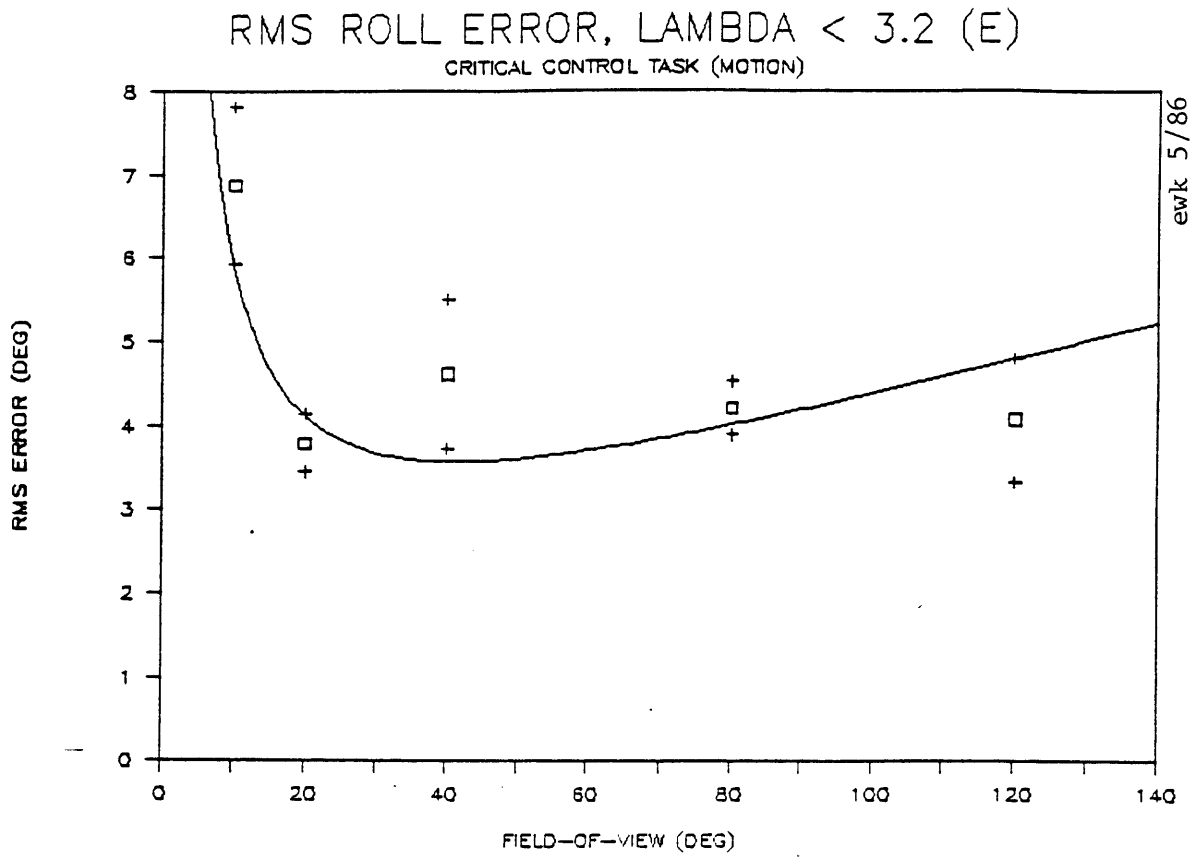

A =	40.668	ΔA =	18.283
B =	1.596	ΔB =	1.228
C =	0.024	ΔC =	0.012

$X^2 = 5.121$ (92%)

Figure 6.9 (e)

6.6 Summary of Results

Both RMS roll errors and time constants showed that the stationary and moving field conditions have nearly opposite effects on subject performance. The results of the Critical Control Experiment shows that subjects tend to perform best at a mid-range field-of-view when they are controlling the motion of a visual field. Subjects tend perform less well in the mid-range field-of-view sizes when controlling the motion of a small center display. These trends were not always significant but no results showed a contrary trend.

END OF PART ONE

PART TWO: THE TRACKING EXPERIMENT

CHAPTER 7: EXPERIMENTAL PROCEDURES FOR THE TRACKING TASK

The Tracking Experiment was a tracking task using a time-invariant system; the instability level remained fixed during a single run. The purpose of this experiment was to develop a quasi-linear model of the human operator. By using a random appearing disturbance signal as an input to the system, and measuring the operator's output through the hand control, the operator's linear transfer function was estimated and compared for different field-of-view sizes. Once the linear transfer function had been calculated the subject's non-linear control response, or remnant, was found.

The purpose of the Tracking Experiment was to gather data which would model the human operator as a quasi-linear system. The linear component of the model gave specific information concerning the subject's control characteristics such as the subject's crossover frequency, phase margin, and gain and phase throughout the range of measurable frequencies. Once a linear model of the subject was formulated, the subject's remnant, or uncorrelated input, was modeled and compared for different fields-of-view. This experiment supplemented the information from the critical control experiment. The critical control experiment only provided information about the subject's time delay and accuracy of control. However, changes in these parameters did not indicate what the basic changes were in the subject's control response. An appropriate mathematical model can show the basic influence of field-of-view size on the subject's transfer function.

7.1 Implementation of the Tracking Experiment

The subject's control response to roll motion was expected to change for different field-of-view sizes. In order to analyze the subject's transfer function for a particular field-of-view the control element in the experiment was a time invariant system. This allowed the subject's transfer function to remain relatively constant over the period of time needed to collect the data.

The basic method used for analyzing the data was be the least squares fit of an output signal with an input signal. In this experiment the displayed roll angle was the input and the subject's control signal from the stick was the output. These signals were sampled at 15 Hz, the update rate of the task program. The least squares method provided a model of the subject transfer function.

With the program running at an update/sampling rate of 15 Hz, a minimum run time of 136.53 seconds for each separate test was chosen. This gave a total of 2048 datapoints for the input and output signals. The actual run time was 146.67 seconds, corresponding to 2200 datapoints which allowed for a buffer at the beginning of the test, where the subject could settle into a stable control state.

A forcing function was added to the system which appeared to the subject as an external disturbance. This disturbance signal was designed to simulate white noise in order to stimulate a wide range of frequency responses from the subject. If the disturbance signal were not added into the system, the subject's transfer function would be difficult to identify. The first order control element was of a lower order than the operator transfer function which was initially estimated

as a second order system. The subject would only respond to frequencies near the natural frequency of the closed-loop system, limiting the valid frequency range of the predicted transfer function [Ljung, personal communication].

The simulated white noise was created by summing thirteen sinusoids. The base run time of 136.53 seconds corresponded to a primary frequency of 0.04602 rad/sec. Each sinusoid making up the disturbance signal had a frequency which was a prime harmonic of the primary frequency, ω_o. The total disturbance signal had a power spectral density, approximated by the first order PSD function

$$\Phi(s) = \frac{K}{s + a}^2 \qquad (3.1)$$

Replacing s with $j\omega$ the PSD function had the form

$$\Phi(\omega) = \frac{K^2}{\omega^2 + a^2} \qquad (3.2)$$

The break frequency, a, indicated where the power density began to drop off, in this experiment $a = 0.5$ rad/sec. The phases of the sinusoids were set randomly. All parameters of the input signal are shown in appendix 7.1.

7.2 Equipment for the Tracking Experiment

The equipment for the Tracking Experiment was virtually the same as the equipment used for the Critical Control Experiment (see section 3). The graphics computer, the Expanded Field Display and the subject's

control input equipment was unchanged. One major element that was modified was the computer program for the Tracking Experiment.

The Tracking Experiment program was simpler than the Critical Control Experiment program. Since the lambda value was held constant the commands which monitored the average roll error of the display were not needed. One addition to the Tracking Experiment program was the forcing function. The forcing function was calculated before the tests as a discretized signal and placed in a separate data file. When the tracking task program ran its initialization process, it read this file and stored it in an array. The elements of this array were accessed in order each time the program passed through the control loop routine. When passing through the program loop, the current disturbance signal value was added to the roll angle which was calculated from the control equations. The resulting angle was used to display the computer generated image.

A low pass filter for attenuating high force stick frequencies was also implemented in the Tracking Experiment. Because the data was analyzed digitally care was taken to insure that the subject's stick output signal was suitable for analysis. The main concern was to remove high frequency components from the stick signal. The roll control program, which included the data sampling commands, ran at an update rate of 15 Hz, therefore frequencies above 7.5 Hz were filtered out since they could not be measured accurately. The analog stick signal was sent through a low pass filter, consisting of a simple RC circuit, with a break frequency of 3.8 Hz, before being converted to a digital signal and entering the computer.

7.3 Design of the Tracking Experiment

There were nine experimental cases for the tracking task experiment based on three instability levels and three fields-of-view. The three field-of-view sizes used for the tracking task were 10°, 40° and 120°. The 10° field stimulated only the central visual field, the 40° field stimulated a portion of the periphery and provided a much greater motion field than the 10° case, and the 120° field stimulated almost all of the peripheral visual field. All subjects ran tests for instability levels of $\lambda = 2.0$ and $\lambda = 3.0$. In addition, each subject ran a series of tests at an instability level that they could just barely control over the test run-time. These cases provided data that showed field-of-view to be more or less critical to performance depending on the difficulty of the task.

A trial was made up of one of each of these nine cases, and there were two trials per subject. A single test lasted two minutes and thirty seconds and the nine tests, including set-up time for each case, lasted approximately forty-five minutes. The subject was allowed to take a five-minute break during the trial.

7.4 Subjects for the Tracking Experiment

Subjects B and E from the Critical Control Experiment were used as the two subjects of the Tracking Experiment. These subjects had the most experience with the Critical Control Experiment where the objective was basically the same as the tracking task: to keep the displayed roll angle as close to 0° as possible. The set-up procedure was also similar

for both tasks. Subjects only needed a few practice runs to become used to the three primary differences; the tracking task lasts longer than the critical control task, two and a half minutes compared to less than fifty seconds; the tracking task had a forcing function acting as an input which was very noticeable at high instability levels; and the dynamics of the tracking task remain constant throughout the test. After both subjects completed ten practice trials they were ready to start the true experiments.

Both subjects were tested at instability levels of $\lambda = 2.0$, and $\lambda = 3.0$. The third instability level was set near to the highest value the subject could control over the run-time of the test. This highest level was determined by trial and error during the training period. Subject B had a maximum controllable instability level of 3.2 and subject E had a maximum controllable instability level of 4.0.

7.5 Conducting the Tracking Experiment

The equipment adjustment procedure for the Tracking Experiment was the same as the Critical Control Experiment. The experimenter gave the command to start the program, specified an output file to which the data was written and set the instability level through the keyboard. The subject adjusted the chair and the Expanded Field Display, the experimenter inserted the desired field-of-view masks which the subject positioned, and the experimenter then started the test.

The problem in the Critical Control Experiment with the computer accessing the hard disk during a run, was solved prior to the Tracking Experiment tests. A test was restarted only if the subject lost control

before the run-time was completed, or if the experimenter had set-up the incorrect case. Both of these situations happened twice during the whole experiment. Once a test was successfully completed, the experimenter exited from the program, saving the data, then restarted the program and set the parameters for the next case.

CHAPTER 8: DATA ANALYSIS OF THE TRACKING EXPERIMENT

8.1 Overview of the Data Analysis for the Tracking Experiment

The data analysis for the Tracking Experiment was designed to show how changes in the subject's field-of-view affected the control of the visually simulated aircraft roll motion. The data from the Tracking Experiment was used to mathematically model the subject's control response as a quasi-linear system. This quasi-linear system consisted of a linear transfer function plus a non-linear element which was uncorrelated with the subject's input signal.

Basic measurements produced by this data analysis are the subject's frequency response, crossover frequency, and remnant. The frequency response shows the magnitude and phase relation between the subject's input and output signals, for a range of frequencies. The crossover frequency indicates the stability of the subject/control element system. Remnant is the non-linear element of the subject's control response; remnant is generally considered to be white-noise, not correlated with the control of the system dynamics and, therefore, a contributor to the subject's control error [Levison, 1969].

The signals from various points of the closed-loop control system provided the raw data for the Tracking Experiment analysis. Figure 8.1 shows the closed-loop control system in which the subject was the active control element. The forcing function signal, r, was a quasi-random disturbance composed of thirteen sinusoids, each sinusoid having a frequency that was a primary multiple of the base frequency of the test. The displayed roll error, e, was the subject's input signal and the

control stick response, u, was the subject's output signal. The output of the control element, y, was summed with the forcing function to produce the displayed error. The only other signal that appears in figure 8.1 is the subject's remnant, n, which was assumed to be injected before the subject's linear transfer function.

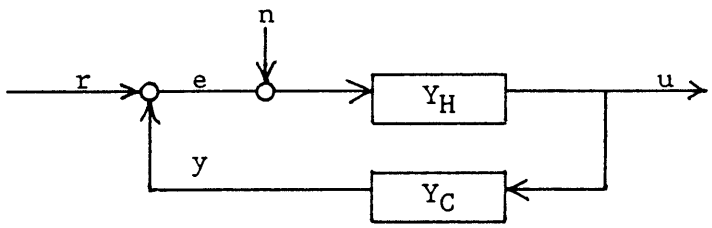

Figure 8.1: Closed-loop control system

Two methods were used to analyze the data from this experiment First, the least squares method of system identification provided the analysis on which the majority of the Tracking Experiment results were based. The least squares method is very versatile since it results in a parametric model for the human operator; numerical values were returned for the coefficients of the subject's transfer function. Once the parametric model was estimated it was very easy to predict other aspects of the subject's control response such as remnant and stability margins.

The least squares method has not been used extensively in past research for analyzing human operator control signals. Therefore, the second method, spectral analysis using the fast fourier transform used frequently in past human operator research, provided a comparison for the least squares data analysis. The fourier transform method does not return a parametric model so it was not as versatile as the least

squares method. However, it does measure directly the correlation between the subject's output and input signals.

8.2 Least Squares Method of System Identification

The least squares method identifies a human operator transfer function using only the input and output signals for the subject, and is based on the assumption that the subject can be modeled as a linear control element. The signals are arrays of numbers representing a constant frequency sample of the original signals. As figure 8.1 shows, the subject acts on the input signal 'e' to produce an output signal 'u'. The least squares method estimates the process which acted on 'e' to produce 'u'; the least squares method is not a procedure which finds the correlation between two signals. The result of the least squares method was a transfer function which produced the best fit of the two signals.

8.2.1 Implementation of the Least Squares Method

The least squares method of system identification was developed for use primarily with digital computers and is therefore a relatively new method for identifying a transfer function. The input and output signals that the least squares method uses must be discrete since the least squares method compares two arrays of numbers with each other. In the Tracking Experiment the two signals were sampled at a rate of 15 Hz, or 94.2 radians per second; the interval between samples, h, was 0.0667

seconds. This sampling frequency allowed the analysis of signal frequencies as high as 47.1 radians per second.

When the tests were run for the Tracking Experiment, 2200 data points were collected for each signal which corresponds to a test run time of 146.7 seconds. The first 100 data points were trimmed from each signal to avoid any subject transients which may have occurred at the beginning of the test. Also, the last 52 data points of each signal were trimmed away leaving a net signal length of 2048 points. The computer used for the least squares analysis did not have the capacity to operate on a signal this long so two least squares analyses were performed on each test: one for the first 1024 points and another for the second 1024 points. Since there were two separate tests for each experimental case, four sets of results were produced by the least squares analysis.

The relation between the input and output signals that the least squares method assumes is:

$$A\,u = B\,e + n \qquad 8.1\ (a)$$

A is a polynomial with coefficients a_1 to a_{na}

B is a polynomial with coefficients b1 to b_{nb}

n is a noise signal assumed to be the subject's remnant

Equation 8.1 can also be written as:

$$u = (B/A)\,e + (1/A)\,n \qquad 8.1\ (b)$$

B/A is the time domain transfer function which is analyzed in frequency domain.

Three initial parameters must be set when using the least squares method. The first two are the orders of the numerator and denominator polynomials of the transfer function. The third parameter was the value of the subject's time delay, which was specified as an integer multiple of the time step, h. The values for these three parameters were chosen based on past human operator research and the results of the Critical Control Experiment described in Part One of this report.

The Critical Control Experiment resulted in values for the subjects' effective time delay as a function of field-of-view size. These effective time delay values were used to determine the time delay for the Tracking Experiment; the integer multiple of the time step, h, which was closest to the effective time delay, was used in the Tracking Experiment Analysis.

Past human operator research has produced a number of operator transfer functions on which the orders of the transfer function polynomials, for the current research, are based. Jex, McDonnel and Phatak, 1966, use the 'precision model' for the human operator to analyze the data from their experiment. The control element dynamics for the Tracking Experiment of the current research are the same as those of the Jex experiment; the subject's control input device and his task are similar to the Jex experiment. Therefore, the precision model described by Jex was a good basis for the transfer function of the current research. The transfer function for the precision model is:

$$Y_{Ph} = \frac{K\, e^{-s\tau_e}\, (T_K s + 1)(T_L s + 1)}{(T_K' s + 1)(T_N s + 1)((s/\omega_N)^2 + (2\zeta_N/\omega_N)s + 1)} \qquad 8.2$$

K = gain

τ_e = effective time delay

T_K and T_K' = low frequency neuromuscular dynamics

T_L = mid frequency equalization parameter

T_N = closed-loop, neuro-muscular, viscous damping

ω_N and ζ_N = stiffness, inertia and damping of arm and control stick system

This function has a fourth order denominator and a second order numerator, however, some modifications were made to this model before it was implemented in the least squares analysis. The subject's mid-frequency response was considered to be the main area of interest since it was the range in which the stability margins of the open-loop system are determined. Therefore, the least squares analysis was not used to find the values for T_K and T_K'. This reduces the denominator and numerator to third and first order polynomials respectively.

Equation 8.2 was developed in the continuous time domain which uses the LaPlace transform variable s. The least squares analysis takes place in the discrete time domain. Transfer functions in the discrete time domain are transforms of the frequency variable z and are called z-transforms. The discrete time domain variable z is related to the continuous time domain variable s, by the equation:

$$z = e^{sT} \qquad 8.3$$

In order for equation 8.2 to work well in the discrete time domain, the effects of converting an equation from the continuous time domain to

the discrete time domain must be accounted for. The poles of a transfer function can be converted directly from one time domain to the other by simply using the bilinear transform:

$$s = \frac{2}{T}\,\frac{z - 1}{z + 1} \qquad 8.4$$

Furthermore, the order of the denominator polynomial remains the same when a transfer function is converted. No such general rule holds for the zeros of the transfer function. The zeros can be estimated by substituting a linear function of for the frequency variable, but the order of the numerator polynomial often changes when the conversion is made from one time domain to the other.

In light of the discussion above, the discrete time domain transfer function chosen for the least squares analysis had the form:

$$Y_h = \left[\frac{b_1 + b_2 z^{-1} + b_3 z^{-2}}{1 + a_1 z^{-1} + a_2 z^{-2} + a_3 z^{-3}}\right] z^{-n_k} \qquad 8.5$$

b_1, b_2 and b_3 are coefficients of the numerator polynomial.

a_1, a_2 and a_3 are coefficients of the denominator polynomial.

n_k is an integer number of time steps, h, in the time delay.

8.2.2 Frequency Response from the Least Squares Method

Once the subject's transfer function has been found, the frequency response of the subject can be easily calculated by measuring the magnitude and the phase of the transfer function for the desired range

of frequencies. The magnitude and phase can be displayed with a bode plot and the values at any frequency can be found since the transfer function is valid for a continuous range of frequencies. The predicted transfer functions can show how the subject's gain and phase are dependent on the field-of-view size.

8.2.3 Crossover Frequency and Phase Margin

Analysis of the open-loop crossover frequency and phase margin can indicate the frequency range in which the subject effectively controls the system dynamics and the relative stability of the closed-loop system. Variations in the crossover frequency or the phase margin due to changes in the field-of-view size, would indicate significant effects of field-of-view on subject performance.

The stability of the closed-loop system depends on the frequency response of the open-loop transfer function $Y_h Y_c$. The closed-loop system is unstable if the output signal 'y' is reinforced, rather than attenuated. One way the signal 'y' is reinforced is if the gain of the open-loop system is greater than unity when the phase drops below 180°. This is the principle on which the crossover frequency is based.

The crossover frequency is defined as the frequency where the gain of the open-loop system drops to unity. For this bandwidth of frequencies the subject responds efficiently to the system dynamics by attenuating the system error.

The phase margin measures the stability of the closed-loop system and is defined in terms of the crossover frequency, ω_c:

$$\text{phase margin} = \text{phase}(Y_h Y_c(\omega_c)) - 180°$$

The closer the open-loop phase is to 180° at this frequency, the closer the system is to becoming unstable. Therefore, a greater phase margin indicates a more stable closed-loop system.

8.2.4 Human Operator Remnant

For the least squares data analysis the subject's remnant was defined as the component of the subject's output signal, u, that cannot be predicted by the subject's linear transfer function. The remnant predicted by the least squares method was approximately white noise which acts to disturb the closed-loop system, increasing the roll error. Remnant is usually describe by a power spectral density curve, or the integrated power of the remnant signal, n. An increase in the remnant power due to a change in the field-of-view size would indicate decrease in the subject's performance.

In order to analyze the subject's remnant signal, the signal's relation to the rest of the transfer function must be understood. For the current research remnant will be modeled as a noise signal that was injected into the display error (see figure 8.1). In other words, the subject's remnant was caused by inaccuracies in estimating the visual roll motion, not by central nervous system processing or by neuromuscular dynamics [Levison, Baron and Kleinman, 1969].

Figure 8.2 shows the injection point of the noise signal, n', which was modeled by the least squares method (see equation 8.1 (b)). The noise signal, n', was calculated simply by filtering the subject's input

signal, e, through the transfer function determined in section 8.2.1 to produce a noise free output signal, u', u' was then compared to the actual subject output signal, u, to determine n'. However, the noise signal produced by the least squares method, n', was not the same as the remnant, n, which is shown in figure 8.1 since they differ in their point of injection.

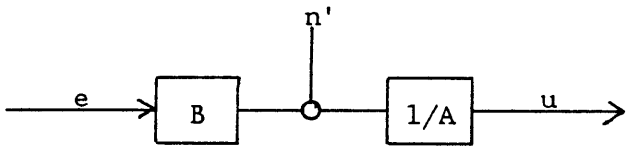

Figure 8.2: Noise injection point for least squares human operator model

Figure 8.2 indicates that the signal, n', can be converted to the corresponding signal, n, by filtering n' through the transfer function 1/B. Care must be taken when filtering n' through 1/B; the roots of B are the zeros of the transfer function, B/A, and may be unstable when used as poles in the transfer function 1/B. If the noise signal, n', is filtered through an unstable transfer function it will not produce a reasonable remnant, n.

To solve this problem any unstable roots of the polynomial B are converted to stable roots, producing a polynomial B'. This conversion is best visualized in the Laplace transform domain. An unstable pole will lie in the right-half-plane having a positive real component. To make this root stable, it was reflected to the left-half-plane so that its real component was negative; the imaginary component remains unchanged. The reflection of the pole into the left-half-plane will

affect the phase but not the gain of the frequency response of 1/B' compared to 1/B. Since the remnant power was not dependent on the phase of the signal, the power spectrum and the integrated power will not be affected by the conversion of the polynomial B.

The procedure stated above results in a time-domain, remnant signal, n, which enters the system as an addition to the display error, e. Once the remnant signal was calculated its power spectrum was found using the formula:

$$P(n) = fft(n) * conj(fft(n)) / n_t \qquad 8.6$$

fft is the fast fourier transform operation

conj is the complex conjugate operation

nt is the number of discrete points in the signal

The resulting power spectrum gives the signal power at discrete frequencies ranging from $2\pi/(hn_t)$ to $\pi/(h)$ radians per second. The frequency interval between discrete values was $2\pi/(hn_t)$. This power spectrum was very noisy so an averaging method was used which gives signal powers for a number of selected frequencies. The selected frequencies are the same thirteen, primary frequencies that make up the forcing function, r. The averaged power density at a primary frequency was found by averaging the power density values for the three points immediately above and the three points immediately below the primary frequency in question. Once the power densities at the thirteen primary frequencies are found they can be summed to produce an estimate of the total integrated power in the remnant signal.

8.3 Human Operator Analysis Using the Fast Fourier Transform

A single fast fourier transform (FFT) analysis will be performed for each individual test. This will produce to sets of data for each experimental case. As for the least squares method, the signals were all trimmed to 2048 data points. The FFT analysis worked better when using all 2048 datapoints compared to using only 1024 datapoints as in the least squares method. The reason the FFT worked best with 2048 points was that the forcing function, r, was made of sinusoids each with a period that was a primary factor of the base period. The base period for the Tracking Experiment was set to correspond to 2048 datapoints when the experiment was planned.

8.3.1 Frequency Response Based on the Fast Fourier Transform

The FFT method calculates the subject's frequency response directly without modeling a parametric transfer function. The FFT method uses the time sampled signals, r, u and e as the raw data for the analysis of the human operator's control response. The FFT method produces a non-parametric transfer function, Y_h, which was an array of complex numbers, representing the subject's frequency response for a range of discrete frequencies.

$$Y_h = \Phi_{ru} / \Phi_{re} \qquad 8.7$$

Φ_{ru} = fft(u) * conj(fft(r)) / n_t

this is the cross-power spectral density of r and u.

Φ_{re} = fft(e) * conj(fft(r)) / n_t

this is the cross-power spectral density of r and e.

The magnitudes of the elements in Y_h are the gains of the transfer function at the discrete frequencies and the angles described by the elements of Y_h are the phases of the transfer function at the discrete frequencies. Due to the characteristics of the FFT analysis, the values of transfer function, Y_h, are only valid at the primary frequencies that are contained in the forcing function, r. Therefore, the results that the FFT method produces are the gain and phase of the subject at thirteen discrete frequencies [Sheridan, 1974].

8.3.2 Remnant Analysis Based on the Fast Fourier Transform

Levison, Baron and Kleinman, 1969, provide the method of subject remnant analysis that was used in conjunction with the FFT method. Levison defines operator remnant as the component of the subject's output, u, that is not correlated with the forcing function, r. This is different from the least squares remnant analysis described in section 8.2.4. The least squares remnant is defined as the component of the signal, u, that cannot be predicted by the subject's linear transfer function. The two separate analysis methods, FFT and least squares, cannot be manipulated to produce compatible remnant models. However, the results can still be compared in light of the difference between the two methods.

Levison, et al, 1969, starts by separating the power spectrum of the signal, u, into a component due to the forcing function, r, and a non-correlated component:

$$\Phi_{uu} = \Phi_{ur} + \Phi_{un} \qquad 8.9$$

Φ_{uu} is the power spectral density of the signal u

Φ_{ur} is the component correlated with the forcing function

Φ_{un} is the uncorrelated component due to the remnant

The relations between signals in the closed-loop system can be used to predict a remnant power spectrum, Φ_{nn}, for the remnant when it is modeled as a disturbance added to the display error, e.

$$\Phi_{nn} = (\Phi_{un} / \Phi_{ur}) * \Phi_{rr} \qquad 8.10$$

Φ_{rr} is the power spectral density of the forcing function

The remnant power spectral density was only valid at the frequencies contained in the forcing function. Therefore, this method of analyzing operator remnant will produce remnant power values for thirteen discrete frequencies.

CHAPTER 9: RESULTS OF THE TRACKING EXPERIMENT

The Tracking Experiment is designed to produce a quasi-linear model of the human operator. This quasi-linear model will show how the control response of the subject is affected by changes in the field-of-view of the visual display. Three areas of subject control response studied in the current research are: the subject's frequency response, the subject's crossover frequency and phase margin, and the subject's remnant. Frequency response, crossover frequency and phase margin describe the linear element of the subject's control response; the remnant describes the non-linear element.

Results for the Tracking Experiment are obtained by two separate methods of data analysis: the least squares method and the fast fourier transform method. The least squares method was relied upon to produce the primary results for this experiment and any statistical conclusions are based on results from the this method. The FFT method was used to corroborate the least squares method whenever a comparison was feasible. Results from the least squares method and the FFT method are presented for the frequency response data and for the remnant data. The FFT method was not used to analyze the crossover frequency or phase margin since it does not produce numerical values for gain or phase over a continuous range of frequencies.

The Tracking Experiment consisted of nine experimental cases. These nine cases were formed by the combination of three field-of-view sizes (10°, 40° and 120°) and three instability levels, lambda (2.0, 3.0 and 4.0). Since the object of this experiment is to show how field-of-

view affects the manual control of roll motion, comparisons will be made primarily between field-of-view sizes, within a set value for lambda.

The results of the Tracking Experiment are presented for subject B only. Data was also collected and analyzed for subject A but those results are not presented primarily to avoid the confusion of too many plots. Subject B had the most experience in the Critical Control Experiment as well as the Tracking Experiment and could explain his RMS roll error and time constant values being generally lower than the other subjects. However, the general trends for subject B in the Critical Control Experiment are similar to those of the other subjects and are not unusual in any obvious way. Therefore, subject B was considered a well trained but typical candidate for the Tracking Experiment.

Section 9.1 presents the frequency response results of the Tracking Experiment. Frequency responses resulting from the least squares method are presented for two example cases. The average values of the least squares transfer functions for two typical cases are plotted along with the values obtained by the FFT method to show practical differences between the two methods. A statistical comparison is then made between field-of-view sizes for a given value of lambda. Section 9.2 presents a statistical comparison of the crossover frequencies and phase margins for each case. Finally, section 9.3 presents the subject's remnant results. The power spectrum for both the least squares method results and the FFT method results are plotted for an example case. A final plot makes a statistical comparison between integrated power values obtained from the least squares method.

9.1 Frequency Response of the Human Operator

The frequency response of the subject is shown with a bode plot which breaks the subject's response into gain and phase. A typical response for this type of task will show a gain slightly above one for the low to mid frequencies, a peak which is caused by the natural frequency of the neuro-muscular and control stick dynamics, and then a rapid fall off in the high frequency range. The phase plot will generally start a 0° phase lag and then drop rapidly around the natural frequency due to the normal out-of-phase, high frequency response and the subject's time delay.

Changes in the frequency response that are relevant to a subject's level of performance are differences in the mid-frequency gain and differences in the phase lag. Higher gain generally means the subject is more sure of his response and therefore able to give a stronger output signal. Less phase lag means the subject can respond to a given frequency at an earlier point in the cycle, therefore having more effective control.

9.1.1 Frequency Response for Each Experimental Case

Bode plots showing the frequency response for two example cases are presented in figures 9.1 (a) and (b). Four frequency response curves, resulting from the four least squares models determined for each case, are superimposed on each plot. These figures show that the frequency response curves, both for gain and phase, are consistent for each experimental case. Figure 9.1 (b) shows the case with the most

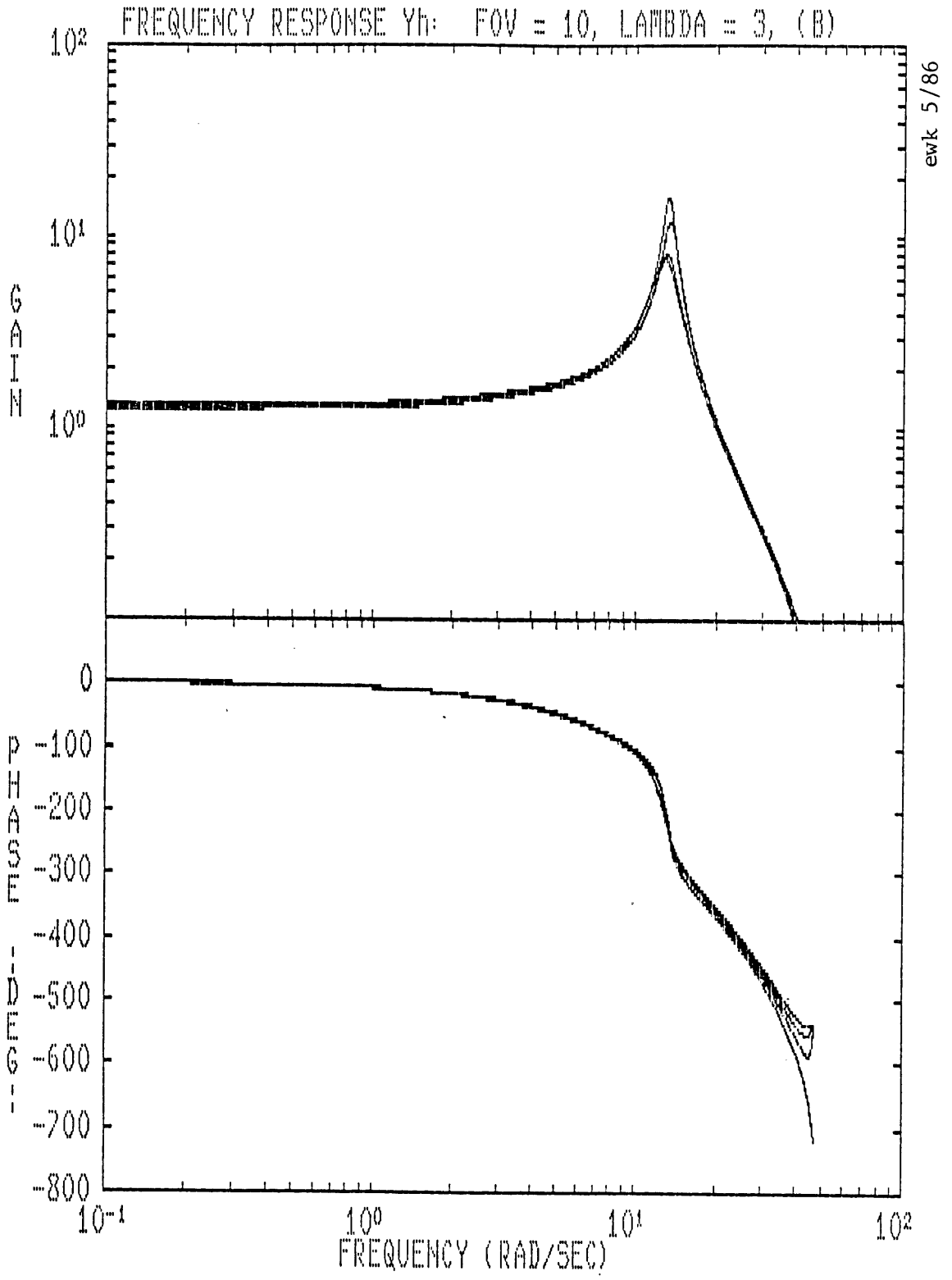
FREQUENCY RESPONSE Yh: FOV = 10, LAMBDA = 3, (B)
ewk 5/86
GAIN
PHASE -- DEG --
FREQUENCY (RAD/SEC)
10²
10¹
10⁰
0
-100
-200
-300
-400
-500
-600
-700
-800
10⁻¹
10⁰
10¹
10²

Figure 9.1 (a)

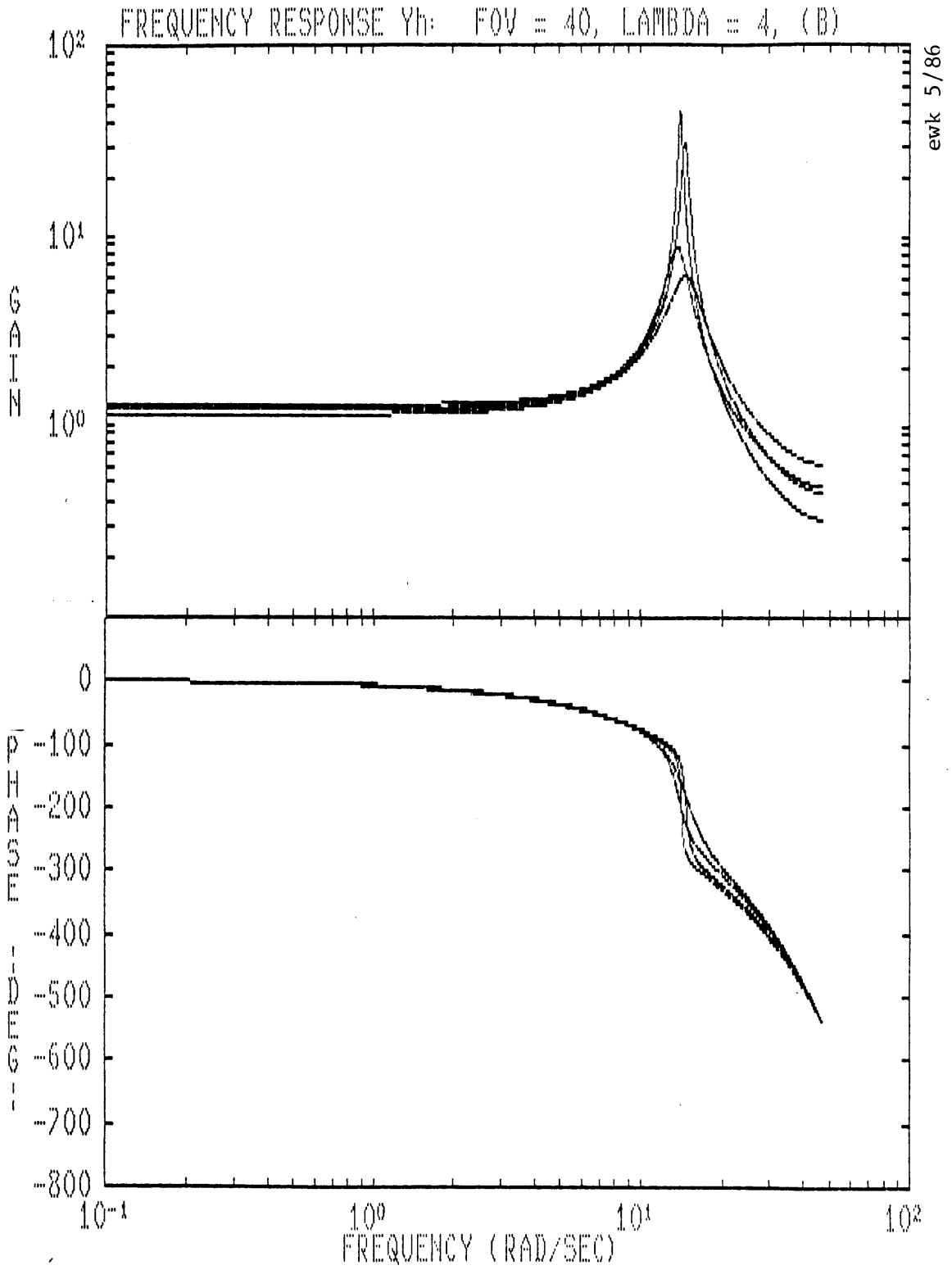
FREQUENCY RESPONSE Yh: FOV = 40, LAMBDA = 4, (B)
ewk 5/86
GAIN
PHASE (DEG)
FREQUENCY (RAD/SEC)
10²
10¹
10⁰
0
-100
-200
-300
-400
-500
-600
-700
-800
10⁻¹
10⁰
10¹
10²

Figure 9.1 (b)

variability between individual curves. The most obvious differences are the heights of the resonant peaks and the high frequency values for the transfer function gain. For all plots there is little difference in the natural frequency or the low frequency gain. Bode plots for all nine experimental cases are shown in appendix 9.1.

9.1.2 Comparison of the Least Squares and the FFT Transfer Functions

The four separate transfer functions, produced by the least squares method, are averaged and plotted for each experimental case. Superimposed on the plots are the FFT values for the transfer function that were obtained from two individual tests. Figures 9.2 (a) and (b) show examples of the best and worst cases of correlation between the least squares and FFT methods. The rest of the figures are contained in appendix 9.2. The comparison shows a very good correlation between the two methods with a couple notable differences. The FFT method shows a slightly higher gain at the lowest measured frequencies while the least squares method does not. This increase in the low frequency gain is due to the low frequency neuro-muscular dynamics which, as stated in section 8.2.1 were not implemented in the least squares analysis. Another difference between the two methods is that the FFT method shows slightly more phase lag in the high frequency range. This may be due to the limited choice of the time delay used in the least squares method.

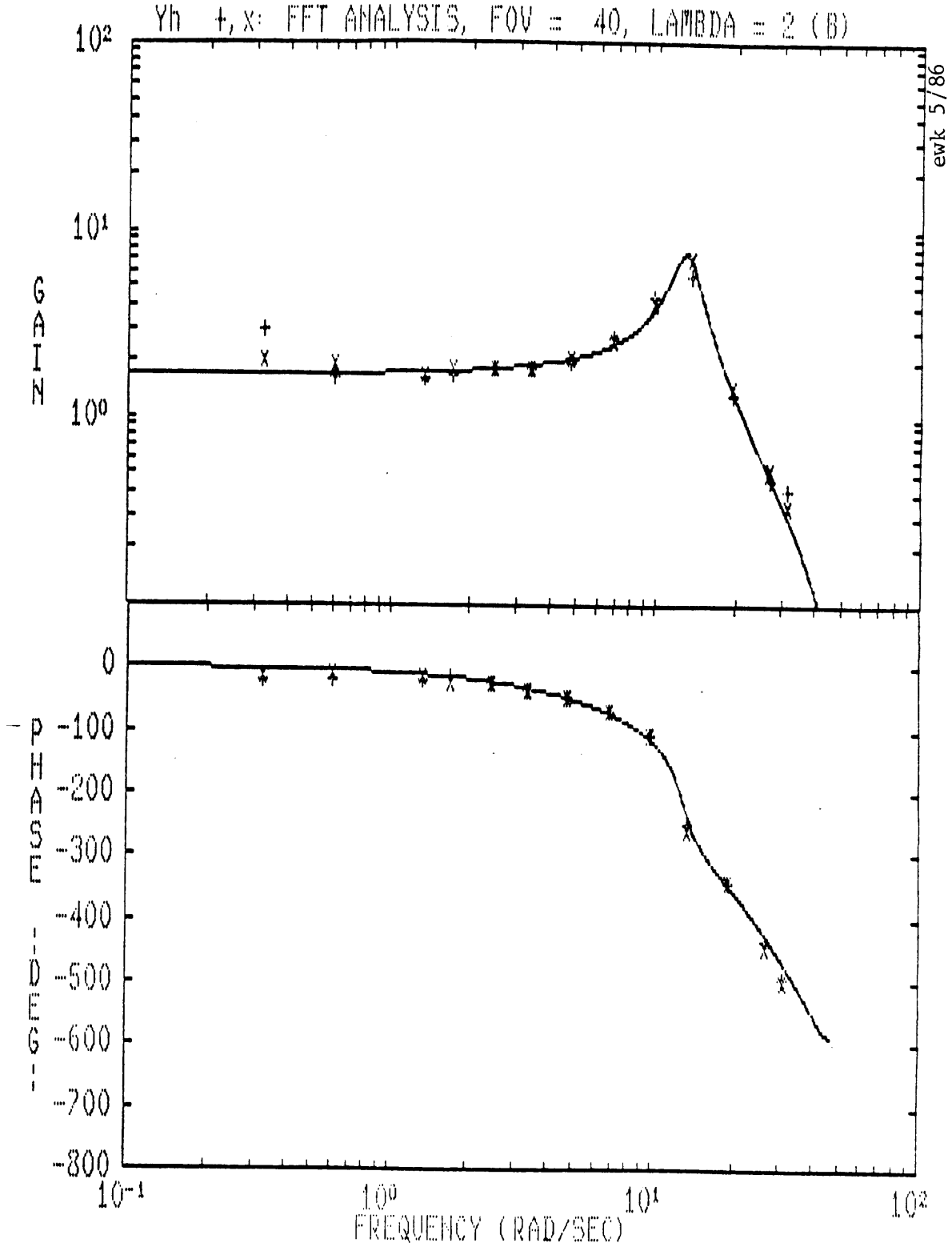
Yh +,x: FFT ANALYSIS, FOV = 40, LAMBDA = 2 (B)
ewk 5/86
GAIN
10^2
10^1
10^0
PHASE - DEG
0
-100
-200
-300
-400
-500
-600
-700
-800
10^{-1}
10^0
10^1
10^2
FREQUENCY (RAD/SEC)

Figure 9.2 (a)

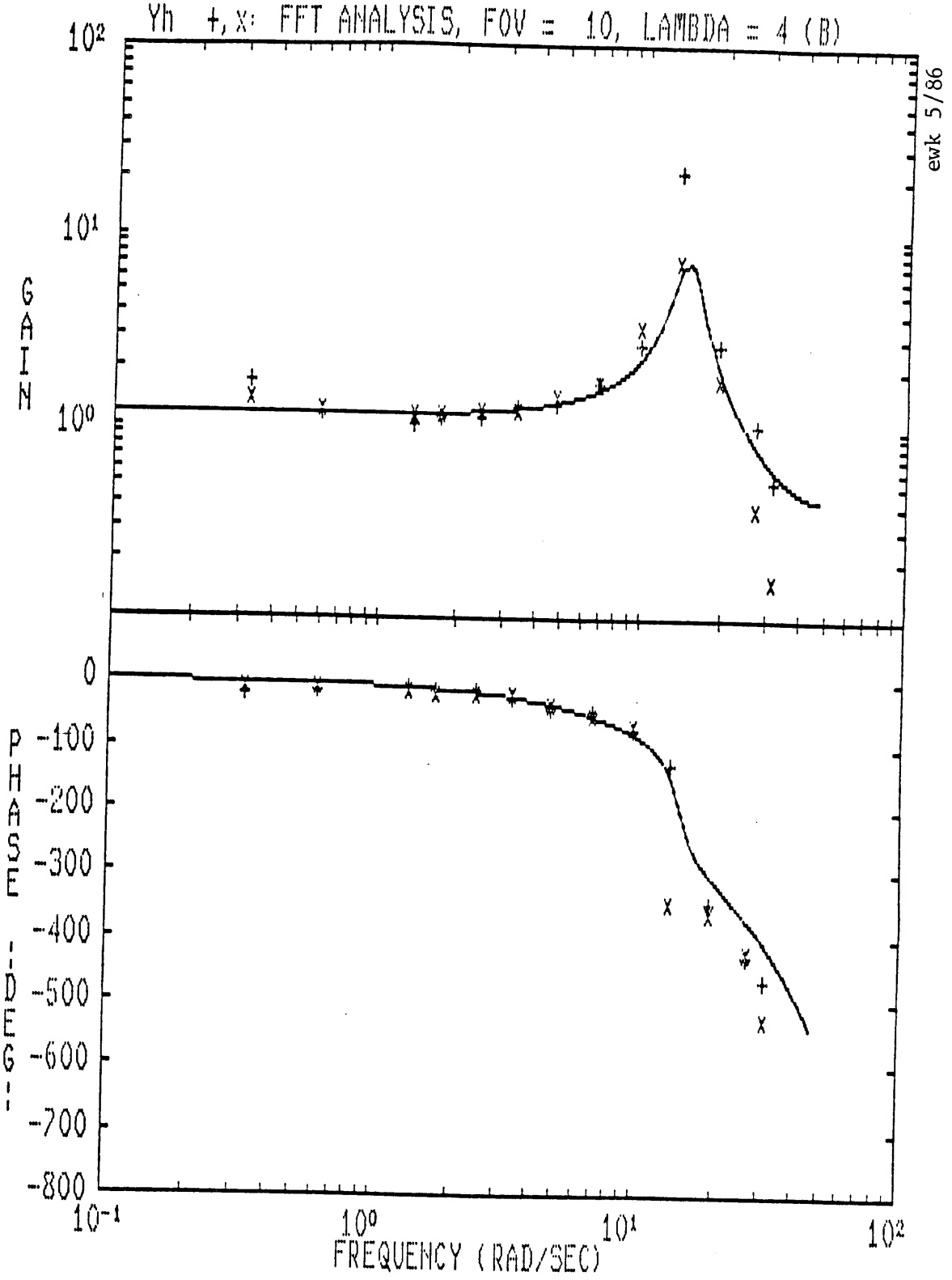
Yh +,x: FFT ANALYSIS, FOV = 10, LAMBDA = 4 (B)
ewk 5/86
GAIN
PHASE --DEG--
FREQUENCY (RAD/SEC)
10²
10¹
10⁰
0
-100
-200
-300
-400
-500
-600
-700
-800
10⁻¹
10⁰
10¹
10²

Figure 9.2 (b)

9.1.3 Effect of Field-of-View on Frequency Response

Three sets of figures, 9.3, 9.4 and 9.5, show the effect of field-of-view on the subject's gain and phase for the three instability levels, 2.0, 3.0 and 4.0 respectively. The (a) figures within each set compare the 10° and 40° field-of-view sizes, the (b) figures compare the 40° and 120° field-of-view sizes and the (c) figures compare the 120° and 10° field-of-view sizes.

Although these figures show the results of the least squares analysis, which predicts a transfer function for a continuous range of frequencies, only thirteen frequencies are shown. The thirteen frequencies shown correspond to the primary frequencies contained in the forcing function, r. Other frequencies could have been shown as well, however, these thirteen frequencies provide a well spaced set of points with which the curves can be compared.

Two symbols, a square and a triangle, are used to represent the two curves that are being compared. The square always represents the first field-of-view size listed at the top of the figure. These symbols represent the mean of the four separate curves that were found for each experimental case. If there is a significant difference between the two curves at a given frequency, an arrow is used to indicate the corresponding points. A single plus sign (+) above the arrow indicates a 95% confidence level that the value corresponding to the square is higher than the value corresponding to the triangle. Two plus signs indicate a 99% confidence level. Minus signs (-) are used if the value represented by the square is lower than the value represented by the triangle. Most

of the significant differences in the mid-frequency range were on the order of 1 db for gain and 5° for phase.

Figures 9.3 (a) to (c) show how field-of-view size affects the subject's transfer function for an instability level of 2.0. The general result is that the 40° and 120° cases provide significant advantages over the 10° case, while there is little difference between 40° and 120°. The phase lag of the 10° case is significantly greater than the phase lag in the two other cases for the mid to high frequency range. The gain of the 10° case is also less than the other two cases for several points in the mid frequency range. Significant differences in gain between the 120° and 10° cases suggest that the subject's natural frequency is greater for the 120° case than for the 10° case.

Figures 9.4 (a) to (c) show the effect of field-of-view size on the subject's transfer function, for an instability level of 3.0. The 40° case shows significantly better performance over the 10° case and the 120° case. The 120° case shows slightly better performance than the 10° case. The 40° case has greater gain and less phases lag than both the 10° and 120° cases, throughout the mid and high frequency ranges. The comparison of 120° with 10° shows a greater gain for the 120° case at low frequencies though it also has greater phase lag. High frequency range phase lag is greater for the 10° case than the 120° case.

Figures 9.5 (a) to (c) show there is little frequency response difference for 10° vs. 40° or 40° vs. 120°. A comparison of 120° with 10° shows the 120° case to have significantly greater gain in the mid frequency range and a trend to have less phase lag throughout the low and mid frequency ranges. The 40° case has greater phase lag than the 120° case in the low frequency range.

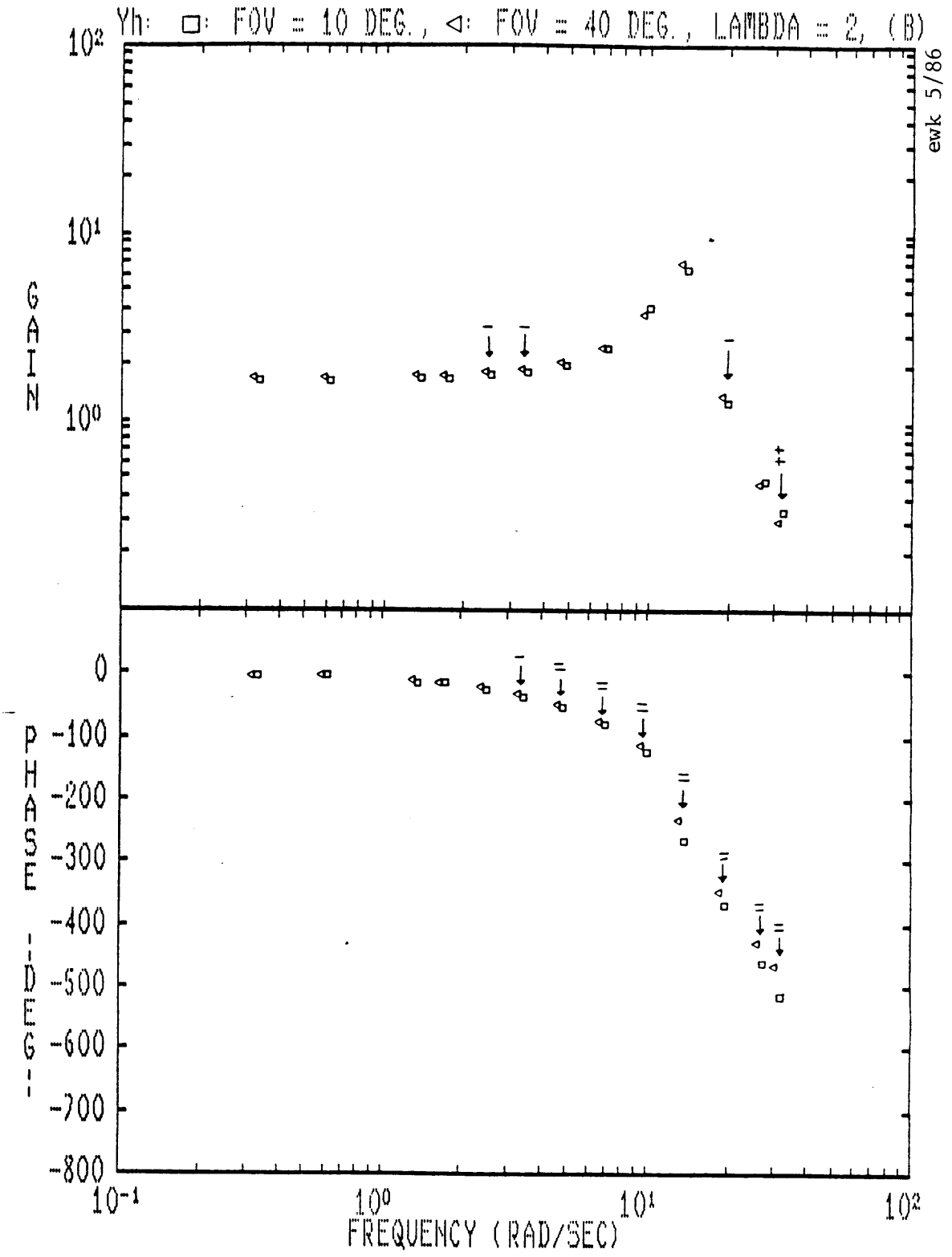
Yh: □: FOV = 10 DEG., ◁: FOV = 40 DEG., LAMBDA = 2, (B)
ewk 5/86
GAIN
PHASE --DEG--
FREQUENCY (RAD/SEC)
10²
10¹
10⁰
0
-100
-200
-300
-400
-500
-600
-700
-800
10⁻¹
10⁰
10¹
10²

Figure 9.3 (a)

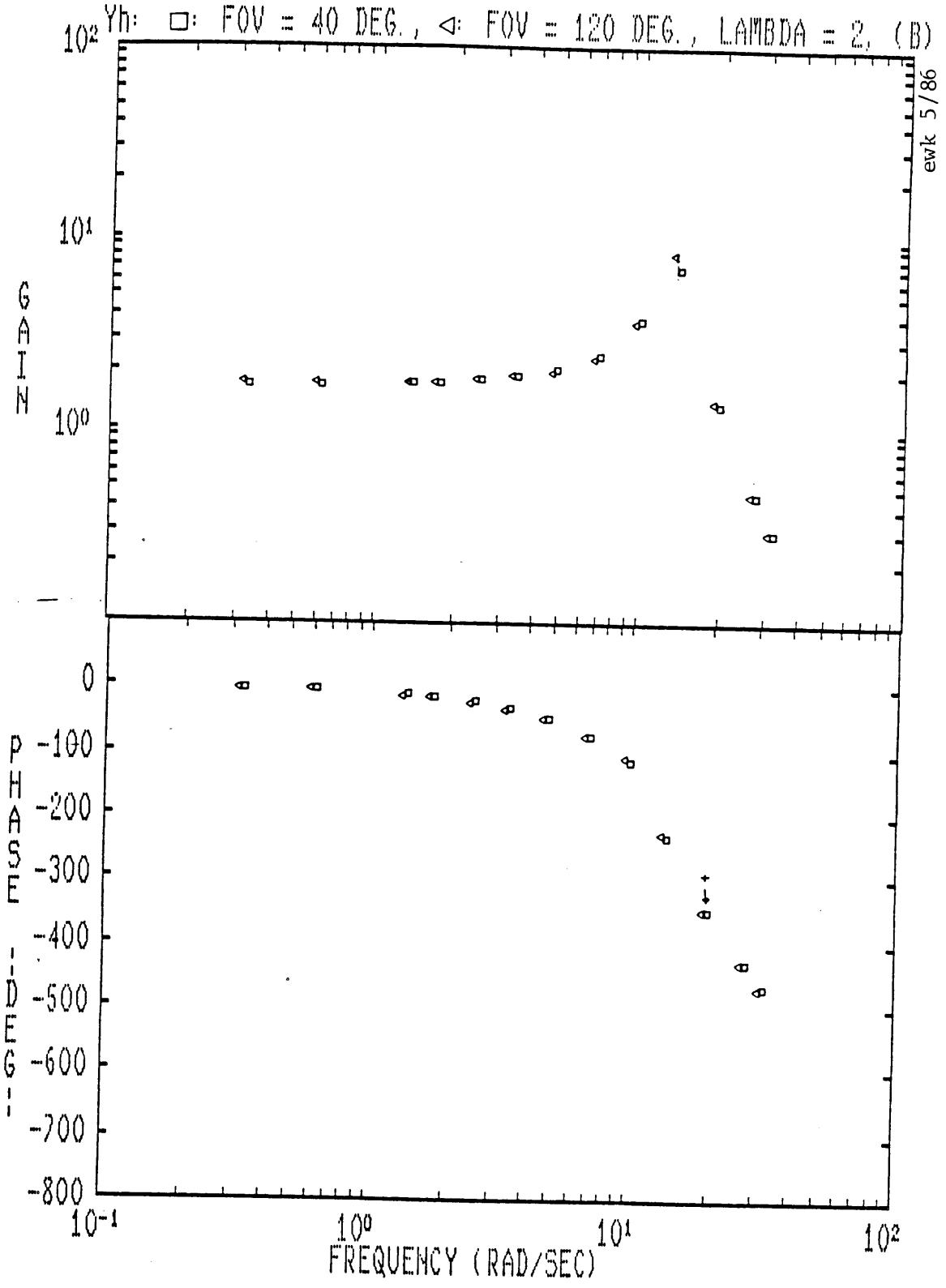
Yh: □: FOV = 40 DEG., ◁: FOV = 120 DEG., LAMBDA = 2. (B)
ewk 5/86
GAIN
10^2
10^1
10^0
PHASE --DEG--
0
-100
-200
-300
-400
-500
-600
-700
-800
10^{-1}
10^0
10^1
10^2
FREQUENCY (RAD/SEC)

Figure 9.3 (b)

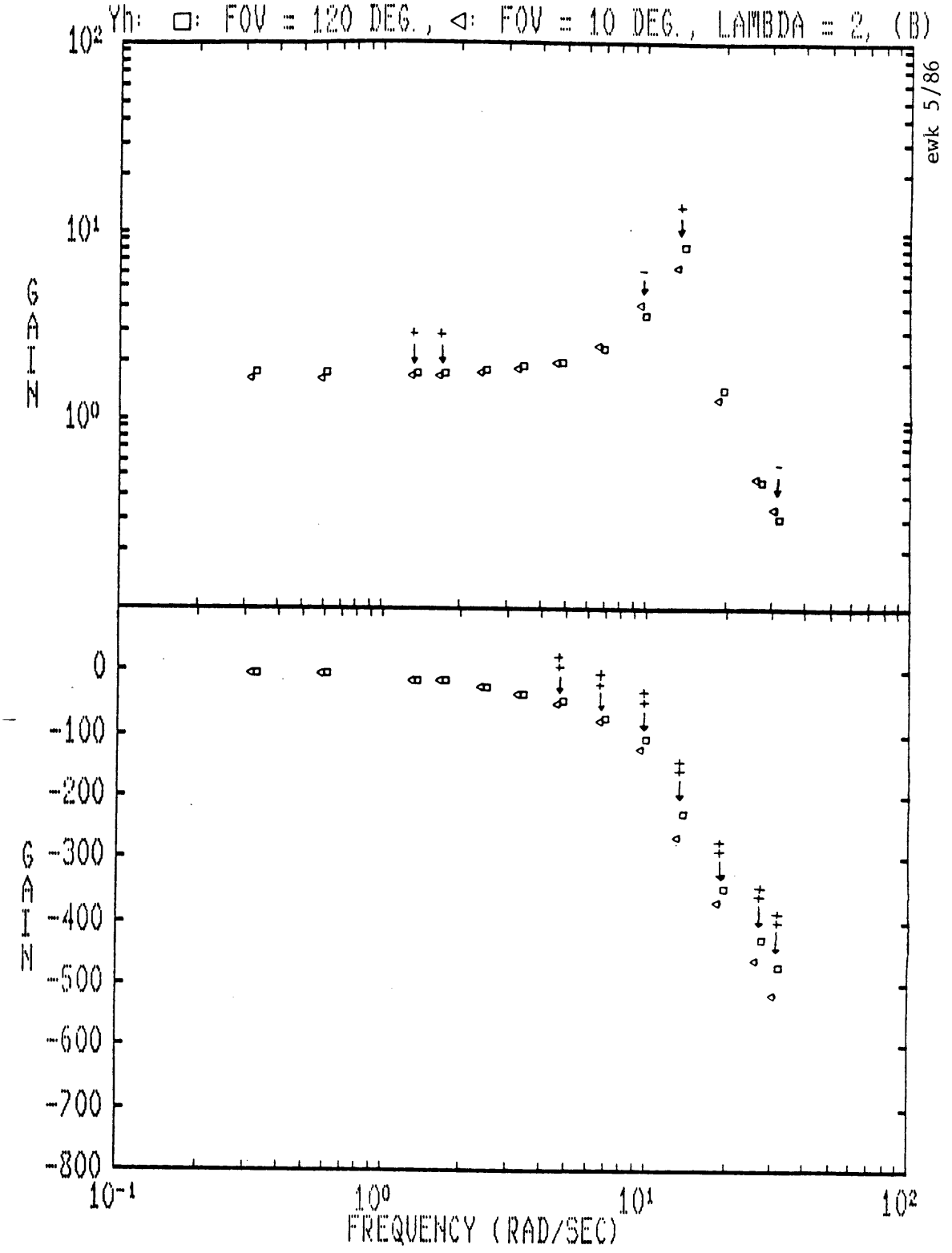
Yh: □: FOV = 120 DEG., △: FOV = 10 DEG., LAMBDA = 2, (B)
ewk 5/86
GAIN
10^2
10^1
10^0
0
-100
-200
-300
-400
-500
-600
-700
-800
10^{-1}
10^0
10^1
10^2
FREQUENCY (RAD/SEC)

Figure 9.3 (c)

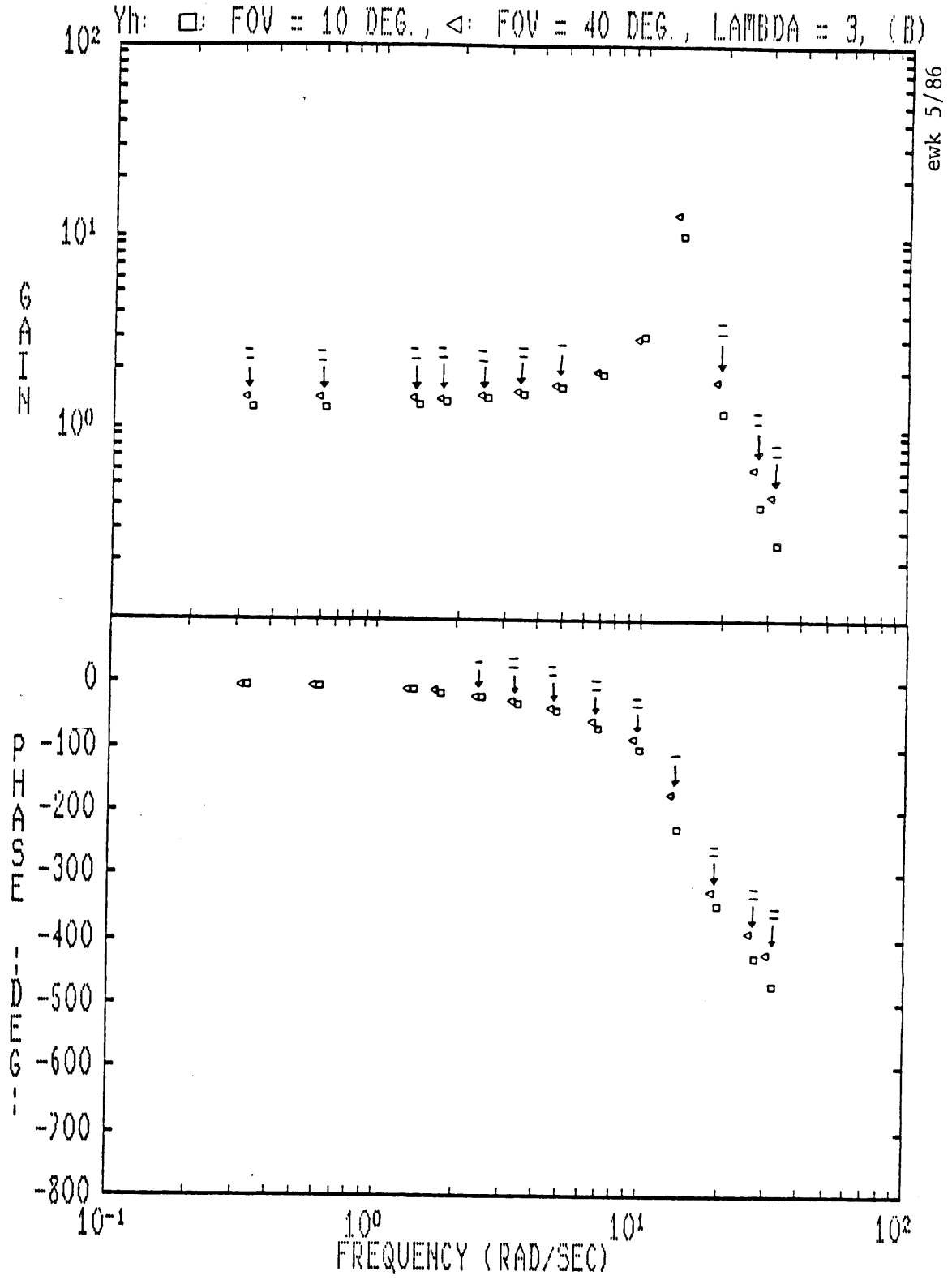
Yh: □: FOV = 10 DEG., ◁: FOV = 40 DEG., LAMBDA = 3, (B)
ewk 5/86
GAIN
PHASE --DEG--
FREQUENCY (RAD/SEC)

Figure 9.4 (a)

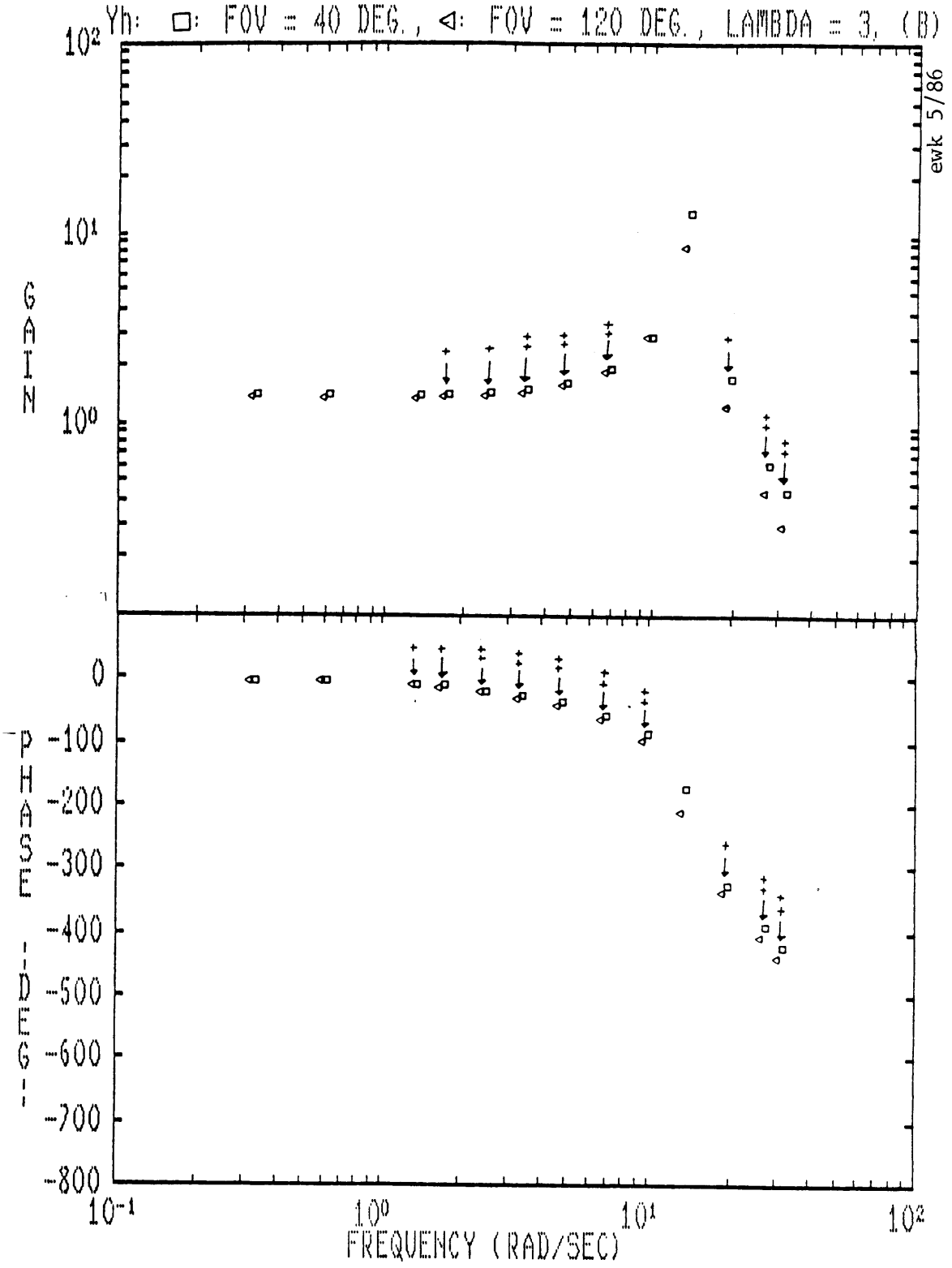
Yh: □: FOV = 40 DEG., ◁: FOV = 120 DEG., LAMBDA = 3. (B)
ewk 5/86
GAIN
PHASE --DEG--
FREQUENCY (RAD/SEC)
10²
10¹
10⁰
10⁻¹
0
-100
-200
-300
-400
-500
-600
-700
-800

Figure 9.4 (b)

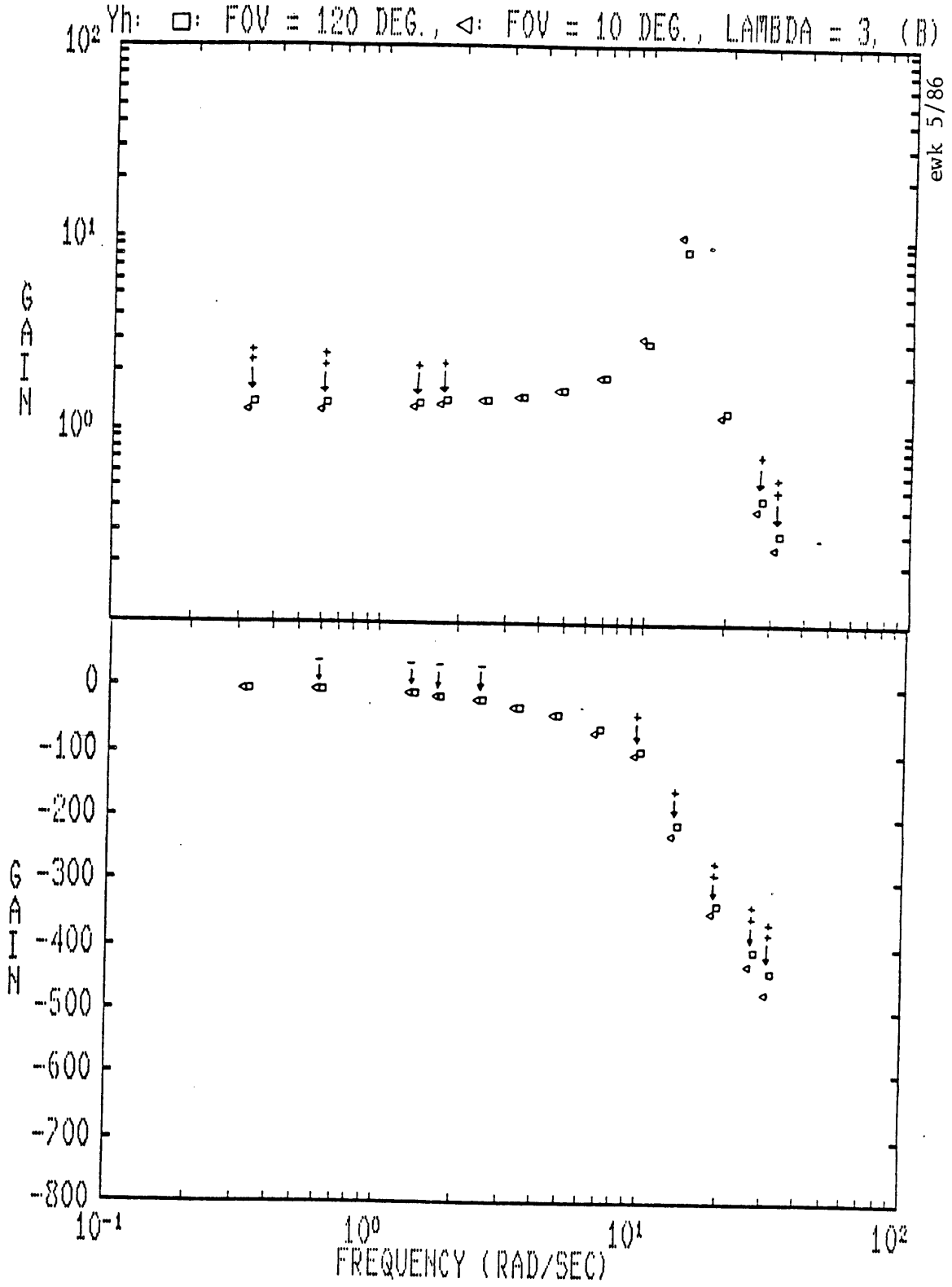
Yh: □: FOV = 120 DEG., △: FOV = 10 DEG., LAMBDA = 3, (B)
ewk 5/86
GAIN
10^2
10^1
10^0
0
-100
-200
-300
-400
-500
-600
-700
-800
10^{-1}
10^0
10^1
10^2
FREQUENCY (RAD/SEC)

Figure 9.4 (c)

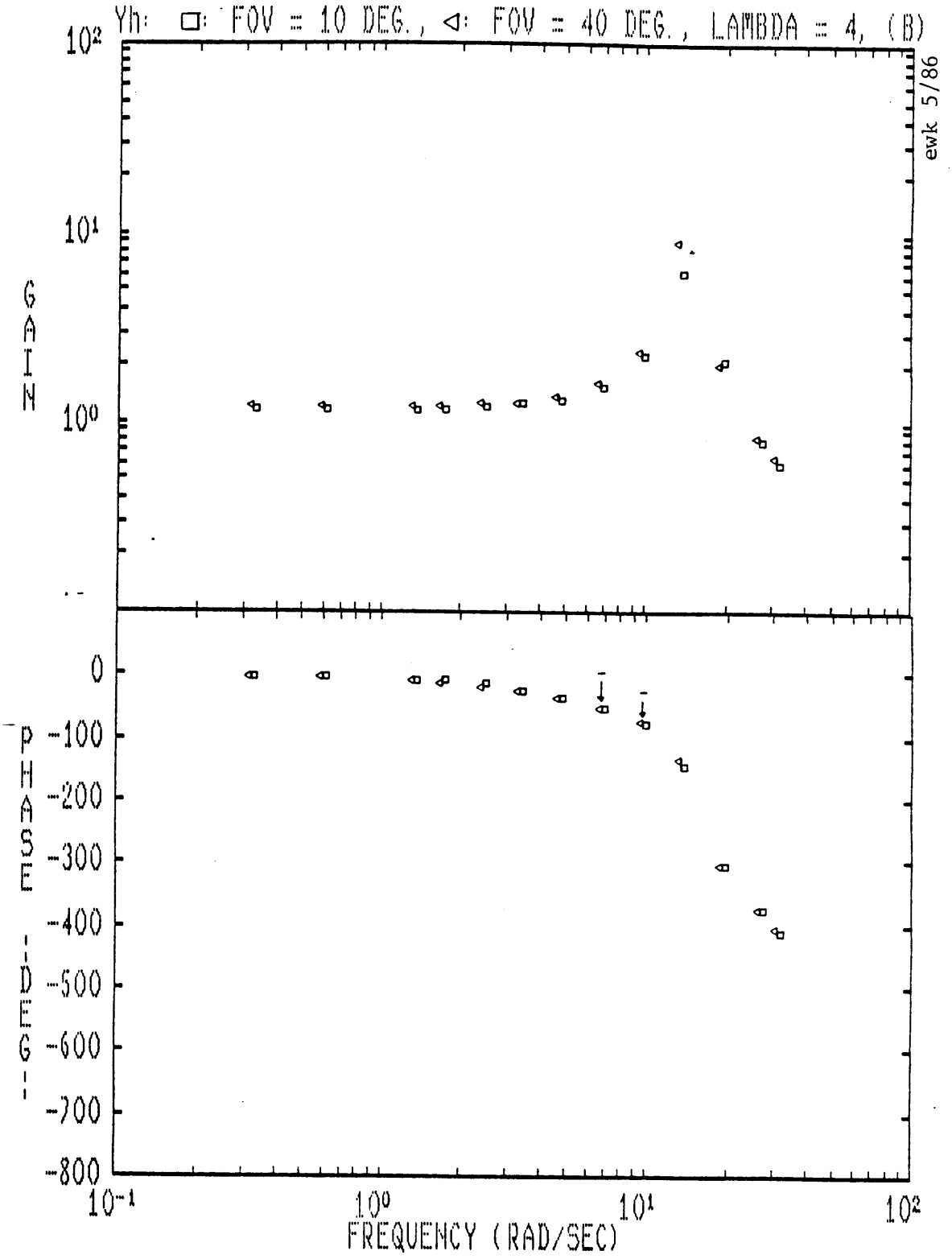
Yh: □: FOV = 10 DEG., ◁: FOV = 40 DEG., LAMBDA = 4, (B)
ewk 5/86
GAIN
PHASE --DEG--
FREQUENCY (RAD/SEC)
10²
10¹
10⁰
0
-100
-200
-300
-400
-500
-600
-700
-800
10⁻¹
10⁰
10¹
10²

Figure 9.5 (a)

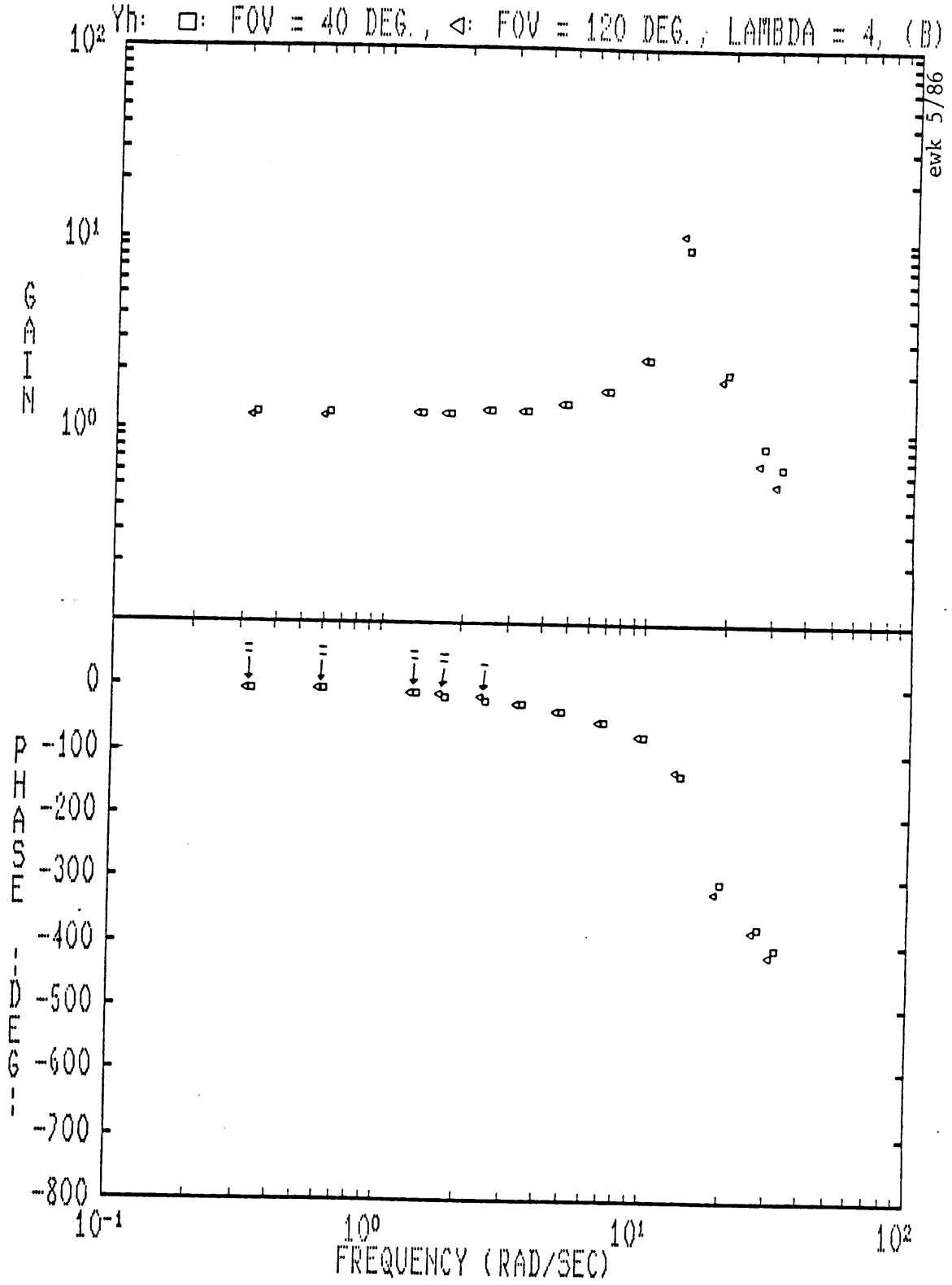
Yh: □: FOV = 40 DEG., ◁: FOV = 120 DEG., LAMBDA = 4, (B)
ewk 5/86
GAIN
PHASE -- DEG --
FREQUENCY (RAD/SEC)

Figure 9.5 (b)

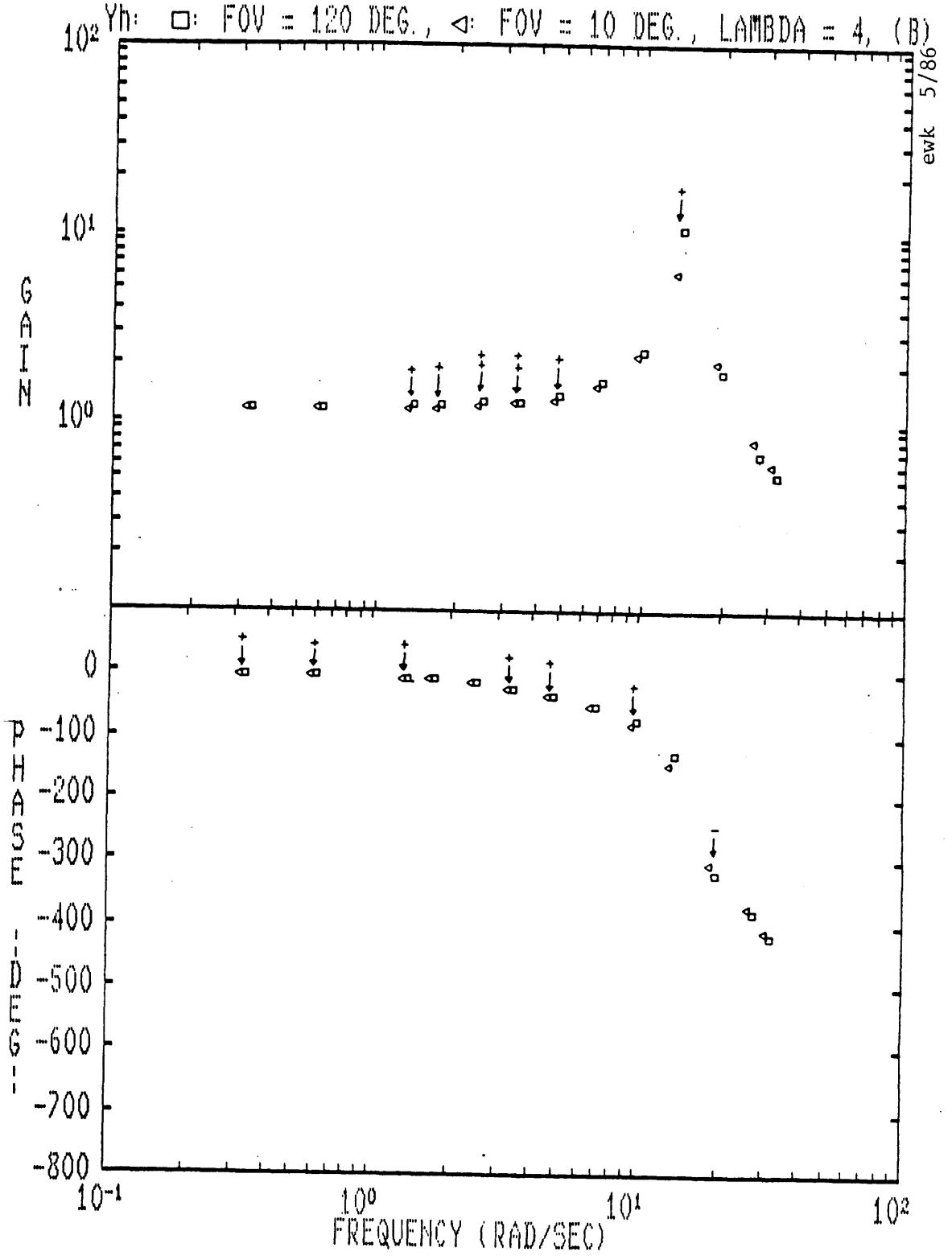
Yh: □: FOV = 120 DEG., ◁: FOV = 10 DEG., LAMBDA = 4, (B)
ewk 5/86
GAIN
PHASE --DEG--
FREQUENCY (RAD/SEC)

Figure 9.5 (c)

The results of the overall frequency response analysis indicate that the 10° field-of-view size decreases operator performance compared to the 40° and 120° field-of-view sizes. However, the effect of field-of-view on the subject's transfer function is not consistent for the range of instability levels tested. For an instability level of 2.0, where the subject's task is relatively easy, there is essentially no difference in subject performance between the 10° case and the 120° case. When the instability level is 3.0 and the task difficulty is moderate, the 40° case produces the best subject performance, but when the instability level is greatest and the task is most difficult, the 120° case produces the best subject performance. This variation in the field-of-view effect, due to the instability level is examined through further data analysis.

9.2 Crossover Frequency and Phase Margin

Figures 9.6 and 9.7 show the crossover frequencies and the phase margins calculated from the least squares transfer functions. The mean of the four values obtained for each case are plotted as squares. The plus signs represent the sample standard deviations of the mean. A table of student-t values is given below each plot. This table indicates the level of significance between the mean values for changes in the field-of-view size. Student-t values marked with a single asterisk (*) indicate a 95% confidence level that one mean is greater than the other. Student-t values marked by a double asterisk (**) indicate a 99% confidence level or greater.

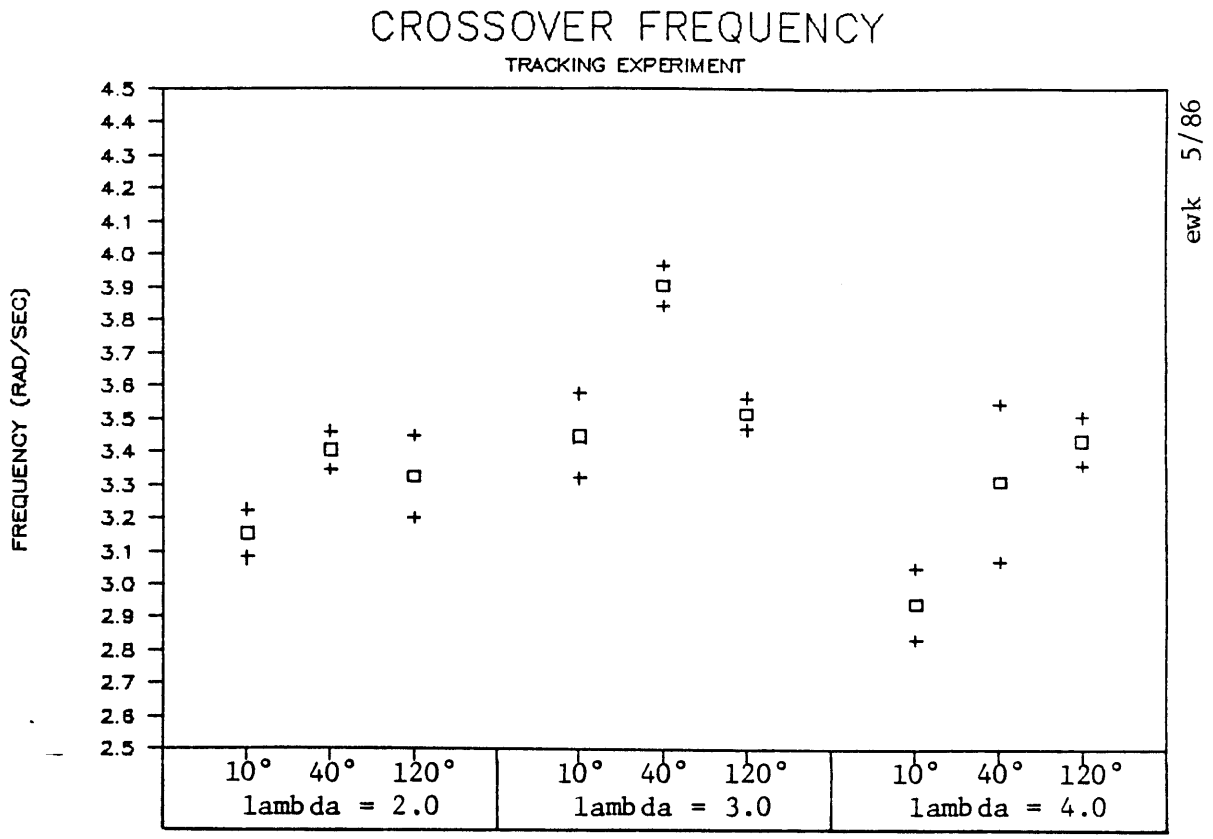

	lambda		
	2.0	3.0	4.0
10° vs. 40°	2.78*	3.21**	1.40
40° vs. 120°	-0.59	-4.96**	0.51
120° vs. 10°	-1.21	-0.50	-3.79**

Figure 9.6: Crossover frequencies with significance levels between field-of-view sizes

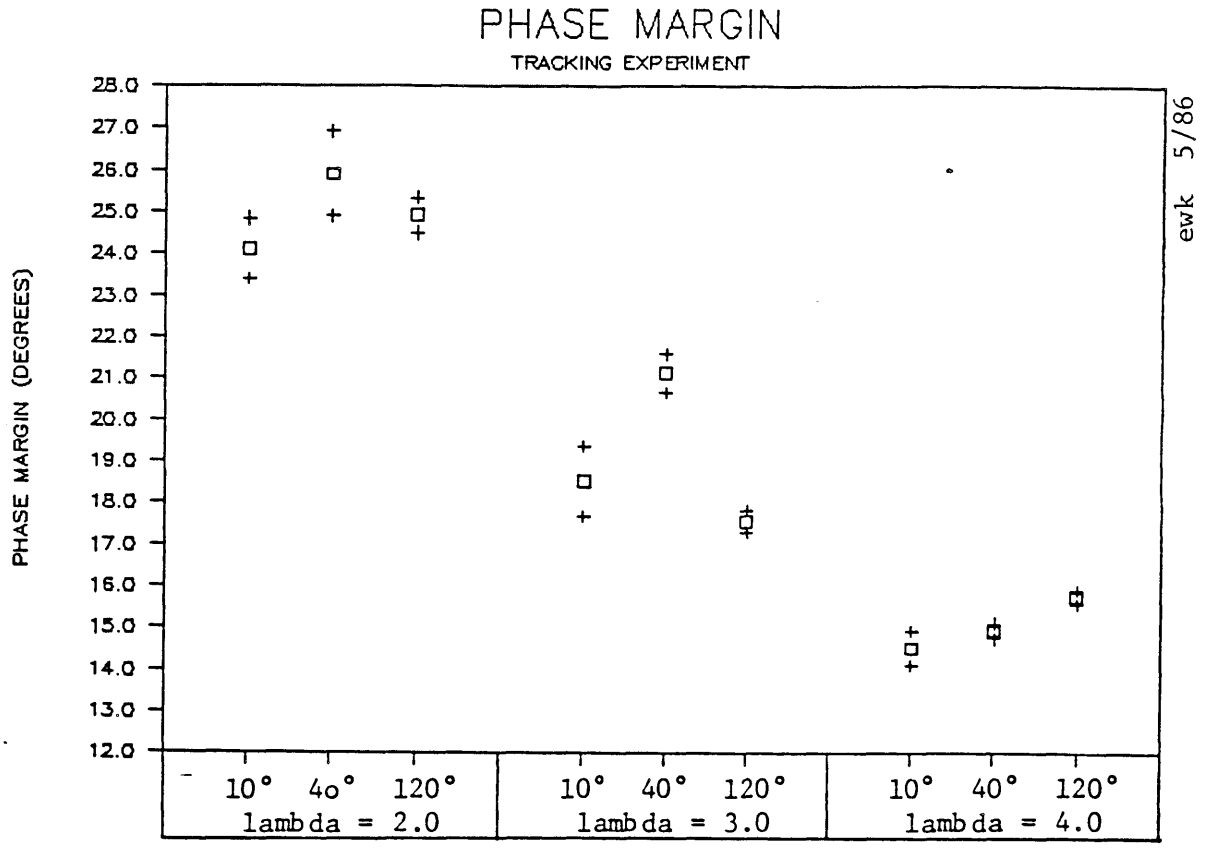

lambda

			2.0	3.0	4.0
10°	vs.	40°	1.43	2.74*	0.92
40°	vs.	120°	-0.88	-6.64**	3.40**
120°	vs.	10°	-0.97	1.07	-2.81*

Figure 9.7: Phase margins with significance levels between field-of-view sizes

The results of the crossover frequency and phase margin analysis seem to roughly match the transfer function analysis of section 9.1. For the low instability level the 40° case is has a significantly higher crossover frequency than the 10° case. The 120° case shows no significant difference with either the 10° or 40° case. For the moderate instability level, the 40° case has a significantly higher crossover frequency and phase margin than either the 10° case or the 120° case. For the high instability level the 120° case has a significantly higher crossover frequency and phase margin than the 10° case, while the 40° case is not significantly different from either the 10° case or the 120° case. These results show more clearly that variations in field-of-view size may have different effects on subject performance depending on the instability of the control system.

The crossover frequencies also provide a quick method of comparing the subject's performance between instability levels. One feature that stands out is the crossover frequency is greatest, for 10° and 40° field-of-view sizes, when lambda is 3.0. The operator appears to adopt a better control response when the task difficulty is moderate.

9.3 Remnant Analysis

Figure 9.8 shows the power spectral density of the subject's remnant for an example case. Power spectral density plots for all cases are shown in appendix 9.3. As stated in section 8.2.4, the remnant was only calculated at the primary frequencies by both the least squares method and the Levison/FFT method. The upper plot shows the mean and standard deviations of the four remnant values produced by the least

squares analysis. The lower plot shows the individual FFT values obtained from two separate tests. Figure 9.9 summarizes the total integrated power values obtained from the least squares remnant analysis. A table below the plot gives the student-t values that indicate confidence levels for differences, caused by changes in the field-of-view size.

The results show that as the instability level increases, the remnant power becomes much greater for the 10° case compared to the 40° or 120° case. Remnant power of the 40° case is essentially equal to the remnant power in the 120° case for all three instability levels.

9.4 Summary of Results

The Tracking Experiment results show that the effect of field-of-view on subject performance changes as the instability of the task changes. For the three instability levels tested the 10° case almost always produced lower levels of performance as seen in the rapid increase in operator remnant for the 10° case over the 40° and 120° cases. However, the performance differences between the 40° and 120° cases went through some significant changes as the instability level increased. The 40° case produced the best performance for the control loop with moderate instability, lambda equal to 4, while the 120° case produced the best performance when the instability was high. Theses differences can be most clearly seen in the analysis of the crossover frequency values.

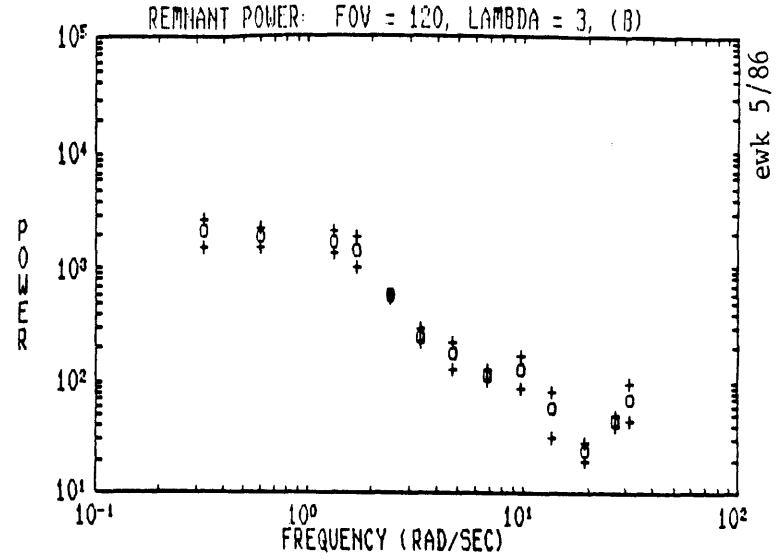

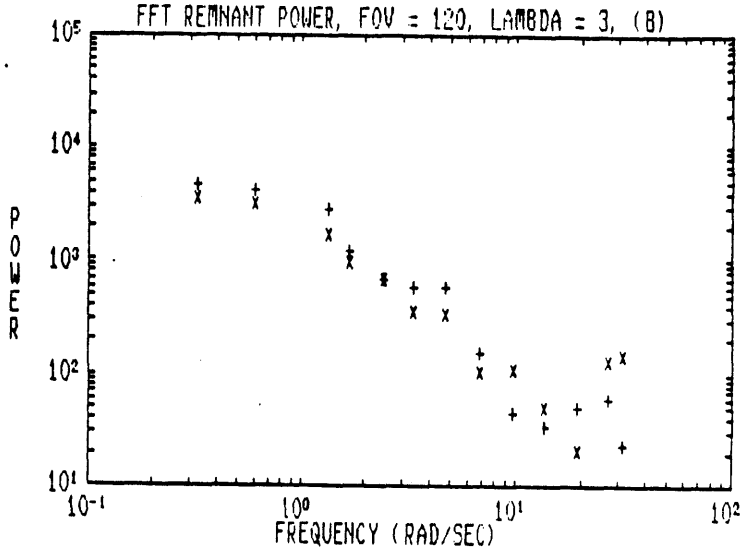

Total integrated power of remnant (arbitrary units)

Least squares: 7280 ± 345

FFT test 1 : 12840

FFT test 2 : 7280

Figure 9.8 (a): Power spectrum of remnant

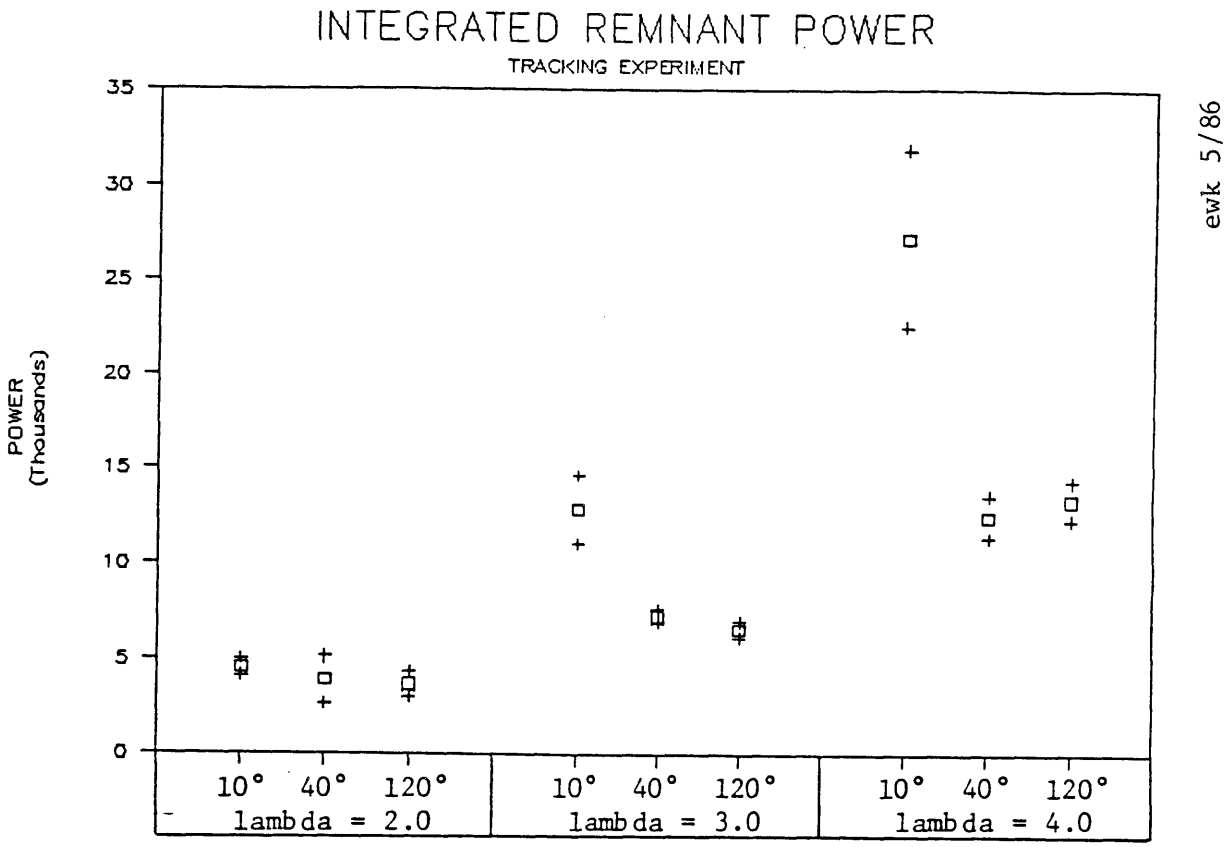

lambda

			2.0	3.0	4.0
10°	vs.	40°	-0.50	-3.08*	-3.10*
40°	vs.	120°	-0.15	-1.27	0.56
120°	vs.	10°	1.08	3.43**	2.94*

Figure 9.9: Integrated remnant power with significance levels between field-of-view sizes

END OF PART TWO

CHAPTER 10: DISCUSSION OF PART ONE AND PART TWO: INTERPRETING THE RESULTS FROM THE CRITICAL CONTROL EXPERIMENT AND THE TRACKING EXPERIMENT

This section is a discussion the overall results and conclusions of this research. Two experiments, the Critical Control Experiment and the Tracking Experiment, were designed to show how limiting a subject's field-of-view affects control response for visually simulated roll motion. The Critical Control Experiment measured the subject's time delay and tracking accuracy. The Tracking Experiment produced a quasi-linear, human operator model. This model showed how the subject's linear control response and non-linear remnant were affected by changing the field-of-view.

Sections 10.1 and 10.2 present two topics of discussion for the combined results from Part One and Part Two. The first topic is optimal field-of-view in the control of visual roll motion. Results from both experiments show the subject's control response is optimized when the field-of-view size is in the mid-range of those tested.

The second topic, presented in Section 10.2, is optimal angular velocity for the control of visual roll motion. When the display moves at this optimal angular velocity the subject's crossover frequency is highest, indicating a greater bandwidth of the control signal. The concept of an optimal angular velocity is supported by the crossover frequency results.

Section 10.3 compares the results from the Critical Control Experiment, of the current research, with the results from the Critical Tracking Task described by Jex, et al [1966]. Section 10.4 presents a

final discussion on the lack of bodily motion when simulating roll in the current research.

10.1 Discussion of an Optimal Field-of-View

At an 'optimal' field-of-view the roll motion of the display most influence on the human operator's perception of motion. The results of Critical Control Experiment give the strongest indication of an optimal field-of-view. The discussion of this experiment is divided into results from the moving field cases, results from the stationary field cases and results from the Tracking Experiment. In the moving field cases the simulated scene rolled according to the system dynamics. In the stationary field cases the simulated scene remained fixed and only a small center display showed the roll motion. Results of the Tracking Experiment indicated an optimal field-of-view for one of the three stability levels tested.

10.1.1 Optimal Field-of-View: Moving Field Cases

The results of the moving field cases, from the Critical Control Experiment, indicated an optimal field-of-view size at which the subject has the greatest accuracy of control. Plots of the results from the moving field cases are shown in Section 6, figures 6.1, 6.3, 6.5 and 6.7.

Figure 6.1 shows the transition time constants for the five subjects. Subject B has a minimum transition time constant at 80° which is significantly less than the time constants at wider or narrower

field-of-view sizes. Three other subjects show a trend for a minimum time constant at a mid-size field-of-view (20°, 40° or 80°). Subject D is the only one with a minimum time constant at an extreme field-of-view size (10° or 120°). Four subject's therefore show a tendency to have an mid-size field-of-view that is optimal in terms of the transition time constant. The critical time constant, shown in figure 6.3, shows little indication of an optimal field-of-view. Only subject B has a critical time constant, at a mid-size field-of-view, that is significantly less than other field-of-view sizes.

The most significant indicator of an optimal field-of-view size is the stage one RMS roll error and the corresponding least squares curve, shown in figure 6.9. Modelling the effect of field-of-view on RMS roll error showed that all subjects had a mid-range, optimal field-of-view size. RMS roll error dropped rapidly from 10° to 40° and then increased slowly from 40° to 120°. Table 10.1 gives the field-of-view sizes, predicted by the least squares fit, at which the RMS roll error was minimized.

	subject				
	A	B	C	D	E
optimal FOV	51°	46°	55°	57°	41°

(mean = 50° standard deviation = 2.9°)

table 10.1

For the stage two RMS error results, shown in figure 6.7, two subject's had minimum RMS errors at a mid-range field-of-view, that was

significantly less than RMS errors for wider or narrow field-of-view sizes. Two subjects showed a trend to have a minimum RMS error at a mid-range field-of-view size while the fifth subject's data was ambiguous, with no clear relation between field-of-view and RMS roll error.

The existence of an optimal field-of-view size where the subject has the greatest accuracy of control is strongly indicated by the time constant results and the RMS roll error results for the moving field condition. While not all subjects showed an optimal field-of-view for each measurement, no subject showed a contrary effect.

10.1.2 Optimal Field-of-View: Stationary Field Cases

The results from the stationary field cases indicate an 'inverse optimal field-of-view'. The inverse optimal field-of-view is the field-of-view size where the stationary simulated scene interferes most with the control of the central roll motion indicator. This interference manifests itself as an increase in the subject's RMS roll error or time constants the mid-range field-of-view sizes.

Four out of the five subjects had critical time constant results that indicated an inverse optimal field-of-view in the stationary field cases. These subjects had significantly minimum time constants at either 10° or 120°, or at both 10° and 120°. The results for the stage one and stage two RMS roll errors show the same trend as the critical time constant results. Three out of the five subjects, A, B and D, have significantly minimum stage one and stage two RMS roll errors for the extreme field-of-view sizes, indicating less accurate control in the mid-size field-of-view range. The other two subjects, C and E, showed

slight trends for minimum RMS errors at the extreme field-of-view sizes.

The above results for the stationary field cases of the Critical Control Experiment show trends for lower time constants and lower RMS roll errors at the extreme field-of-view sizes. The conclusion based on these results and the results of the moving field cases is that a mid-range field-of-view exists where the visual field has the most influence on the subject's control response.

In the moving field cases the optimum field-of-view helps the subject control the roll motion since the subject's task is to control the motion of the simulated scene. In the stationary field cases the 'optimal' field-of-view interferes with the subject's control response since the subject's task is to control a small center display, while the visual field remains fixed.

A direct comparison of the moving and stationary field conditions shows a nearly opposite affect on subject performance. Both curves for RMS and time constant values bow downward for the motion cases and upwards for the stationary cases. The numerical difference between the two curves is highest for the mid field-of-view sizes.

This result is relevant to controlling an aircraft using only instruments for motion information. The results from the stationary condition indicate that an instrument would be most effective when it is either the only object in the pilot's field-of-view or it is surrounded by a visual field that extends well into the periphery. If the visual field surrounding the instrument extends only partially into the periphery, such as a well lighted instrument panel, a perceptual conflict may occur which would hinder the pilot's control response.

10.1.3 Optimal Field-of-View: Tracking Experiment

The crossover frequency results from the Tracking Experiment show that the subject's control response is optimal at 40° when lambda = 3.0, but when lambda = 4.0 control response is optimized at 120°. Similar results are shown by the comparisons of frequency responses. The subject's gain when lambda = 3.0 is significantly higher, over a wide range of frequencies, when the field-of-view was 40° as compared to 10° and 120°. The subject's also had significantly less phase lag at 40° than at 10° and 120°. These results of the Tracking Experiment, for the moderate instability level, correspond to the results for the Critical Control Experiment which predicted a mid-range optimal field-of-view.

10.2 Optimal Velocity Discussion

Results from the Tracking Experiment indicate an optimal roll velocity at which the subject's crossover frequency is greatest. Values for RMS roll velocity are shown in table 10.2 for each of the nine cases. When comparing the crossover frequencies with RMS velocity it is

	lambda		
FOV	2.0	3.0	4.0
10°	2.65 ± 0.14	4.85 ± 0.21	9.77 ± 0.27
40°	2.32 ± 0.16	4.46 ± 0.26	7.49 ± 0.40
120°	2.41 ± 0.12	3.78 ± 0.21	7.61 ± 0.57

Table 10.2 RMS angular velocity (degrees/sec)

apparent that the crossover frequency is greatest for a lambda value of 3.0 corresponding to moderate RMS velocity. These crossover frequencies are plotted in section 9, figure 9.6. For the 10° and 40° field-of-view sizes, the crossover frequency is highest, by significant margins, when lambda = 3.0 as compared to 2.0 or 4.0. The 120° field-of-view cases show no significant variation in the crossover frequency for different levels of lambda. These results indicate that the subject's control response is optimized when the task difficulty and angular velocity are moderate.

A possible explanation for the optimal velocity is that low angular velocities are difficult to detect while high angular velocities are difficult to judge. Subjects of these experiments often made comment that when the instability level was very low, the roll motion was slightly disorientating to the point where the subject sometimes perceived self-motion as opposed to the display motion. When the angular velocity is high, the motion is difficult to judge due to visual noise. This noise is the result of being unable to distinguish between different roll velocities, since the magnitude of the velocity overwhelms the subject's perception.

A possible connection exists between the optimal angular velocity and the optimal field-of-view. This connection is based on the fact that the true velocity of a point in the visual field is dependent on the angular roll velocity and the radial distance of the point from the center of rotation. Points in the periphery of the visual field will have much higher linear velocities than points nearer to the center and may produce a much greater amount of perceptual noise.

10.3 Comparison of the Critical Control Experiment with Past Research

This section makes a brief comparison between the results of the Critical Control Experiment of the current research and the Critical Tracking Task, conducted by Jex, et al [1966]. The results that are compared are the critical time constants and the frequency response characteristics. The critical time constants obtained in the Jex experiments leveled off at a minimum level of approximately 0.15 seconds. The best critical time constants obtained by a subject in the Critical Control Experiment reached a minimum level of about 0.2. The time constant difference between these two experiments was significant.

The frequency responses of the two experiments also showed significant differences. The natural frequency, ω_N, of the stick/subject system, which produces the characteristic spike in the bode gain diagram, had an average value of 13 radians/second in the Critical Control Experiment and an average value of 21 radians/second in the Jex Critical Tracking Task. This natural frequency, which could be due primarily to the force-stick itself, may have affected the critical time constant.

10.4 Absence of Bodily Motion in the Experiments

Due to lack of access to a moving-base simulator, the experiments of the current research were performed using only visually simulated roll motion. Therefore, the results do not apply directly to the control of aircraft in actual flight. Expected changes in the subject's control response, due to the addition of bodily motion, would be a

increase in the phase lead, due to information from the vestibular system. This phase lead would not theoretically decrease the critical time constant since the subject is not able to adopt lead or lag equalization at the critical instability level. However, increased phase lead would improve the stability of the closed-loop system.

10.5 Summary

The results of these experiments show that a mid-size field-of-view has the greatest influence on a subject's ability to control roll motion. This 'optimal' field-of-view can both help and hinder the subject's control response depending on the exact nature of the task. If the subject is trying only to control motion in the center of his visual field, visual information in the periphery may distort the subject's perception of that motion.

The results of the crossover frequency analysis show that the optimal field-of-view theory may be relevant only for tasks with moderate levels of stability. Since the Critical Control Experiment measured the subject's performance while the stability level went from low to high, the results may be showing effects of the predominant stability level during the task.

Crossover frequency analysis also indicates that the velocity of roll motion effects a subject's control response. A moderate RMS roll velocity enables the subject to adopt a higher bandwidth control response as indicated by a greater crossover frequency.

Appendix 3.1 Equipment Information

Projection lenses for EFD: 80 mm, f = 2.8, Corygon lenses, Rolyn Optics, part no. 30.1451

Ground Glass for EFD: Rolyn Optics, part no. 55.3050

Fresnel Lens for EFD: Rolyn Optics, part no. 16.7200

Hand control: force stick, model no. 435DC, manufactured by Measurement Systems, Inc.

Signal generator for driving control stick: Hewlett-Packard audio oscillator, model no. 201C

A/D card: multibus compatible, memory mapped, manufactured by Analog Devices, model no. RTI-732.

Signal Generator for generating clock signal: Krohn-Hite, model 5100A

Appendix 3.2 Program Code for the Critical Control Experiment
Program language: C

```
/*************************************************************
*                                                            *
*       task.c is a roll control task program. This          *
*       section of the program contains the "main"           *
*       program call, the main program, variable ini-        *
*       tialization, and the dynamics equations.             *
*                                                            *
*************************************************************/


#include "define.h"

#define true 1
#define false 0

main (argc,argv)
int argc;
char *argv[];
{

/***  variable declaration ***/

    short count_dn, start_task,          Boolean variables for selecting
      _   end_task, letter,                 program options
          adcon, motion, efd,
          stage_one, baseline;

    Angle theta_screen;                  Roll angle of display (1/100's deg)

    int i, j,                            Integer increments
        change_pt,                       Count when instability rate changes
        max_roll,                        Maximum roll angle of screen
        filt_error,                      Average roll error over 10 cycles
        error_max,                          and criterion for rate change
        point[10];                       Array for storing roll error values

    int val1, val2,                      Values read from A/D card
        xcard, scan,                     Secondary assignments of values
        off_i;                           Integer value of mid-stick position

    int stick_array[1500],               Arrays for storing input and output
        roll_array[1500],                   data
        pulse_array[2][1500],
        scan_array[1500];

    char charbuf[8];                     Character buffer
```

```
    float theta, x, h,                  Real values of roll, stick, time-step
        lambda, lambda_c,               Current lambda, critical lambda
        d_lambda, min_lamb,             Lambda rate, min lambda for rate change
        d_lambda1, d_lambda2,           First lambda rate, second lambda rate
        k1, k2, k3,                     Coefficients for dynamics equtions
        offset, x_factor;               Stick offset, stick gain

    FILE *fpw, *fopen();                Initialize and read data files
    FILE *fpr, *fopen();

    fpw = fopen("DATA","w");
    fpr = fopen("param","r");
    fscanf (fpr,"%f %f %f %f %f %f %f %d %d",
        &h, &offset, &x_factor, &k3, &d_lambda1, &d_lambda2, &min_lamb,
        &error_max, &max_roll);

/***  variable initialization ***/

    count_dn = start_task = end_task = baseline = false;
    efd = adcon = stage_one = motion = true;

    off_i = (int) (offset);
    theta = 0.0;
    theta_screen = 0;
    scan = xcard = 0;
    x = 0.0;
    lambda = 1.5;
    d_lambda = d_lambda1;
    filt_error = 0;
    for (i = 0; i <= 9; i++) point[i] = 0;
    for (i = 0; i <= 1999; i++) pulse_array[0][i] = pulse_array[1][i] = 0;
    i = 0;
    j = 45;

    system_init ();

/***. main program loop ***/

    while (!end_task)                   Enter loop if subject has not
    {                                   lost control.
        if (baseline) color(black);     Set background color to black
        else color(skyblue);            or blue and create graphics
        callobj (FIELD_FORMAT);         window.

        while (qtest ())                Read keyboard inputs.
        {
            qread (&letter);
            switch (letter)
            {
                case 'g':               Start test
                    count_dn = true;
                    break;
```

```
            case 'm':                          Use stationary visual field,
                motion = !motion;              display horizon indicator.
                break;

            case 'b':                          Do not show landscape, only
                baseline = !baseline;          10 deg horizon indicator.
                motion = !motion;
                break;

            case 'v':                          Display scene upsidedown for
                efd = !efd;                    use with EFD.
                break;

            case 'r':                          Restart and initialize task.
                theta = x = 0.0;
                theta_screen = xcard = scan = 0;
                count_dn = start_task = false;
                stage_one = true;
                lambda = 1.5;
                d_lambda = d_lambda1;
                filt_error = 0;
                for (i = 0; i <= 9; i++) point[i] = 0;
                for (i = 0; i <= 1999; i++)
                    pulse_array[0][i] = pulse_array[1][i] = 0;
                i = 0;
                j = 45;
                fclose(fpw);
                fpw = fopen("DATA","w");
                break;

            case 'e':                          Exit from program, saving data.
                end_task = true;
                break;
        }
    }

    if (stage_one)                             Calculate performance criteria.
    {
        filt_error = filt_error - point[i];        Sum roll error.
        point[i] = abs(theta_screen);
        filt_error = filt_error + point[i];
        i++;
        if (i == 10) i = 0;
        if (filt_error > error_max && lambda > min_lamb)
        {
            d_lambda = d_lambda2;                  Switch to second rate.
            stage_one = false;
            change_pt = j;
            lambda_c = lambda;
        }
    }

    while(new_ad(9) > 0x7ff) pulse_array[0][j]++;   Wait for 15 Hz timing
    while(new_ad(9) < 0x7ff) pulse_array[1][j]++;   signal.
```

```
        if (start_task)                         If task has started...
        {
            val1 = new_ad(1);                   Read analog stick value.
            xcard = val1;
            x = (float) (xcard);

            val2 = new_ad(10);                  Read test signal value.
            scan = val2;

            x = (x - offset) / x_factor;        Unbias stick signal.
            lambda = lambda + d_lambda;         Increment lambda by current
                                                rate.

/***  calculate roll motion ***/

            k1 = exp(h * lambda);               Coefficient 'A'
            k2 = k1 - 1.0;                      Coefficient 'B'

            theta = k1 * theta - k2 * x;        Calculate roll
            theta_screen = (int) (theta * k3);  Multiply by display 'gain'.

            stick_array[j] = xcard;             Store data in arrays.
            roll_array[j] = theta_screen;
            scan_array[j] = scan;

            if (theta_screen > max_roll ||
                theta_screen < -max_roll)
                start_task = false;             Criterion for loss of control.
            ++j;                                Increment cycle count.
        }

        if (efd) rotate (1800,'z');             Rotate display 180 deg for EFD
        if (motion)                             Display moving visual field.
        {
            rotate (-theta_screen,'z');         Display the field with the
            callobj (TERA);                     calculated roll angle.
            rotate (theta_screen,'z');
            callobj (ROLL_INDICATOR);           Display fixed cross-hairs.
        }
        else                                    Display stationary visual field
        {                                       or display no visual field.
            if (!baseline) callobj(TERA);
            rotate (-theta_screen,'z');         Display horizon indicator
            callobj(TILT_INDICATOR);            with calculated roll angle.
            rotate (theta_screen,'z');
            callobj (ROLL_INDICATOR);           Display fixed cross-hairs.
        }
        color(blue);
        cmov2i(9,35);
        sprintf(charbuf,"%3.1f", lambda);       Display lambda value to subject.
        charstr(charbuf);
        if (efd) rotate (1800,'z');             Return roll angle to zero deg.
```

```
        if (count_dn)                          Before task actually starts
        {                                      display a short starting
            color(red);                        sequence to alert the subject.
            move2i(-j>>1, -20);
            rdr2i(0, 40);
            move2i(j>>1, -20);
            rdr2i(0, 40);
            j--;
            if (j == 0)
            {
                count_dn = false;
                start_task = true;
            }
            color(blue);
        }

        if (!stage_one) color(red);            Display lambda to person running
        cmov2i(-375,-280);                     the experiment.
        sprintf(charbuf,"%5.3f", lambda);
        charstr(charbuf);

        swapbuffers ();                        Send the graphics display to
    }                                          the monitor.

                                               End of program loop, continue
                                               if subject has not lost control.

/***-send all the output data to a file ***/

    fprintf(fpw,"%5d %8.3f %5d %8.3f\n", j, lambda, change_pt, lambda_c);
    for (i = 0; i <= j; i++)
        fprintf(fpw,"%5d %8d %8d %8d %5d %5d\n", i, stick_array[i] - off_i,
            roll_array[i], scan_array[i], pulse_array[0][i], pulse_array[1][i]);
    fprintf (fpw,"    -1\n");
    fclose (fpw);
    unqdevice (KEYBD);
    greset ();
    printf("critical lambda = %4.2f  cycles = %5d\n", lambda, j);
    gexit ();
}
```

Appendix 4.1 Description of Subjects

Subject A

age: 37 sex: M handedness: right

general physical and mental health: good

current medication: none

visual perception anomalies: none

motor coordination anomalies: none

aircraft flight experience: 10 hours in flight simulators

Subject B

age: 23 sex: M handedness: right

general physical and mental health: good

current medication: none

visual perception anomalies: none

motor coordination anomalies: none

aircraft flight experience: 50 hours in light aircraft

Subject C

age: 24 sex: M handedness: right

general physical and mental health: good

current medication: none

visual perception anomalies: none

motor coordination anomalies: none

aircraft flight experience: none

Subject D

age: 22 sex: M handedness: ambidextrous

general physical and mental health: good

current medication: none

visual perception anomalies: none

motor coordination anomalies: none

aircraft flight experience: 2 hours in light aircraft

Subject E

age: 21 sex: M handedness: right

general physical and mental health: good

current medication: none

visual perception anomalies: none (20/40 far vision)

motor coordination anomalies: none

aircraft flight experience: none

Appendix 4.2 Written Instructions for Subjects

INFORMATION AND INSTRUCTIONS FOR SUBJECTS

GENERAL INFORMATION

There are ten tests in this experiment. A trial will consist of the ten tests, run in a random order. A test lasts between 20 and 60 seconds, the time between tests will be about 1 1/2 minutes, therefore, a trial will last about 20 minutes.

On each of the three days prior to the final experiments, one trial will be run for practice.

Two days will be required for the final experiment. On these days three trials will be run with a five minute break between trials.

Since this experiment depends on manual control, the subject should be free of the influence of any drug. This includes caffeine (no coffee or cola 4 hours prior to the experiment), alcohol (12 hours), cold medicines (12 hours), narcotics, hallucinogens, hostess twinkies, etc.

Please follow the schedule as closely as possible. Due to scheduling constraints it is important that you, the subject, arrive on time. If you cannot make it at the scheduled time call as soon as possible. At the very least, we can reschedule the experiment.

Please fill out the general questionnaire before the experiments. On each day prior to running the tests, you will be asked a few additional questions concerning your physical and mental state. Please respond to the best of your ability, all answers will be kept strictly confidential.

INSTRUCTIONS FOR EXPERIMENT

1) Seat yourself comfortably in the chair, checking viewer and control stick position.

2) Adjust chin rest and check image quality.

3) To adjust masks.

   a) Looking through one eye at a time, roughly adjust each mask so that the crosshairs are centered.

   b) Using both eyes, finely adjust the mask position. Sight a detail in the scene that is very close to the left hand boarder of the masks. Adjust the masks using the visual detail as a reference. Do the same for the top, right hand and finally the bottom boarders.

4) Signal the operator when you are ready to start.

5) During a test, hold the stick between the thumb and the side of the side of the index finger. Keep the eyes fixed on the crosshairs. If you look any place else, you will be turned into a newt.

6) Concentrate and do your best. Remember, this is a CRITICAL control task; it should measure the limits of your ability.

7) IF YOU DO WELL:
   All subjects will receive a six-pack of their favorite beverage. (It is not your favorite beverage if you cannot afford it yourself). The subject with the highest average instability level, over the five days of experiments, will receive an additional six-pack as will the subject with the highest individual score.

Thank you for your participation in this experiment.

Appendix 4.3 Terminal Session Information

```
login: root

# edt

# gotask [data file name]          (Critical Control Experiment)

keyboard input:

     test designation
     m: select stationary or moving field condition
     b: baseline case (10° FOV, stationary field)
     v: rotate display 180°

     test control
     g: start test
     r: restart test
     e: exit and save data to named file

# gotrack [data file name]         (Tracking Experiment)

keyboard input:

     test designation
     m: select stationary or moving field condition
     b: baseline case (10° FOV, stationary field)
     l: increment lambda value (cycles to lower limit after
        reaching 4.5)
     v: rotate display 180°

     test control
     g: start test
     r: restart test
     e: exit and save data to named file
```

Appendix 6.1 Data for transition and critical time constants

Statistical analysis of cases for each subject.
1st column: case designation

2nd through 5th columns: transition time constant information
2nd column: mean of six tests
3rd column: standard deviation of individual points
4th column: mean minus the standard deviation of the mean
5th column: mean plus the standard deviation of the mean

6th through 9th columns: critical time constant information
6th column: mean of six tests
7th column: standard deviation of individual points
8th column: mean minus the standard deviation of the mean
9th column: mean plus the standard deviation of the mean

units: degrees

case designation code
1: 10° 2: 20° 3: 40° 4: 80° 5: 120°
s: stationary field condition
m: moving field condition

subject A

s1	t:	0.300	0.016	: 0.293	: 0.306	c:	0.252	0.008	: 0.249 : 0.255
s2	t:	0.309	0.005	: 0.307	: 0.311	c:	0.268	0.015	: 0.262 : 0.274
s3	t:	0.297	0.020	: 0.289	: 0.305	c:	0.251	0.013	: 0.246 : 0.256
s4	t:	0.304	0.008	: 0.301	: 0.308	c:	0.262	0.016	: 0.255 : 0.269
s5	t:	0.299	0.014	: 0.293	: 0.305	c:	0.265	0.017	: 0.258 : 0.272
m1	t:	0.297	0.011	: 0.292	: 0.301	c:	0.264	0.013	: 0.259 : 0.269
m2	t:	0.286	0.019	: 0.278	: 0.293	c:	0.247	0.010	: 0.243 : 0.251
m3	t:	0.264	0.024	: 0.254	: 0.274	c:	0.237	0.009	: 0.233 : 0.240
m4	t:	0.249	0.018	: 0.242	: 0.257	c:	0.234	0.013	: 0.229 : 0.240
m5	t:	0.269	0.027	: 0.258	: 0.280	c:	0.228	0.015	: 0.222 : 0.234

subject B

s1	t:	0.258	0.030	: 0.245	: 0.270	c:	0.214	0.013	: 0.209 : 0.219
s2	t:	0.285	0.027	: 0.274	: 0.296	c:	0.221	0.010	: 0.217 : 0.225
s3	t:	0.268	0.021	: 0.259	: 0.277	c:	0.218	0.007	: 0.216 : 0.221
s4	t:	0.271	0.016	: 0.264	: 0.278	c:	0.225	0.013	: 0.220 : 0.231
s5	t:	0.278	0.020	: 0.270	: 0.286	c:	0.214	0.006	: 0.211 : 0.216
m1	t:	0.263	0.011	: 0.258	: 0.267	c:	0.221	0.013	: 0.216 : 0.227
m2	t:	0.235	0.020	: 0.227	: 0.244	c:	0.200	0.009	: 0.196 : 0.203
m3	t:	0.223	0.025	: 0.213	: 0.233	c:	0.200	0.014	: 0.194 : 0.205
m4	t:	0.207	0.011	: 0.202	: 0.211	c:	0.195	0.005	: 0.194 : 0.197
m5	t:	0.257	0.017	: 0.250	: 0.264	c:	0.203	0.004	: 0.202 : 0.205

subject C

s1	t:	0.291	0.019	: 0.283	: 0.299	c:	0.219	0.014	: 0.213 : 0.225
s2	t:	0.298	0.015	: 0.292	: 0.304	c:	0.239	0.025	: 0.229 : 0.249
s3	t:	0.308	0.007	: 0.305	: 0.311	c:	0.239	0.009	: 0.235 : 0.242
s4	t:	0.289	0.017	: 0.283	: 0.296	c:	0.240	0.018	: 0.233 : 0.247
s5	t:	0.294	0.014	: 0.288	: 0.300	c:	0.236	0.021	: 0.227 : 0.245
m1	t:	0.284	0.023	: 0.275	: 0.293	c:	0.223	0.013	: 0.218 : 0.229
m2	t:	0.283	0.015	: 0.277	: 0.289	c:	0.213	0.012	: 0.208 : 0.218
m3	t:	0.256	0.032	: 0.243	: 0.269	c:	0.222	0.013	: 0.216 : 0.227
m4	t:	0.252	0.029	: 0.240	: 0.264	c:	0.218	0.005	: 0.216 : 0.220
m5	t:	0.265	0.018	: 0.258	: 0.273	c:	0.218	0.002	: 0.217 : 0.218

subject D

s1	t:	0.300	0.011	: 0.295	: 0.304	c:	0.234	0.016	: 0.228 : 0.241
s2	t:	0.300	0.013	: 0.295	: 0.305	c:	0.244	0.017	: 0.237 : 0.251
s3	t:	0.299	0.006	: 0.296	: 0.301	c:	0.257	0.023	: 0.248 : 0.267
s4	t:	0.307	0.004	: 0.306	: 0.309	c:	0.260	0.009	: 0.256 : 0.263
s5	t:	0.289	0.020	: 0.281	: 0.297	c:	0.245	0.011	: 0.241 : 0.250
m1	t:	0.301	0.014	: 0.295	: 0.306	c:	0.248	0.029	: 0.236 : 0.260
m2	t:	0.296	0.020	: 0.288	: 0.305	c:	0.230	0.012	: 0.225 : 0.234
m3	t:	0.273	0.021	: 0.264	: 0.281	c:	0.234	0.009	: 0.230 : 0.238
m4	t:	0.267	0.022	: 0.258	: 0.276	c:	0.232	0.007	: 0.229 : 0.235
m5	t:	0.250	0.022	: 0.241	: 0.259	c:	0.229	0.015	: 0.223 : 0.235

subject E

s1	t:	0.302	0.016	: 0.296	: 0.309	c:	0.274	0.005	: 0.272 : 0.276
s2	t:	0.307	0.008	: 0.304	: 0.310	c:	0.284	0.015	: 0.278 : 0.290
s3	t:	0.298	0.017	: 0.291	: 0.306	c:	0.285	0.020	: 0.277 : 0.293
s4	t:	0.307	0.011	: 0.303	: 0.312	c:	0.286	0.008	: 0.283 : 0.289
s5	t:	0.308	0.008	: 0.305	: 0.312	c:	0.293	0.013	: 0.288 : 0.299
m1	t:	0.303	0.009	: 0.299	: 0.307	c:	0.283	0.009	: 0.279 : 0.287
m2	t:	0.291	0.021	: 0.282	: 0.300	c:	0.270	0.023	: 0.261 : 0.280
m3	t:	0.284	0.025	: 0.274	: 0.295	c:	0.257	0.017	: 0.251 : 0.264
m4	t:	0.270	0.024	: 0.260	: 0.280	c:	0.252	0.019	: 0.244 : 0.260
m5	t:	0.290	0.018	: 0.283	: 0.298	c:	0.251	0.014	: 0.245 : 0.257

Individual test values

test name designation
1st character: subject
2nd and 3rd characters: date of month
4th character: trial/day
5th character: test/trial

time constants: subject A

test	transition	critical
A1115s1	0.302	0.249
A1129s1	0.277	0.251
A1132s1	0.312	0.251
A1216s1	0.312	0.268
A1221s1	0.312	0.248
A1234s1	0.281	0.245
A1116s2	0.312	0.287
A1125s2	0.312	0.278
A1134s2	0.310	0.271
A1211s2	0.307	0.255
A1226s2	0.300	0.271
A1235s2	0.312	0.247
A1112s3	0.309	0.267
A1127s3	0.301	0.246
A1138s3	0.307	0.265
A1210s3	0.258	0.252
A1227s3	0.293	0.242
A1231s3	0.312	0.235
A1113s4	0.294	0.253
A1128s4	0.312	0.289
A1136s4	0.309	0.254
A1215s4	0.303	0.254
A1229s4	0.296	0.276
A1239s4	0.312	0.246
A1118s5	0.312	0.257
A1121s5	0.282	0.260
A1137s5	0.312	0.281
A1213s5	0.285	0.238
A1224s5	0.293	0.284
A1230s5	0.309	0.272

A1111m1	0.288	0.268
A1126m1	0.309	0.251
A1135m1	0.284	0.252
A1219m1	0.293	0.279
A1225m1	0.312	0.277
A1237m1	0.294	0.255
A1119m2	0.290	0.262
A1120m2	0.312	0.236
A1130m2	0.280	0.247
A1214m2	0.268	0.246
A1223m2	0.300	0.238
A1238m2	0.264	0.254
A1117m3	0.263	0.240
A1122m3	0.278	0.240
A1131m3	0.304	0.251
A1217m3	0.238	0.230
A1220m3	0.246	0.230
A1236m3	0.255	0.230
A1110m4	0.272	0.243
A1123m4	0.266	0.249
A1139m4	0.239	0.225
A1212m4	0.252	0.241
A1222m4	0.243	0.234
A1232m4	0.223	0.213
A1114m5	0.255	0.233
A1124m5	0.270	0.248
A1133m5	0.256	0.212
A1218m5	0.231	0.210
A1228m5	0.298	0.236
A1233m5	0.301	0.230

Individual test values

time constants: subject B

test	transition	critical
B1818s1	0.246	0.218
B1823s1	0.298	0.209
B1836s1	0.289	0.212
B1910s1	0.250	0.207
B1929s1	0.242	0.236
B1935s1	0.220	0.199
B1813s2	0.259	0.226
B1820s2	0.307	0.209
B1834s2	0.246	0.237
B1918s2	0.291	0.211
B1922s2	0.297	0.218
B1931s2	0.312	0.224
B1811s3	0.291	0.212
B1822s3	0.261	0.213
B1835s3	0.248	0.224
B1913s3	0.254	0.227
B1925s3	0.299	0.213
B1936s3	0.256	0.221
B1810s4	0.272	0.234
B1824s4	0.278	0.212
B1832s4	0.249	0.218
B1914s4	0.256	0.239
B1924s4	0.294	0.212
B1933s4	0.278	0.239
B1817s5	0.259	0.202
B1826s5	0.300	0.219
B1838s5	0.252	0.214
B1915s5	0.286	0.214
B1927s5	0.298	0.217
B1937s5	0.274	0.218

B1814m1	0.252	0.226
B1827m1	0.278	0.215
B1830m1	0.252	0.209
B1916m1	0.258	0.220
B1923m1	0.263	0.214
B1932m1	0.273	0.245
B1819m2	0.229	0.189
B1825m2	0.218	0.197
B1831m2	0.217	0.198
B1912m2	0.230	0.210
B1926m2	0.252	0.210
B1934m2	0.268	0.193
B1815m3	0.203	0.177
B1828m3	0.197	0.187
B1839m3	0.224	0.205
B1919m3	0.267	0.213
B1920m3	0.219	0.210
B1939m3	0.229	0.206
B1816m4	0.208	0.201
B1821m4	0.202	0.191
B1837m4	0.198	0.194
B1917m4	0.222	0.201
B1928m4	0.193	0.190
B1938m4	0.216	0.195
B1812m5	0.277	0.198
B1829m5	0.261	0.200
B1833m5	0.245	0.207
B1911m5	0.237	0.205
B1921m5	0.275	0.207
B1930m5	0.247	0.203

Individual test values

time constants: subject C

test	transition	critical
C1011s1	0.312	0.227
C1029s1	0.287	0.225
C1030s1	0.300	0.224
C1116s1	0.256	0.236
C1123s1	0.292	0.203
C1138s1	0.299	0.200
C1015s2	0.312	0.282
C1021s2	0.299	0.208
C1032s2	0.303	0.243
C1114s2	0.312	0.227
C1126s2	0.291	0.231
C1134s2	0.273	0.241
C1010s3	0.308	0.232
C1020s3	0.312	0.250
C1038s3	0.308	0.244
C1110s3	0.312	0.226
C1122s3	0.312	0.242
C1132s3	0.295	0.236
C1019s4	0.265	0.226
C1023s4	0.291	0.249
C1037s4	0.277	0.272
C1118s4	0.300	0.229
C1121s4	0.312	0.239
C1136s4	0.291	0.226
C1018s5	0.273	0.220
C1025s5	0.295	0.224
C1035s5	0.294	0.256
C1115s5	0.284	0.225
C1127s5	0.307	0.269
C1139s5	0.312	0.223

C1016m1	0.265	0.233
C1026m1	0.287	0.245
C1033m1	0.250	0.217
C1112m1	0.291	0.216
C1128m1	0.312	0.216
C1135m1	0.300	0.212
C1012m2	0.295	0.206
C1028m2	0.278	0.225
C1036m2	0.300	0.204
C1119m2	0.292	0.208
C1129m2	0.262	0.232
C1131m2	0.269	0.204
C1017m3	0.221	0.198
C1024m3	0.274	0.233
C1031m3	0.268	0.228
C1117m3	0.246	0.221
C1125m3	0.224	0.215
C1137m3	0.304	0.234
C1014m4	0.228	0.214
C1027m4	0.247	0.211
C1034m4	0.303	0.220
C1113m4	0.266	0.223
C1124m4	0.244	0.217
C1130m4	0.225	0.223
C1013m5	0.245	0.221
C1022m5	0.285	0.218
C1039m5	0.257	0.215
C1111m5	0.264	0.217
€1120m5	0.289	0.219
C1133m5	0.253	0.215

Individual test values

time constants: subject D

test	transition	critical
D1618s1	0.312	0.227
D1627s1	0.301	0.265
D1634s1	0.295	0.233
D1715s1	0.296	0.234
D1723s1	0.312	0.227
D1736s1	0.284	0.219
D1615s2	0.294	0.248
D1624s2	0.304	0.250
D1633s2	0.312	0.263
D1713s2	0.312	0.256
D1724s2	0.279	0.229
D1735s2	0.298	0.219
D1610s3	0.301	0.274
D1621s3	0.294	0.272
D1639s3	0.290	0.281
D1716s3	0.303	0.240
D1729s3	0.305	0.223
D1739s3	0.298	0.254
D1613s4	0.304	0.269
D1629s4	0.312	0.245
D1635s4	0.306	0.266
D1712s4	0.312	0.262
D1721s4	0.307	0.264
D1737s4	0.303	0.252
D1619s5	0.296	0.254
D1625s5	0.292	0.245
D1637s5	0.302	0.257
D1717s5	0.289	0.230
D1725s5	0.307	0.251
D1731s5	0.251	0.235

D1612m1	0.305	0.234
D1622m1	0.312	0.276
D1631m1	0.312	0.289
D1710m1	0.302	0.245
D1727m1	0.295	0.218
D1730m1	0.276	0.224
D1611m2	0.302	0.234
D1620m2	0.312	0.244
D1638m2	0.301	0.238
D1719m2	0.312	0.222
D1728m2	0.258	0.229
D1738m2	0.294	0.212
D1616m3	0.278	0.247
D1626m3	0.303	0.234
D1636m3	0.285	0.236
D1711m3	0.255	0.240
D1722m3	0.272	0.225
D1733m3	0.244	0.223
D1617m4	0.281	0.235
D1623m4	0.283	0.227
D1630m4	0.234	0.227
D1718m4	0.256	0.245
D1726m4	0.255	0.232
D1732m4	0.292	0.227
D1614m5	0.228	0.219
D1628m5	0.243	0.224
D1632m5	0.273	0.255
D1714m5	0.271	0.221
D1720m5	0.263	0.238
D1734m5	0.222	0.218

Individual test values

time constants: subject E

test	transition	critical
E1612s1	0.277	0.267
E1626s1	0.312	0.274
E1634s1	0.312	0.274
E1711s1	0.312	0.283
E1720s1	0.288	0.272
E1735s1	0.312	0.274
E1617s2	0.298	0.272
E1629s2	0.296	0.277
E1638s2	0.312	0.288
E1714s2	0.312	0.282
E1725s2	0.312	0.273
E1734s2	0.312	0.311
E1615s3	0.312	0.305
E1621s3	0.312	0.303
E1633s3	0.297	0.281
E1719s3	0.270	0.255
E1728s3	0.312	0.295
E1730s3	0.286	0.272
E1610s4	0.284	0.282
E1628s4	0.312	0.275
E1637s4	0.312	0.290
E1718s4	0.312	0.287
E1722s4	0.312	0.297
E1733s4	0.311	0.286
E1616s5	0.312	0.309
E1623s5	0.312	0.308
E1636s5	0.292	0.281
E1712s5	0.308	0.284
E1723s5	0.312	0.297
E1738s5	0.312	0.282

E1618m1	0.292	0.291
E1620m1	0.304	0.283
E1631m1	0.312	0.294
E1717m1	0.312	0.269
E1726m1	0.291	0.282
E1739m1	0.307	0.279
E1614m2	0.309	0.293
E1624m2	0.312	0.306
E1635m2	0.274	0.259
E1710m2	0.269	0.258
E1721m2	0.309	0.246
E1731m2	0.272	0.260
E1611m3	0.286	0.284
E1625m3	0.312	0.256
E1639m3	0.290	0.260
E1716m3	0.271	0.239
E1724m3	0.304	0.263
E1736m3	0.242	0.241
E1613m4	0.310	0.287
E1622m4	0.287	0.255
E1632m4	0.247	0.244
E1713m4	0.271	0.251
E1727m4	0.256	0.245
E1737m4	0.251	0.230
E1619m5	0.298	0.264
E1627m5	0.270	0.246
E1630m5	0.312	0.271
E1715m5	0.290	0.246
E1729m5	0.268	0.245
E1732m5	0.305	0.233

Appendix 6.2 Data for Stage One RMS roll errors

Stage one RMS roll error: statistical analysis of cases for each subject.

1st column: case designation
2nd column: mean of six tests
3rd column: standard deviation of individual points
4th column: mean minus the standard deviation of the mean
5th column: mean plus the standard deviation of the mean

units: degrees

case designation code
1: 10° 2: 20° 3: 40° 4: 80° 5: 120°
s: stationary field condition
m: moving field condition

subject A					
s1	:	6.38 :	1.82 :	5.64 :	7.12
s2	:	9.28 :	3.04 :	7.92 :	10.64
s3	:	9.79 :	2.30 :	8.85 :	10.73
s4	:	7.56 :	3.70 :	6.05 :	9.07
s5	:	6.21 :	2.09 :	5.36 :	7.07
m1	:	5.17 :	1.83 :	4.42 :	5.91
m2	:	3.45 :	1.15 :	2.98 :	3.92
m3	:	2.85 :	1.23 :	2.35 :	3.35
m4	:	2.57 :	0.56 :	2.34 :	2.80
m5	:	3.33 :	0.80 :	3.01 :	3.66
subject B					
s1	:	2.56 :	0.85 :	2.19 :	2.94
s2	:	3.44 :	1.10 :	2.99 :	3.88
s3	:	5.03 :	2.70 :	3.93 :	6.13
s4	:	4.35 :	1.35 :	3.80 :	4.90
s5	:	3.70 :	1.37 :	3.09 :	4.31
m1	:	4.59 :	2.05 :	3.75 :	5.42
m2	:	2.88 :	1.13 :	2.42 :	3.34
m3	:	1.96 :	0.46 :	1.77 :	2.14
m4	:	2.12 :	0.58 :	1.89 :	2.36
m5	:	3.05 :	0.61 :	2.80 :	3.30

subject C				
s1	6.05	0.76	5.74	6.36
s2	6.48	1.94	5.68	7.27
s3	7.07	2.35	6.11	8.03
s4	6.84	2.33	5.79	7.88
s5	5.99	2.16	5.03	6.96
m1	5.63	2.26	4.71	6.55
m2	3.56	1.07	3.12	3.99
m3	2.06	0.68	1.78	2.33
m4	2.11	0.62	1.86	2.37
m5	2.79	0.62	2.53	3.04
subject D				
s1	5.19	0.75	4.88	5.49
s2	5.94	1.44	5.29	6.58
s3	5.60	1.62	4.93	6.26
s4	7.06	2.37	6.09	8.03
s5	5.04	1.01	4.63	5.45
m1	5.68	1.79	4.95	6.41
m2	3.57	1.11	3.11	4.02
m3	3.24	0.72	2.94	3.53
m4	3.13	0.84	2.79	3.47
m5	3.37	1.55	2.74	4.01
subject E				
s1	8.15	2.52	7.12	9.18
s2	10.05	5.63	7.75	12.34
s3	10.41	4.65	8.51	12.31
s4	10.11	4.90	8.11	12.11
s5	9.81	4.66	7.91	11.71
m1	6.87	2.30	5.93	7.81
m2	3.79	0.77	3.45	4.14
m3	4.62	1.99	3.73	5.51
m4	4.22	0.78	3.90	4.54
m5	4.08	1.81	3.34	4.82

Individual Test Values

Test name designation
1st character: subject
2nd and 3rd characters: date of month
4th character: trial/day
5th character: test/trial

stage one rms values, subject A

test	rms error (deg)	
A1115s1 :	5.09	
A1129s1 :	5.58	
A1132s1 :	6.32	
A1216s1 :	6.34	
A1221s1 :	5.04	
A1234s1 :	9.90	
A1116s2 :	24.78	outlier: not included in data analysis
A1125s2 :	9.47	
A1134s2 :	9.94	
A1211s2 :	12.15	
A1226s2 :	4.16	
A1235s2 :	10.69	
A1112s3 :	10.51	
A1127s3 :	11.46	
A1138s3 :	8.44	
A1210s3 :	8.48	
A1227s3 :	6.80	
A1231s3 :	13.07	
A1113s4 :	5.84	
A1128s4 :	14.28	
A1136s4 :	4.36	
A1215s4 :	9.18	
A1229s4 :	4.93	
A1239s4 :	6.77	
A1118s5 :	9.66	
A1121s5 :	4.56	
A1137s5 :	7.83	
A1213s5 :	4.90	
A1224s5 :	4.54	
A1230s5 :	5.80	

A1111m1	:	6.31
A1126m1	:	3.20
A1135m1	:	8.05
A1219m1	:	3.61
A1225m1	:	5.53
A1237m1	:	4.30
A1119m2	:	3.06
A1120m2	:	5.32
A1130m2	:	2.64
A1214m2	:	2.03
A1223m2	:	3.84
A1238m2	:	3.82
A1117m3	:	1.92
A1122m3	:	1.47
A1131m3	:	5.02
A1217m3	:	3.08
A1220m3	:	2.95
A1236m3	:	2.66
A1110m4	:	2.21
A1123m4	:	2.74
A1139m4	:	2.97
A1212m4	:	1.74
A1222m4	:	3.31
A1232m4	:	2.44
A1114m5	:	2.58
A1124m5	:	2.92
A1133m5	:	4.33
A1218m5	:	3.44
A1228m5	:	2.52
A1233m5	:	4.22

Individual test scores

stage one rms error subject B

test	rms error (deg)	
B1818s1 :	2.02	
B1823s1 :	17.59	outlier: not included in data analysis
B1836s1 :	2.72	
B1910s1 :	2.56	
B1929s1 :	1.65	
B1935s1 :	3.87	
B1813s2 :	2.80	
B1820s2 :	2.91	
B1834s2 :	3.25	
B1918s2 :	3.96	
B1922s2 :	2.32	
B1931s2 :	5.38	
B1811s3 :	5.97	
B1822s3 :	2.98	
B1835s3 :	4.13	
B1913s3 :	5.01	
B1925s3 :	2.28	
B1936s3 :	9.82	
B1810s4 :	2.96	
B1824s4 :	4.05	
B1832s4 :	4.52	
B1914s4 :	2.85	
B1924s4 :	6.21	
B1933s4 :	5.51	
B1817s5 :	2.92	
B1826s5 :	2.88	
B1838s5 :	4.31	
B1915s5 :	2.55	
B1927s5 :	9.88	outlier: not included in data analysis
B1937s5 :	5.84	

B1814m1	:	3.44
B1827m1	:	3.06
B1830m1	:	5.89
B1916m1	:	4.61
B1923m1	:	2.55
B1932m1	:	7.96
B1819m2	:	2.90
B1825m2	:	1.68
B1831m2	:	3.75
B1912m2	:	4.62
B1926m2	:	1.93
B1934m2	:	2.38
B1815m3	:	1.64
B1828m3	:	2.60
B1839m3	:	2.16
B1919m3	:	2.19
B1920m3	:	1.85
B1939m3	:	1.30
B1816m4	:	3.28
B1821m4	:	1.99
B1837m4	:	1.68
B1917m4	:	2.01
B1928m4	:	1.98
B1938m4	:	1.81
B1812m5	:	4.11
B1829m5	:	2.35
B1833m5	:	2.80
B1911m5	:	2.83
B1921m5	:	2.85
B1930m5	:	3.39

Individual test scores

stage one rms values, subject C

test	rms error (deg)	
C1011s1 :	6.03	
C1029s1 :	6.61	
C1030s1 :	4.74	
C1116s1 :	5.98	
C1123s1 :	6.96	
C1138s1 :	5.96	
C1015s2 :	9.43	
C1021s2 :	5.25	
C1032s2 :	5.64	
C1114s2 :	5.79	
C1126s2 :	4.44	
C1134s2 :	8.30	
C1010s3 :	3.85	
C1020s3 :	9.16	
C1038s3 :	6.63	
C1110s3 :	9.67	
C1122s3 :	8.21	
C1132s3 :	4.90	
C1019s4 :	5.29	
C1023s4 :	7.08	
C1037s4 :	6.33	
C1118s4 :	4.79	
C1121s4 :	15.05	outlier: not included in data analysis
C1136s4 :	10.69	
C1018s5 :	6.18	
C1025s5 :	5.36	
C1035s5 :	4.88	
C1115s5 :	3.98	
C1127s5 :	9.58	
C1139s5 :	13.35	outlier: not included in data analysis

C1016m1 : 2.86
C1026m1 : 4.23
C1033m1 : 6.25
C1112m1 : 9.27
C1128m1 : 6.67
C1135m1 : 4.51
C1012m2 : 2.33
C1028m2 : 2.47
C1036m2 : 4.56
C1119m2 : 4.92
C1129m2 : 3.82
C1131m2 : 3.24
C1017m3 : 1.85
C1024m3 : 2.07
C1031m3 : 1.69
C1117m3 : 1.87
C1125m3 : 1.47
C1137m3 : 3.37
C1014m4 : 1.19
C1027m4 : 1.99
C1034m4 : 3.12
C1113m4 : 1.95
C1124m4 : 2.16
C1130m4 : 2.28
C1013m5 : 3.56
C1022m5 : 2.93
C1039m5 : 2.51
C1111m5 : 2.44
C1120m5 : 3.38
C1133m5 : 1.91

Individual test scores

stage one rms values, subject D

test	rms error (deg)	
D1618s1 :	5.99	
D1627s1 :	6.22	
D1634s1 :	4.59	
D1715s1 :	4.67	
D1723s1 :	5.15	
D1736s1 :	4.50	
D1615s2 :	4.89	
D1624s2 :	5.55	
D1633s2 :	5.84	
D1713s2 :	8.42	
D1724s2 :	11.05	outlier: not included in data analysis
D1735s2 :	4.99	
D1610s3 :	4.53	
D1621s3 :	5.19	
D1639s3 :	6.81	
D1716s3 :	8.32	
D1729s3 :	4.41	
D1739s3 :	4.33	
D1613s4 :	5.45	
D1629s4 :	5.22	
D1635s4 :	6.12	
D1712s4 :	5.53	
D1721s4 :	9.13	
D1737s4 :	10.90	
D1619s5 :	5.07	
D1625s5 :	3.64	
D1637s5 :	6.14	
D1717s5 :	4.03	
D1725s5 :	5.88	
D1731s5 :	5.45	

D1612m1	:	5.78
D1622m1	:	6.32
D1631m1	:	8.84
D1710m1	:	4.13
D1727m1	:	4.00
D1730m1	:	5.02
D1611m2	:	1.60
D1620m2	:	3.97
D1638m2	:	4.29
D1719m2	:	3.82
D1728m2	:	4.69
D1738m2	:	3.04
D1616m3	:	4.13
D1626m3	:	2.90
D1636m3	:	3.07
D1711m3	:	2.11
D1722m3	:	3.81
D1733m3	:	3.41
D1617m4	:	2.83
D1623m4	:	1.83
D1630m4	:	4.08
D1718m4	:	3.80
D1726m4	:	2.67
D1732m4	:	3.58
D1614m5	:	3.04
D1628m5	:	1.87
D1632m5	:	5.11
D1714m5	:	2.79
D1720m5	:	5.45
D1734m5	:	1.99

Individual test scores

stage one rms values, subject E

test	rms error (deg)
E1612s1	9.02
E1626s1	5.61
E1634s1	11.27
E1711s1	4.70
E1720s1	9.86
E1735s1	8.43
E1617s2	6.57
E1629s2	3.48
E1638s2	10.03
E1714s2	7.12
E1725s2	14.28
E1734s2	18.80
E1615s3	15.40
E1621s3	10.39
E1633s3	3.84
E1719s3	15.67
E1728s3	10.27
E1730s3	6.90
E1610s4	7.45
E1628s4	10.62
E1637s4	12.13
E1718s4	5.59
E1722s4	18.66
E1733s4	6.21
E1616s5	12.65
E1623s5	15.62
E1636s5	4.12
E1712s5	4.93
E1723s5	12.84
E1738s5	8.71

E1618m1	:	5.75	
E1620m1	:	6.38	
E1631m1	:	8.24	
E1717m1	:	9.99	
E1726m1	:	7.59	
E1739m1	:	3.28	
E1614m2	:	3.83	
E1624m2	:	15.44	outlier: not included in data analysis
E1635m2	:	4.55	
E1710m2	:	3.28	
E1721m2	:	4.51	
E1731m2	:	2.79	
E1611m3	:	7.36	
E1625m3	:	13.25	outlier: not included in data analysis
E1639m3	:	5.93	
E1716m3	:	2.86	
E1724m3	:	4.13	
E1736m3	:	2.82	
E1613m4	:	5.42	
E1622m4	:	3.79	
E1632m4	:	4.03	
E1713m4	:	3.13	
E1727m4	:	4.36	
E1737m4	:	4.60	
E1619m5	:	3.81	
E1627m5	:	3.86	
E1630m5	:	6.66	
E1715m5	:	2.62	
E1729m5	:	1.87	
E1732m5	:	5.67	

Appendix 6.3 Data for Stage Two RMS roll errors

Statistical analysis of cases for each subject.

1st column: case designation
2nd column: mean of six tests
3rd column: standard deviation of individual points
4th column: mean minus the standard deviation of the mean
5th column: mean plus the standard deviation of the mean

units: degrees

case designation code
1: 10° 2: 20° 3: 40° 4: 80° 5: 120°
s: stationary field condition
m: moving field condition

subject A				
s1	25.71	4.64	23.64	27.79
s2	27.83	3.02	26.48	29.18
s3	25.83	4.67	23.74	27.92
s4	32.98	1.73	32.21	33.76
s5	28.80	3.34	27.30	30.29
m1	29.01	4.12	27.17	30.86
m2	23.97	3.42	22.44	25.49
m3	17.37	0.68	17.07	17.67
m4	16.00	2.45	14.90	17.10
m5	21.29	4.10	19.46	23.12
subject B				
s1	20.10	3.24	18.64	21.55
s2	25.24	4.07	23.42	27.06
s3	23.68	4.03	21.88	25.49
s4	22.33	3.44	20.80	23.87
s5	21.35	1.88	20.51	22.20
m1	22.63	4.76	20.50	24.76
m2	16.98	3.95	15.22	18.75
m3	14.70	2.83	13.43	15.97
m4	13.47	2.52	12.34	14.59
m5	17.36	2.76	16.13	18.60

subject C				
s1	26.45	3.68	24.80	28.09
s2	23.70	2.30	22.67	24.73
s3	27.80	3.62	26.18	29.42
s4	26.03	4.36	24.08	27.98
s5	26.12	5.18	23.80	28.43
m1	24.12	3.41	22.59	25.65
m2	21.45	2.79	20.20	22.70
m3	19.47	4.81	17.32	21.62
m4	17.22	3.36	15.72	18.72
m5	18.33	3.94	16.57	20.10
subject D				
s1	23.91	2.80	22.65	25.16
s2	28.79	4.00	27.00	30.58
s3	26.03	5.07	23.77	28.30
s4	26.60	5.45	24.17	29.04
s5	23.59	4.90	21.40	25.79
m1	28.62	3.38	27.11	30.13
m2	22.39	3.56	20.79	23.98
m3	17.44	4.37	15.48	19.39
m4	21.33	3.85	19.61	23.05
m5	15.72	2.64	14.54	16.90
subject E				
s1	24.89	5.48	22.44	27.35
s2	27.85	6.77	24.83	30.88
s3	26.30	10.49	21.61	30.99
s4	32.20	10.19	27.65	36.76
s5	34.82	10.45	30.14	39.49
m1	30.86	7.08	27.69	34.03
m2	21.01	8.61	17.16	24.86
m3	21.54	5.04	19.28	23.79
m4	16.43	3.21	14.99	17.87
m5	19.22	3.40	17.71	20.74

Individual Test Values

Test name designation
1st character: subject
2nd and 3rd characters: date of month
4th character: trial/day
5th character: test/trial

stage two rms values, subject A

test	rms error (deg)	points in rms calculation
A1115s1	32.56	366
A1129s1	20.98	243
A1132s1	21.19	387
A1216s1	31.41	266
A1221s1	22.78	416
A1234s1	26.03	307
A1116s2	36.49	141
A1125s2	27.16	195
A1134s2	28.49	236
A1211s2	28.17	337
A1226s2	25.11	191
A1235s2	25.84	422
A1112s3	23.96	256
A1127s3	29.42	390
A1138s3	29.03	262
A1210s3	14.18	141
A1227s3	20.98	389
A1231s3	29.19	525
A1113s4	31.90	301
A1128s4	32.20	131
A1136s4	35.19	355
A1215s4	30.68	328
A1229s4	31.55	147
A1239s4	34.41	428
A1118s5	28.97	343
A1121s5	31.09	198
A1137s5	35.30	181
A1213s5	28.24	385
A1224s5	23.95	83
A1230s5	24.11	229

A1111m1	25.30	164
A1126m1	33.15	377
A1135m1	23.29	267
A1219m1	24.62	111
A1225m1	33.56	206
A1237m1	29.47	284
A1119m2	23.53	213
A1120m2	26.46	520
A1130m2	22.72	286
A1214m2	15.74	236
A1223m2	25.86	449
A1238m2	25.55	151
A1117m3	17.39	266
A1122m3	16.53	336
A1131m3	17.97	359
A1217m3	18.17	200
A1220m3	16.42	261
A1236m3	17.82	315
A1110m4	15.57	282
A1123m4	21.54	200
A1139m4	16.49	256
A1212m4	15.45	196
A1222m4	13.74	198
A1232m4	13.98	277
A1114m5	15.24	279
A1124m5	16.09	227
A1133m5	23.13	496
A1218m5	17.16	369
A1228m5	26.72	466
A1233m5	23.10	526

Individual test values

stage two rms values, subject B

test	rms error (deg)	points in rms calculation
B1818s1	20.77	371
B1823s1	19.75	731
B1836s1	24.04	667
B1910s1	21.23	519
B1929s1	12.24	173
B1935s1	15.63	417
B1813s2	24.38	368
B1820s2	22.24	770
B1834s2	13.15	187
B1918s2	27.10	679
B1922s2	25.81	628
B1931s2	30.41	635
B1811s3	21.72	672
B1822s3	20.20	519
B1835s3	20.91	322
B1913s3	25.47	333
B1925s3	30.42	695
B1936s3	20.53	400
B1810s4	20.84	362
B1824s4	18.60	614
B1832s4	18.95	397
B1914s4	22.14	233
B1924s4	26.53	689
B1933s4	26.18	347
B1817s5	18.71	631
B1826s5	21.83	631
B1838s5	22.12	454
B1915s5	19.55	626
B1927s5	24.27	646
B1937s5	21.86	532

B1814m1	16.97	328
B1827m1	30.19	587
B1830m1	20.23	506
B1916m1	22.44	422
B1923m1	23.66	514
B1932m1	15.98	274
B1819m2	21.26	619
B1825m2	9.91	434
B1831m2	15.94	408
B1912m2	11.89	358
B1926m2	19.29	493
B1934m2	18.92	790
B1815m3	18.20	587
B1828m3	12.17	386
B1839m3	14.21	379
B1919m3	15.80	552
B1920m3	8.61	276
B1939m3	15.14	402
B1816m4	10.97	301
B1821m4	15.14	374
B1837m4	10.96	295
B1917m4	15.63	410
B1928m4	9.77	300
B1938m4	15.92	443
B1812m5	13.98	775
B1829m5	18.48	668
B1833m5	17.07	494
B1911m5	16.05	463
B1921m5	16.77	659
B1930m5	22.89	547

Individual test values

stage two rms values, subject C

test	rms error (deg)	points in rms calculation
C1011s1	22.62	600
C1029s1	25.19	516
C1030s1	23.51	584
C1116s1	21.15	259
C1123s1	28.45	782
C1138s1	31.72	848
C1015s2	19.08	171
C1021s2	25.38	749
C1032s2	22.87	423
C1114s2	25.90	598
C1126s2	23.41	477
C1134s2	19.51	310
C1010s3	30.42	537
C1020s3	27.06	399
C1038s3	26.29	427
C1110s3	22.07	608
C1122s3	29.44	461
C1132s3	32.92	445
C1019s4	18.27	407
C1023s4	24.42	321
C1037s4	18.28	89
C1118s4	27.38	539
C1121s4	30.29	490
C1136s4	28.96	528
C1018s5	24.16	506
C1025s5	19.75	566
C1035s5	24.07	277
C1115s5	34.14	510
C1127s5	20.93	235
C1139s5	29.69	639

C1016m1	15.63	334
C1026m1	23.83	332
C1033m1	22.07	413
C1112m1	25.54	623
C1128m1	24.62	712
C1135m1	27.71	708
C1012m2	19.43	763
C1028m2	15.75	479
C1036m2	24.05	798
C1119m2	21.52	719
C1129m2	24.57	332
C1131m2	23.15	659
C1017m3	18.02	436
C1024m3	14.62	384
C1031m3	22.93	397
C1117m3	27.96	339
C1125m3	12.01	259
C1137m3	19.81	504
C1014m4	16.12	301
C1027m4	22.11	455
C1034m4	17.31	636
C1113m4	14.80	434
C1124m4	18.87	372
C1130m4	9.20	189
C1013m5	13.70	342
C1022m5	24.93	576
C1039m5	19.34	471
C1111m5	19.32	484
C1120m5	14.03	586
C1133m5	16.90	445

Individual test values

stage two rms values, subject D

test	rms error (deg)	points in rms calculation
D1618s1	23.86	599
D1627s1	20.45	239
D1634s1	20.38	473
D1715s1	25.22	465
D1723s1	28.47	594
D1736s1	22.49	565
D1615s2	22.42	340
D1624s2	29.38	362
D1633s2	24.97	300
D1713s2	35.92	355
D1724s2	30.99	446
D1735s2	28.13	619
D1610s3	28.60	178
D1621s3	19.56	160
D1639s3	26.67	87
D1716s3	33.14	446
D1729s3	21.04	609
D1739s3	27.29	315
D1613s4	27.24	225
D1629s4	30.50	441
D1635s4	20.87	253
D1712s4	34.76	305
D1721s4	25.45	273
D1737s4	19.24	351
D1619s5	18.77	298
D1625s5	21.11	359
D1637s5	26.63	306
D1717s5	22.27	478
D1725s5	32.60	367
D1731s5	18.31	241

D1612m1	28.38	510
D1622m1	25.52	209
D1631m1	35.65	126
D1710m1	33.74	402
D1727m1	28.26	624
D1730m1	24.56	480
D1611m2	21.99	472
D1620m2	29.37	449
D1638m2	25.41	459
D1719m2	20.64	650
D1728m2	18.21	337
D1738m2	19.78	689
D1616m3	14.31	278
D1626m3	19.05	500
D1636m3	25.43	403
D1711m3	13.04	224
D1722m3	15.62	446
D1733m3	13.14	317
D1617m4	27.04	397
D1623m4	20.46	478
D1630m4	12.54	206
D1718m4	18.80	182
D1726m4	22.23	286
D1732m4	21.64	516
D1614m5	11.42	249
D1628m5	15.51	296
D1632m5	18.54	188
D1714m5	17.76	480
D1720m5	17.28	284
D1734m5	11.88	213

Individual test values

stage two rms values, subject E

test	rms error (deg)	points in rms calculation
E1612s1	15.14	117
E1626s1	23.56	226
E1634s1	28.45	221
E1711s1	27.54	161
E1720s1	16.73	136
E1735s1	30.90	223
E1617s2	19.71	183
E1629s2	21.86	139
E1638s2	30.02	133
E1714s2	34.17	172
E1725s2	30.87	230
E1734s2	78.43	5
E1615s3	56.15	38
E1621s3	39.76	49
E1633s3	24.69	120
E1719s3	19.27	177
E1728s3	34.17	92
E1730s3	17.92	129
E1610s4	19.61	59
E1628s4	34.63	219
E1637s4	28.72	123
E1718s4	24.95	141
E1722s4	59.12	80
E1733s4	28.72	141
E1616s5	71.17	16
E1623s5	48.48	24
E1636s5	29.32	95
E1712s5	24.46	140
E1723s5	48.05	83
E1738s5	34.61	174

E1618m1	17.51	37
E1620m1	28.60	131
E1631m1	42.79	99
E1717m1	24.59	257
E1726m1	32.05	84
E1739m1	37.45	170
E1614m2	41.07	96
E1624m2	47.67	34
E1635m2	17.86	170
E1710m2	17.12	152
E1721m2	16.55	416
E1731m2	22.01	147
E1611m3	16.59	50
E1625m3	24.68	348
E1639m3	21.53	232
E1716m3	18.16	309
E1724m3	27.74	268
E1736m3	10.80	136
E1613m4	19.42	131
E1622m4	16.51	254
E1632m4	12.93	136
E1713m4	12.16	214
E1727m4	15.03	181
E1737m4	20.73	286
E1619m5	14.70	234
E1627m5	15.52	243
E1630m5	21.75	243
E1715m5	24.23	338
E1729m5	16.02	242
E1732m5	20.05	520

Appendix 7.1 Parameters of the forcing function

component	harmonic	frequency (rad/sec)	amplitude	phase 1	phase 2
1	7	0.322	1.698	5.60	1.37
2	13	0.598	1.166	4.71	4.76
3	29	1.33	0.872	4.07	6.04
4	37	1.70	0.565	4.86	4.03
5	53	2.44	0.520	4.47	1.03
6	73	3.36	0.440	2.11	2.11
7	103	4.74	0.386	6.09	0.93
8	149	6.86	0.324	4.22	3.68
9	211	9.71	0.265	4.61	5.44
10	293	13.5	0.225	3.88	3.58
11	419	19.3	0.191	0.10	3.39
12	587	27.0	0.138	5.69	0.39
13	683	31.4	0.098	5.84	5.30

Appendix 9.1 Superposition of the four frequency response curves predicted by the least squares models. One bode plot for each case.

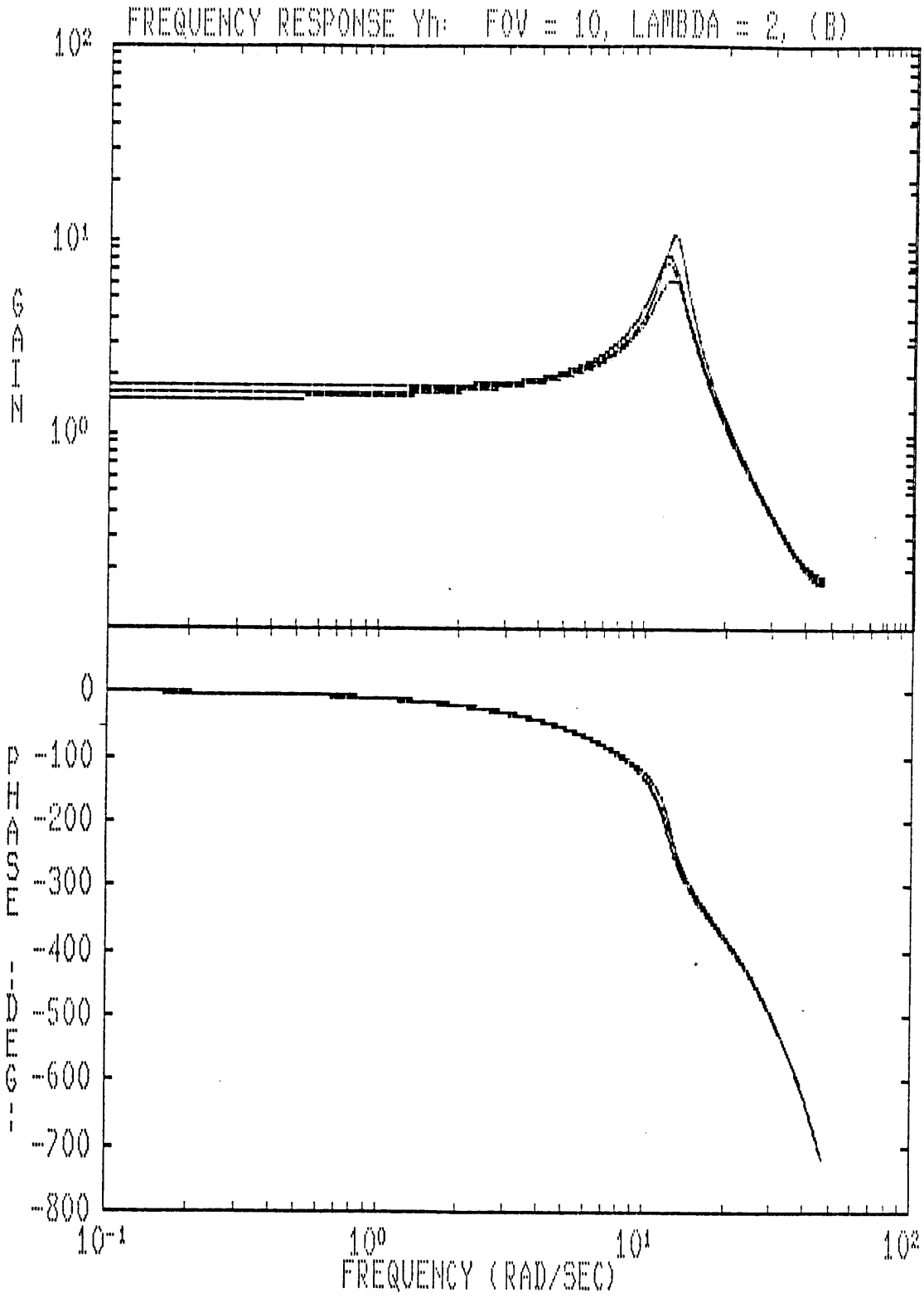
FREQUENCY RESPONSE Yh: FOV = 10, LAMBDA = 2, (B)
GAIN
PHASE --DEG--
FREQUENCY (RAD/SEC)

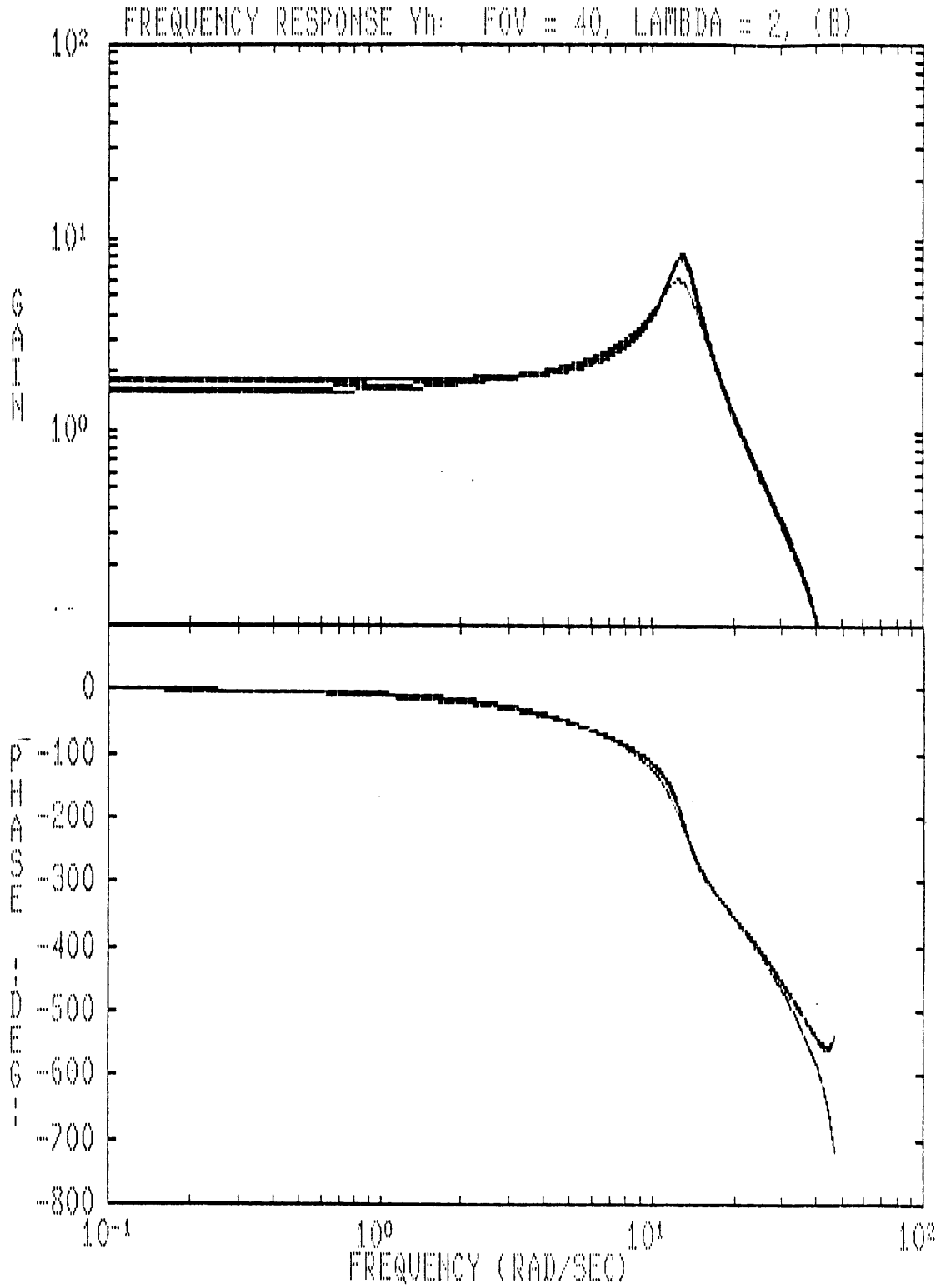
FREQUENCY RESPONSE Yh: FOV = 40, LAMBDA = 2, (B)
GAIN
PHASE --DEG--
FREQUENCY (RAD/SEC)
10²
10¹
10⁰
0
-100
-200
-300
-400
-500
-600
-700
-800
10⁻¹
10⁰
10¹
10²

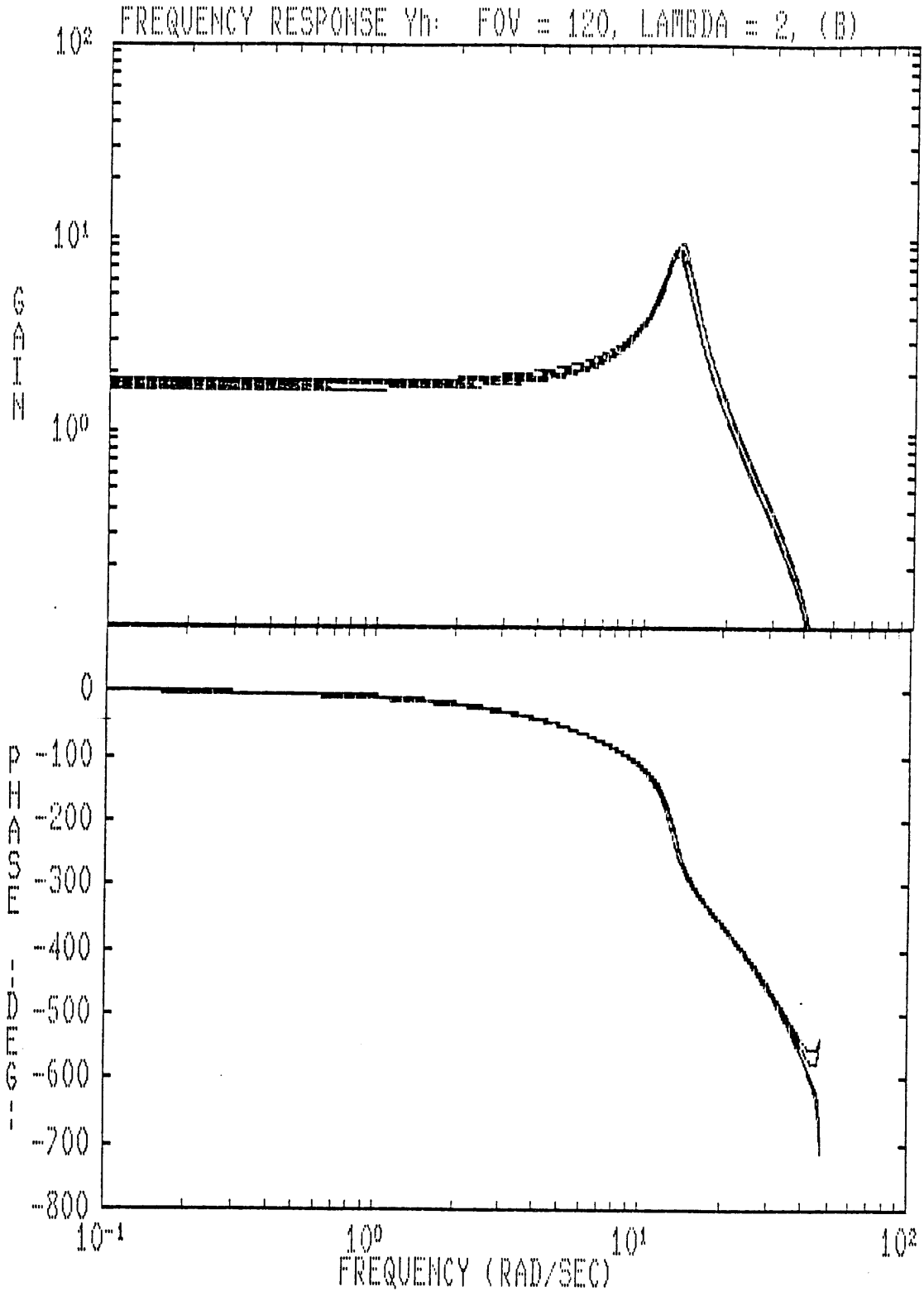
FREQUENCY RESPONSE Yh: FOV = 120, LAMBDA = 2, (B)
GAIN
PHASE --DEG--
FREQUENCY (RAD/SEC)
10²
10¹
10⁰
0
-100
-200
-300
-400
-500
-600
-700
-800
10⁻¹
10⁰
10¹
10²

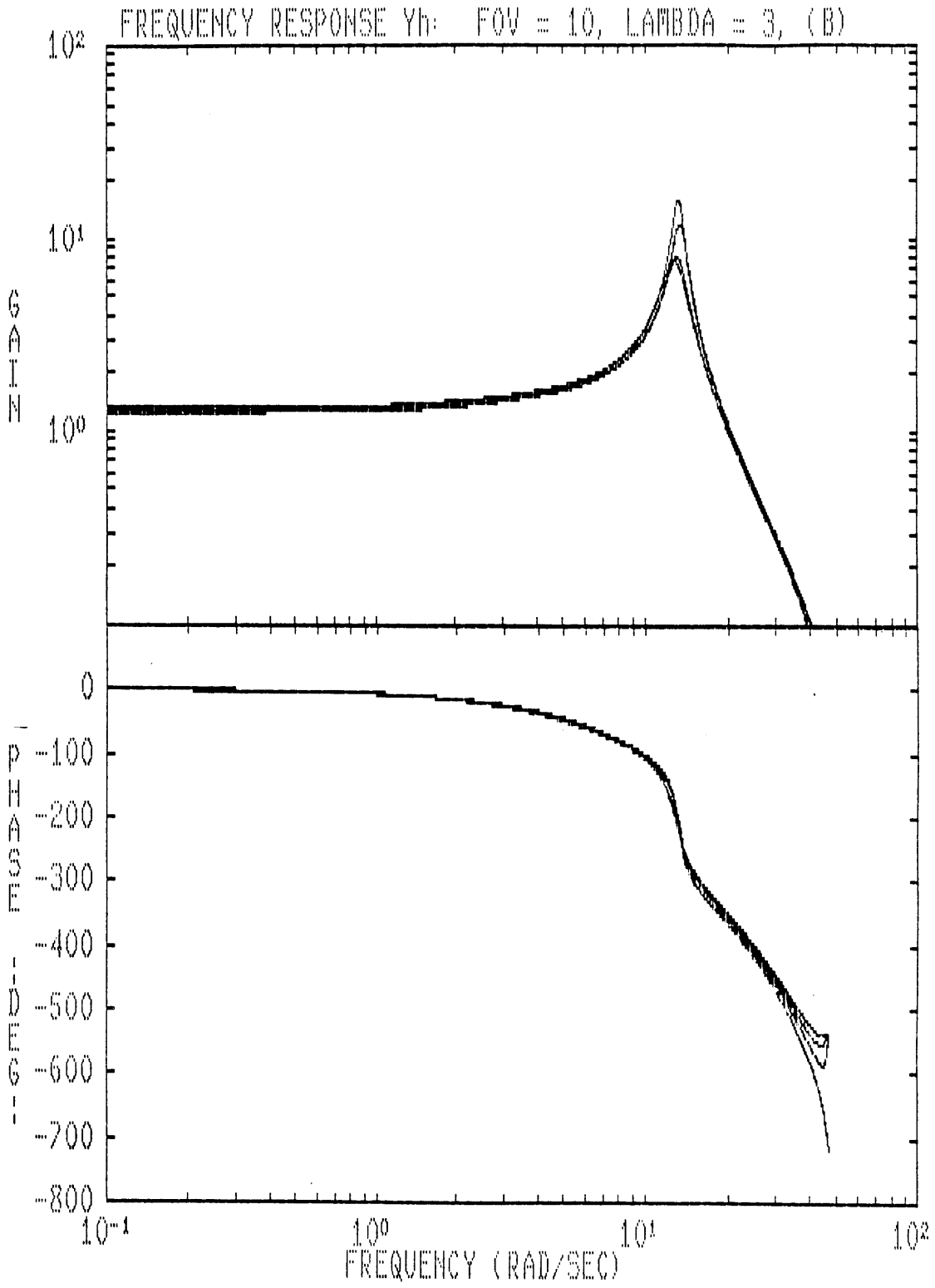
FREQUENCY RESPONSE Yh: FOV = 10, LAMBDA = 3, (B)
GAIN
PHASE --DEG--
FREQUENCY (RAD/SEC)

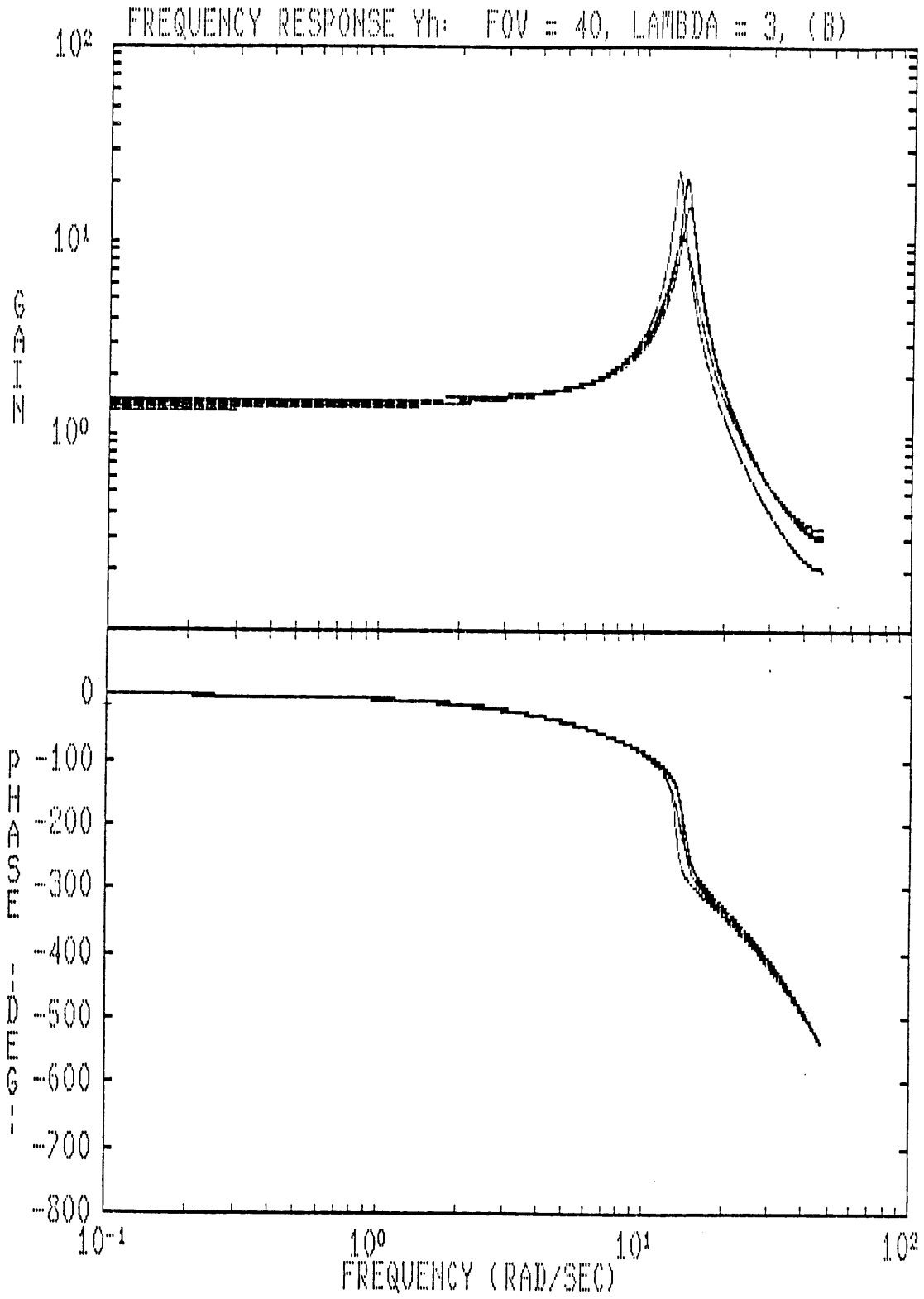
FREQUENCY RESPONSE Yh: FOV = 40, LAMBDA = 3, (B)
GAIN
PHASE --DEG--
FREQUENCY (RAD/SEC)

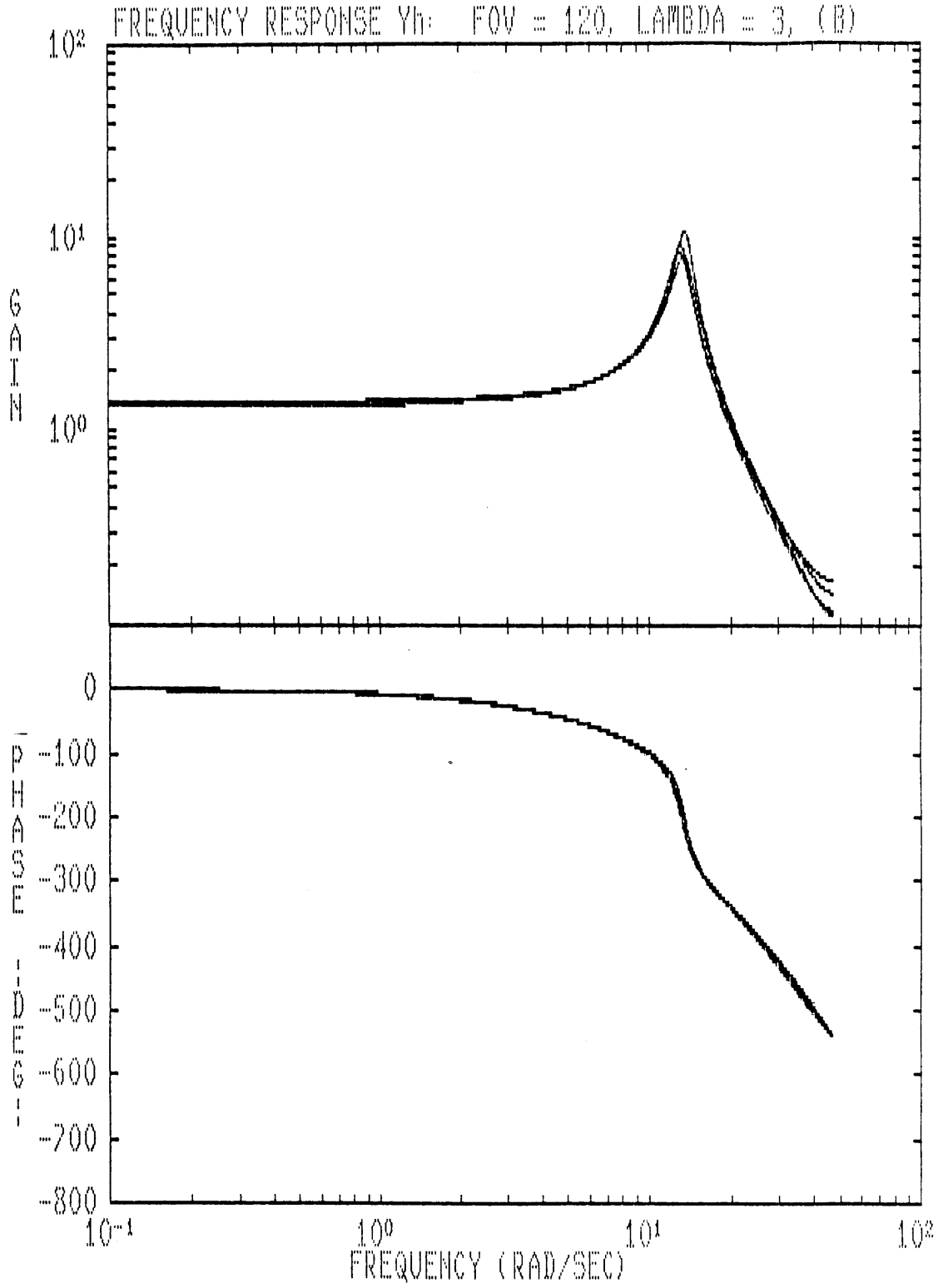
FREQUENCY RESPONSE Yh: FOV = 120, LAMBDA = 3, (B)
GAIN
PHASE --DEGS--
FREQUENCY (RAD/SEC)

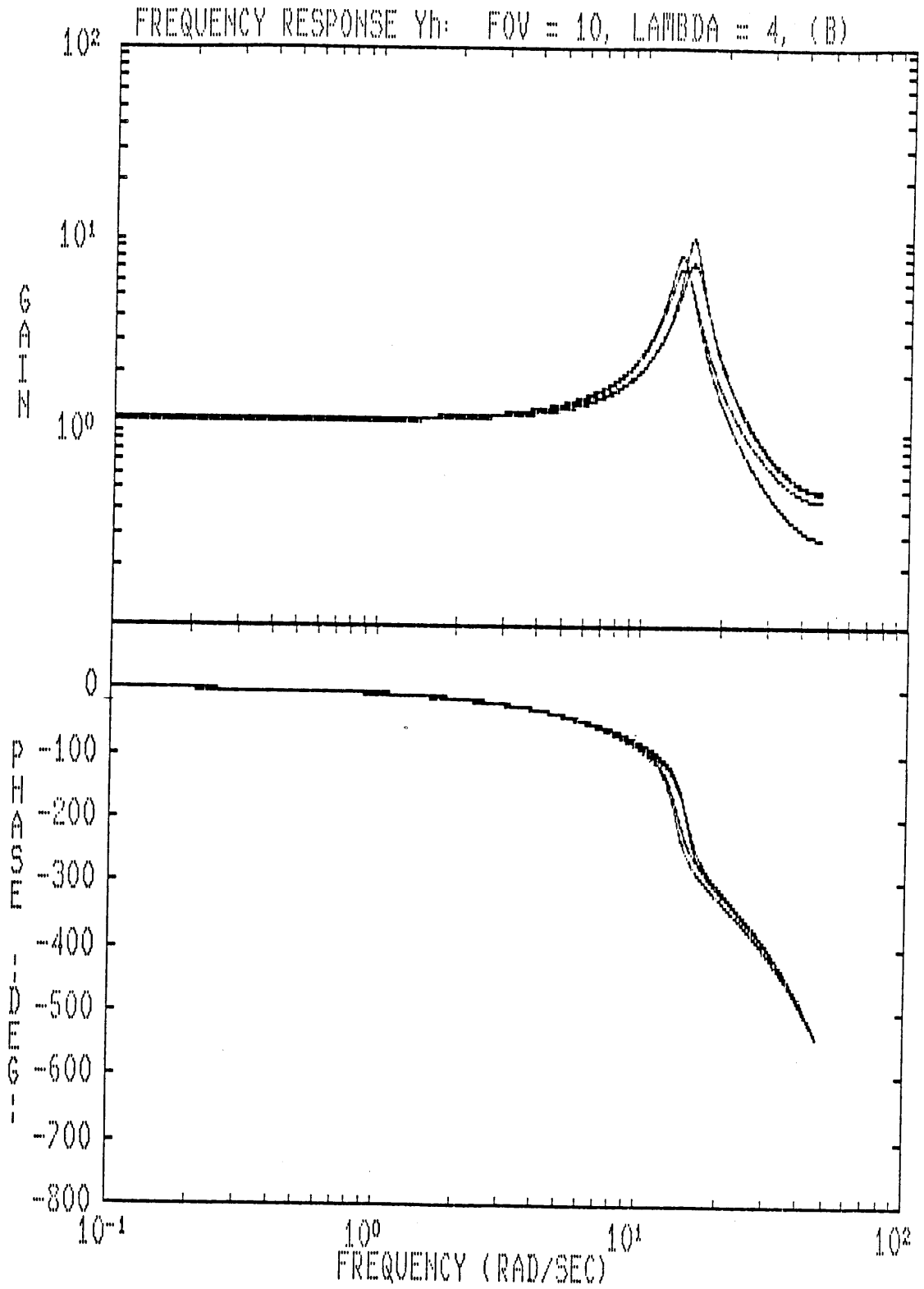
FREQUENCY RESPONSE Yh: FOV = 10, LAMBDA = 4, (B)
GAIN
PHASE -- DEGREES --
FREQUENCY (RAD/SEC)

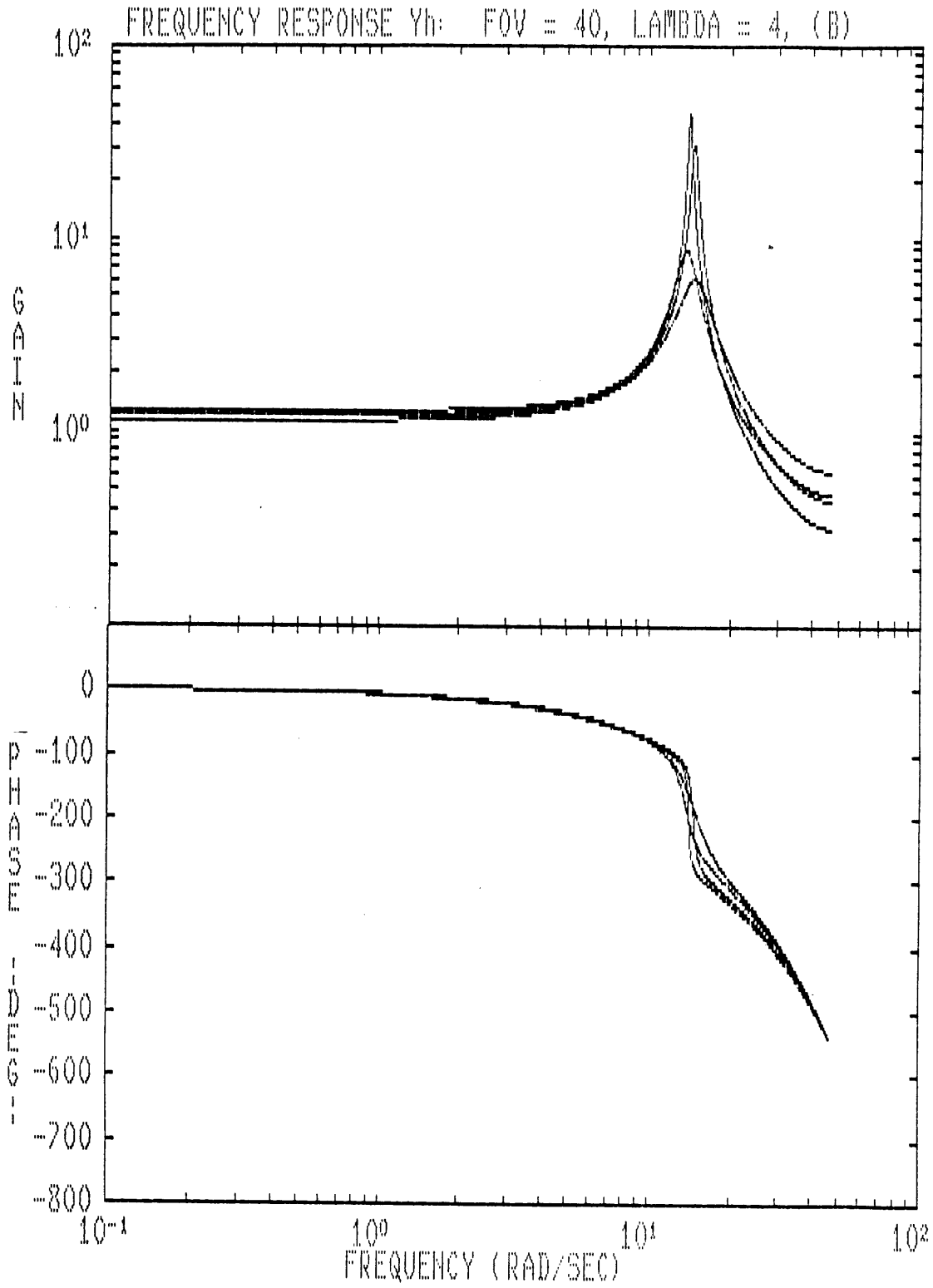
FREQUENCY RESPONSE Yh: FOV = 40, LAMBDA = 4, (B)
GAIN
PHASE -- DEG --
FREQUENCY (RAD/SEC)
10²
10¹
10⁰
0
-100
-200
-300
-400
-500
-600
-700
-800
10⁻¹
10⁰
10¹
10²

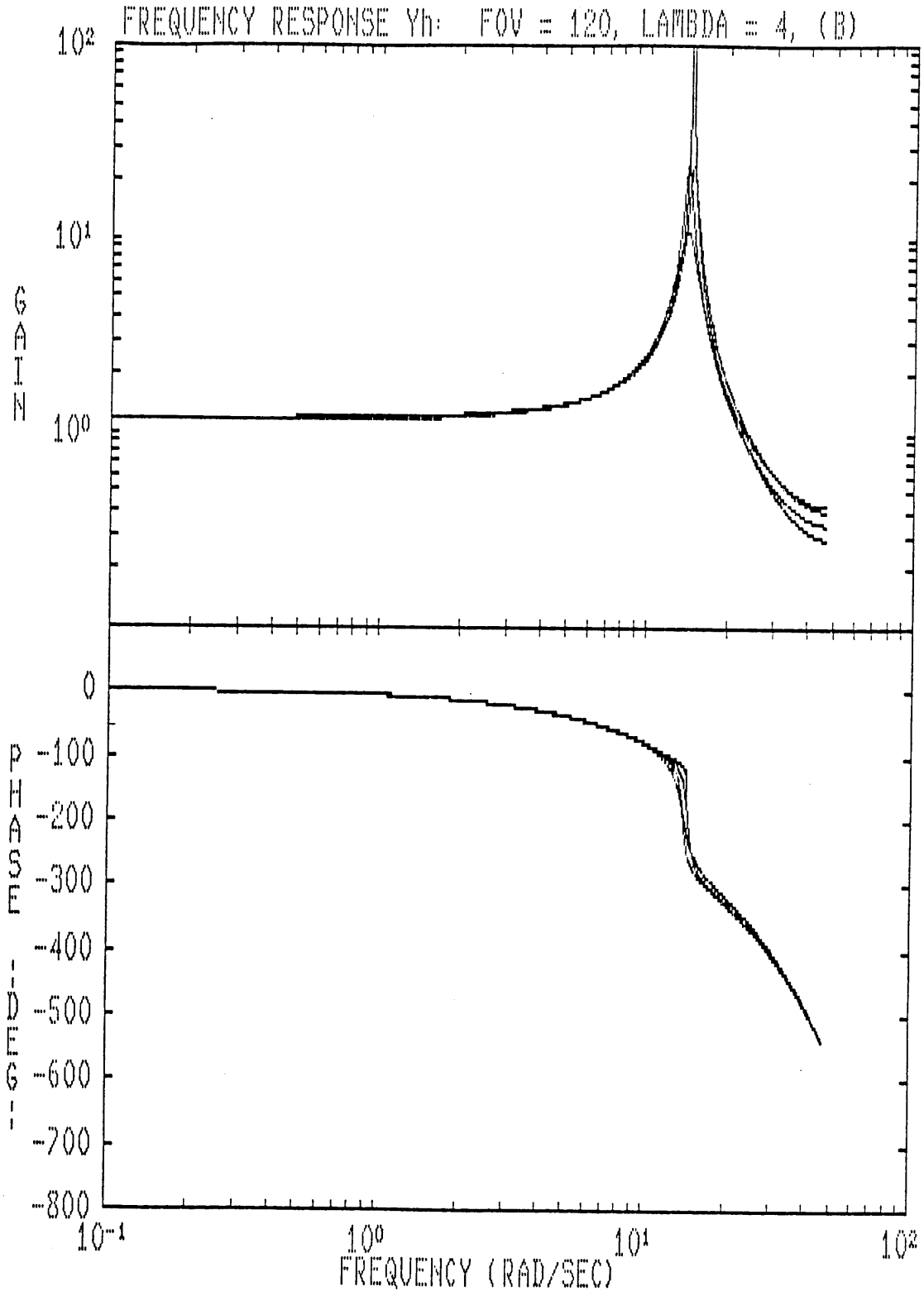
FREQUENCY RESPONSE Yh: FOV = 120, LAMBDA = 4, (B)
GAIN
10^2
10^1
10^0
PHASE --DEG--
0
-100
-200
-300
-400
-500
-600
-700
-800
10^{-1}
10^0
10^1
10^2
FREQUENCY (RAD/SEC)

Appendix 9.2 Comparison of the least squares and FFT frequency responses. One bode plot for each case.

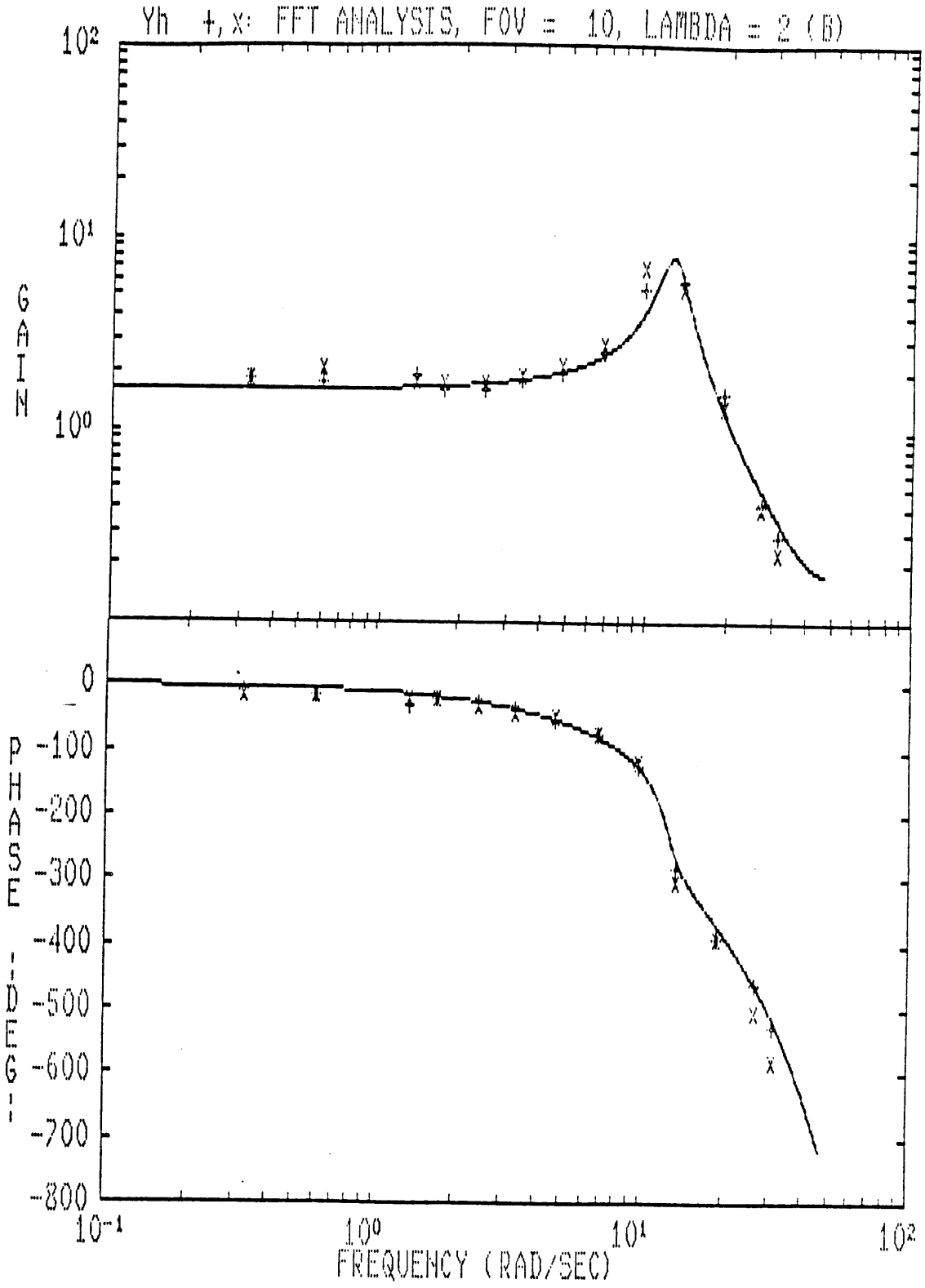
Yh +,x: FFT ANALYSIS, FOV = 10, LAMBDA = 2 (B)
GAIN
PHASE --DEG--
FREQUENCY (RAD/SEC)

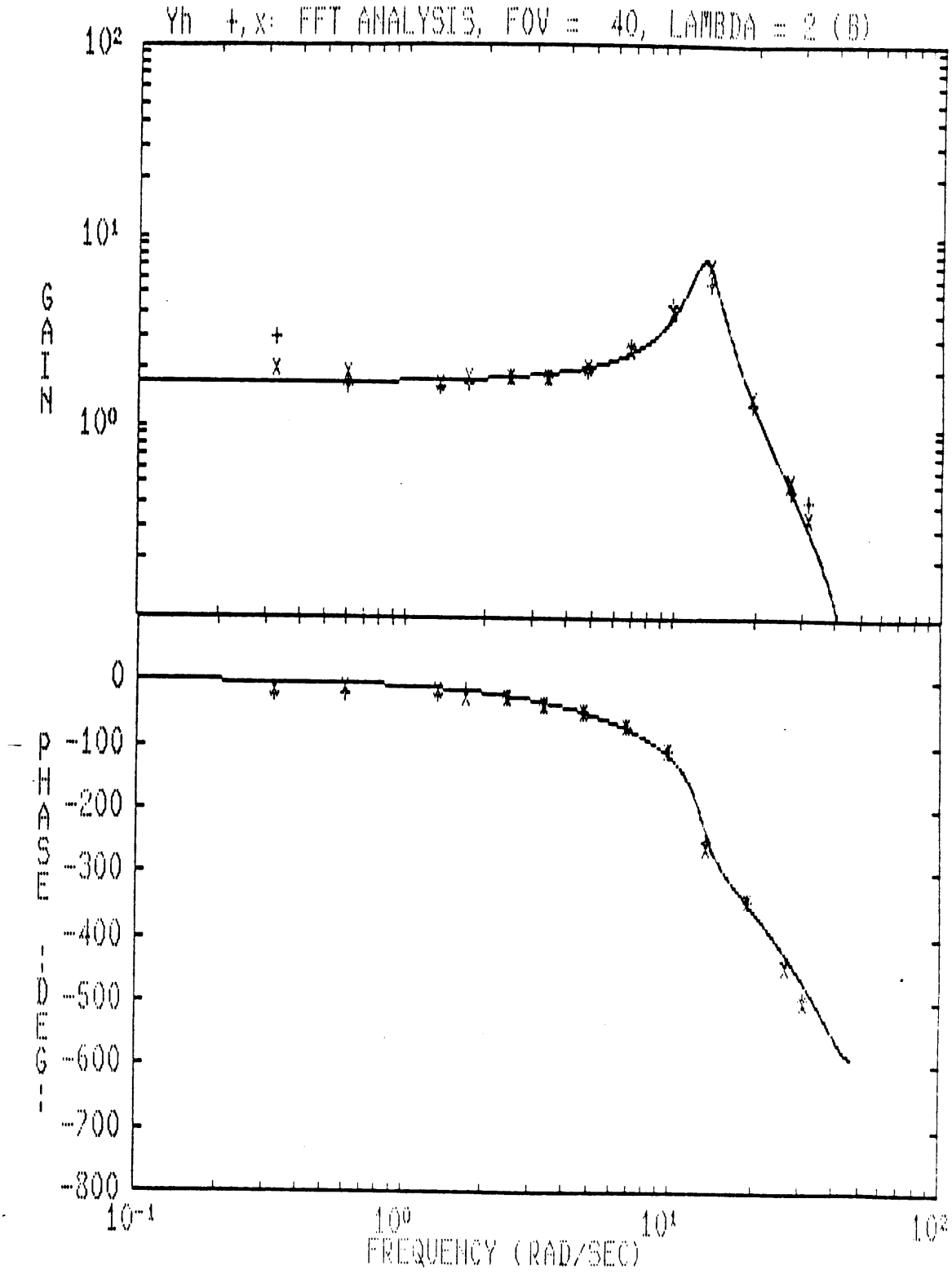
Yh +,x: FFT ANALYSIS, FOV = 40, LAMBDA = 2 (B)
GAIN
10^2
10^1
10^0
PHASE --DEG--
0
-100
-200
-300
-400
-500
-600
-700
-800
10^{-1}
10^0
10^1
10^2
FREQUENCY (RAD/SEC)

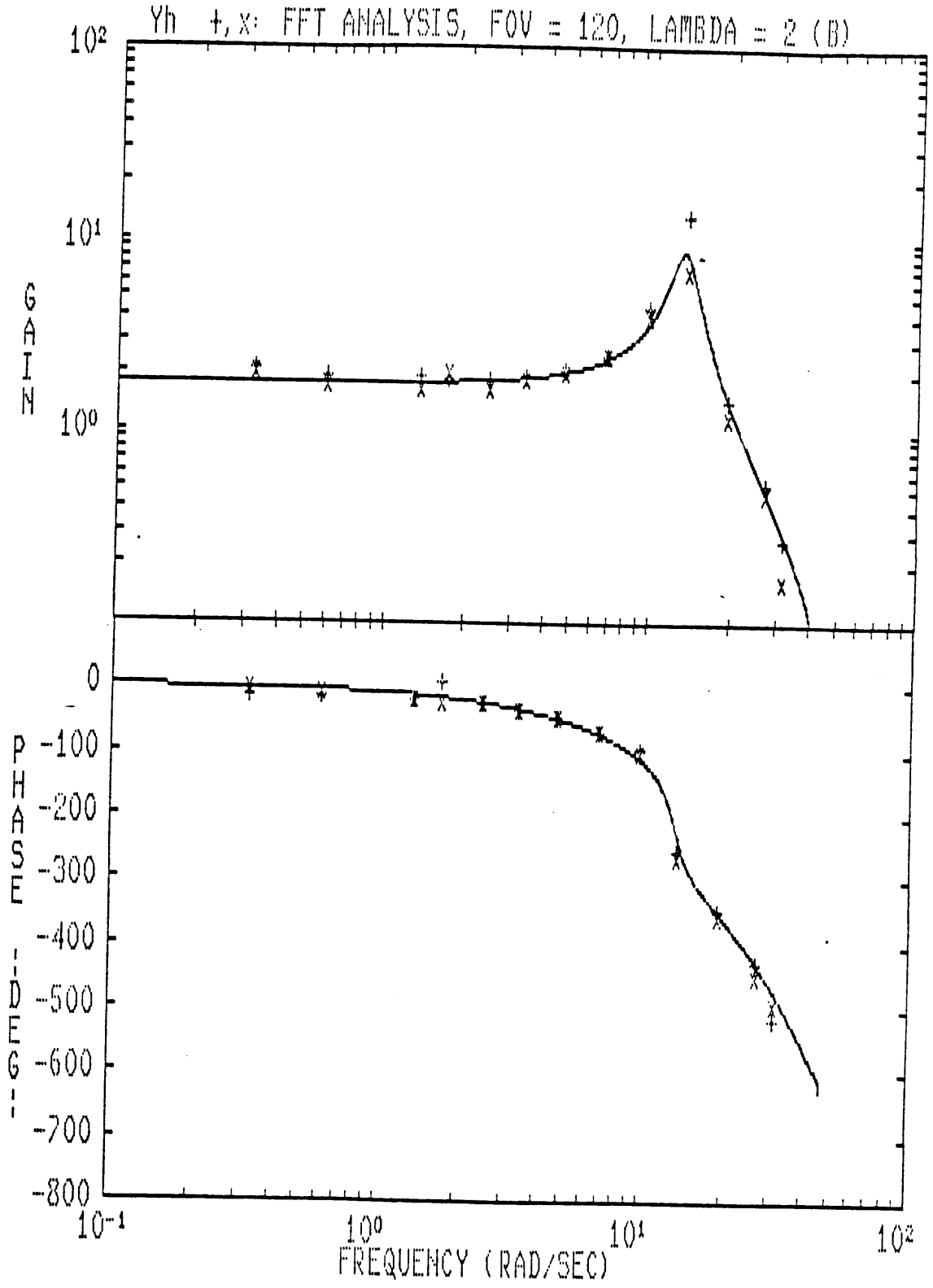
Yh +, x: FFT ANALYSIS, FOV = 120, LAMBDA = 2 (B)
GAIN
PHASE --DEG--
FREQUENCY (RAD/SEC)

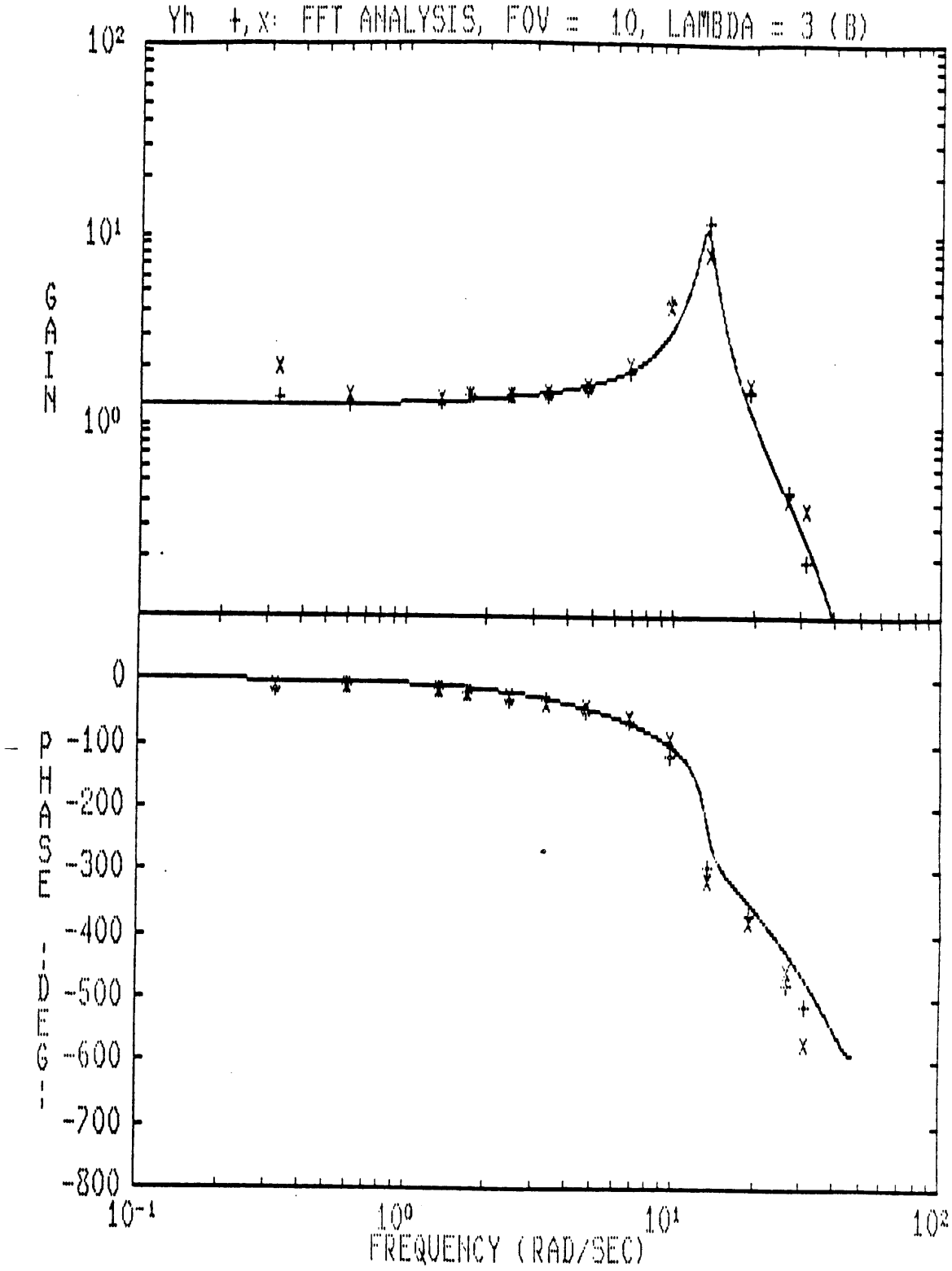
Yh +,x: FFT ANALYSIS, FOV = 10, LAMBDA = 3 (B)
GAIN
PHASE --DEG--
FREQUENCY (RAD/SEC)

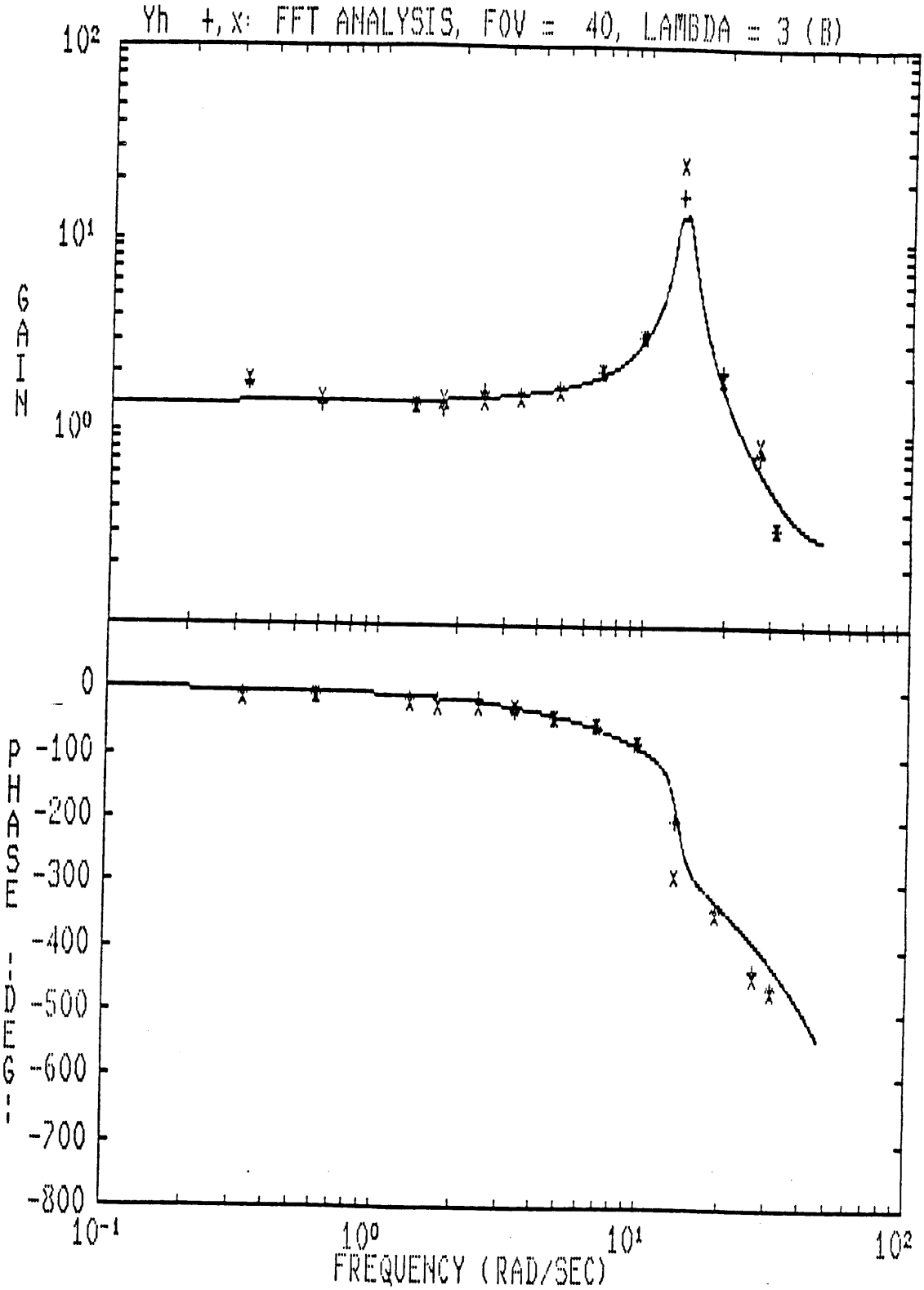
Yh +,x: FFT ANALYSIS, FOV = 40, LAMBDA = 3 (B)
10²
10¹
10⁰
GAIN
0
-100
-200
-300
-400
-500
-600
-700
-800
PHASE --DEG--
10⁻¹
10⁰
10¹
10²
FREQUENCY (RAD/SEC)

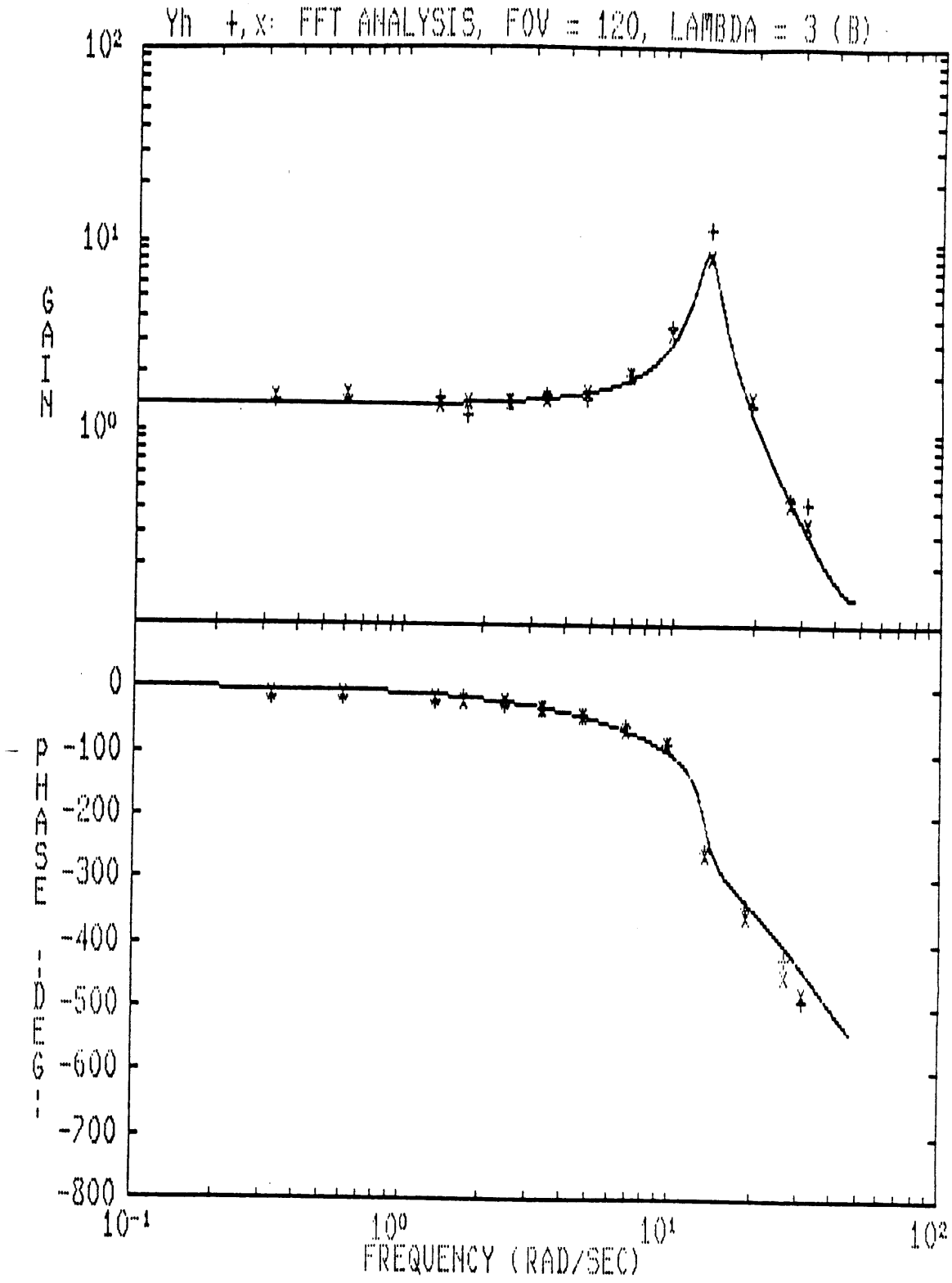
Yh +,x: FFT ANALYSIS, FOV = 120, LAMBDA = 3 (B)
GAIN
PHASE --DEG--
FREQUENCY (RAD/SEC)

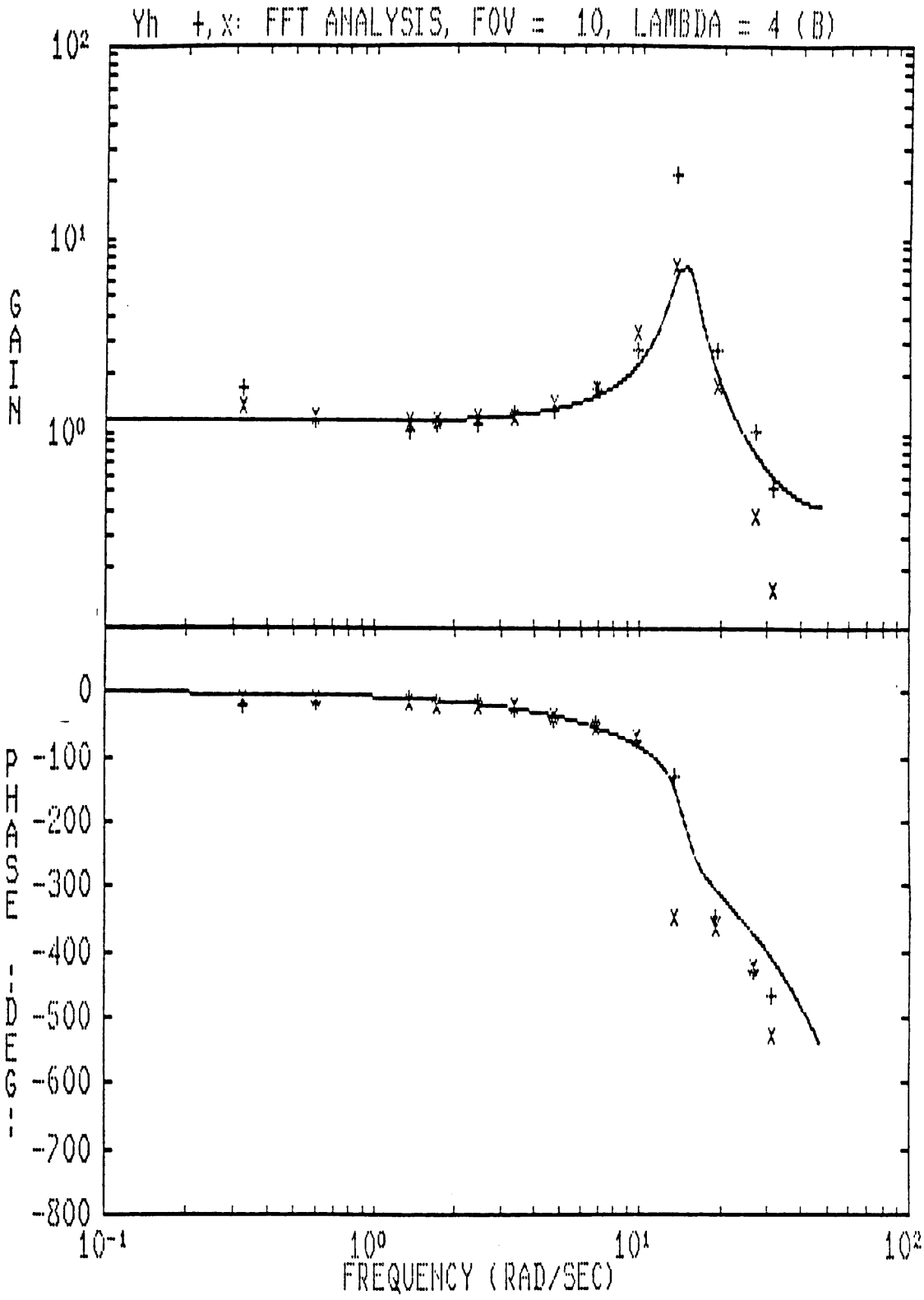
Yh +, x: FFT ANALYSIS, FOV = 10, LAMBDA = 4 (B)
GAIN
PHASE --DEG--
FREQUENCY (RAD/SEC)

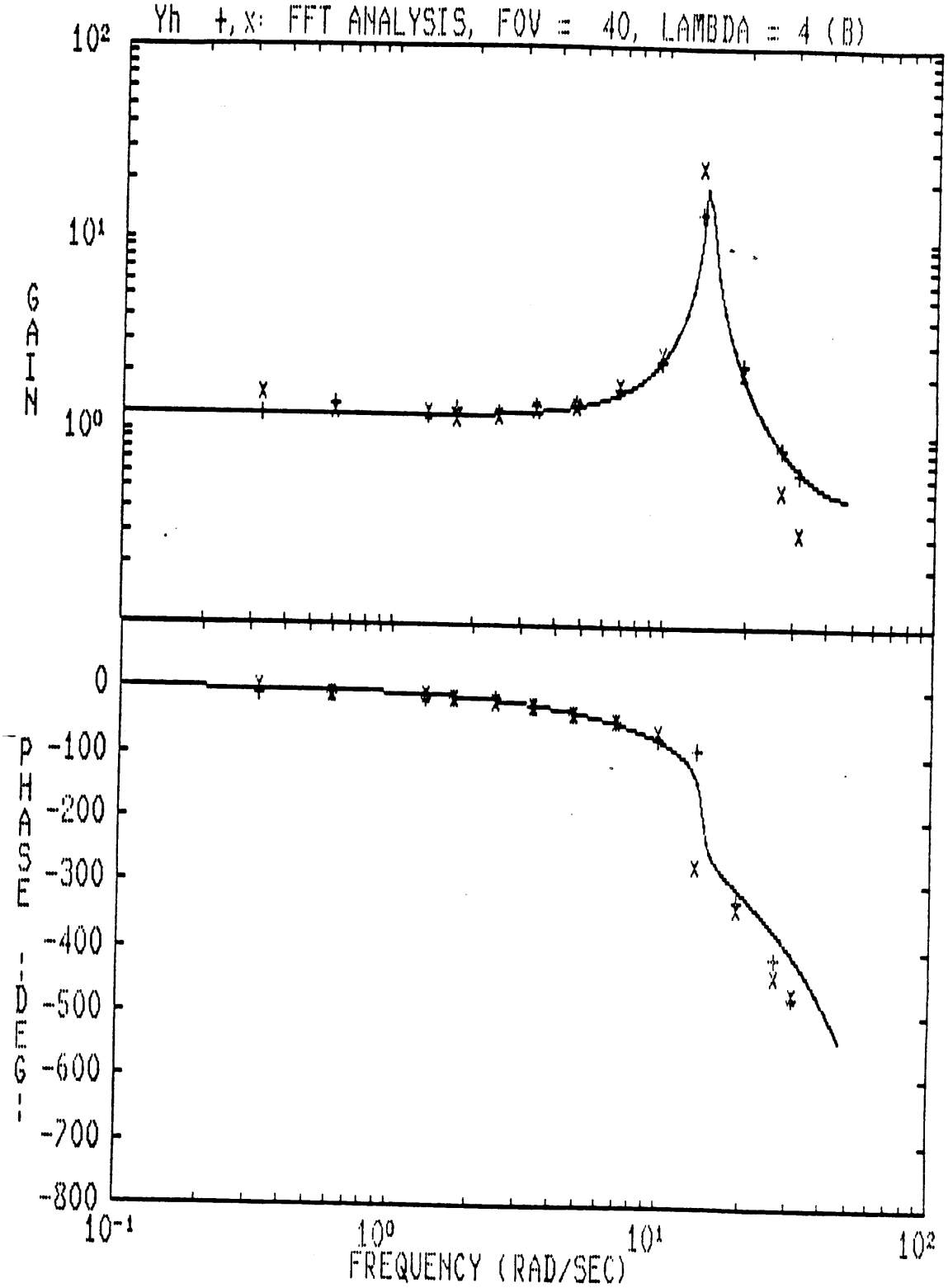
Yh +,x: FFT ANALYSIS, FOV = 40, LAMBDA = 4 (B)
GAIN
PHASE --DEG--
FREQUENCY (RAD/SEC)

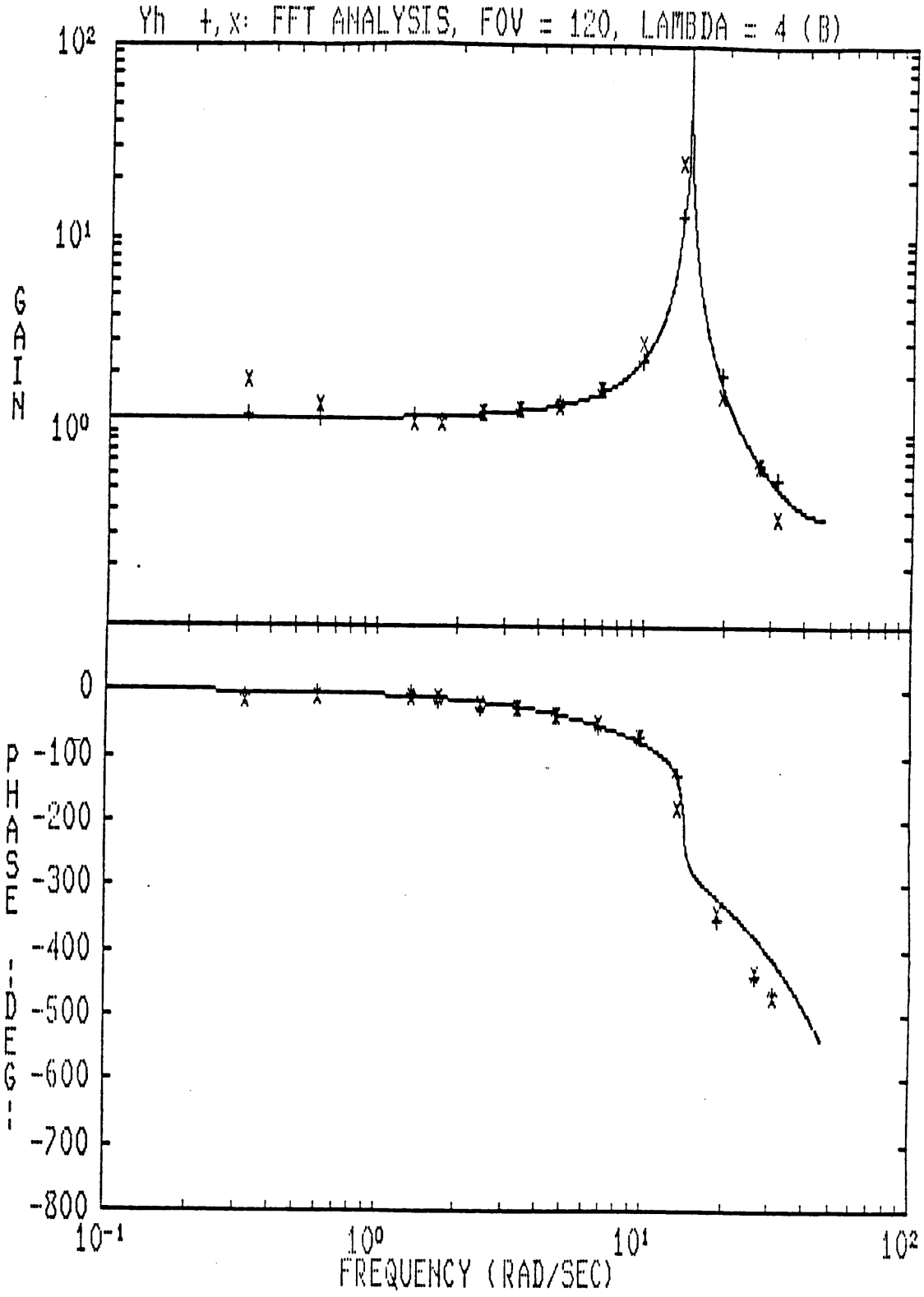
Yh +,x: FFT ANALYSIS, FOV = 120, LAMBDA = 4 (B)
GAIN
PHASE -DEG-
FREQUENCY (RAD/SEC)

Appendix 9.3 Power spectral densities from least squares and FFT methods. Two plots for each case.

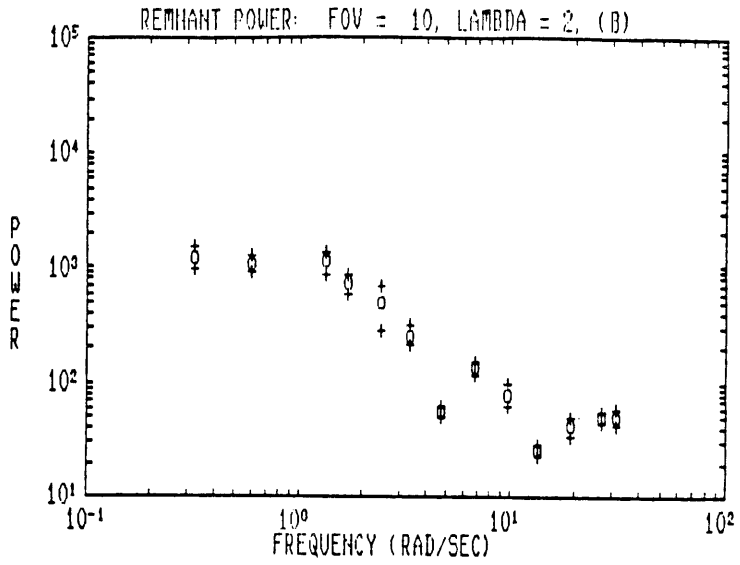

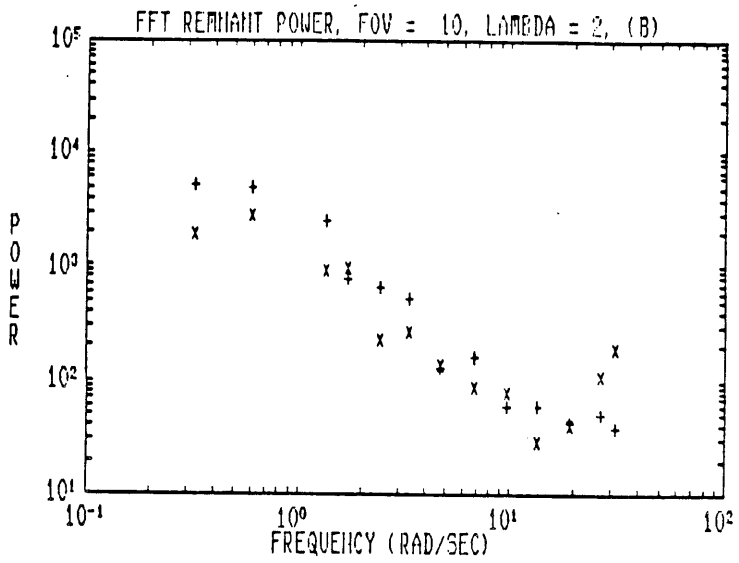

Total integrated power of remnant (arbitrary units)

Least squares: 4542 ± 430

FFT test 1 : 9476

FFT test 2 : 6858

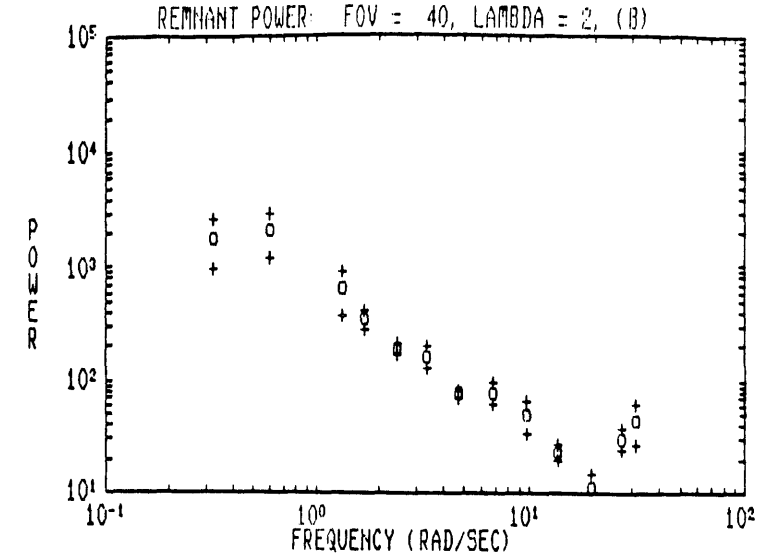

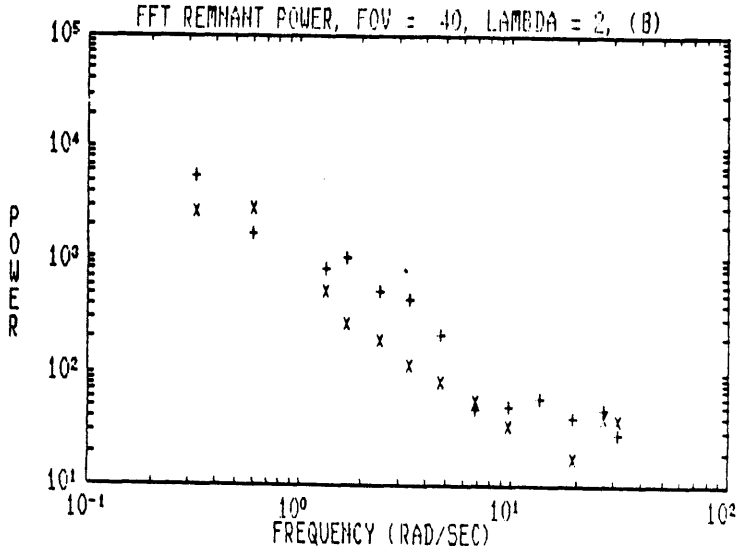

Total integrated power of remnant (arbitrary units)

Least squares: 3893 ± 1230

FFT test 1 : 6748

FFT test 2 : 4270

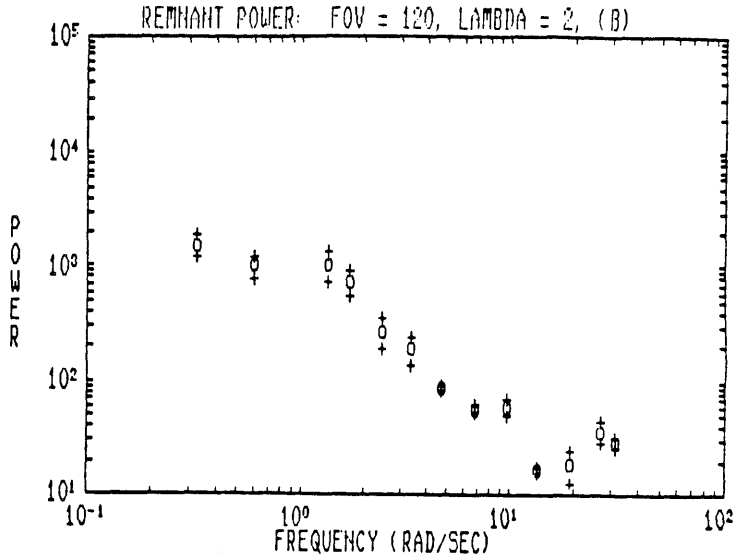

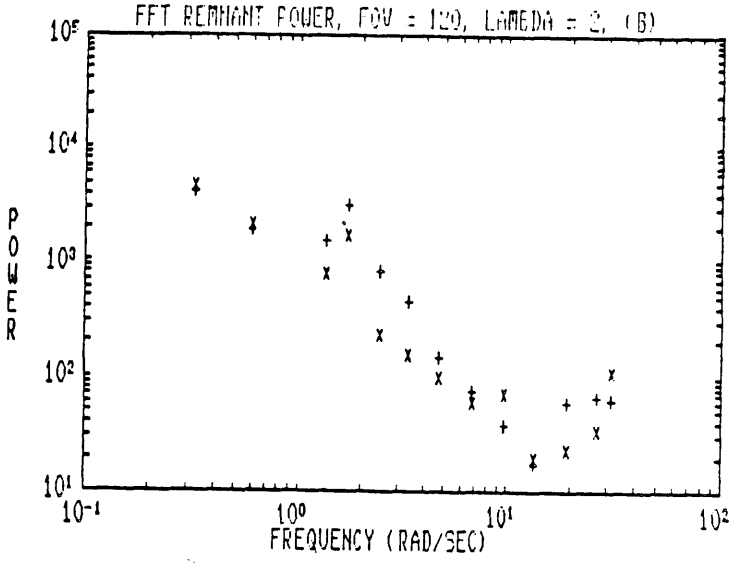

Total integrated power of remnant (arbitrary units)

Least squares: 3685 ± 666

FFT test 1 : 8358

FFT test 2 : 6429

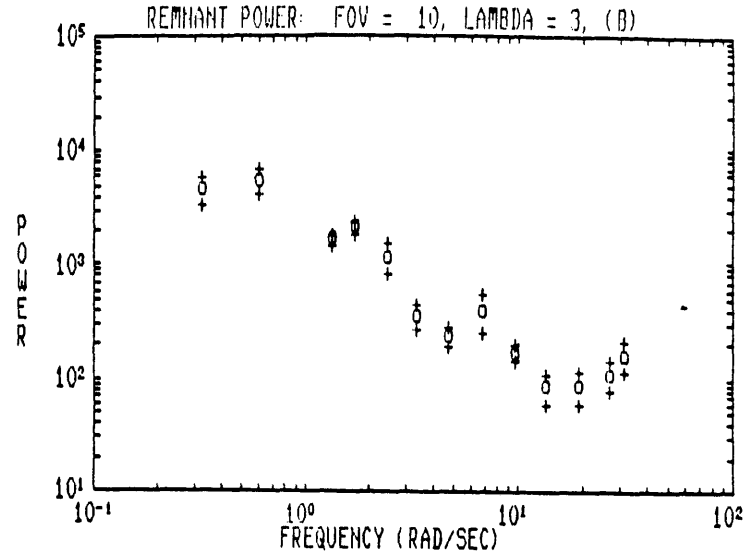

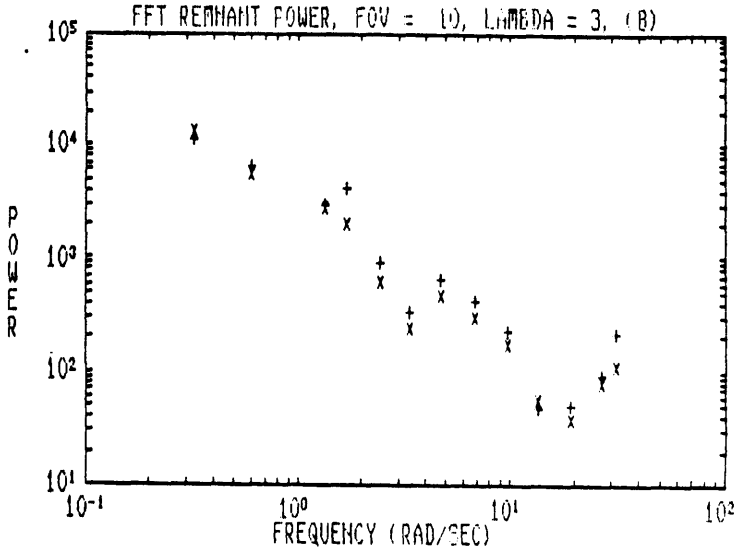

Total integrated power of remnant (arbitrary units)

Least squares: 12890 ± 1790

FFT test 1 : 18690

FFT test 2 : 15620

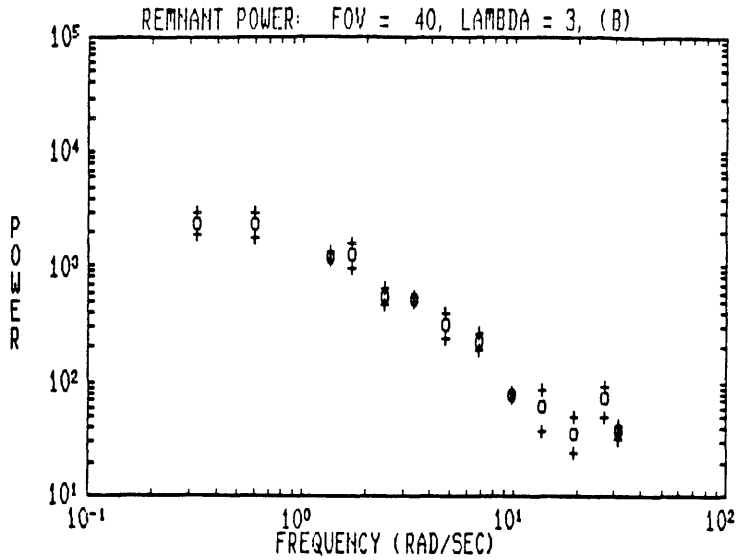

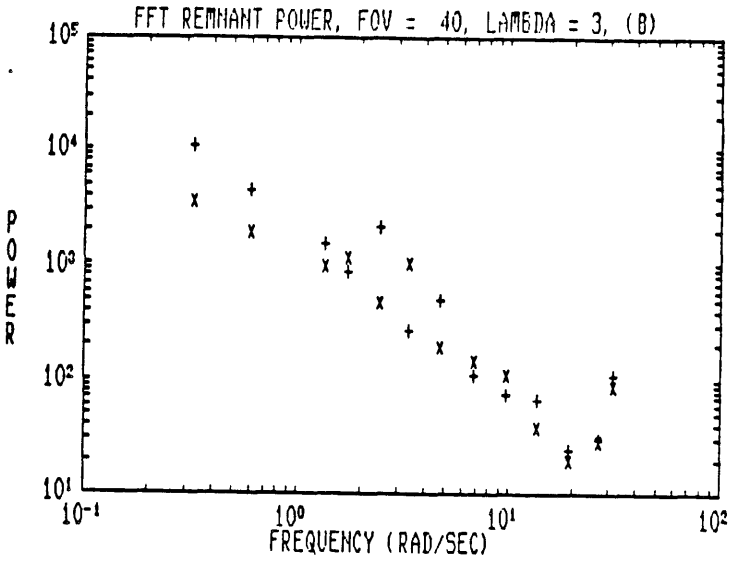

Total integrated power of remnant (arbitrary units)

Least squares: 7277 ± 345

FFT test 1 : 12840

FFT test 2 : 7279

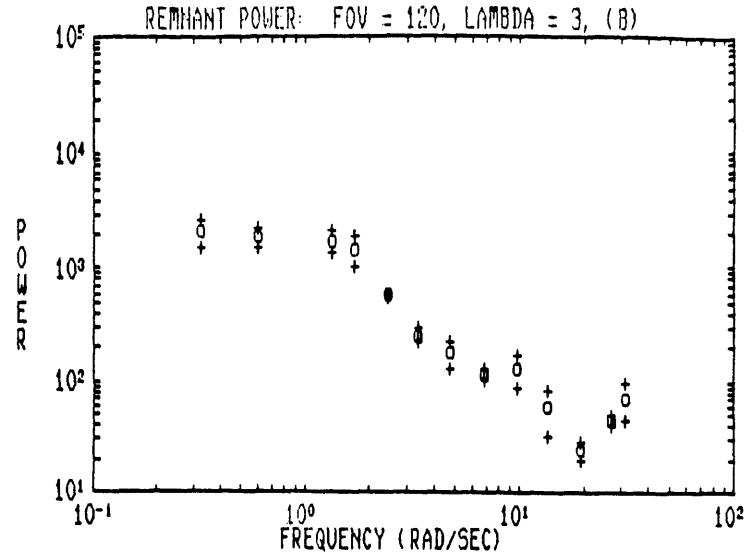

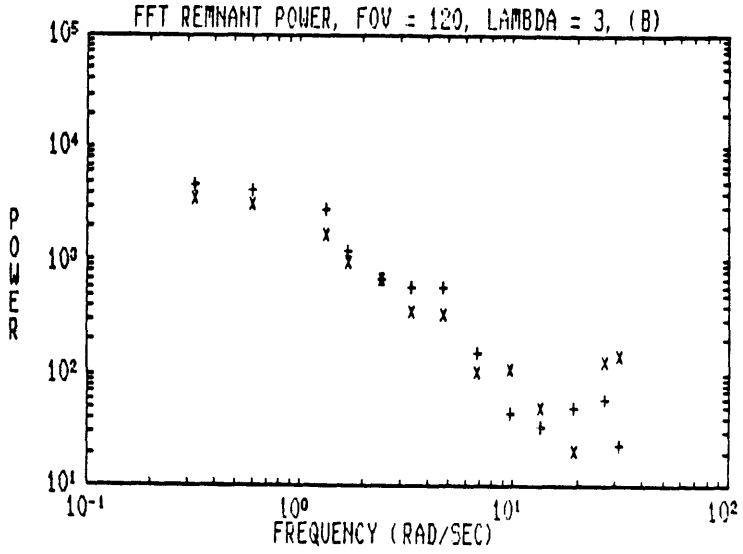

Total integrated power of remnant (arbitrary units)

Least squares: 6590 ± 419

FFT test 1 : 10120

FFT test 2 : 8903

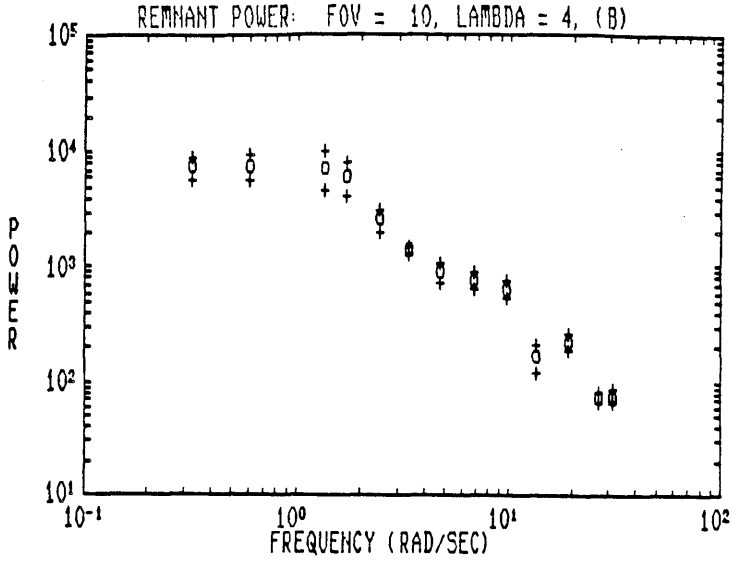

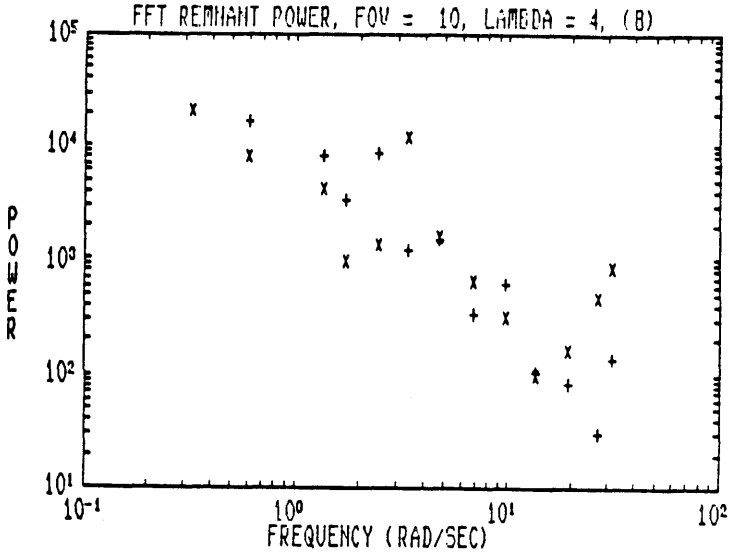

Total integrated power of remnant (arbitrary units)

Least squares: 27250 ± 4620

FFT test 1 : 102000

FFT test 2 : 46100

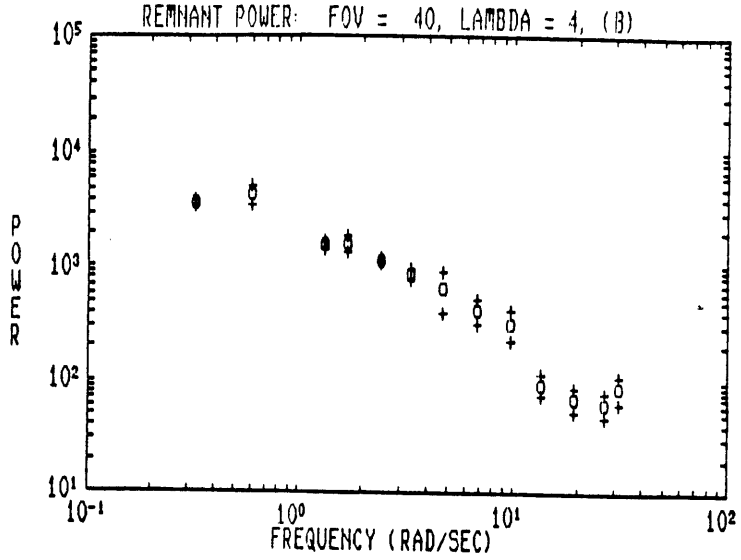

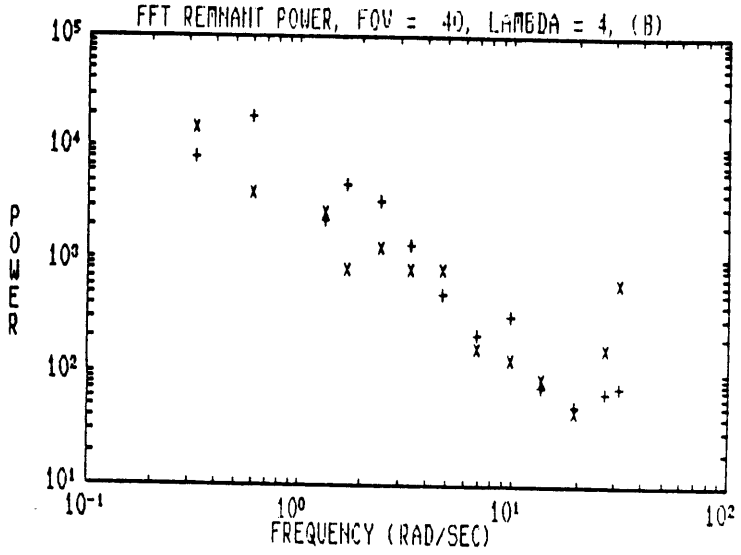

Total integrated power of remnant (arbitrary units)

Least squares: 12550 ± 1100

FFT test 1 : 25100

FFT test 2 : 20200

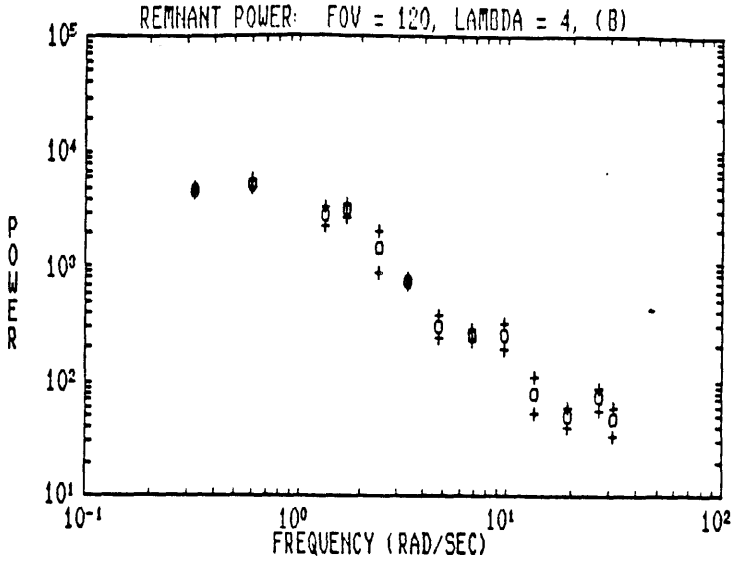

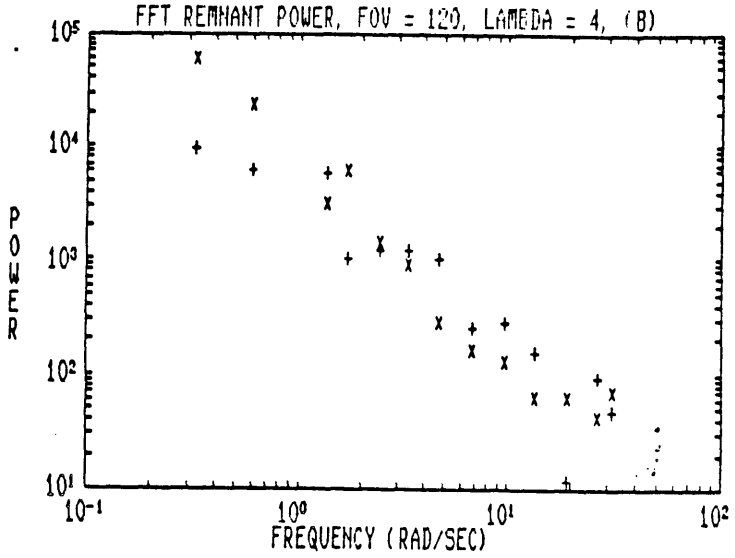

Total integrated power of remnant (arbitrary units)

Least squares: 13380 ± 1020

FFT test 1 : 18100

FFT test 2 : 46800

REFERENCES

Aviation Week and Space Technology, November 5, 1984, "720 Completes Tests Before Crash", McGraw-Hill Publications.

Aviation Week and Space Technology, January 14, 1985, "Virtual Cockpit's Panoramic Displays Afford Advanced Mission Capabilities", McGraw-Hill Publications.

Brandt, Dichgans, Koenig, Differential Effects of Central Versus Peripheral Vision on Egocentric and Exocentric Motion Perception, Experimental Brain Research, 16,476-491 (1973).

Cornsweet, Visual Perception, Academic Press, 1970

Held, Leibowitz, Teuber, Handbook of Sensory Physiology, Volume VIII, Perception, Springer-Verlag, 1978

Howlett, Wide Angle Color Photography Method and System, United States Patent Office, #4,406,537.

Jex, McDonnell, Phatak, A Critical Tracking Task for Man-Machine Research Related to the Operator's Effective Time Delay. Part I: Theory and Experiments with a First-Order Divergent Control Element, NASA CR-616, 1966.

Levison, Baron, Kleinman, A Model for Human Controller Remnant, Transactions on Man-Machine Systems, Vol. MMS-10, No. 4, 1969.

McDonnel, Jex, A Critical Tracking Task for Man-Machine Research Related to the Operator's Effective Time Delay. Part II: Experimental Effects of System Input Spectra, Control Stick Stiffness, and Controlled Element Order, NASA CR-674, 1967.

Pirenne, Visual Perception, 1967

Orear, Notes on Statistics for Physicists, U.S. Atomic Energy Commission, UCRL-8417, 1958

Sheridan, Ferrel, Man-Machine Systems, MIT Press, 1974.

Zacharias, Caglayan, Sinacori, A Visual Cuing Model for Terrain Following Applications, AIAA Journal of Guidance, Vol. 8, No. 2, March-April 1983.

Zacharias, Levison, A Performance Analyzer for Identifying Changes in Human Operator Tracking Strategies, Aerospace Medical Research, Laboratory, AMRL-TR-70-17, 1979.